

**Neutrino oscillation phenomenology
with fermions beyond the standard model**

A thesis

submitted to

Tata Institute of Fundamental Research, Mumbai

for the degree of

Doctor of Philosophy in Physics

by

Shamayita Ray

Department of Theoretical Physics,

**Tata Institute of Fundamental Research,
Mumbai, India**



April, 2010

*To
My Parents*

Declaration

This thesis is a presentation of my original research work. Wherever contributions of others are involved, every effort is made to indicate this clearly, with due reference to the literature, and acknowledgement of collaborative research and discussions.

The work was done under the guidance of Professor Amol Dighe, at the Tata Institute of Fundamental Research, Mumbai.

Shamayita Ray

In my capacity as supervisor of the candidates thesis, I certify that the above statements are true to the best of my knowledge.

Amol Dighe

Date

Acknowledgment

I would like to acknowledge my thesis supervisor Prof. Amol Dighe for introducing me to the exciting field of neutrino physics. I am extremely thankful to him for his constant support, encouragement and guidance.

I would also like to thank all my collaborators for their kind co-operation and continuous support. I am truly thankful to all the former and present students of the department with whom I have shared the office and who helped me a lot day in and day out. I would like to take this opportunity to thank all the faculty members and the non-academic members of our department.

Finally without the support and help of family members and my friends it would have been impossible for me to finish this thesis work. I am thankful to all of them.

Synopsis

S.1 Introduction

The field of neutrino physics has made immense progress in the last decade, which was initiated when the Super-Kamiokande experiment in Japan [1] reported the evidence for oscillations in the atmospheric neutrinos. Afterwards oscillations in the solar neutrinos were established by the SNO experiment [2], which solved the long-standing solar neutrino puzzle. Results from the controlled source experiments KamLAND [3] and K2K [4, 5] provided further confirmation of the oscillation phenomena. Various short baseline experiments also probed the neutrino mixing parameter space in different regions.

There have also been experiments that indicated the presence of neutrino mixing beyond three flavors. The first such experiment showing the positive indication for the neutrino oscillation beyond the three-neutrino paradigm was the Los Alamos LSND [6] experiment, but the KARMEN [7] experiment strongly constrained the LSND parameter space. Currently MiniBooNE [8] experiment at Fermilab has probed the entire LSND parameter region but has not observed any neutrino oscillations.

If the controversial LSND claim is set aside for the moment, the current knowledge about the neutrinos is that there are three neutrino flavors (ν_α , $\alpha \in \{e, \mu, \tau\}$), which mix to form three neutrino mass eigenstates (ν_i , $i \in \{1, 2, 3\}$). These mass eigenstates are separated by $\Delta m_{ij}^2 \equiv m_i^2 - m_j^2$ where, $m_{i,j}$ denote mass eigenvalues with $i, j \in \{1, 2, 3\}$. The two sets of eigenstates are connected through $\nu_\alpha = (U_{\text{PMNS}})_{\alpha i} \nu_i$, where U_{PMNS} is the Pontecorvo-Maki-Nakagawa-Sakata neutrino mixing matrix [9, 10, 11, 12] in the basis where the charged lepton mass matrix is diagonal. This matrix is parametrized as

$$U_{\text{PMNS}} = P \cdot \mathcal{U} \cdot Q, \quad (1)$$

where

$$\mathcal{U} = U_{23}(\theta_{23}, 0) U_{13}(\theta_{13}, \delta) U_{12}(\theta_{12}, 0), \quad Q = \text{Diag}\{e^{-i\phi_1}, e^{-i\phi_2}, 1\}. \quad (2)$$

Here $U_{ij}(\theta_{ij}, \delta_{ij})$ is the complex rotation matrix in the i - j plane, δ is the Dirac CP violating phase, ϕ_i are the Majorana phases, and P is the flavor phase matrix (Sometimes the flavor phases are called as the unphysical phases since they do not play a role in the phenomenology of neutrino mixing or in neutrino beta decays.) The current best-fit values and 3σ ranges for these parameters are summarized in Table 1.1. It is still not known whether the neutrino mass ordering is normal ($m_1 < m_2 < m_3$) or inverted ($m_3 < m_1 < m_2$). Many

	Best fit	3σ range
Δm_{21}^2 [10^{-5}eV^2]	7.65	7.05 - 8.34
$ \Delta m_{31}^2 $ [10^{-3}eV^2]	2.40	2.07 - 2.75
$\sin^2 \theta_{12}$	0.304	0.25 - 0.37
$\sin^2 \theta_{23}$	0.50	0.36 - 0.67
$\sin^2 \theta_{13}$	0.01	≤ 0.056

Table 1: The present best-fit values and 3σ ranges of oscillation parameters [13, 14, 15].

high precision oscillation experiments are going on and also being planned in order to measure the neutrino oscillation parameters with higher accuracy and to determine the neutrino mass ordering. Though the neutrino oscillation experiments are not sensitive to the absolute neutrino masses, the current bound from cosmology on the sum of the three neutrino masses is $\sum m_i \lesssim 1.5$ eV [16]. The upcoming beta-decay experiments like KATRIN [17] will aim at measuring the absolute neutrino mass scale.

Recently it has been pointed out [18] that with two or more sterile neutrinos, having $\Delta m^2 \sim \mathcal{O}(1)$ eV², it is possible to satisfy both LSND and MiniBooNE data simultaneously. Sterile neutrinos, with masses ~ 0.1 eV or higher and obeying all the constraints from the terrestrial experiments, can also play an important role in astrophysics and cosmology [19]. The matter enhanced active-sterile neutrino transformation can have a great effect on r-process nucleosynthesis in the core-collapse supernovae [20], and can also influence the explosion dynamics [21]. Presence of sterile neutrinos can explain the large observed velocities of pulsars [22]. The Chandra blank sky observations

also allow keV neutrinos to be viable dark matter candidates [23], which can help in the production of supermassive black holes [24]. These are excellent dark matter candidates in ν MSM [25, 26, 27, 28] and can also explain masses of active neutrinos and baryon asymmetry of the universe. Thus the main requirements for the astrophysically and cosmologically relevant sterile neutrinos are that they be heavier than the three active neutrinos ($m \sim 1\text{--}10$ eV or \sim keV) and that they mix weakly with the electron and muon neutrino (in order to satisfy the MiniBooNE constraints).

In this thesis we explore the neutrino oscillation phenomenology, with fermions beyond the standard model (SM), on two fronts. First, we study the effect of the presence of one or more \sim eV–keV sterile neutrinos on the signals expected at the upcoming long baseline experiments. Second, we examine neutrino mass models where new fermions with masses \sim TeV or higher participate through the Type-III seesaw mechanism [29].

In the first part we find out the analytic expression for the survival and conversion probabilities of the neutrinos when the \sim eV–keV sterile neutrinos are present and examine some of the possible signatures of sterile neutrino mixing on the signals at a neutrino factory setup with near and far detectors. We also estimate bounds on the sterile neutrino parameters that can be obtained at such long baseline experiments [30].

One of the most distinctive features emerging out of the current experimental values given in the Table 1 is that the neutrinos are massive and the absolute masses of neutrinos are orders of magnitude smaller than those of quarks and charged leptons. In the framework of the SM, since there is no right-handed neutrino, the neutrinos are massless at the tree-level. Moreover, because of the presence of only one helicity state of the neutrino per generation, neutrinos cannot have a Dirac mass even at loop level. So the only other possibility is the lepton number violating Majorana mass term. But lepton number is a symmetry of the SM, though accidental, and if that symmetry is to be obeyed, Majorana masses also cannot be generated at loop level. It can also be seen that the Planck scale (M_{Pl}) effect cannot introduce the required neutrino mass in the SM as it can only generate a neutrino mass $\sim \mathcal{O}(v_{EW}^2/M_{\text{Pl}}) \approx \mathcal{O}(10^{-5}\text{eV})$, and hence cannot explain the atmospheric mass squared difference. Hence generally the neutrino masses are incorporated at the tree-level by adding new particles to the SM. The most favored mechanisms

to generate such small neutrino masses are the so called seesaw mechanisms which need the introduction of one or more heavy fields, while maintains the $SU(3)_C \times SU(2)_L \times U(1)_Y$ gauge group structure of the SM.

The low energy effective Lagrangian needed to explain the non-zero neutrino mass can in general be expressed as a series of non-renormalizable operators, the dominant one being the dimension-5 operator given as [31]

$$\mathcal{L} = \kappa_5 l_L l_L \phi \phi , \quad (3)$$

where l_L and ϕ are respectively the lepton and Higgs doublets belonging to the SM. Here κ_5 is the effective coupling which can be expressed in terms of a dimensionless coupling a_5 as $\kappa_5 = a_5/\Lambda$ with Λ some high energy scale. In this picture the SM serves as an effective theory valid up to the mass scale Λ , which can be taken to be the mass of the lightest of the heavy fields. Such an operator violates lepton number by two units and hence gives rise to Majorana masses for neutrinos: $m_\nu \sim \frac{1}{2}\kappa_5 v^2$, where v is the vacuum expectation value of the Higgs field ϕ after spontaneous symmetry breaking. Taking $v \sim 246$ eV, a neutrino mass of ~ 0.05 eV implies $\Lambda \sim 10^{15}$ GeV if $a_5 \sim 1$.

Since the neutrino mass is generated at the high scale while the neutrino masses and mixing parameters are measured experimentally at a low scale, the renormalization group (RG) evolution effects need to be included. The current experimental data in Table 1 shows that in the neutrino sector two of the three mixing angles are large, while the third one is small, which is rather different from the quark sector where all three mixing angles are small. Because of the large values of the two mixing angles, RG evolution of the neutrino masses and the mixing plays an important role in the neutrino sector, which is not the case with the quark sector. RG evolution will be even larger if the neutrinos happen to be quasi-degenerate.

The effect of RG induced quantum corrections on leptonic masses and mixings have been studied extensively in the literature [32, 33, 34, 35, 36, 37]. These effects can have interesting consequences such as the generation of large mixing angles [38, 39, 40, 41, 42, 43, 44], small mass splittings for degenerate neutrinos [45, 46, 47, 48, 49, 50, 51, 52, 53], or radiative generation of θ_{13} starting from a zero value at the high scale [54, 55, 56, 57]. RG induced deviations from various high scale symmetries and correlations with low scale observables have been explored. Such effects can have significant contributions from the threshold

corrections [58, 59, 60]. The RG evolution of the neutrino mass operator in the SM and the Minimal Supersymmetric Standard Model (MSSM) in the context of Type-I seesaw [59, 61, 62] and Type-II seesaw [63, 64] have been studied in the literature. In the context of Type-III seesaw with degenerate heavy fermions, the impact of the RG evolution on the vacuum stability and perturbativity bounds of the Higgs Boson has been explored in [65].

Here we study the RG evolution of the neutrino masses and mixing in the Type-III seesaw with non-degenerate heavy fermions [29] and discuss the salient features through an illustrative example. Then the RG evolution of all these parameters is studied in the effective low energy theory. Analytical expressions for the evolution of these parameters are obtained through an expansion in the small parameter θ_{13} [34, 35]. However, some subtle issues are present when $\theta_{13} = 0$ is reached, either at the high scale or during the evolution. We try to analyze the problem for a better understanding and also present an alternative formalism [57]. Then for the class of neutrino mass models with $\theta_{13} = 0$ at the high scale, we calculate the maximum value of θ_{13} that can be generated through the RG evolution. This gives correlated constraints on θ_{13} and the lightest neutrino mass m_0 , with the SM serving as the low energy effective theory.

S.2 Signature of sterile neutrinos at long baseline experiments

S.2.1 Analytic computation of probabilities

Motivated by the concept of sterile neutrinos important in astrophysics and cosmology, we consider the sterile neutrinos with masses ~ 0.1 eV or higher. With only one sterile species present, the neutrino mixing matrix becomes a 4×4 matrix U_4 , instead of U_{PMNS} defined in Eq. (1.1), and is given as $U_4 = \mathcal{U}_4 \cdot Q_4$ with

$$Q_4 = \text{Diag}(e^{-i\phi_1}, e^{-i\phi_2}, e^{-i\phi_3}, 1), \quad (4)$$

$$\mathcal{U}_4 = U_{14}(\theta_{14}, \delta_{14}) U_{34}(\theta_{34}, 0) U_{24}(\theta_{24}, \delta_{24}) U_{23}(\theta_{23}, 0) U_{13}(\theta_{13}, \delta_{13}) U_{12}(\theta_{12}, 0), \quad (5)$$

where $U_{ij}(\theta_{ij}, \delta_{ij})$ is the complex rotation matrix in the i - j plane and Q_4 is the Majorana phase matrix, which will not contribute to the neutrino oscillations. Here we do not write the “flavor phases” explicitly. The limit when the sterile neutrino is completely decoupled – or when it does not exist – is obtained simply by setting $\theta_{14}, \theta_{24}, \theta_{34} \rightarrow 0$ and $\phi_3 \rightarrow 0$ so that $U_4 \rightarrow U_{\text{PMNS}}$, apart from the unphysical “flavor phase” part.

We expect θ_{14}, θ_{24} and θ_{34} , the mixing angles involving the sterile neutrino, to be small due to the constraints from the short baseline appearance [7, 8, 66, 67] and disappearance [68] experiments. The atmospheric neutrino data restrict the deviation of θ_{23} from maximality to be small [69], and the CHOOZ data [70] combined with solar, atmospheric and KamLAND experiments constrain θ_{13} to be less than 0.2 rad at 3σ C.L. [13, 14, 15]. Hence one can write

$$\theta_{13} \equiv \chi_{13}\lambda, \quad \theta_{23} \equiv \frac{\pi}{4} + \chi_{23}\lambda, \quad \theta_{14} \equiv \chi_{14}\lambda, \quad \theta_{24} \equiv \chi_{24}\lambda, \quad \theta_{34} \equiv \chi_{34}\lambda, \quad (6)$$

where $\lambda \equiv 0.2$ is an auxiliary small parameter and all the χ_{ij} are $\mathcal{O}(1)$ quantities. In the long baseline neutrino experiments of typical energy $E \sim \mathcal{O}(\text{GeV})$, owing to the small value of $\Delta m_{\odot}^2 L / (4E)$, the oscillations due to Δm_{\odot}^2 do not have enough time to develop, and the effect of Δm_{\odot}^2 may be viewed as a perturbation to the dominating Δm_{atm}^2 oscillations. Hence we can define

$$\Delta m_{21}^2 / \Delta m_{32}^2 \equiv \eta \lambda^2. \quad (7)$$

Note that η is positive (negative) for the normal (inverted) neutrino mass ordering.

When neutrinos pass through the earth matter, there are matter effects that give rise to an effective potential $V_e = \sqrt{2}G_F N_e$ for the electron neutrino as compared to the other neutrinos by virtue of the its charged current forward scattering interactions. Here G_F is the Fermi constant and N_e is the number density of electrons. In addition, all the active neutrinos also get an effective potential $V_n = -G_F N_n / \sqrt{2}$ compared to the sterile neutrino by virtue of their neutral current forward scattering reactions. Here N_n is the number density of neutrons. For anti-neutrinos, the signs of V_e and V_n are reversed. The effective

Hamiltonian in the flavor basis is then

$$H_f \approx \frac{1}{2E} \left[\mathcal{U}_0 \begin{pmatrix} -\Delta m_{21}^2 & 0 & 0 & 0 \\ 0 & 0 & 0 & 0 \\ 0 & 0 & \Delta m_{32}^2 & 0 \\ 0 & 0 & 0 & \Delta m_{42}^2 \end{pmatrix} \mathcal{U}_0^\dagger + \begin{pmatrix} A_e + A_n & 0 & 0 & 0 \\ 0 & A_n & 0 & 0 \\ 0 & 0 & A_n & 0 \\ 0 & 0 & 0 & 0 \end{pmatrix} \right], \quad (8)$$

where $A_{e(n)} \equiv 2EV_{e(n)}$, and \mathcal{U}_0 is the mixing matrix in vacuum, whose form is given in Eq. (2.2). Let H_f be diagonalized by a unitary matrix \mathcal{U}_m to give the diagonal matrix H_D . If we assume that the density encountered by the neutrinos during their passage through the earth is a constant, the flavor conversion probabilities may be written as

$$P_{\alpha\beta} \equiv P(\nu_\alpha \rightarrow \nu_\beta) = \left| \sum_i [\mathcal{U}_m]_{\alpha i} [\mathcal{U}_m]_{\beta i}^* \exp \left[i \frac{(-\tilde{m}_i^2)L}{2E} \right] \right|^2, \quad (9)$$

where \tilde{m}_i are the effective masses of the interaction eigenstates in matter. This approximation is valid as long as the neutrino trajectories do not pass through the core, and the neutrino energy is not close to the θ_{13} resonance energy in the earth.

It can be checked that the Rayleigh-Schrödinger perturbation theory in the small parameter λ can be used in this framework to calculate \tilde{m}_i and \mathcal{U}_m , correct up to any required order in λ . Here we will calculate the probabilities accurate up to $\mathcal{O}(\lambda^2)$. The neutrino flavor conversion (or survival) probabilities for an initial ν_μ , correct up to $\mathcal{O}(\lambda^2)$, may be written as

$$P_{\mu e} \approx 2\theta_{13}^2 \Delta_{32}^2 \frac{\sin^2(\Delta_e - \Delta_{32})}{(\Delta_e - \Delta_{32})^2} + \mathcal{O}(\lambda^3), \quad (10)$$

$$\begin{aligned} P_{\mu\mu} \approx & \cos^2 \Delta_{32} + 4\tilde{\theta}_{23}^2 \sin^2 \Delta_{32} - \Delta_{21} \sin^2 \theta_{12} \sin 2\Delta_{32} \\ & + \frac{\theta_{13}^2 \Delta_{32}}{(\Delta_e - \Delta_{32})^2} \{ +\Delta_e(\Delta_e - \Delta_{32}) \sin 2\Delta_{32} \\ & - 2\Delta_{32} \cos \Delta_{32} \sin \Delta_e \sin(\Delta_e - \Delta_{32}) \} \\ & - 2\theta_{24}^2 \cos^2 \Delta_{32} + 2\theta_{24}\theta_{34}\Delta_n \cos \delta_{24} \sin 2\Delta_{32} + \mathcal{O}(\lambda^3), \end{aligned} \quad (11)$$

$$\begin{aligned} P_{\mu\tau} \approx & \sin^2 \Delta_{32} - 4\tilde{\theta}_{23}^2 \sin^2 \Delta_{32} + \Delta_{21} \sin^2 \theta_{12} \sin 2\Delta_{32} \\ & + \frac{\theta_{13}^2 \Delta_{32}}{(\Delta_e - \Delta_{32})^2} \{ -\Delta_e(\Delta_e - \Delta_{32}) \sin 2\Delta_{32} \\ & 2\Delta_{32} \sin \Delta_{32} \cos \Delta_e \sin(\Delta_e - \Delta_{32}) \} - (\theta_{24}^2 + \theta_{34}^2) \sin^2 \Delta_{32} \\ & - \theta_{24}\theta_{34} (2\Delta_n \cos \delta_{24} + \sin \delta_{24}) \sin 2\Delta_{32} + \mathcal{O}(\lambda^3), \end{aligned} \quad (12)$$

where we have defined the dimensionless quantities $\Delta_{ij} \equiv \Delta m_{ij}^2 L / (4E)$ and $\Delta_{e,n} \equiv A_{e,n} L / (4E)$ for convenience. To arrive at these simple expressions for the probabilities given in Eqs. (2.15)–(2.17), which also provide with important physical insights, we have used the following approximations. We assumed that the neutrinos travelled through a constant matter density and then (taking the density of the Earth mantle ~ 5 gm/cc) $|A_{e,n}| \ll |\Delta m_{42}^2|$ through out the energy range 1 – 50 GeV. Also since $|\Delta m_{32}^2| \ll |\Delta m_{42}^2|$ and $|\Delta m_{32}^2 L / E| \sim \mathcal{O}(1)$, for the experimental set-ups under consideration we have $|\Delta m_{42}^2 L / E| \gg 1$ and the oscillating terms of the form $\cos(\Delta m_{42}^2 L / E)$ may be averaged out. However, these analytic expressions are not expected to be valid in the θ_{13} resonance region where $\Delta_e \approx \Delta_{32}$, or for large L/E where Δ_{21} would become $\mathcal{O}(\lambda)$ and higher order terms in Δ_{21} are to be taken into account. The validity and limitations of these approximations have been checked with the exact numerical simulations. Probabilities for the antiparticles are obtained simply by replacing $\Delta_{e,n} \rightarrow -\Delta_{e,n}$ and $\delta_{ij} \rightarrow -\delta_{ij}$. As can be seen, only one CP violating phase δ_{24} contributes to the CP violation in these channels up to $\mathcal{O}(\lambda^2)$.

For an initial ν_e beam, the relevant neutrino flavor conversion probabilities are

$$P_{ee} \approx 1 - 4\theta_{13}^2 \Delta_{32}^2 \frac{\sin^2(\Delta_e - \Delta_{32})}{(\Delta_e - \Delta_{32})^2} - 2\theta_{14}^2 + \mathcal{O}(\lambda^3), \quad (13)$$

$$P_{e\mu} \approx P_{e\tau} \approx 2\theta_{13}^2 \Delta_{32}^2 \frac{\sin^2(\Delta_e - \Delta_{32})}{(\Delta_e - \Delta_{32})^2} + \mathcal{O}(\lambda^3), \quad (14)$$

where we have used the same approximations as above. Thus only P_{ee} bears the signature of the sterile neutrino at this order and the contribution is CP conserving.

S.2.2 Signatures at long baseline experiments

In order to demonstrate the capability of future long baseline experiments in distinguishing the sterile neutrino contribution to the neutrino flavor conversion probabilities, we choose a typical neutrino factory setup [71], with a 0.5 kt “near” detector 1 km away and a 50 kt “far” detector 7000 km away, with the charge identification capability. We implement the propagation of the neutrinos through the earth using the PREM profile [72] and take care of the detector characteristics using the General Long Baseline Experiment

Simulator (GLOBES) [73, 74]. The energy range is chosen to be 10–50 GeV, where the analytic expressions are valid for the chosen baseline of 7000 km.

We study the asymmetries $\mathcal{A}_{\mu(\tau)}(E)$ and the integrated asymmetries $\tilde{\mathcal{A}}_{\mu(\tau)}$ defined as

$$\begin{aligned}\mathcal{A}_{\mu(\tau)}(E) &\equiv \frac{N_{\mu(\tau)}^{\text{far}}(E)}{N_{\mu}^{\text{near}}(E)} - \frac{\overline{N}_{\mu(\tau)}^{\text{far}}(E)}{\overline{N}_{\mu}^{\text{near}}(E)}, \\ \tilde{\mathcal{A}}_{\mu(\tau)}(E) &\equiv \frac{N_{\mu(\tau)}^{\text{far}}(E > 15\text{GeV})}{N_{\mu}^{\text{near}}(E > 15\text{GeV})} - \frac{\overline{N}_{\mu(\tau)}^{\text{far}}(E > 15\text{GeV})}{\overline{N}_{\mu}^{\text{near}}(E > 15\text{GeV})},\end{aligned}\quad (15)$$

where N_{ℓ} (\overline{N}_{ℓ}) is the number of ℓ^- (ℓ^+) observed at the near or far detector. Here the events observed in the near detector act as a normalizing factor, and help in canceling out the systematic errors due to fluxes, cross sections and efficiencies in each energy bin. It is found that for $\theta_{24}\theta_{34} \gtrsim 0.005$, the sterile contribution to neutrino conversions can be discernible from the three neutrino mixing results at 3σ C.L. in the worst case scenario. If the value of θ_{13} is bounded further, the reach of neutrino factories for the sterile mixing is enhanced. In addition, the actual value of θ_{13} also affects the discovery potential of sterile mixing. Since the asymmetries depend on the sign of Δm_{32}^2 , sterile mixing can also distinguish between the two mass orderings.

If we have a 50 kt detector that can detect e^-/e^+ and identify their charge, we can use the observable $\mathcal{R}_e(E)$ and integrated quantity $\tilde{\mathcal{R}}_e$

$$\mathcal{R}_e(E) \equiv \frac{N_e^{\text{far}}(E)}{N_e^{\text{near}}(E)}, \quad \tilde{\mathcal{R}}_e \equiv \frac{N_e^{\text{far}}(E > 25\text{GeV})}{N_e^{\text{near}}(E > 25\text{GeV})}, \quad (16)$$

for detecting the sterile neutrino contribution. In this case for $\theta_{14} \gtrsim 0.06$, the sterile mixing signals can be clearly discerned at 3σ C.L. in worst case scenario. If the bound on θ_{13} becomes stronger, even smaller values of θ_{14} may be identified, while a higher actual value of θ_{13} helps in the identification of sterile mixing even at lower θ_{14} . No difference between the two hierarchies, or between ν_e and $\bar{\nu}_e$, is expected.

S.2.3 Generalization to any number of sterile neutrinos

Currently it has been proposed that two or more sterile neutrinos with $\Delta m_{j1}^2 \sim 1$ eV ($j > 3$) and $|\mathcal{U}_{ej}\mathcal{U}_{\mu j}| \sim \mathcal{O}(0.01\text{--}0.1)$ are consistent with all data [18]. It is

therefore desirable to extend our formalism to more than one sterile neutrinos. The analytical treatment in Sec. S.2.1 for the case of one sterile neutrino may be generalized easily to any arbitrary number n of sterile neutrinos. The $(3+n) \times (3+n)$ mixing matrix \mathcal{U}_{3+n} may be written in the block form as

$$\begin{aligned} \mathcal{U}_{3+n} &\equiv \begin{pmatrix} [U^{AA}]_{3 \times 3} & [U^{AS}]_{3 \times n} \\ [U^{SA}]_{n \times 3} & [U^{SS}]_{n \times n} \end{pmatrix} \equiv \mathcal{W} \cdot \mathcal{V} \\ &\equiv \begin{pmatrix} [W^{AA}]_{3 \times 3} & [W^{AS}]_{3 \times n} \\ [W^{SA}]_{n \times 3} & [W^{SS}]_{n \times n} \end{pmatrix} \begin{pmatrix} [V^{AA}]_{3 \times 3} & [0]_{3 \times n} \\ [0]_{n \times 3} & [V^{SS}]_{n \times n} \end{pmatrix}, \end{aligned} \quad (17)$$

where V^{AA} is the standard mixing matrix for three active neutrino flavors, and V^{SS} is the matrix that mixes the n sterile neutrinos among themselves and hence can be chosen to be identity matrix. The matrix \mathcal{W} parametrizes the mixing between active and sterile states. In addition, we assume that all the active-sterile mixing is small [18]. This allows us to write $W^{AS} \equiv \lambda X^{AS}$. Up to $\mathcal{O}(\lambda^2)$, the unitary matrix \mathcal{W} may be written in its most general form as

$$\mathcal{W} = \begin{pmatrix} \left[I - \lambda^2 \frac{X^{AS}(X^{AS})^\dagger}{2} \right]_{3 \times 3} & [\lambda X^{AS}]_{3 \times n} \\ [-\lambda (X^{AS})^\dagger]_{n \times 3} & \left[I - \lambda^2 \frac{(X^{AS})^\dagger X^{AS}}{2} \right]_{n \times n} \end{pmatrix} + \mathcal{O}(\lambda^3). \quad (18)$$

Finally using the same approximations and assumptions as in Sec. S.2.1, the sterile contribution to the CP violation up to $\mathcal{O}(\lambda^2)$ becomes

$$P_{\mu\mu} - P_{\bar{\mu}\bar{\mu}} \approx (P_{\mu\mu} - P_{\bar{\mu}\bar{\mu}})_{3\nu} + 4\text{Re}[W^{\tau S}(W^{\mu S})^\dagger] \Delta_n \sin 2\Delta_{32}, \quad (19)$$

$$\begin{aligned} P_{\mu\tau} - P_{\bar{\mu}\bar{\tau}} &\approx (P_{\mu\tau} - P_{\bar{\mu}\bar{\tau}})_{3\nu} - 4\text{Re}[W^{\tau S}(W^{\mu S})^\dagger] \Delta_n \sin 2\Delta_{32} \\ &\quad - 2\text{Im}[W^{\tau S}(W^{\mu S})^\dagger] \sin 2\Delta_{32}, \end{aligned} \quad (20)$$

for an incident ν_μ beam, while the only sterile neutrino contribution is in P_{ee} for an incident ν_e beam, as before, and is given by

$$P_{ee} \approx 1 - 4\theta_{13}^2 \Delta_{32}^2 \frac{\sin^2(\Delta_e - \Delta_{32})}{(\Delta_e - \Delta_{32})^2} - 2[W^{eS}(W^{eS})^\dagger] + \mathcal{O}(\lambda^3). \quad (21)$$

As a result, the bounds obtained on $\theta_{14}, \theta_{24}, \theta_{34}$ and δ_{24} in the 4-neutrino analysis can be directly translated to bounds on the combinations $[W^{eS}(W^{eS})^\dagger]$, $[W^{\mu S}(W^{\mu S})^\dagger]$, $[W^{\tau S}(W^{\tau S})^\dagger]$ as well as the real and the imaginary parts of $[W^{\tau S}(W^{\mu S})^\dagger]$.

S.3 RG evolution: Type-III seesaw scenario

S.3.1 The Type-III seesaw model and the effective low energy theory

In Type-III seesaw model three heavy fermions are added to each family of the SM. These fermions have zero weak hypercharge. However, under the $SU(2)_L$ gauge, they transform as a triplet in the adjoint representation. For the sake of simplicity, we define the quantity $\Sigma \equiv \Sigma_R + \Sigma_R^C$, where Σ_R is the $SU(2)_L$ triplet given as

$$\Sigma_R \equiv \begin{pmatrix} \Sigma_R^0/\sqrt{2} & \Sigma_R^+ \\ \Sigma_R^- & -\Sigma_R^0/\sqrt{2} \end{pmatrix}, \quad (22)$$

and Σ_R^C is the CP conjugate field. Clearly, Σ also transforms in the adjoint representation of $SU(2)_L$. Note that though formally $\Sigma = \Sigma^C$, the individual elements of Σ are not all Majorana particles. The neutral components are indeed Majorana spinors, while the others are charged Dirac spinors.

Introduction of the fermionic triplets Σ introduce new terms in the Lagrangian to give

$$\mathcal{L} = \mathcal{L}_{SM} + \mathcal{L}_\Sigma, \quad (23)$$

$$\mathcal{L}_\Sigma = \mathcal{L}_{\Sigma,kin} + \mathcal{L}_{\Sigma,mass} + \mathcal{L}_{\Sigma,Yukawa}, \quad (24)$$

with

$$\begin{aligned} \mathcal{L}_{\Sigma,kin} &= \text{Tr}[\bar{\Sigma} i \not{D} \Sigma], \\ \mathcal{L}_{\Sigma,mass} &= -\frac{1}{2} \text{Tr}[\bar{\Sigma} \mathbb{M}_\Sigma \Sigma], \\ \mathcal{L}_{\Sigma,Yukawa} &= -\bar{l}_L \sqrt{2} Y_\Sigma^\dagger \Sigma \tilde{\phi} + \text{h.c.} . \end{aligned} \quad (25)$$

Here ε is the completely anti-symmetric tensor in the $SU(2)_L$ space. \mathbb{M}_Σ is the Majorana mass matrix of the heavy fermion triplets and Y_Σ is the Yukawa coupling. The covariant derivative of the triplet Σ is defined as $D_\mu \Sigma = \partial_\mu \Sigma + ig_2 [W_\mu, \Sigma]$, where g_2 is the $SU(2)_L$ gauge coupling.

In the low energy limit of the extended SM, we have an effective theory which will be described by the SM Lagrangian with the additional operators obtained

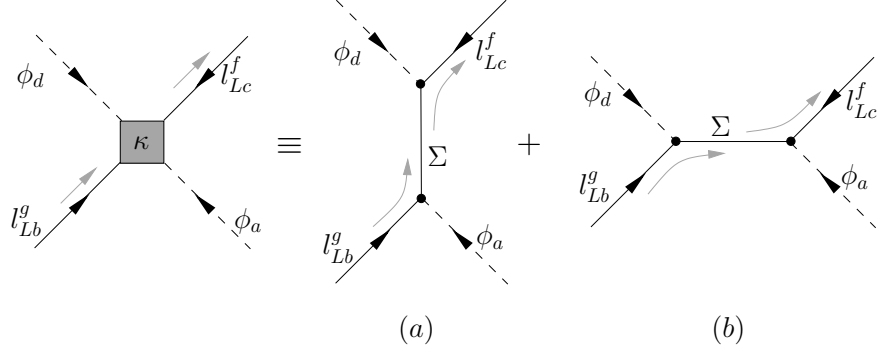


Figure 1: The effective vertex κ at an energy $\mu \ll M_1$, after all the heavy fermions have been decoupled from the theory. $f, g \in \{1, 2, 3\}$ are the generation indices. The $SU(2)_L$ and generation indices for Σ are not shown explicitly since they are summed over.

by integrating out the heavy fermion triplets added at high scale. The lowest dimensional one of such operators is the dimension-5 operator

$$\mathcal{L}_\kappa = \kappa_{fg} \left(\overline{l}_L^C \sigma^i \varepsilon \phi \right) \left(\phi^T \sigma^i \varepsilon l_L^g \right) + \text{h.c.} , \quad (26)$$

where κ is a complex symmetric matrix with mass dimension (-1). Generation indices $f, g \in \{1, 2, 3\}$ are shown explicitly and $a, b, c, d \in \{1, 2\}$ are the $SU(2)_L$ indices.

The relevant diagrams in the complete theory giving rise to the effective operators in the low energy limit are shown in Fig 1. The “shaded box” on the left hand side represents the effective low energy vertex κ , and the equality in the figure is obtained with the identification

$$\kappa = 2Y_\Sigma^T M_\Sigma^{-1} Y_\Sigma . \quad (27)$$

S.3.2 Radiative corrections in Type-III seesaw

Sequential decoupling of heavy fermions

Let us consider the most general case when there are r triplets having masses $M_1 < M_2 < \dots < M_{r-1} < M_r$. Above the heaviest mass M_r , all the r -triplets are coupled to the theory and will contribute to the neutrino mass through seesaw mechanism. Below the lowest mass M_1 , all the heavy triplets will get

decoupled and will contribute through the effective low energy operator. In between, in the energy range $M_n > \mu > M_{n-1}$, triplets with masses M_n – M_r are already decoupled, while the lighter triplets with masses M_1 – M_{n-1} are still coupled and the effective mass of the neutrinos will be given as

$$\mathbb{m}_\nu^{(n)} = -\frac{v^2}{4} \left(\mathcal{K}^{(n)} + 2Q^{(n)} \right), \quad (28)$$

where $Q \equiv Y_\Sigma^T \mathbb{M}_\Sigma^{-1} Y_\Sigma$. Here $Y_\Sigma^{(n)}$ is the Yukawa matrix for the coupled triplets. Appropriate matching condition is to be applied at the threshold $\mu = M_{n-1}$.

Dimensional regularization and renormalization: The β -functions

We use the dimensional regularization and the minimal subtraction scheme for renormalization. However, the final results will be independent of the particular regularization as well as the renormalization scheme used for the calculations. All the calculations are done in the general renormalizable R_ξ gauge, and the GUT normalization of the gauge couplings has been used [32]. Finally, functional differentiation method as in [75] is used to find the β functions.

Since the fermion triplets have non-zero $SU(2)_L$ charge, they will affect the RG evolution of the gauge coupling g_2 via $16\pi^2\beta_{g_2} = b_2 g_2^3$, where $b_2 = -19/6 + 4(n-1)/3$, showing that the sign of b_2 changes for $n \geq 3$. Also, one can check that addition of fermion triplets shifts the g_1 - g_2 intersection to higher energy scales, and the g_2 - g_3 intersection to lower energy scales, as can be seen from Fig. 2 and thus can facilitate gauge coupling unification.

The running equations of the Yukawa couplings Y_e and Y_Σ are given as

$$16\pi^2\beta_{Y_e} = Y_e \left(\frac{3}{2} Y_e^\dagger Y_e + \frac{15}{2} Y_\Sigma^\dagger Y_\Sigma + T - \frac{9}{4} g_1^2 - \frac{9}{4} g_2^2 \right), \quad (29)$$

$$16\pi^2\beta_{Y_\Sigma} = Y_\Sigma \left(\frac{5}{2} Y_e^\dagger Y_e + \frac{5}{2} Y_\Sigma^\dagger Y_\Sigma + T - \frac{9}{20} g_1^2 - \frac{33}{4} g_2^2 \right), \quad (30)$$

where $T = \text{Tr} \left[Y_e^\dagger Y_e + 3Y_\Sigma^\dagger Y_\Sigma + Y_u^\dagger Y_u + Y_d^\dagger Y_d \right]$.

Separating the components of different chirality, the running of the Majorana

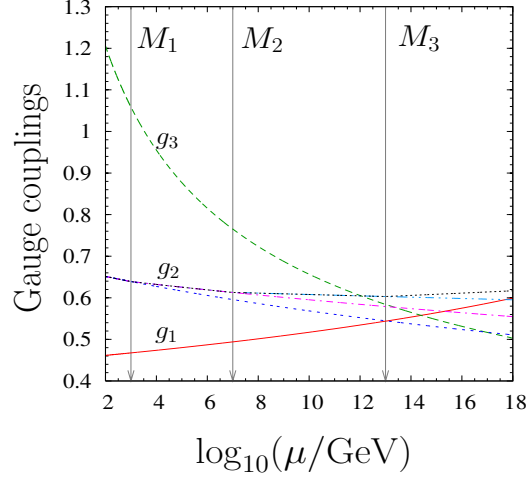


Figure 2: The solid (red) line and the dashed (green) lines show the energy scale variations of g_1 and g_3 respectively in the SM, which is unaffected in Type-III seesaw. The dotted (blue) line gives the SM running of g_2 , while dot-dashed (magenta), dot-dot-dashed (sky) and densely dotted (black) lines show the running if there were one, two or three fermion triplets respectively.

mass matrix is obtained to be

$$16\pi^2\beta_{\mathbb{M}_\Sigma} = \begin{pmatrix} (n) & (n)_i \\ Y_\Sigma & Y_\Sigma^\dagger \end{pmatrix} \mathbb{M}_\Sigma + \mathbb{M}_\Sigma \begin{pmatrix} (n) & (n)_i \\ Y_\Sigma & Y_\Sigma^\dagger \end{pmatrix}^T - 12g_2^2\mathbb{M}_\Sigma. \quad (31)$$

The gauge coupling term produces a large running of \mathbb{M}_Σ , a distinctive feature of Type-III seesaw over Type-I.

As seen from Eq. (3.36), the RG evolution of the light neutrino mass matrix $\mathbb{m}_\nu^{(n)}$ is controlled by the evolutions of both $\kappa^{(n)}$ and $Q^{(n)}$, which are given by

$$16\pi^2\beta_x = \alpha_x^{(n)} x + P_x^T x + x P_x, \quad (32)$$

with $x = \kappa, Q$ and P_x, α_x are functions of $Y_\Sigma^{(n)}, Y_e, T, \lambda, g_1$ and g_2 in general. We have calculated P_x, α_x explicitly and obtained them to be

$$P_\kappa = \frac{3}{2}Y_\Sigma^\dagger Y_\Sigma - \frac{3}{2}Y_e^\dagger Y_e \quad ; \quad \alpha_\kappa = 2T + \lambda - 3g_2^2, \quad (33)$$

$$P_Q = \frac{3}{2}Y_\Sigma^\dagger Y_\Sigma + \frac{5}{2}Y_e^\dagger Y_e \quad ; \quad \alpha_Q = 2T - \frac{9}{10}g_1^2 - \frac{9}{2}g_2^2. \quad (34)$$

S.3.3 RG evolution of neutrino masses and mixing angles: Illustrative example

Using the beta-functions given in Eqs. (3.58), (3.59) and (32), we determine the running of the neutrino masses, mixing angles and phases, using a procedure similar to that in [34, 61]. In a basis where Y_e is diagonal, $U_{\text{PMNS}} = U_\nu$ with U_{PMNS} defined in Eq. (1.1). A subtle point is that even if we start with a diagonal Y_e at the high scale, the $Y_\Sigma^\dagger Y_\Sigma$ term in Eq. (3.58) will generate off-diagonal terms and the neutrino mixing matrix will be given as $U_{\text{PMNS}} = U_e^\dagger U_\nu$, where U_e is the unitary matrix that diagonalizes $Y_e^\dagger Y_e$ by a unitary transformation.

We numerically calculate the RG running for some typical parameter values, including the impact of running between the thresholds. We consider three triplets to be present with masses $M_1 < M_2 < M_3$. In Fig. 3.5, we illustrate the RG evolution of parameters when the neutrino masses are quasi-degenerate. From the top left panel it is observed that the running of θ_{23} , θ_{13} is substantial between the thresholds. It should be noted that though the running of θ_{12} , being proportional to $1/\Delta m_\odot^2$, is expected to be large, in this case θ_{12} running is quite small owing to the special choice of Majorana phases $|\phi_2 - \phi_1| \sim 90^\circ$ for the quasi-degenerate neutrinos. It illustrates that Majorana phases play an important role in the RG evolution of neutrino parameters. The Dirac phase, which was chosen to vanish at μ_0 , is generated by the RG evolution. The running of Dirac as well as Majorana phases is thus also substantial between the thresholds, as can be seen from the top right panel. The right hand bottom panel of Fig. 3.5 shows the evolution of $m_\beta \equiv \sqrt{\sum_i |U_{ei}|^2 m_i^2}$, the effective neutrino mass measured in the Tritium beta decay experiments [17], as well as $m_{ee} \equiv |\sum_i U_{ei}^2 m_i|$, the effective neutrino Majorana mass in the neutrinoless double beta decay. The large running of these masses suggests that, even if the beta decay experiments were to bound m_β to ≤ 0.3 eV, or the neutrinoless double beta decay experiments were to bound m_{ee} to ≤ 0.1 eV, the value of m_0 generated at the high scale can still be substantially larger.

As can be observed, the running of masses is quite substantial in Type-III seesaw. It has also been checked that the values of m_0 required to cause substantial running of mixing angles may be quite small. The Majorana phases also play an important role in determining the nature of running of the different parameters. However the exact dependence on the value of m_0 , mass thresholds

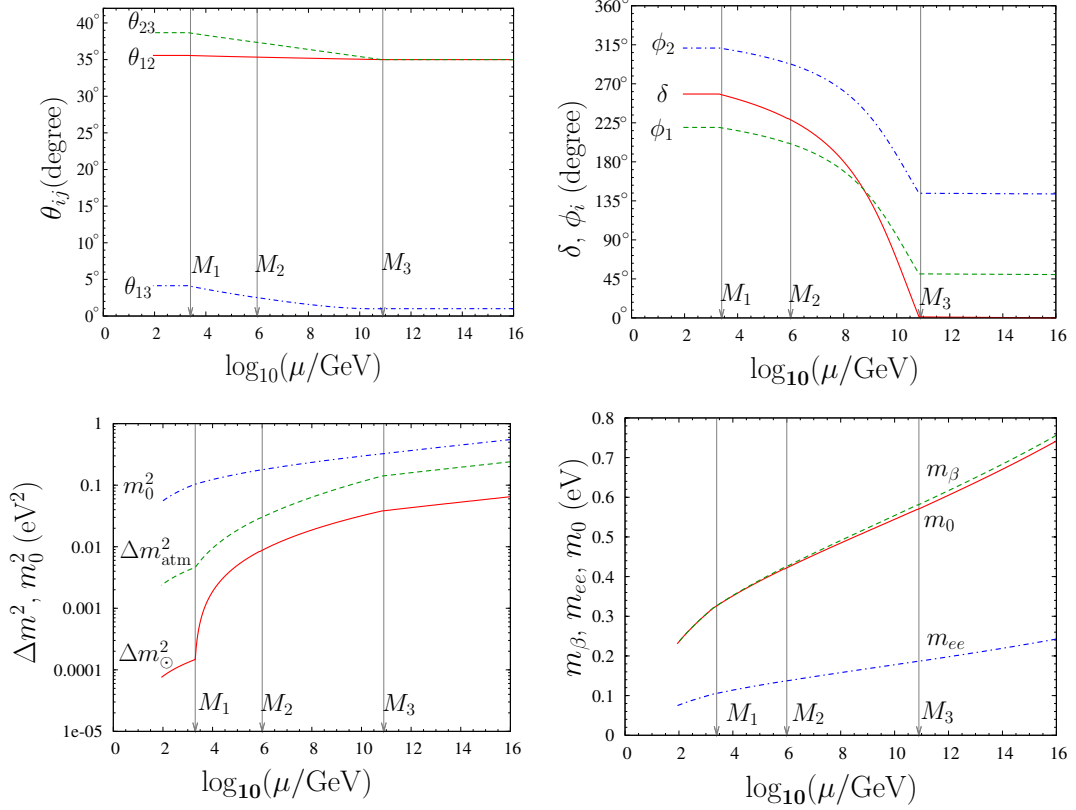


Figure 3: RG evolution of mixing angles, mass squared differences, and CP violating phases, for quasi-degenerate neutrino masses and normal mass ordering. The values of parameters at the high scale have been chosen such that the Δm^2 's and g_2 at the low scale are reproduced. Note that for the Majorana phases ϕ_i , the regions $(0^\circ - 180^\circ)$ and $(180^\circ - 360^\circ)$ should be identified with each other.

and CP violating phases needs to be studied in further detail for a better understanding of the allowed neutrino parameter space at high energies.

S.4 RG evolution of neutrino mixing: The subtlety at $\theta_{13} = 0$

S.4.1 Apparent singularity in δ and evolution in the complex \mathcal{U}_{e3} plane

When one writes down the analytic expressions for the evolution equations for the neutrino masses, mixing angles and phases, it is seen that for a quantity

$X \in \{m_i, \theta_{ij}, \phi_i\}$, the evolution can be written as

$$\dot{X} = A_X + \mathcal{O}(\theta_{13}), \quad (35)$$

where dot represents the derivative with respect to $t \equiv \ln(\mu/GeV)/(16\pi^2)$. Here A_X is independent of θ_{13} , but is a function of $m_i, \theta_{12}, \theta_{23}, \phi_i$ in general, while only A_{13} depends on δ also. The evolution of δ formally takes the form

$$\dot{\delta} = \frac{D_\delta}{\theta_{13}} + A_\delta + \mathcal{O}(\theta_{13}), \quad (36)$$

and thus the derivative of δ formally diverges at vanishing θ_{13} , indicating an apparent singularity. This is an unphysical singularity: all the elements of the mixing matrix U_{PMNS} evolve continuously, and the peculiar evolution of δ is related to the fact that δ is undefined at $\theta_{13} = 0$. This argument is in fact used in [34, 35] to assert that D_δ identically vanishes when $\theta_{13} = 0$, which in the effective theory leads to the condition

$$\cot \delta = \frac{m_1 \cos 2\phi_1 - (1 + \zeta)m_2 \cos 2\phi_2 - \zeta m_3}{m_1 \sin 2\phi_1 - (1 + \zeta)m_2 \sin 2\phi_2}, \quad (37)$$

where $\zeta = \Delta m_\odot^2/\Delta m_{\text{atm}}^2$. While this prescription for choosing δ at $\theta_{13} = 0$ works practically when one starts with vanishing θ_{13} , a few conceptual problems remain. First, when $\theta_{13} = 0$, the value of δ chosen should not make a difference to the RG evolution since δ is an unphysical quantity at this point. Secondly, it is not *a priori* clear whether the prescription would work when $\theta_{13} = 0$ is reached during the process of RG evolution, which seems like fine tuning. The problem also propagates to the evolution of θ_{13} , since it depends in turn on δ . The evolution of all the other quantities, *viz.* $\theta_{12}, \theta_{23}, m_i, \phi_i$ is independent of δ up to $\mathcal{O}(\theta_{13}^0)$ [34, 35], so these quantities do not concern us here.

In order to understand the nature of the apparent singularity in δ , we explore the RG evolution of the complex quantity $\mathcal{U}_{e3} = \sin \theta_{13} e^{-i\delta}$. We start with three representative values of δ at the energy scale $\mu_0 = 10^{12}$ GeV, with the other parameters chosen such that $\theta_{13} \lesssim 10^{-3}$ at $\mu \approx 10^9$ GeV. The left panel of Fig. 4.1 shows the evolution in the complex \mathcal{U}_{e3} plane. It is seen that fine tuning is needed to reach $\theta_{13} = 0$. But as the limit is reached, the value of δ

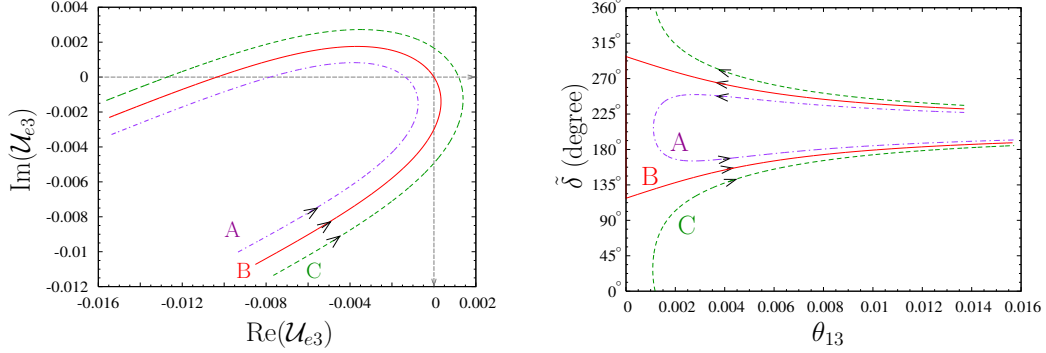


Figure 4: The left panel shows the evolution in the $\text{Re}(\mathcal{U}_{e3})$ – $\text{Im}(\mathcal{U}_{e3})$ parameter plane, whereas the right panel shows the corresponding evolution in the θ_{13} – $\tilde{\delta}$ plane. The values of the parameters chosen at $\mu_0 = 10^{12}$ GeV are: $\tan \beta = 50$, $m_0 = 0.0585$ eV², $\Delta m_{\odot}^2 = 4.22 \times 10^{-5}$ eV², $\Delta m_{\text{atm}}^2 = 3.91 \times 10^{-3}$ eV², $\theta_{12} = 32.84^\circ$, $\theta_{23} = 43.71^\circ$ and $\theta_{13} = 0.014$ rad. The Majorana phases are taken to be $\phi_1 = 58.9^\circ$ and $\phi_2 = 159.15^\circ$. The Dirac CP phase is 124.0° for case A (violet, dash-dotted line), 128.447° for case B (red, solid line) and 133.0° for case C (green, dashed line).

at the origin is well-defined by

$$\begin{aligned} \cot \tilde{\delta}_0 &\equiv \lim_{\substack{\text{Re}(\mathcal{U}_{e3}) \rightarrow 0 \\ \text{Im}(\mathcal{U}_{e3}) \rightarrow 0}} \frac{\text{Re}(\mathcal{U}_{e3})}{\text{Im}(\mathcal{U}_{e3})} = \lim_{\substack{\text{Re}(\mathcal{U}_{e3}) \rightarrow 0 \\ \text{Im}(\mathcal{U}_{e3}) \rightarrow 0}} \frac{\frac{d}{dt} \text{Re}(\mathcal{U}_{e3})}{\frac{d}{dt} \text{Im}(\mathcal{U}_{e3})} \\ &= -\frac{m_1 \cos 2\phi_1 - (1 + \zeta)m_2 \cos 2\phi_2 - \zeta m_3}{m_1 \sin 2\phi_1 - (1 + \zeta)m_2 \sin 2\phi_2}, \end{aligned} \quad (38)$$

where $\tilde{\delta} \equiv 2\pi - \delta$ and we have used L'Hospital's rule to compute the limit. This gives the value of $\cot \delta_0$ which is the same as that prescribed in [34, 35].

S.4.2 RG running in the new basis \mathcal{P}_J

The net evolution of θ_{13} and δ as functions of the energy scale is shown in the top panels of Fig. 4.2. Though the origin of the discontinuity in δ in the scenario B is well-understood now, it is important to have a clear evolution of parameters that reflect the continuous nature of the evolution of elements of U_{PMNS} . The evolutions of $(\text{Re}(\mathcal{U}_{e3}), \text{Im}(\mathcal{U}_{e3}))$ and $(J_{\text{CP}}, J'_{\text{CP}})$ are shown in the

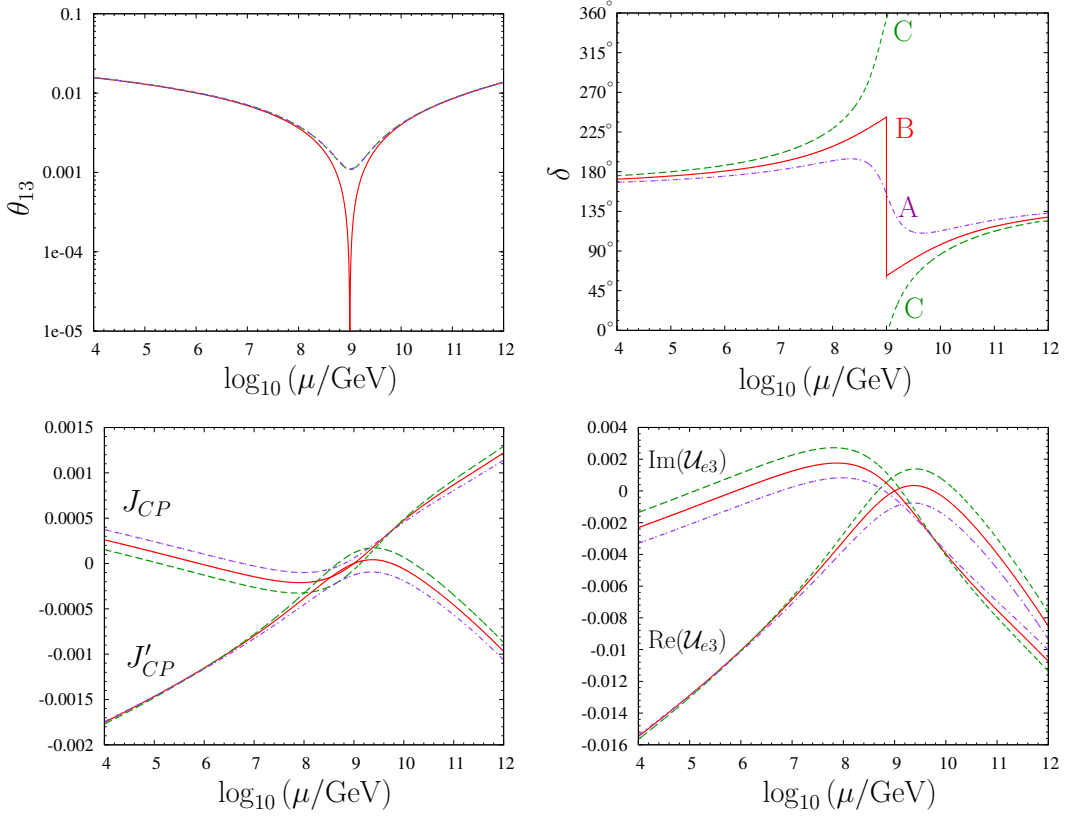


Figure 5: The evolution of θ_{13} , δ , $\text{Re}(\mathcal{U}_{e3})$, $\text{Im}(\mathcal{U}_{e3})$, J_{CP} and J'_{CP} as functions of the energy scale μ , in the scenarios A (violet, dash-dotted line), B (red, solid line) and C (green, dashed line).

bottom panels of Fig. 4.2, where the quantities J_{CP} , J'_{CP} are defined as

$$J_{CP} \equiv \frac{1}{2} \sin \theta_{12} \cos \theta_{12} \sin \theta_{23} \cos \theta_{23} \sin \theta_{13} \cos^2 \theta_{13} \sin \delta, \quad (39)$$

$$J'_{CP} \equiv \frac{1}{2} \sin \theta_{12} \cos \theta_{12} \sin \theta_{23} \cos \theta_{23} \sin \theta_{13} \cos^2 \theta_{13} \cos \delta. \quad (40)$$

As can be seen, the evolutions of (J_{CP}, J'_{CP}) are very similar to those of $(\text{Re}(\mathcal{U}_{e3}), \text{Im}(\mathcal{U}_{e3}))$ and more importantly are continuous at every point including $\theta_{13} \rightarrow 0$. Calculations show that the RG evolution equations for (J_{CP}, J'_{CP}) can be written in the same form as in Eq. (35), with A_X being a function of θ_{12} , θ_{23} , m_i , ϕ_i , J_{CP} , J'_{CP} and independent of δ . We also choose to write the RG evolution for θ_{13}^2 instead of θ_{13} and this quantity turns out to have a nonsingular behavior at $\theta_{13} = 0$. Since $\theta_{13} \geq 0$ by convention, the complete information about θ_{13} lies within θ_{13}^2 .

Thus the evolution equations in basis $\mathcal{P}_J \equiv \{m_i, \theta_{12}, \theta_{23}, \theta_{13}^2, \phi_i, J_{\text{CP}}, J'_{\text{CP}}\}$ are all non-singular and continuous at every point. The agreement between the evolutions of the different parameters in the two bases (up to $\mathcal{O}(\theta_{13})$) has also been checked against the exact numerical running [57].

S.4.3 Bounds on θ_{13} at low scale

We consider all the theories that predict $\theta_{13} = 0$ at the high scale $\mu_0 = 10^{12}$ GeV and consider the SM to be the low energy effective theory. The values of the other parameters at high energy are chosen such that their low scale values are compatible with experiments. Then the maximum value that θ_{13} can gain through radiative corrections can be estimated as

$$\begin{aligned} \theta_{13} &\equiv \left| \int_{t_0}^t A_{13} dt + \mathcal{O}(\theta_{13}) \right| & (41) \\ &\approx \frac{|C| \Delta_\tau m_3}{2|\Delta m_{31}^2|} \sin 2\theta_{12} \sin 2\theta_{23} \times \\ &\quad |m_1 \cos(2\phi_1 - \delta) - (1 + \zeta)m_2 \cos(2\phi_2 - \delta) - \zeta m_3 \cos \delta|. & (42) \end{aligned}$$

Here we have $C = -3/2$ for the SM and we define $t_0 \equiv \ln(\mu_0/\text{GeV})/(16\pi^2)$, and $\Delta_\tau = -(1/32\pi^2)(g_2 m_\tau/M_W)^2 \approx -1.4 \times 10^{-5}$, where g_2 is the $\text{SU}(2)_L$ gauge coupling, whereas m_τ and M_W are the τ lepton and W boson masses respectively. We keep the leading order terms in Δ_τ and θ_{13} , both of which are small parameters.

We analytically obtain the maximum possible value of θ_{13} from Eq. (4.22) (when θ_{12} and θ_{23} can take any value within the experimentally allowed range) and compare with the experimental results. In Fig. 4.4 each point represents a different high energy theory with $\theta_{13} = 0$ at the high scale. Thus it is seen that the maximum value gained radiatively by θ_{13} is rather small, being $\lesssim 3 \times 10^{-3}$ in the range $0 \leq m_0 \leq 0.5$ eV for both the mass orderings. Hence if future experiments measure θ_{13} greater than this limit, all the theories with $\theta_{13} = 0$ at the high scale and SM as the low energy effective theory will be ruled out completely. If the upper limit for m_0 is brought down by KATRIN [17] to $m_0 \lesssim 0.2$ eV, even lower θ_{13} values will be excluded for this class of theories. Note that for m_0 of this order, the effective electron neutrino mass m_β as measured by KATRIN, will essentially be the same as m_0 .

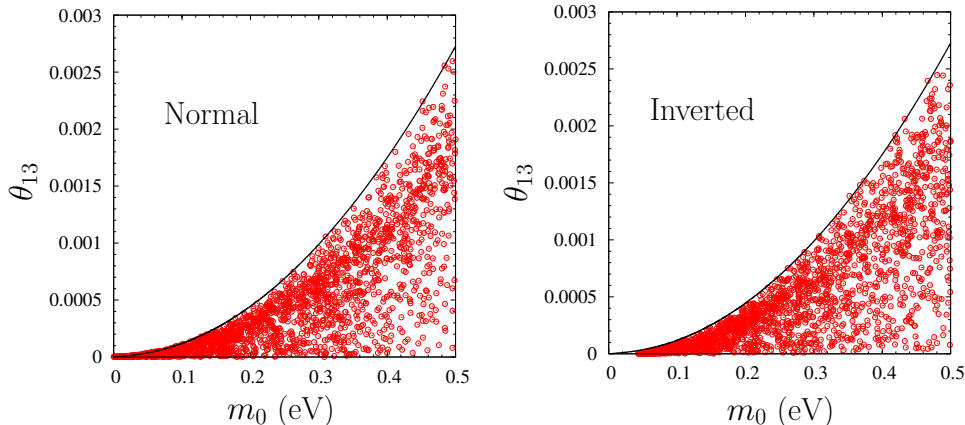


Figure 6: Scatter points show the low energy θ_{13} as a function of the lightest neutrino mass m_0 at the low scale, for both normal (left panel) and inverted (right panel) mass ordering. Each point represents a different high energy theory with $\theta_{13} = 0$. The solid (black) line gives the maximum attainable θ_{13} for a given m_0 , the current 3σ limits of the masses and mixings, and the proper choices of the phase values.

S.5 Conclusion

Heavy sterile neutrinos may play an important role in astrophysics and cosmology, for example in r-process nucleosynthesis or as dark matter. Neutrino oscillation experiments, mainly the short baseline ones, have already put severe constraints on the extent of mixing of these sterile neutrinos with the active ones. Recently it has been pointed out that to satisfy both LSND and Mini-BooNE data simultaneously, at least two sterile neutrinos with $\Delta m^2 \sim \mathcal{O}(1)$ eV² are in fact needed.

At the same time, the current experimental values of the mass squared differences of the three active neutrinos, combined with the bound on the sum of the neutrino masses coming from cosmology and astrophysics, indicate that neutrino masses are orders of magnitude smaller than the masses of the quarks and the charged leptons. The most favored mechanisms to generate such small neutrino masses are the seesaw mechanisms. In this scenario small active neutrino masses will be generated by seesaw at some high energy scale, while the experimental data are available at the laboratory energy scales and hence one need to include the effects of renormalization group (RG) evolution. Unlike the quark sector where all the mixing angles being small RG evolutions are

also quite small, the effect of RG evolution on the neutrino masses and the mixing parameters are important as two of the mixing angles θ_{12} , θ_{23} are large in this case. If the neutrinos are quasi-degenerate, the effect of RG evolution will be even more.

In this thesis we explore the neutrino oscillation phenomenology on two fronts. In the first part we check whether the sterile neutrinos obeying the constraints from astrophysics, cosmology and neutrino oscillation data can still give rise to observable signals at future long baseline experiments, and whether these signals can be cleanly identified in spite of our current lack of knowledge of the parameters in the mixing of three active neutrinos. We also estimate the bounds on the sterile neutrino parameters that can be obtained at these experiments.

The sterile neutrinos required to fit all the oscillation data, help r-process nucleosynthesis or act as the warm dark matter are too light to serve as the seesaw particles giving small active neutrino masses at the high scale. On the other hand, if we have a heavy right-handed Majorana fermion in the high energy renormalizable theory to generate the neutrino mass via seesaw (Type-I or Type-III), the mixing angle with the active species will be $\lesssim 3 \cdot 10^{-5}$ for a mass $\gtrsim 10$ keV, and hence will not affect the signal at the future long baseline experiments.

In the second part of the thesis we consider the Type-III seesaw scenario when heavy right-handed Majorana fermion triplets are added to the standard model (SM) at the high energy scale, so that they produce the small active neutrino masses through the Type-III seesaw mechanism. At energies lower than the mass of the respective heavy fermion, the particle gets decoupled from the theory, and contributes to the active neutrino masses through the non-renormalizable effective operator. We use the dimensional regularization and the minimal subtraction scheme to compute the beta functions in the renormalizable R_ξ gauge and study the RG evolution of the neutrino masses and mixing parameters in the high energy renormalizable theory as well as the low energy effective theory. We point out some salient features of the RG evolution of the neutrino masses and the mixing parameters in this model, and also the important role of the threshold effects and Majorana phases in the evolution of mixing angles through an illustrative example.

Some subtle issues are present when $\theta_{13} = 0$ is reached, either at the high

scale or during evolution. This is essentially because of the fact that the Dirac CP phase δ becomes unphysical when $\theta_{13} = 0$. We analyze this problem for a better understanding and also present an alternative formalism which enables one to determine analytically the change in the neutrino masses and mixing parameters due to RG evolution unambiguously, even when the evolution involves the $\theta_{13} = 0$ point. Finally we consider the models which predict $\theta_{13} = 0$ at the high scale and estimate the maximum value of θ_{13} that can be generated through RG evolution. We obtain a correlated constraint on θ_{13} and the lightest neutrino mass m_0 , for both the mass orderings and with the SM as the low energy effective theory. It is seen that for both the mass orderings, $\theta_{13} \lesssim 3 \times 10^{-3}$ for $0 \leq m_0 \leq 0.5$ eV and future measurements of θ_{13} and m_0 may be able to rule out this whole class of models considered here.

List of Publications

1. S. Goswami, S. Petcov, S. Ray and W. Rodejohann, “Large U_{e3} and Tribimaximal Mixing,” Phys. Rev. D **80**, 053013 (2009) [arXiv:0907.2869 [hep-ph]].
2. J. Chakraborty, A. Dighe, S. Goswami and S. Ray, “Renormalization group evolution of neutrino masses and mixing in the Type-III seesaw mechanism,” Nucl. Phys. B **820**, 116 (2009) [arXiv:0812.2776 [hep-ph]].
3. A. K. Alok, A. Dighe and S. Ray, “CP asymmetry in the decays $B \rightarrow (X_s, X_d)\mu^+\mu^-$ with four generations,” Phys. Rev. D **79**, 034017 (2009) [arXiv:0811.1186 [hep-ph]].
4. A. Dighe, S. Goswami and S. Ray, “Renormalization group evolution of neutrino mixing parameters near $\theta_{13} = 0$ and models with vanishing θ_{13} at the high scale,” Phys. Rev. D **79**, 076006 (2009) [arXiv:0810.5680 [hep-ph]].
5. A. Dighe and S. Ray, “CPT violation in long baseline neutrino experiments: a three flavor analysis,” Phys. Rev. D **78**, 036002 (2008) [arXiv:0802.0121 [hep-ph]].
6. A. Dighe and S. Ray, “Signatures of heavy sterile neutrinos at long baseline experiments,” Phys. Rev. D **76**, 113001 (2007) [arXiv:0709.0383 [hep-ph]].

Contents

Declaration	v
Acknowledgment	vii
Synopsis	ix
S.1 Introduction	ix
S.2 Signature of sterile neutrinos at long baseline experiments . . .	xiii
S.3 RG evolution: Type-III seesaw scenario	xix
S.4 RG evolution of neutrino mixing: The subtlety at $\theta_{13} = 0$. . .	xxiv
S.5 Conclusion	xxix
List of Publications	xxxiii
1 Introduction	1
1.1 The light sterile neutrinos	6
1.2 Seesaw mechanisms and neutrino mass	8
1.3 Renormalization group evolution	12
2 Signature of sterile neutrinos in the upcoming experiments	15
2.1 Introduction	15
2.2 Analytic computation of neutrino flavor conversion probabilities	18
2.3 Signatures at long baseline experiments	26
2.4 Generalization to any number of sterile neutrinos	33
2.5 Summary	37
3 Type-III seesaw: RG evolution of neutrino masses and mixing	41
3.1 Introduction	41
3.2 The Type-III seesaw model	43
3.3 Radiative corrections in Type-III seesaw	48
3.4 RG running of neutrino masses and mixing angles	57

CONTENTS

3.5	Illustrative examples of RG running of the masses and mixing	63
3.6	Summary	68
4	RG evolution near $\theta_{13} = 0$	71
4.1	Introduction	71
4.2	Apparent singularity in δ -evolution at $\theta_{13} = 0$ and RG evolution in the complex \mathcal{U}_{e3} plane	74
4.3	RG evolution equations in terms of the parameter set \mathcal{P}_J . . .	79
4.4	Bounds on θ_{13} at low scale	80
4.5	Summary	88
5	Conclusions	91
Appendices		
A	Calculation of neutrino flavor survival/conversion probabilities	95
B	Feynman diagrams in Type-III seesaw	103
C	Calculation of renormalization constants	109
D	RG evolution equations of masses and mixing parameters	129
	Bibliography	133

Chapter 1

Introduction

The field of neutrino physics has made immense progress in the last decade, which was initiated when the Super-Kamiokande (SK) experiment in Japan [1] reported the evidence for oscillations in the atmospheric neutrinos. Now there is compelling evidence that solar, atmospheric, accelerator and reactor neutrinos oscillate, which implies that the neutrinos are massive and the leptons mix among themselves.

The atmospheric neutrinos are produced in the Earth's atmosphere by cosmic rays. The flux of cosmic rays that lead to neutrinos with energies above a few GeV is isotropic. Hence one expects the downward and the upward-going fluxes of multi-GeV neutrinos of a given flavor to be equal. The underground SK detector found that for multi-GeV atmospheric muon neutrinos the zenith-angle dependence deviates from this expectation and the deviation can be explained when one invokes $\nu_\mu \rightarrow \nu_\tau$ oscillations. The oscillations of muon neutrinos into other flavors have also been confirmed by the energy spectrum obtained from the controlled source experiments K2K [5] and MINOS [76]. The allowed region for the oscillation parameters, Δm_{atm}^2 and $\sin^2 2\theta_{\text{atm}}$, is shown in Fig 1.1. As can be seen from the figure, the MINOS data is capable of measuring Δm_{atm}^2 with high precision, while SK put stronger bound on $\sin^2 2\theta_{\text{atm}}$. The results from the short-baseline (SBL) experiments (like NOMAD [67], CDHS [68] etc.) show that the $\nu_\mu \rightarrow \nu_e$ oscillations can be present only as small sub-dominant effects and also put strong bounds on the active-sterile mixing angles in $\nu_\mu \rightarrow \nu_s$ oscillations, an oscillation channel whose sub-dominant effect is not yet ruled out completely.

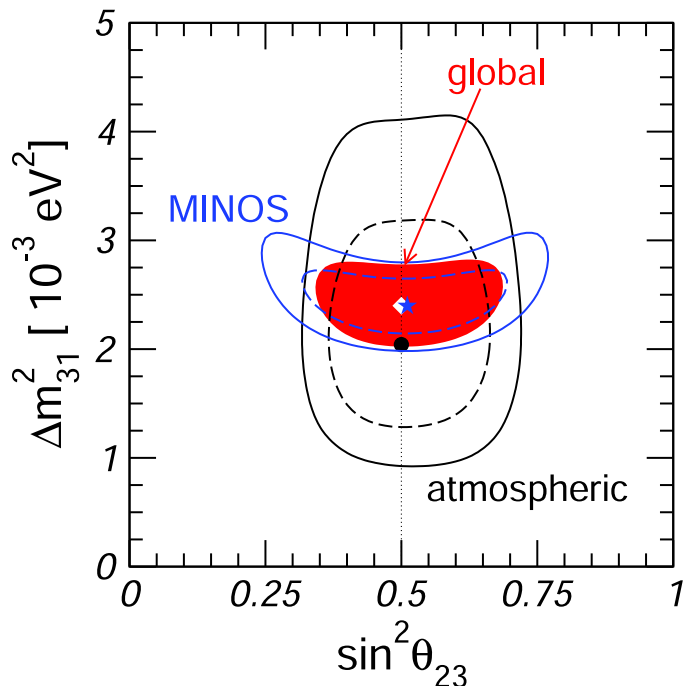


Figure 1.1: The region of the atmospheric oscillation parameters Δm_{atm}^2 and $\sin^2 2\theta_{\text{atm}}$ obtained from the SK, K2K and MINOS experiments [13].

The pioneering solar neutrino experiment by Davis and collaborators using ^{37}Cl reported a solar electron neutrino flux significantly smaller than that predicted by the standard solar model (SSM), and this deficit in the number of electron neutrinos is known as the “solar neutrino problem”. The puzzle persisted in the literature for about 30 years, and then the charged current (CC) and the neutral current (NC) data from the SNO experiment [2], combined with the SK solar neutrino data [77], provided direct evidence for neutrino oscillations in solar neutrinos. However, four different solutions were there to explain the solar neutrino oscillations [78]: (i) the LMA or large mixing angle solution ($\Delta m_{\odot}^2 = 5.0 \cdot 10^{-5} \text{ eV}^2$, $\tan^2 \theta_{\odot} = 0.42$), (ii) the low mass solution ($\Delta m_{\odot}^2 = 7.9 \cdot 10^{-8} \text{ eV}^2$, $\tan^2 \theta_{\odot} = 0.61$), (iii) the vacuum solution ($\Delta m_{\odot}^2 = 4.6 \cdot 10^{-10} \text{ eV}^2$, $\tan^2 \theta_{\odot} = 1.8$) and (iv) the SMA or small mixing angle solution ($\Delta m_{\odot}^2 = 5.0 \cdot 10^{-6} \text{ eV}^2$, $\tan^2 \theta_{\odot} = 1.5 \cdot 10^{-3}$). The results from the controlled source experiment KamLAND [3] confirmed the LMA solution and ruled out the other two possibilities. Fig 1.2 shows the allowed region of the solar neutrino oscillation parameters Δm_{\odot}^2 and $\tan^2 \theta_{\odot}$.

Combining the results obtained from the solar, atmospheric and the reac-

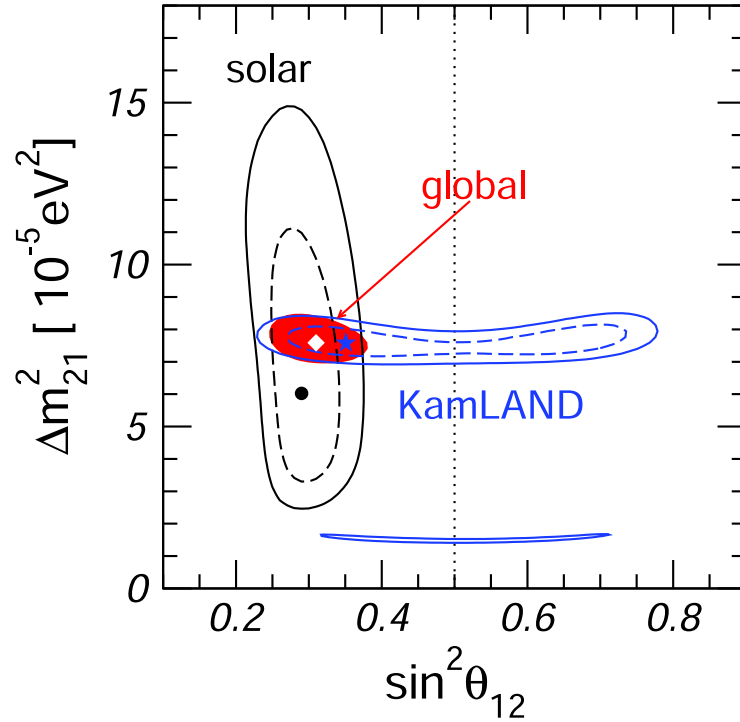


Figure 1.2: The allowed region in the neutrino oscillation parameter space from solar neutrino data and KamLAND experiment [13].

tor neutrino oscillation experiments described above, the current knowledge about the neutrinos is that there are three neutrino flavors ($\nu_\alpha, \alpha \in \{e, \mu, \tau\}$), which mix to form three neutrino mass eigenstates ($\nu_i, i \in \{1, 2, 3\}$). These mass eigenstates are separated by $\Delta m_{ij}^2 \equiv m_i^2 - m_j^2$ where, $m_{i,j}$ denote mass eigenvalues with $i, j \in \{1, 2, 3\}$. The two sets of eigenstates are connected through $\nu_\alpha = (U_{\text{PMNS}})_{\alpha i} \nu_i$, where U_{PMNS} is the Pontecorvo-Maki-Nakagawa-Sakata neutrino mixing matrix [9, 10, 11, 12] in the basis where the charged lepton mass matrix is diagonal. This matrix is parametrized as

$$U_{\text{PMNS}} = P \cdot \mathcal{U} \cdot Q, \quad (1.1)$$

where

$$\mathcal{U} = U_{23}(\theta_{23}, 0) U_{13}(\theta_{13}, \delta) U_{12}(\theta_{12}, 0), \quad Q = \text{Diag}\{e^{-i\phi_1}, e^{-i\phi_2}, 1\}. \quad (1.2)$$

Here $U_{ij}(\theta, \delta)$ is the complex rotation matrix in the i - j plane, δ is the Dirac CP violating phase, ϕ_i are the Majorana phases, and P is the flavor phase matrix (Sometimes the flavor phases are called as the unphysical phases since they

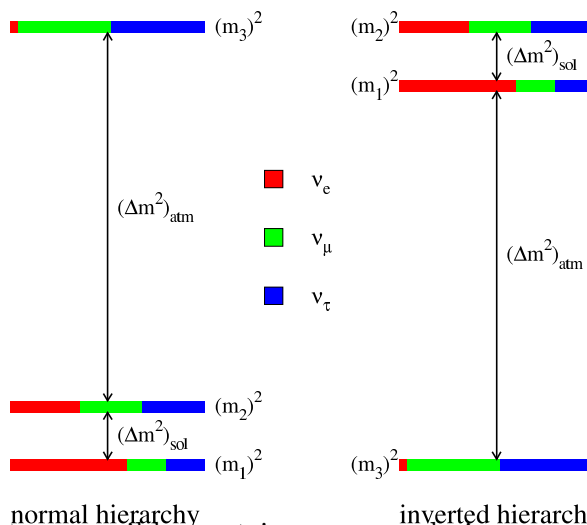


Figure 1.3: The two possible neutrino mass orderings: normal ($m_1 < m_2 < m_3$) and inverted ($m_3 < m_1 < m_2$).

	Best fit	3σ range
Δm_{21}^2 [10^{-5}eV^2]	7.65	7.05 - 8.34
$ \Delta m_{31}^2 $ [10^{-3}eV^2]	2.40	2.07 - 2.75
$\sin^2 \theta_{12}$	0.304	0.25 - 0.37
$\sin^2 \theta_{23}$	0.50	0.36 - 0.67
$\sin^2 \theta_{13}$	0.01	≤ 0.056

Table 1.1: The present best-fit values and 3σ ranges of oscillation parameters [13, 14, 15].

do not play any role in the phenomenology of neutrino mixing or beta-decay.) Finally, with all the above definitions, \mathcal{U} takes the form

$$\mathcal{U} = \begin{pmatrix} c_{12}c_{13} & s_{12}c_{13} & s_{13}e^{-i\delta} \\ -c_{23}s_{12} - s_{23}s_{13}c_{12}e^{i\delta} & c_{23}c_{12} - s_{23}s_{13}s_{12}e^{i\delta} & s_{23}c_{13} \\ s_{23}s_{12} - c_{23}s_{13}c_{12}e^{i\delta} & -s_{23}c_{12} - c_{23}s_{13}s_{12}e^{i\delta} & c_{23}c_{13} \end{pmatrix}, \quad (1.3)$$

where c_{ij} and s_{ij} are the cosines and sines respectively of the mixing angle θ_{ij} . The current best-fit values and 3σ ranges for these parameters are summarized in Table 1.1. It is still not known whether the neutrino mass ordering is normal ($m_1 < m_2 < m_3$) or inverted ($m_3 < m_1 < m_2$), these two possibilities are shown in Fig. 1.3. Many other high precision oscillation experiments are going on and also being planned in order to measure the neutrino oscillation parameters with higher accuracy and to determine the neutrino mass ordering.

While the neutrino oscillation experiments are not sensitive to the absolute neutrino masses, the beta decay and the neutrinoless double beta decay ($0\nu\beta\beta$) processes are. At the same time, it is possible to estimate $\sum_i m_i$ from cosmology also. In case of the beta decay, the non-zero neutrino mass would modify the Kurie plot, regardless of whether the neutrinos are Dirac or Majorana particles. The effect will depend on $m_\beta = (\sum_i |U_{ei}|^2 m_i^2)^{1/2}$, and if the neutrino masses are small, it will be visible only near the end point of the Kurie plot. The Mainz [79] experiment has placed the upper limit of $m_\beta \leq 2.3$ eV. The upcoming beta-decay experiments like KATRIN [17] will be sensitive to $m_\beta > 0.2$ eV and will thus improve the bound by an order of magnitude. The $0\nu\beta\beta$ decay, on the other hand, is sensitive to the effective Majorana mass of the electron neutrinos, defined as $m_{ee} \equiv |\sum_i U_{ei}^2 m_i|$, and will be observed only if the neutrinos are Majorana particles. A non-zero signal for the $0\nu\beta\beta$ decay will put bound on the specific combination of the neutrino masses and the Majorana phases given by m_{ee} . The current limit put by the Heidelberg-Moscow experiment [80] is $m_{ee} \lesssim 0.9$ eV. The cosmic microwave background radiation (CMBR) carries the imprint of the neutrino masses since in the standard Big Bang model, for the standard model (SM) interactions of the neutrinos, the neutrinos are abundant like the photons till the epoch of nucleosynthesis when they decouple from the thermal bath of the photons. It is also possible to get information about the neutrino masses from the study of the large scale structure as an active neutrino species of mass m_ν will tend to wash out all structures upto a scale $\sim 1/m_\nu$ by free-streaming. Recent results from the Wilkinson Microwave Anisotropy Probe (WMAP) and the surveys on the large scale structure put the limit $\sum_i m_i \leq 0.67 - 2.0$ eV [16, 81]. However it must be noticed that none of the processes discussed above can provide any information about the lightest neutrino mass when there is a strong hierarchy amongst the neutrinos, *i.e.* when the lightest neutrino mass is $\lesssim 0.1$ eV.

There have also been experiments that indicated the presence of neutrino mixing beyond three flavors. The first such experiment showing the positive indication for the neutrino oscillations beyond the three-neutrino paradigm was the Los Alamos LSND [6] experiment, but the KARMEN [7] experiment strongly constrained the region of the neutrino parameter space allowed by the LSND. Currently MiniBooNE [8] experiment at Fermilab has probed the entire LSND parameter region but has not observed any neutrino oscillations.

The very fact that the active neutrinos are massive demands an extension of

the SM. One way is to extend it by addition of extra fermionic fields which are heavy ($m \sim 10^{11} - 10^{15}$ GeV for Type-I seesaw and \sim TeV for Type-III seesaw) and hence can give rise to light active neutrino masses through seesaw mechanisms. Light singlet fermions with $m \sim 1$ eV are also predicted to explain the neutrino oscillation data when LSND, MiniBooNE and the SBL appearance experiments are considered together [18]. They can also play an important role in stellar astrophysics, while singlet fermions with $m \sim$ keV can serve the purpose of warm dark matter in cosmology. In this thesis we explore the neutrino oscillation phenomenology, with fermions beyond the SM, on two fronts. First, we study the effect of the presence of one or more \sim eV–keV sterile neutrinos on the signals expected at the upcoming long baseline experiments. Second, we examine neutrino mass models where new fermions \sim TeV or higher participate through the Type-III seesaw mechanism [82].

1.1 The light sterile neutrinos

Recently it has been pointed out [18] that with two sterile neutrinos, having $\Delta m^2 \sim \mathcal{O}(1)$ eV², it is possible to satisfy both LSND and MiniBooNE data simultaneously. Fig. 1.4 shows the allowed regions in the Δm_{41}^2 - Δm_{51}^2 plane, when both LSND and MiniBooNE (MB475) data are considered along with the SBL appearance data. It has also been shown that the introduction of more than two sterile species does not introduce any significant changes in the allowed values.

Sterile neutrinos, with masses ~ 0.1 eV or higher and obeying all the constraints from the terrestrial experiments, can also play an important role in astrophysics and cosmology [19]. The matter enhanced active-sterile neutrino transformation can produce a significant effect on r-process nucleosynthesis in the core-collapse supernovae [20] by reducing the number of electron neutrinos available for $\nu_e n \rightarrow p e^-$ and thereby increasing the number of neutrons. Since the sterile neutrinos interact very weakly with the nuclear matter, they can transport heat out of the star very efficiently and thus can influence the explosion dynamics of supernovae [21]. Presence of sterile neutrinos can explain the large observed velocities of pulsars [22]. The Chandra blank sky observations also allow keV neutrinos to be viable dark matter candidates [23]. Such keV sterile neutrinos can help in the production of supermassive black holes [24].

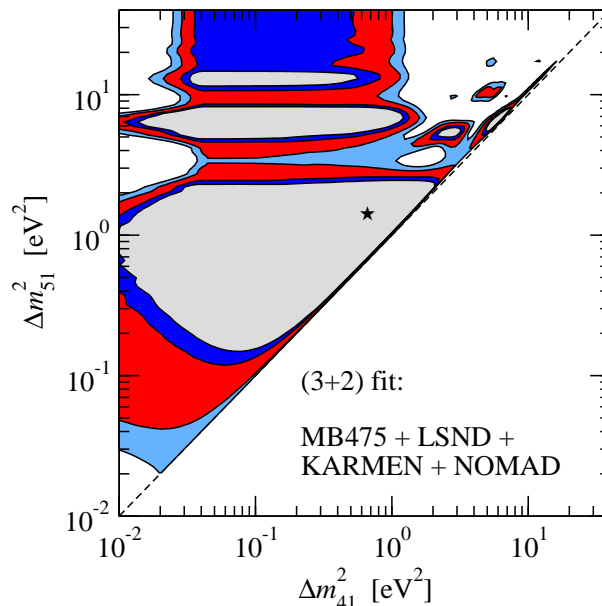


Figure 1.4: Allowed regions for SBL appearance data in (3+2) schemes at 90%, 95%, 99%, 99.73% C.L. (2 dof) in the plane of Δm_{41}^2 and Δm_{51}^2 . All other parameters have been minimized [18]. MB475 implies that the MiniBooNE data points in the range energy < 475 MeV have not been considered.

These are excellent dark matter candidates in ν MSM [25, 26, 27, 28], which explain masses of active neutrinos and baryon asymmetry of the universe. Sterile neutrinos may leave their imprints in the supernova neutrino burst [83, 84], or in the ultrahigh energy neutrino signals observed at the neutrino telescopes [85].

Thus the main requirements for the astrophysically and cosmologically relevant sterile neutrinos are that they should be heavier than the three active neutrinos ($m \sim 1\text{--}10$ eV or \sim keV) and that they mix weakly with the electron and muon neutrino (in order to satisfy the MiniBooNE and SBL appearance constraints).

In the first part of the thesis we find out the analytic expressions for the survival and conversion probabilities of neutrinos when the $m \sim$ eV–keV sterile neutrinos are present and examine some of the possible signatures of sterile neutrino mixing on the signals at a neutrino factory setup with near and far detectors. We also estimate bounds on the sterile neutrino parameters that can be obtained at such long baseline experiments [30].

1.2 Seesaw mechanisms and neutrino mass

One of the most distinctive features emerging out of the current experimental values given in the Table 1.1, when combined with the present bound on the absolute neutrino masses from cosmology and the beta-decay experiments, is that the neutrinos are massive and the absolute masses of neutrinos are orders of magnitude smaller than those of quarks and charged leptons. In the framework of the SM, since there is no right-handed neutrino, the neutrinos are massless at the tree-level, and they cannot have a Dirac mass even at loop level. So the only other possibility is the lepton number violating Majorana mass term. But lepton number is a symmetry of the SM, though accidental, and if that symmetry is to be obeyed, Majorana masses also cannot be generated at loop level. It can also be seen that the Planck scale (M_{Pl}) effect cannot introduce the required neutrino mass in the SM as it can only generate a neutrino mass $\sim \mathcal{O}(v_{EW}^2/M_{\text{Pl}}) \approx \mathcal{O}(10^{-5}\text{eV})$, and hence cannot explain the atmospheric mass squared difference. Hence generally the neutrino masses are incorporated at the tree-level by adding new particles to the SM. The most favored mechanisms to generate such small neutrino masses are the so called seesaw mechanisms which need the introduction of one or more heavy fields, while maintains the $SU(3)_C \times SU(2)_L \times U(1)_Y$ gauge group structure of the SM.

1.2.1 The seesaw

The simplest extension of the SM to incorporate small active neutrino mass is to introduce right-handed singlet fermions N_R in the theory, which are singlets under the SM gauge group. Hence these N_R fields are essentially right-handed neutrinos. Presence of these new fields allows new terms in the Lagrangian

$$\mathcal{L}_N = \frac{1}{2}\bar{N}(i\partial)N - \frac{1}{2}\bar{N}M_N N - \left(\bar{N}Y_N\tilde{\phi}^\dagger l_L + \text{h.c.}\right), \quad (1.4)$$

where l_L and ϕ are respectively the lepton and Higgs doublets belonging to the SM. Here we do not write the generation or the $SU(2)_L$ indices explicitly. The field N is defined as $N \equiv N_R + N_R^C$, where N_R^C is the CP conjugate of the right-handed field N_R . Y_N is the Yukawa coupling for the singlet fermion and

\mathbb{M}_N is the mass matrix. Thus the complete Lagrangian of the theory becomes

$$\mathcal{L} = \mathcal{L}_{\text{SM}} + \mathcal{L}_N , \quad (1.5)$$

and it is possible to write the neutrino mass terms as

$$- \mathcal{L}_{\nu_{\text{mass}}} = \frac{1}{2} \begin{pmatrix} \bar{\nu}_L & \overline{N}_R^C \end{pmatrix} \begin{pmatrix} 0 & \mathbf{m}_D \\ \mathbf{m}_D^T & \mathbb{M}_N \end{pmatrix} \begin{pmatrix} \nu_L^C \\ N_R \end{pmatrix} + \text{h.c.} , \quad (1.6)$$

where $\mathbf{m}_D = (v/\sqrt{2})Y_N^T$ is the Dirac mass matrix for the neutrinos generated after the electroweak symmetry breaking when the Higgs gets the vacuum expectation value (vev) v such that

$$\langle \phi^0 \rangle = v/\sqrt{2} . \quad (1.7)$$

Thus the complete mass matrix for the neutrinos becomes

$$\mathcal{M}_\nu = \begin{pmatrix} 0 & \mathbf{m}_D \\ \mathbf{m}_D^T & \mathbb{M}_N \end{pmatrix} , \quad (1.8)$$

which when block-diagonalized gives the eigenvalues

$$\mathbf{m}_1 \approx -\mathbf{m}_D \mathbb{M}_N^{-1} \mathbf{m}_D^T , \quad (1.9)$$

$$\mathbf{m}_2 \approx \mathbb{M}_N , \quad (1.10)$$

where we have assumed that $\mathbb{M}_N \gg \mathbf{m}_D$, *i.e.* the eigenvalues of \mathbb{M}_N are much larger than the eigenvalues of \mathbf{m}_D . Thus Eqs. (1.10) and (1.9) show respectively that eigenvalues of the matrix \mathbf{m}_2 are large, while those of \mathbf{m}_1 are small and hence the eigenstates corresponding to these small eigenvalues should serve the purpose of the mass eigenstates of the light active neutrinos. Thus the presence of the heavy right-handed neutrinos will produce the light active neutrino masses and this mechanism of making one particle light at the expense of making another one heavy is called the seesaw mechanism. The seesaw obtained by adding heavy right-handed singlet fermions to the SM is called the Type-I seesaw [86, 87, 88, 89, 90].

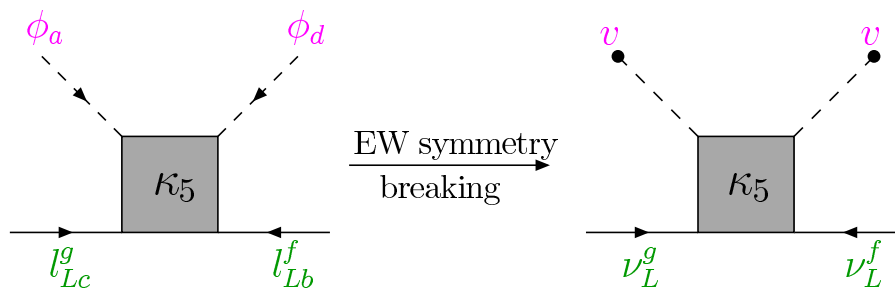


Figure 1.5: Generation of the Majorana neutrino mass from the low energy effective Lagrangian given in Eq. (1.11) after spontaneous symmetry breaking.

1.2.2 The effective theory

The low energy effective Lagrangian needed to explain the non-zero active neutrino masses can in general be expressed as a series of non-renormalizable operators, the dominant one being the dimension-5 operator given as [31]

$$\mathcal{L} = \kappa_5 l_L l_L \phi \phi . \quad (1.11)$$

Here κ_5 is the effective coupling which can be expressed in terms of a dimensionless coupling a_5 as $\kappa_5 = a_5/\Lambda$ with Λ some high energy scale. In this picture the SM serves as an effective theory valid upto the mass scale Λ , which can be taken to be the mass of the lightest of the heavy fields. However the specific form of κ_5 will depend on the high energy field content and the interactions present at the high scale. The operator shown in Eq. (1.11) violates lepton number by two units and hence gives rise to Majorana masses for neutrinos after spontaneous symmetry breaking, $m_\nu \sim \frac{1}{2}\kappa_5 v^2$, as shown in the Fig. 1.5. Here v is the vev of the Higgs field ϕ , as given in Eq. (1.7). Taking $v \sim 246$ eV, a neutrino mass of ~ 0.05 eV implies $\Lambda \sim 10^{15}$ GeV if $a_5 \sim 1$.

Clearly the sterile neutrinos considered in Section 1.1 are too light to give the seesaw masses to the active species. In the second part of this thesis we consider the right-handed Majorana fermions capable of producing the light active neutrino mass via seesaw. As can be seen from Fig. 1.6, for neutrinos with a mass $\gtrsim \mathcal{O}(10 \text{ keV})$ the mixing angle becomes $\lesssim 3 \cdot 10^{-5}$ [19] and hence the heavy seesaw particles having masses $\gg 10 \text{ keV}$ will not affect the phenomenology at the long baseline experiments discussed before.

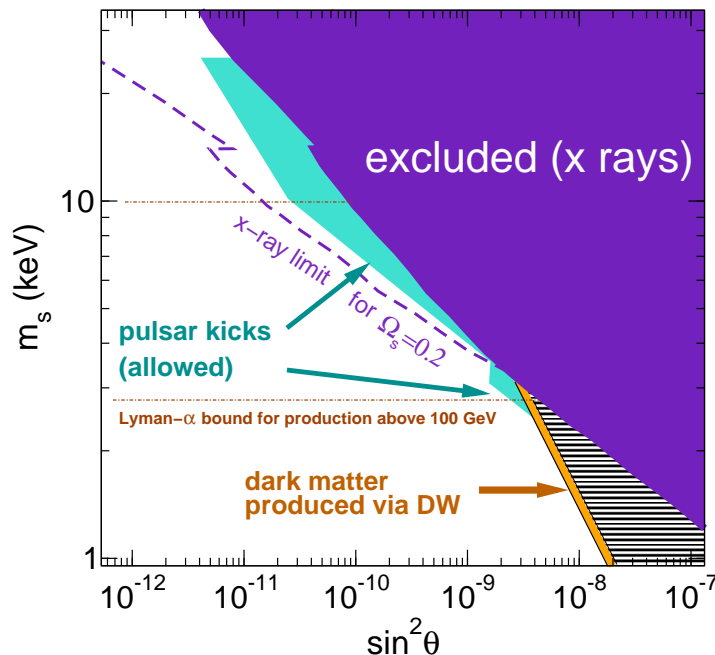


Figure 1.6: Constraints on the sterile neutrino mass and the mixing angle from astrophysics and cosmology data [19].

1.2.3 Different seesaw mechanisms

There are four possible ways to form a dimension-5 gauge singlet term as given in Eq. (1.11) at low energy through the tree-level exchange of a heavy particle at the high energy: (i) each l_L - ϕ pair forms a fermion singlet, (ii) each of the l_L - l_L and ϕ - ϕ pair forms a scalar triplet, (iii) each l_L - ϕ pair forms a fermion triplet, and (iv) each of the l_L - l_L and ϕ - ϕ pair forms a scalar singlet. Case (i) can arise from the tree-level exchange of a right handed fermion singlet and this corresponds to the Type-I seesaw mechanism, as discussed in the Section 1.2.1 in detail. Case (ii) arises when the heavy particle is a Higgs triplet giving rise to the Type-II seesaw mechanism [91, 92]. For case (iii) the exchanged particle should be a right-handed fermion triplet, which corresponds to the Type-III seesaw mechanism [82, 93], which will be discussed in detail in Chapter 3. The last scenario gives terms only of the form $\overline{\nu}_L^c e_L$, which cannot generate a neutrino mass.

A summary of the form of κ_5 and hence the effective light neutrino mass at the low scale in different types of seesaw is given in Table 1.2.

	The effective vertex	κ_5
Type-I		$\kappa_5 = 2Y_N^T M_N^{-1} Y_N$
Type-II		$\kappa_5 = -2 \frac{Y_\Delta \Lambda_6}{M_\Delta^2}$
Type-III		$\kappa_5 = 2Y_\Sigma^T M_\Sigma^{-1} Y_\Sigma$

Table 1.2: Summary of the low energy effective couplings and the effective neutrino mass $m_\nu \equiv -\frac{v^2}{4}\kappa_5$ in the three seesaw scenarios. Here, $Y_N(Y_\Sigma)$ are the Yukawa couplings for the heavy singlet(triplet) fermion present in Type-I(Type-III) seesaw and $M_N(M_\Sigma)$ is the mass matrix ($N \equiv N_R + N_R^C$; $\Sigma \equiv \Sigma_R + \Sigma_R^C$). In Type-II seesaw, M_Δ is the mass of the heavy triplet Higgs, Y_Δ is its Yukawa coupling with the SM lepton doublet l_L , and Λ_6 is its coupling with the SM Higgs ϕ .

1.3 Renormalization group evolution

Since the neutrino mass is generated at the high scale via seesaw mechanisms while the neutrino masses and mixing parameters are measured experimentally at a low scale, the renormalization group (RG) evolution effects need to be included. The current experimental data in Table 1.1 shows that in the neutrino sector two of the three mixing angles are large, while the third one is small, which is rather different from the quark sector where all three mixing angles are small. Because of the large values of the two mixing angles, RG evolution of the neutrino masses and the mixing parameters plays an important role in the neutrino sector, which is not the case with the quark sector. RG evolution will be even larger if the neutrinos happen to be quasi-degenerate.

The radiative corrections in different types of seesaws are expected to be different since the heavy particles couple differently to the SM fields present.

However below the mass scale of the lightest of the heavy particles the effect of all heavy degrees of freedom are integrated out and the effective mass operators in these scenarios become identical, as seen from the Section 1.2.2, and so does the RG evolution in different seesaw scenarios.

The effect of RG induced quantum corrections on leptonic masses and mixings have been studied extensively in the literature [32, 33, 34, 35, 36, 37, 94]. These effects can have interesting consequences such as the generation of large mixing angles [38, 39, 40, 41, 42, 43, 44], small mass splittings for degenerate neutrinos [45, 46, 47, 48, 49, 50, 51, 52, 53], or radiative generation of θ_{13} starting from a zero value at the high scale [54, 55, 56, 57]. RG induced deviations from various high scale symmetries and correlations with low scale observables have been explored. Such effects can have significant contributions from the threshold corrections [58, 59, 60]. The RG evolution of the neutrino mass operator in the SM and the Minimal Supersymmetric Standard Model (MSSM) in the context of Type-I seesaw [59, 61, 62] and Type-II seesaw [63, 64] have been studied in the literature. In the context of Type-III seesaw with degenerate heavy fermions, the impact of the RG evolution on the vacuum stability and perturbativity bounds of the Higgs Boson have been explored in [65].

In the second part of this thesis we study the RG evolution of the neutrino masses and mixing in the Type-III seesaw scenario with non-degenerate heavy fermions [29]. We consider the effect of sequential decoupling of the heavy particles as the energy scale becomes equal to the mass, which is known as the threshold effect. Finally, we study the RG evolution of all these parameters in the effective low energy theory. Analytical expressions for the RG evolution of these parameters have been obtained through an expansion in the small parameter θ_{13} [34, 35]. However, some subtle issues are present when $\theta_{13} = 0$ is reached, either at the high scale or during the evolution. We try to analyze the problem for a better understanding and also present an alternative formalism [57].

Chapter 2

Signature of sterile neutrinos in the upcoming experiments

In this chapter we consider the effects of one or more heavy sterile neutrinos, with masses greater than 1 eV, on the survival and conversion probabilities of the three active neutrino species and in turn on the signals of the upcoming long-baseline experiments.

2.1 Introduction

In the framework of the Standard model (SM) of particle physics, there are only three neutrinos, one each with the electron, muon and tau flavor. The LEP experiments have determined the number of light neutrinos that couple with the Z boson through electroweak interactions to be 2.984 ± 0.008 [95], thus closing the door on any more generations of “active” neutrinos. However, there still may exist sterile neutrinos that do not have electroweak interactions. Though they cannot be detected in the Z decay, they may mix with the active neutrinos and hence participate in neutrino oscillations. The LSND experiment [6] has reported a positive signal for $\bar{\nu}_\mu \rightarrow \bar{\nu}_e$ conversion, which would necessitate the inclusion of a sterile neutrino in the standard framework of neutrino masses and mixing. The extent of sterile neutrino participation in solar neutrino data is severely restricted from the neutral current data from SNO [96, 97]. The atmospheric neutrino data show that the major contribution to the muon neutrino disappearance has to be from $\nu_\mu \leftrightarrow \nu_\tau$

oscillations, however a small admixture of sterile neutrinos cannot be ruled out [98, 99, 100, 101]. Short baseline experiments sensitive to sterile neutrinos in the ~ 1 eV range [7, 66, 67, 68] have given strong upper bounds on sterile mixing. The parameter space consistent with the LSND results would be further restricted at the CNGS experiment [102] or at a neutrino factory with the baseline as short as 10 km [103] through the $\nu_\mu \rightarrow \nu_{e,\tau}$ channel, and at a long baseline neutrino factory through the $\nu_e \rightarrow \nu_\mu$ channel [104]. The MiniBooNE experiment [8] has virtually ruled out any effect of sterile neutrinos in the LSND parameter space if there were only one sterile neutrino species. However, recently it has been pointed out [18] that with two or more sterile neutrinos, it is possible to be in agreement with LSND, MiniBooNE and the short baseline (SBL) appearance data.

Even if the LSND results are ignored, so that there is no longer any need for sterile neutrinos for explaining the neutrino oscillation data, sterile neutrinos that obey all the constraints from the terrestrial experiments can still play a crucial role in astrophysics and cosmology [19], as discussed in the Chapter 1. Finally combining all the above aspects, the main requirements for the astrophysically and cosmologically relevant sterile neutrinos are that they be heavy ($m \sim 1\text{--}10$ eV for r-process nucleosynthesis, and $m \sim$ keV for the dark matter candidates) and that they mix weakly with the electron and muon neutrino (in order to satisfy the MiniBooNE and the SBL appearance experiment constraints). In the first part of this chapter, we consider the case with one such sterile neutrino, which may influence neutrino oscillation experiments. We perform the complete 4- ν analysis, taking into account all the three additional mixing angles of the sterile neutrino ν_s with the active ones, and the two additional CP violating phases. We only concentrate on heavy neutrinos, such that if m_4 is the mass of the neutrino eigenstate with a dominant sterile component, $\Delta m_{\text{st}}^2 \equiv |m_4^2 - m_i^2| \gtrsim 0.1 \text{ eV}^2$ for all other neutrino mass eigenstates ν_i . The oscillations due to Δm_{st}^2 are rather rapid, and can be taken to be averaged out in the long baseline data. As a result, the data are expected to be insensitive to the exact value of Δm_{st}^2 in the long baseline experiments. However, the additional mixing angles θ_{i4} may leave their signatures in the data.

We treat the effects of the sterile neutrino as a perturbation parameterized by a small auxiliary parameter $\lambda \equiv 0.2$. To this end, we represent the active-sterile mixing angles $\theta_{14}, \theta_{24}, \theta_{34}$, the deviation of θ_{23} from maximality, the

reactor angle θ_{13} as well as the ratio $\Delta m_{\odot}^2/\Delta m_{\text{atm}}^2$, formally as some power of λ times $\mathcal{O}(1)$ numbers, so that a systematic expansion in powers of λ may be carried out. Averaging out the fast oscillations due to Δm_{st}^2 allows us to obtain simple analytic approximations for the flavor conversion probabilities of neutrinos. The expressions thus obtained describe the dependence of relevant conversion or survival probabilities on the parameters in a transparent manner.

We analyze, using analytical as well as numerical means, how the parameters involving sterile neutrinos – constrained by the data from solar, atmospheric, and short baseline experiments – affect the results at the long baseline experiments. We illustrate this effect quantitatively in the case of a neutrino factory setup involving a near and a far detector that are capable of lepton charge identification. In particular, we consider the CP asymmetry in μ and τ channels as the observables and calculate how far the limits on the sterile mixing parameters can be brought down. We also consider the electron channel, where signals of sterile neutrino mixing can still be established by the counting of the total number of events above a threshold.

This chapter is organized as follows. In Sec. 2.2, we explain our formalism of a systematic expansion of all quantities in an auxiliary small parameter λ and the use of perturbation theory to obtain the neutrino flavor conversion probabilities. In Sec. 2.3 we examine some of the possible signatures of sterile neutrino mixing on the signals at a neutrino factory setup with near and far detectors, where we also estimate bounds that can be obtained at such long baseline experiments. However, as stated in the Chapter 1, [18] shows that it is possible to be in agreement with the data from LSND, MiniBooNE and the SBL appearance experiments simultaneously if two or more light sterile neutrinos are considered. In Sec. 2.4, we generalize our formalism to any number of sterile species and point out that only certain combinations of the sterile mixing parameters are relevant, independent of the number of sterile species. Sec. 2.5 summarizes the chapter.

2.2 Analytic computation of neutrino flavor conversion probabilities

We work in the 4- ν framework, where $(\nu_e, \nu_\mu, \nu_\tau, \nu_s)$ form the basis of neutrino flavor eigenstates and $(\nu_1, \nu_2, \nu_3, \nu_4)$ form the basis of neutrino mass eigenstates. The mass eigenstates are numbered according to the convention $|\Delta m_{42}^2| \gg |\Delta m_{32}^2| \gg \Delta m_{21}^2 > 0$, where $\Delta m_{ij}^2 \equiv m_i^2 - m_j^2$. We have $\Delta m_{\text{st}}^2 \approx |\Delta m_{42}^2|$, $\Delta m_{\text{atm}}^2 \approx |\Delta m_{32}^2|$ and $\Delta m_{\odot}^2 \approx \Delta m_{21}^2$. Note that the sign of Δm_{32}^2 is as yet unknown, a positive (negative) Δm_{32}^2 corresponds to the normal (inverted) mass ordering of neutrinos.

The mass and flavor eigenstates of neutrinos are connected through a unitary matrix \mathcal{U} , such that

$$\nu_\alpha = \mathcal{U}_{\alpha i} \nu_i, \quad (2.1)$$

where $\alpha \in \{e, \mu, \tau, s\}$ and $i \in \{1, 2, 3, 4\}$. Here mixing matrix \mathcal{U} is a 4×4 matrix \mathcal{U}_4 and may be parameterized as

$$\mathcal{U}_4 = U_{14}(\theta_{14}, \delta_{14}) U_{34}(\theta_{34}, 0) U_{24}(\theta_{24}, \delta_{24}) U_{23}(\theta_{23}, 0) U_{13}(\theta_{13}, \delta_{13}) U_{12}(\theta_{12}, 0), \quad (2.2)$$

where $U_{ij}(\theta_{ij}, \delta_{ij})$ is the complex rotation matrix in the i - j plane, whose elements $[U_{ij}]_{pq}$ are defined as

$$[U_{ij}(\theta, \delta)]_{pq} = \begin{cases} \cos \theta & p = q = i \text{ or } p = q = j \\ 1 & p = q \neq i \text{ and } p = q \neq j \\ \sin \theta e^{-i\delta} & p = i \text{ and } q = j \\ -\sin \theta e^{i\delta} & p = j \text{ and } q = i \\ 0 & \text{otherwise.} \end{cases} \quad (2.3)$$

In the four neutrino basis, the PMNS matrix will look like

$$U_4 = \mathcal{U}_4 \cdot Q_4, \quad (2.4)$$

where Q_4 is the Majorana phase matrix given by

$$Q_4 = \text{Diag}(e^{-i\phi_1}, e^{-i\phi_2}, e^{-i\phi_3}, 1), \quad (2.5)$$

and here we do not write the flavor phase matrix explicitly, which will not contribute to the neutrino oscillations. The limit when the sterile neutrino

is completely decoupled – or when it does not exist – is obtained simply by setting $\theta_{14}, \theta_{24}, \theta_{34} \rightarrow 0$ and $\phi_3 \rightarrow 0$ so that $U_4 \rightarrow U_{\text{PMNS}}$ as given by Eq. (1.1), apart from the unphysical “flavor phase” part.

We expect θ_{14}, θ_{24} and θ_{34} , the mixing angles involving the sterile neutrino, to be small. Indeed, though the 4ν analysis of atmospheric neutrinos give a rather weak bound of $\theta_{24}^2 \approx |[\mathcal{U}_4]_{\mu 4}|^2 < 0.19$ (90% C.L.) [99, 100, 101], short baseline disappearance experiments [68] constrain $\theta_{24}^2 < 0.013$ (90% C.L.), whereas the short baseline appearance experiments [7, 8, 66, 67] give a bound of $\theta_{14}\theta_{24} \approx |[\mathcal{U}_4]_{e4}[\mathcal{U}_4]_{\mu 4}| < 0.02$. The atmospheric neutrino data restrict the deviation of θ_{23} from maximality to be < 0.15 rad at 90% C.L. [69], and the CHOOZ data [70] combined with solar, atmospheric and KamLAND experiments constrain θ_{13} to be less than 0.2 rad at 3σ C.L. [105]. In order to keep track of the smallness of quantities, we introduce an auxiliary number $\lambda \equiv 0.2$ and define the small parameters to be of the form $a\lambda^n$. This allows us to perform a systematic expansion in powers of λ . For the sterile mixing angles, we define

$$\theta_{14} \equiv \chi_{14}\lambda \quad \theta_{24} \equiv \chi_{24}\lambda \quad \theta_{34} \equiv \chi_{34}\lambda \quad , \quad (2.6)$$

whereas for the active mixing angles, we define

$$\theta_{13} \equiv \chi_{13}\lambda \quad , \quad \theta_{23} \equiv \frac{\pi}{4} + \tilde{\theta}_{23} \equiv \frac{\pi}{4} + \chi_{23}\lambda \quad . \quad (2.7)$$

Here, all the χ_{ij} are taken to be $\mathcal{O}(1)$ quantities. We also treat the solar mixing angle, $\theta_{12} \approx 0.6$, as an $\mathcal{O}(1)$ quantity. The limits on the other θ_{ij} s mentioned above translate to $\chi_{24} < 0.6$, $\chi_{14}\chi_{24} < 0.5$, $\chi_{23} < 0.75$ and $\chi_{13} < 1$.

In the long baseline neutrino experiments, the dominating term in flavor conversions oscillates as $\sin^2[\Delta m_{\text{atm}}^2 L/(4E)]$. Owing to the small value of $\Delta m_{\odot}^2 L/(4E)$, the oscillations due to Δm_{\odot}^2 do not have enough time to develop, and the effect of Δm_{\odot}^2 may be viewed as a perturbation to the dominating Δm_{atm}^2 oscillations. We treat the ratio $\Delta m_{\odot}^2/|\Delta m_{\text{atm}}^2| \approx 0.03$ as a small parameter, and define

$$\Delta m_{21}^2/\Delta m_{32}^2 \equiv \eta\lambda^2 \quad . \quad (2.8)$$

Note that η is positive (negative) for the normal (inverted) neutrino mass ordering.

When neutrinos pass through the earth matter, there are matter effects that give rise to an effective potential $V_e = \sqrt{2}G_F N_e$ for the electron neutrino as

compared to the other neutrinos by virtue of the its charged current forward scattering interactions. Here G_F is the Fermi constant and N_e is the number density of electrons. In addition, all the active neutrinos also get an effective potential $V_n = -G_F N_n / \sqrt{2}$ compared to the sterile neutrino by virtue of their neutral current forward scattering reactions. Here N_n is the number density of neutrons. For anti-neutrinos, the signs of V_e and V_n are reversed. The effective Hamiltonian in the flavor basis is then

$$H_f \approx \frac{1}{2E} \left[\mathcal{U}_0 \begin{pmatrix} -\Delta m_{21}^2 & 0 & 0 & 0 \\ 0 & 0 & 0 & 0 \\ 0 & 0 & \Delta m_{32}^2 & 0 \\ 0 & 0 & 0 & \Delta m_{42}^2 \end{pmatrix} \mathcal{U}_0^\dagger + \begin{pmatrix} A_e + A_n & 0 & 0 & 0 \\ 0 & A_n & 0 & 0 \\ 0 & 0 & A_n & 0 \\ 0 & 0 & 0 & 0 \end{pmatrix} \right],$$

where $A_{e(n)} \equiv 2EV_{e(n)}$, and \mathcal{U}_0 is the 4×4 mixing matrix in vacuum, whose form is given in Eq. (2.2). Let H_f be diagonalized by a unitary matrix \mathcal{U}_m , such that

$$H_D = \mathcal{U}_m^\dagger H_f \mathcal{U}_m, \quad (2.9)$$

where H_D is the diagonal matrix. The elements $[H_D]_{ii}$, being the eigenvalues of H_f , give the relative values of $\tilde{m}_i^2 / (2E)$, where \tilde{m}_i are the effective masses of the interaction eigenstates in matter. If we assume that the density encountered by the neutrinos during their passage through the earth is a constant, the flavor conversion probabilities may be written in terms of \tilde{m}_i^2 and the elements of \mathcal{U}_m as

$$P_{\alpha\beta} \equiv P(\nu_\alpha \rightarrow \nu_\beta) = \left| \sum_i [\mathcal{U}_m]_{\alpha i} [\mathcal{U}_m]_{\beta i}^* \exp \left[i \frac{(-\tilde{m}_i^2)L}{2E} \right] \right|^2. \quad (2.10)$$

This approximation is valid as long as the neutrino trajectories do not pass through the core, and the neutrino energy is not close to the θ_{13} resonance energy in the earth.

In order to calculate \mathcal{U}_m , it is convenient to work in the basis of neutrino mass

eigenstates in vacuum. The effective Hamiltonian in this basis is

$$\begin{aligned}
 H_v &= \mathcal{U}_0^\dagger H_f \mathcal{U}_0 \\
 &= \left[\begin{pmatrix} -\frac{\Delta m_{21}^2}{2E} & 0 & 0 & 0 \\ 0 & 0 & 0 & 0 \\ 0 & 0 & \frac{\Delta m_{32}^2}{2E} & 0 \\ 0 & 0 & 0 & \frac{\Delta m_{42}^2}{2E} \end{pmatrix} + \mathcal{U}_0^\dagger \begin{pmatrix} \frac{A_e + A_n}{2E} & 0 & 0 & 0 \\ 0 & \frac{A_n}{2E} & 0 & 0 \\ 0 & 0 & \frac{A_n}{2E} & 0 \\ 0 & 0 & 0 & 0 \end{pmatrix} \mathcal{U}_0 \right],
 \end{aligned} \tag{2.11}$$

which can be diagonalized by the unitary matrix \tilde{U} defined through

$$\mathcal{U}_m = \mathcal{U}_0 \tilde{U} \tag{2.12}$$

such that

$$H_D = \tilde{U}^\dagger \mathcal{U}_0^\dagger H_f \mathcal{U}_0 \tilde{U} = \tilde{U}^\dagger H_v \tilde{U}. \tag{2.13}$$

Using the formal representation of the elements of \mathcal{U}_0 as well as Δm_{21}^2 in terms of λ as shown in Eqs. (2.6), (2.7), and (2.8), the matrix H_v can now be expanded formally in powers of λ as

$$H_v = \frac{\Delta m_{32}^2}{2E} [h_0 + \lambda h_1 + \lambda^2 h_2 + \mathcal{O}(\lambda^3)]. \tag{2.14}$$

The elements of $h_{0,1,2}$ are functions of all the neutrino mixing angles, mass squared differences and CP violating phases in general; the exact expressions are given in Appendix A. All the elements of the matrices h_1 and h_2 are of $\mathcal{O}(1)$ or smaller, so that the techniques of Rayleigh-Schrödinger perturbation theory can be used to calculate the eigenvalues and eigenvectors of H_v that are accurate up to $\mathcal{O}(\lambda^2)$. The complete set of four normalized eigenvectors gives the unitary matrix \tilde{U} that diagonalizes H_v through Eq. (2.13). Using Eq. (2.12), one obtains the unitary matrix \mathcal{U}_m that diagonalizes H_f through Eq. (2.9). The matrix \mathcal{U}_m and the eigenvalues of H_v (or H_f) allow us to calculate the neutrino flavor conversion probabilities from Eq. (2.10).

The flavor conversion probabilities of neutrinos, accurate to $\mathcal{O}(\lambda^2)$, obtained by assuming the neutrinos to travel through a constant matter density, are given in Appendix A. These expressions seem rather complicated. However, we can make certain approximations that will simplify these expressions and bring forth some important physical insights. Since we are interested in heavy sterile

neutrinos, we may take $|\Delta m_{32}^2| \ll |\Delta m_{42}^2|$. Also, since $|\Delta m_{32}^2 L/E| \sim \mathcal{O}(1)$, we have $|\Delta m_{42}^2 L/E| \gg 1$ and the oscillating terms of the form $\cos(\Delta m_{42}^2 L/E)$ may be averaged out. In the long baseline experiments, we are interested in the energy range 1–50 GeV. Even at the higher end of the energy spectrum, taking the density of the earth mantle to be ≈ 5 g/cc, we get $A_e \approx 2 \times 10^{-2}$ eV² and $A_n \approx -1 \times 10^{-2}$ eV² for neutrinos, so we also approximate $|A_{e,n}| \ll |\Delta m_{42}^2|$ wherever appropriate. With these approximations, the neutrino flavor conversion (or survival) probabilities for an initial ν_μ may be written as

$$P_{\mu e} \approx 2\theta_{13}^2 \Delta_{32}^2 \frac{\sin^2(\Delta_e - \Delta_{32})}{(\Delta_e - \Delta_{32})^2} + \mathcal{O}(\lambda^3), \quad (2.15)$$

$$\begin{aligned} P_{\mu\mu} \approx & \cos^2 \Delta_{32} + 4\tilde{\theta}_{23}^2 \sin^2 \Delta_{32} - \Delta_{21} \sin^2 \theta_{12} \sin 2\Delta_{32} \\ & + \frac{\theta_{13}^2 \Delta_{32}}{(\Delta_e - \Delta_{32})^2} \times \\ & \left\{ -2\Delta_{32} \cos \Delta_{32} \sin \Delta_e \sin(\Delta_e - \Delta_{32}) + \Delta_e(\Delta_e - \Delta_{32}) \sin 2\Delta_{32} \right\} \\ & - 2\theta_{24}^2 \cos^2 \Delta_{32} + 2\theta_{24}\theta_{34}\Delta_n \cos \delta_{24} \sin 2\Delta_{32} + \mathcal{O}(\lambda^3), \end{aligned} \quad (2.16)$$

$$\begin{aligned} P_{\mu\tau} \approx & \sin^2 \Delta_{32} - 4\tilde{\theta}_{23}^2 \sin^2 \Delta_{32} + \Delta_{21} \sin^2 \theta_{12} \sin 2\Delta_{32} \\ & + \frac{\theta_{13}^2 \Delta_{32}}{(\Delta_e - \Delta_{32})^2} \times \\ & \left\{ 2\Delta_{32} \sin \Delta_{32} \cos \Delta_e \sin(\Delta_e - \Delta_{32}) - \Delta_e(\Delta_e - \Delta_{32}) \sin 2\Delta_{32} \right\} \\ & - (\theta_{24}^2 + \theta_{34}^2) \sin^2 \Delta_{32} - \theta_{24}\theta_{34} (2\Delta_n \cos \delta_{24} + \sin \delta_{24}) \sin 2\Delta_{32} + \mathcal{O}(\lambda^3), \end{aligned} \quad (2.17)$$

where we have defined the dimensionless quantities $\Delta_{ij} \equiv \Delta m_{ij}^2 L/(4E)$ and $\Delta_{e,n} \equiv A_{e,n} L/(4E)$ for convenience. The following observations may be made from the above expressions:

- The leading $\mathcal{O}(1)$ terms are of the form $\sin^2 \Delta_{32}$ or $\cos^2 \Delta_{32}$, corresponding to the dominating atmospheric neutrino oscillations. There is no subleading term of $\mathcal{O}(\lambda)$.
- For $P_{\mu e}$, there is no sterile contribution up to $\mathcal{O}(\lambda^2)$. Indeed, the leading order sterile contribution to $P_{\mu e}$ is proportional to $\theta_{14}^2 \theta_{24}^2$, which is $\mathcal{O}(\lambda^4)$.
- In the expression for $P_{\mu\mu}$ or $P_{\mu\tau}$, the first line contains the leading oscillating term as well as the subleading terms due to the deviation of θ_{23} from maximality and due to the nonzero value of Δm_{21}^2 . The next

line gives the contribution from θ_{13}^2 , which matches the one obtained in [106]. The last line contains the contribution from sterile neutrinos. Whereas it is enough to have either θ_{24} or θ_{34} nonzero for the sterile mixing to have an effect on $P_{\mu\tau}$, the sterile contribution to $P_{\mu\mu}$ will be present only for nonzero θ_{24} .

- Only one CP violating phase, δ_{24} , is relevant for the flavor conversion probabilities up to this order. The phases δ_{13} and δ_{14} appear only at $\mathcal{O}(\lambda^3)$ or higher. In particular, the CP violating terms proportional to $(\Delta m_{21}^2/\Delta m_{32}^2)\theta_{13}$, as given in [106], are absent since they are of $\mathcal{O}(\lambda^3)$.
- Note that the leading sterile contribution at the long baseline experiments is found to be at $\mathcal{O}(\lambda^2)$. This may be compared with the CP violation in the active sector, whose leading contribution appears at $\mathcal{O}(\lambda^3)$ and the short baseline appearance experiments, whose positive results would appear only at $\mathcal{O}(\lambda^4)$ or higher. The $\mathcal{O}(\lambda^2)$ sterile contribution to $P_{\mu\tau}$, which is proportional to $\sin \Delta_{32}$, is absent in the short baseline appearance experiments where in general $|\Delta_{42}| \sim \mathcal{O}(1)$ and $|\Delta_{32}| \ll 1$, so that $\sin \Delta_{32} \approx 0$. MARK
- When $\Delta_e \approx \Delta_{32}$, the θ_{13} contribution is enhanced due to the factor $(\Delta_e - \Delta_{32})^{-2}$. The analytical approximation is expected to fail in this region since even the higher order terms in θ_{13} may become significant.
- The analytic expressions are not expected to be valid for large L/E where Δ_{21} would become $\mathcal{O}(\lambda)$ and higher order terms in Δ_{21} would also contribute to the probability in Eqs. (2.16) and (2.17) at $\mathcal{O}(\lambda^2)$.
- The probabilities given in Eqs. (2.15), (2.16) and (2.17) do not involve Δm_{st}^2 , and have no information on whether the mainly sterile neutrino ν_4 is heavier or lighter than the other three. This is due to our approximation of averaging out the fast oscillations due to Δm_{st}^2 . This approximation will be more and more accurate as Δm_{st}^2 increases.

The probabilities for the antiparticles are obtained simply by replacing $\Delta_{e,n} \rightarrow -\Delta_{e,n}$ and $\delta_{ij} \rightarrow -\delta_{ij}$. The sterile contribution to the CP violation is therefore

given by

$$P_{\mu\mu} - P_{\bar{\mu}\bar{\mu}} \approx (P_{\mu\mu} - P_{\bar{\mu}\bar{\mu}})_{3\nu} + 4\theta_{24}\theta_{34}\Delta_n \cos \delta_{24} \sin 2\Delta_{32} , \quad (2.18)$$

$$P_{\mu\tau} - P_{\bar{\mu}\bar{\tau}} \approx (P_{\mu\tau} - P_{\bar{\mu}\bar{\tau}})_{3\nu} - 4\theta_{24}\theta_{34}\Delta_n \cos \delta_{24} \sin 2\Delta_{32} \\ - 2\theta_{24}\theta_{34} \sin \delta_{24} \sin 2\Delta_{32} . \quad (2.19)$$

The CP violating contribution of sterile neutrinos to $P_{\mu\mu} - P_{\bar{\mu}\bar{\mu}}$ is entirely from the earth matter effects, whereas for $P_{\mu\tau} - P_{\bar{\mu}\bar{\tau}}$, the contribution comes from both the earth matter effects (through the Δ_n term) as well as the vacuum mixing matrix \mathcal{U}_0 (from the $\sin \delta_{24}$ term).

For an initial ν_e , the relevant neutrino flavor conversion probabilities are

$$P_{ee} \approx 1 - 4\theta_{13}^2\Delta_{32}^2 \frac{\sin^2(\Delta_e - \Delta_{32})}{(\Delta_e - \Delta_{32})^2} - 2\theta_{14}^2 + \mathcal{O}(\lambda^3) , \quad (2.20)$$

$$P_{e\mu} \approx 2\theta_{13}^2\Delta_{32}^2 \frac{\sin^2(\Delta_e - \Delta_{32})}{(\Delta_e - \Delta_{32})^2} + \mathcal{O}(\lambda^3) , \quad (2.21)$$

$$P_{e\tau} \approx 2\theta_{13}^2\Delta_{32}^2 \frac{\sin^2(\Delta_e - \Delta_{32})}{(\Delta_e - \Delta_{32})^2} + \mathcal{O}(\lambda^3) , \quad (2.22)$$

where we have used the approximations $|\Delta_{e,n}| \ll |\Delta_{42}|$, and have averaged out terms that oscillate as fast as $\sin \Delta_{42}$. The complete expressions accurate to $\mathcal{O}(\lambda^2)$ may be found in Appendix A. Clearly, sterile neutrinos have no effect at this order on these probabilities except on P_{ee} , and there is no sterile contribution to the CP violation in any of these three channels.

We demonstrate the validity (and limitations) of our analytic approximations in Fig. 2.1, where we show $P_{\mu\mu}$ and $P_{\mu\tau}$ as a function of energy for three baselines, 3000 km, 7000 km and 10000 km. In each panel, we show the probabilities with $\theta_{14} = \theta_{24} = \theta_{34} = 0.2$ rad and $\theta_{13} = 0$, for $\Delta m_{\text{st}}^2 = 0.1$ eV² and $\Delta m_{\text{st}}^2 = 1$ eV²: the complete 4-neutrino numerical simulation with the Preliminary Reference Earth Model (PREM) [72] for the density of the earth, as well as our analytical approximation that uses the average density along the path of the neutrino and averages out the high frequency approximations.¹ In order to estimate whether nonzero θ_{13} can mimic the signatures of sterile mixing, we also show the probability for all the sterile mixing angles vanishing, but $\theta_{13} = 0.2$ rad.

¹For a baseline of 10000 km, we only show $\Delta m_{\text{st}}^2 = 0.1$ eV², otherwise the oscillation frequency would be too high.

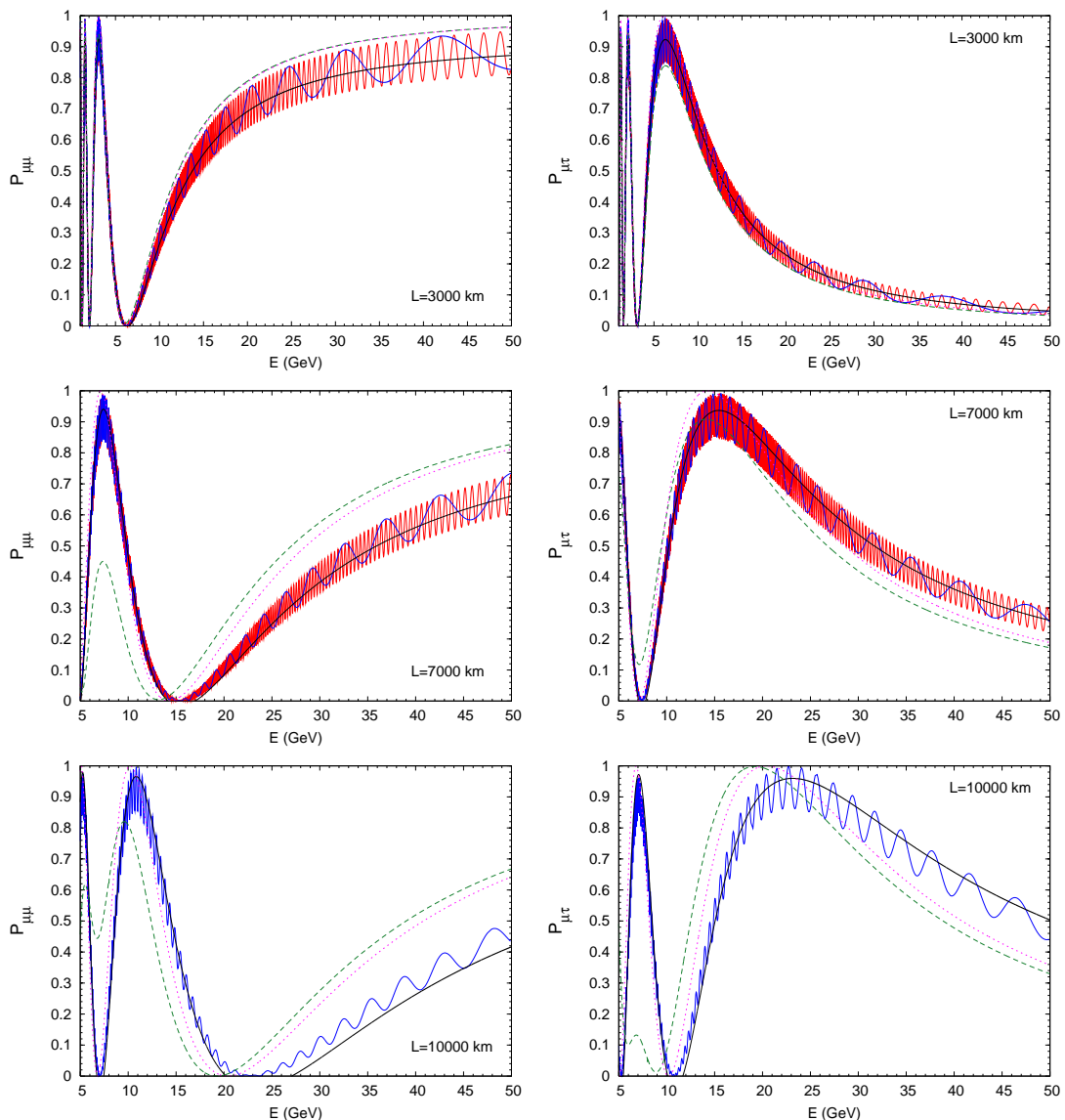


Figure 2.1: Probabilities $P_{\mu\mu}$ and $P_{\mu\tau}$ as functions of energy, and the comparisons with the analytic expressions in Eqs. (2.16) and (2.17). In all the plots, we take $\Delta m_{\odot}^2 = 8 \times 10^{-5}$ eV², $\Delta m_{\text{atm}}^2 = 2.5 \times 10^{-3}$ eV², $\theta_{23} = 45^\circ$, and $\theta_{12} = 33.2^\circ$. The magenta (dotted) curve corresponds to the situation with no sterile contribution and vanishing θ_{13} . The blue (red) curve with rapid (extremely rapid) oscillations corresponds to $\Delta m_{\text{st}}^2 = 0.1$ (1.0) eV², with $\theta_{14} = \theta_{24} = \theta_{34} = 0.2$ rad and $\theta_{13} = 0$. The black curve that passes through the rapidly oscillating curves denotes the analytical approximation, which is independent of the value of Δm_{st}^2 since the high frequency oscillations are averaged out. The green (dashed) curve represents the situation with $\theta_{14} = \theta_{24} = \theta_{34} = 0$, but $\theta_{13} = 0.2$ rad.

The following observations may be made:

- The analytical approximation agrees well with the average of the exact numerical results for $L = 3000$ km and 7000 km. For $L = 10000$ km, though the analytic approximation predicts the qualitative behavior of the averaged probabilities, the exact numerical values have an error of $\sim 5\%$. This is due to the large L making $\Delta_{21} \sim \mathcal{O}(\lambda)$ in the energy range under consideration, so that higher order terms in Δ_{21}^2 contribute to the probabilities in Eqs. (2.16) and (2.17).
- The dominant effect of the sterile contribution is to pull down the value of $P_{\mu\mu}$, which mimics the deviation of θ_{23} from its maximal value. Such a mimicking is also possible through a nonzero θ_{13} , however the effect of θ_{i4} may be significantly larger, beyond what is possible with the current limit on θ_{13} . Moreover, at energies much larger than the θ_{13} resonance, the θ_{13} contribution is suppressed by the factor $\Delta_{32}/(\Delta_e - \Delta_{32})$ in earth matter, whereas the sterile contribution does not undergo any suppression since $|\Delta_n| \ll |\Delta_{42}|$ in the whole energy range of interest. One therefore expects that distinguishing the sterile contribution would be easier at high energies.
- Sterile contribution to $P_{\mu\mu}$ as well as $P_{\mu\tau}$ is larger at longer baselines, due to the Δ_n term present in the Eqs. (2.16) and (2.17), which increases with increasing L . On the other hand, at low L/E values, the sterile contribution to $P_{\mu\tau}$ is highly suppressed by the factor $\sin \Delta_{32}$ in Eq. (2.17).

2.3 Signatures at long baseline experiments

The analytical expressions given in Eqs. (2.15)–(2.17) indicate that at $E \gtrsim 10$ GeV where $|\Delta_e| \gg |\Delta_{32}|$, the contribution of the currently unknown θ_{13} is suppressed by a factor $\sim \Delta_{32}/\Delta_e$. There is no such suppression for the sterile contribution, since $|\Delta_{e,n}| \ll |\Delta_{42}|$ for $E < 50$ GeV. For $E \sim 5$ – 10 GeV, the earth matter effects cause an enhancement through the factor $(\Delta_e - \Delta_{32})^{-2}$. This energy range is therefore unsuitable for searching for a sterile contribution to the conversion probabilities. At $E < 5$ GeV also, since the contribution due to the currently unknown θ_{13} is at least of the same order

as the maximum allowed sterile contribution, discriminating between θ_{13} and sterile contributions to the probabilities would need data from more than one experiment. A high energy neutrino experiment is therefore preferred.

In order to demonstrate the capability of future long baseline experiments in distinguishing the sterile neutrino contribution to the neutrino flavor conversion probabilities, we choose a typical neutrino factory setup [107], with a 50 GeV muon beam directed to a 0.5 kt “near” detector 1 km away, and a 50 kt “far” detector 7000 km away. The detectors may be magnetized iron calorimeters [108], which can identify the charge of the lepton produced from the charged current interaction of the neutrino or anti-neutrino. The number of useful muons in the storage ring is taken to be $1.066 \cdot 10^{21}$, which corresponds to approximately two years of running with μ^- and μ^+ each at the neutrino factory, using the NuFact-II parameters in [71]. We implement the propagation of the neutrinos through the earth using the 5-density model of the Earth, where the density of each layer has been taken to be the average of the densities encountered by the neutrinos along their path in that layer with the PREM profile [72]. We take care of the detector characteristics using the General Long Baseline Experiment Simulator (GLOBES) [73, 74]. The cross-sections used are taken from [109, 110] and the simulation includes an energy resolution of $\sigma_E/E = 15\%$, an overall detection efficiency of 75% for all charged leptons, as well as additional energy dependent post-efficiencies that are taken care of bin-by-bin. We assume perfect lepton charge identification, and neglect any error due to wrong sign leptons produced from the oscillations of the antiparticles. These can be taken care of in the complete simulation of the detector once its detailed characteristics are known.

In Fig. 2.2, we display the asymmetries

$$\mathcal{A}_\mu(E) \equiv \frac{N_\mu^{\text{far}}(E)}{N_\mu^{\text{near}}(E)} - \frac{\overline{N}_\mu^{\text{far}}(E)}{\overline{N}_\mu^{\text{near}}(E)}, \quad \mathcal{A}_\tau(E) \equiv \frac{N_\tau^{\text{far}}(E)}{N_\mu^{\text{near}}(E)} - \frac{\overline{N}_\tau^{\text{far}}(E)}{\overline{N}_\mu^{\text{near}}(E)}, \quad (2.23)$$

where N_ℓ (\overline{N}_ℓ) is the number of ℓ^- (ℓ^+) observed at the near or far detector. These asymmetries roughly correspond to $\mathcal{A}_\mu \approx P_{\mu\mu} - P_{\bar{\mu}\bar{\mu}}$ and $\mathcal{A}_\tau \approx P_{\mu\tau} - P_{\bar{\mu}\bar{\tau}}$, where the events observed in the near detector act as a normalizing factor, and help in canceling out the systematic errors due to fluxes, cross sections and efficiencies in each energy bin. Note that we do not expect any τ^\pm at the near detector, hence the number of events of τ^\pm at the far detector needs to be

normalized to the number of events of μ^\pm at the near detector.

In the absence of any sterile neutrinos, and in the limit of vanishing θ_{13} , the asymmetries \mathcal{A}_μ and \mathcal{A}_τ vanish, as can be seen from Eqs. (2.16) and (2.17). The θ_{13} contribution is indeed suppressed at high energies, as discussed above. In the figure, we show a band corresponding to the possible signals in the absence of any sterile neutrinos, where we vary over the allowed values of the angles θ_{23}, θ_{13} , the CP phase δ_{13} and both the normal as well as inverted mass ordering. For $\Delta m_{\text{atm}}^2, \Delta m_{\odot}^2$ and θ_{12} we only take the current best-fit values, since the variation in these parameters is not expected to cause any significant change in our results. We choose to take $\theta_{24} = \theta_{34}$ and $\delta_{24} = 0$ for illustration, since from the Eqs. (2.18) and (2.19) we expect the asymmetries to be identical in magnitude and proportional to the product $\theta_{24}\theta_{34}$ with vanishing δ_{24} . Any discrepancy between these two asymmetries would indicate a nonzero δ_{24} , and hence CP violation in the sterile sector. The third sterile mixing angle, θ_{14} , is taken to be vanishing since it is not expected to affect the relevant neutrino conversions.

It may be observed from Fig. 2.2 that for $E > 15$ GeV, the sterile contribution results in an deficit (excess) of the asymmetry for normal (inverted) hierarchy in the μ channel. In the τ channel, the situation is the reverse. This is as expected from our analytic expressions in Eqs. (2.18) and (2.19). The asymmetry integrated over energy may therefore be expected to serve as an efficient discriminator between the scenarios with and without sterile neutrinos. In Fig. 2.3, we show the integrated asymmetries

$$\begin{aligned}\tilde{\mathcal{A}}_\mu &\equiv \frac{N_\mu^{\text{far}}(E > 15\text{GeV})}{N_\mu^{\text{near}}(E > 15\text{GeV})} - \frac{\overline{N}_\mu^{\text{far}}(E > 15\text{GeV})}{\overline{N}_\mu^{\text{near}}(E > 15\text{GeV})}, \\ \tilde{\mathcal{A}}_\tau &\equiv \frac{N_\tau^{\text{far}}(E > 15\text{GeV})}{N_\mu^{\text{near}}(E > 15\text{GeV})} - \frac{\overline{N}_\tau^{\text{far}}(E > 15\text{GeV})}{\overline{N}_\mu^{\text{near}}(E > 15\text{GeV})}.\end{aligned}\quad (2.24)$$

The figure indicates that for $\theta_{24}\theta_{34} \gtrsim 0.005$, the sterile contribution to neutrino conversions can be discernable from the three neutrino mixing results at 3σ C.L. in the worst case scenario. The width of the band is determined essentially by the allowed range of θ_{13} . If the value of θ_{13} is bounded further, the reach of neutrino factories for the sterile mixing is enhanced. In addition, the actual value of θ_{13} also affects the discovery potential of sterile mixing by influencing the integrated asymmetries $\tilde{\mathcal{A}}_\mu, \tilde{\mathcal{A}}_\tau$, as shown in the figure. Note that since the

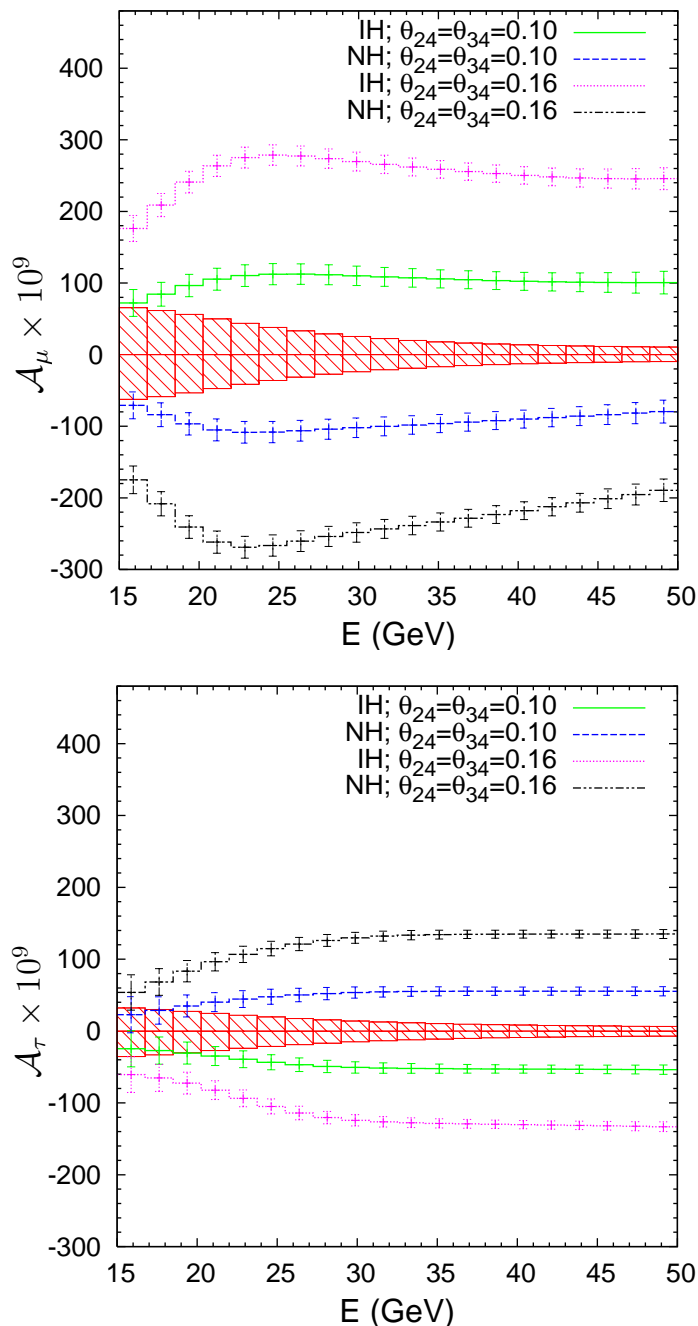


Figure 2.2: The asymmetries $\mathcal{A}_\mu(E)$ and $\mathcal{A}_\tau(E)$ as functions of energy at a neutrino factory. The band corresponds to allowed values of the asymmetries without any sterile mixing, with θ_{23} , θ_{13} and δ_{13} allowed to vary over all their allowed ranges, and with both the normal (NH) and inverted (IH) hierarchies. The plots for showing the dependence on sterile components are with $\theta_{23} = \pi/4$, $\delta_{24} = 0$, and $\Delta m_{42}^2 = 0.1 \text{ eV}^2$. The results will not change if Δm_{42}^2 has higher values. No significant dependence on θ_{14} is expected from the Eqs. (2.16) and (2.17), hence we use $\theta_{14} = 0$. The errors shown are only statistical.

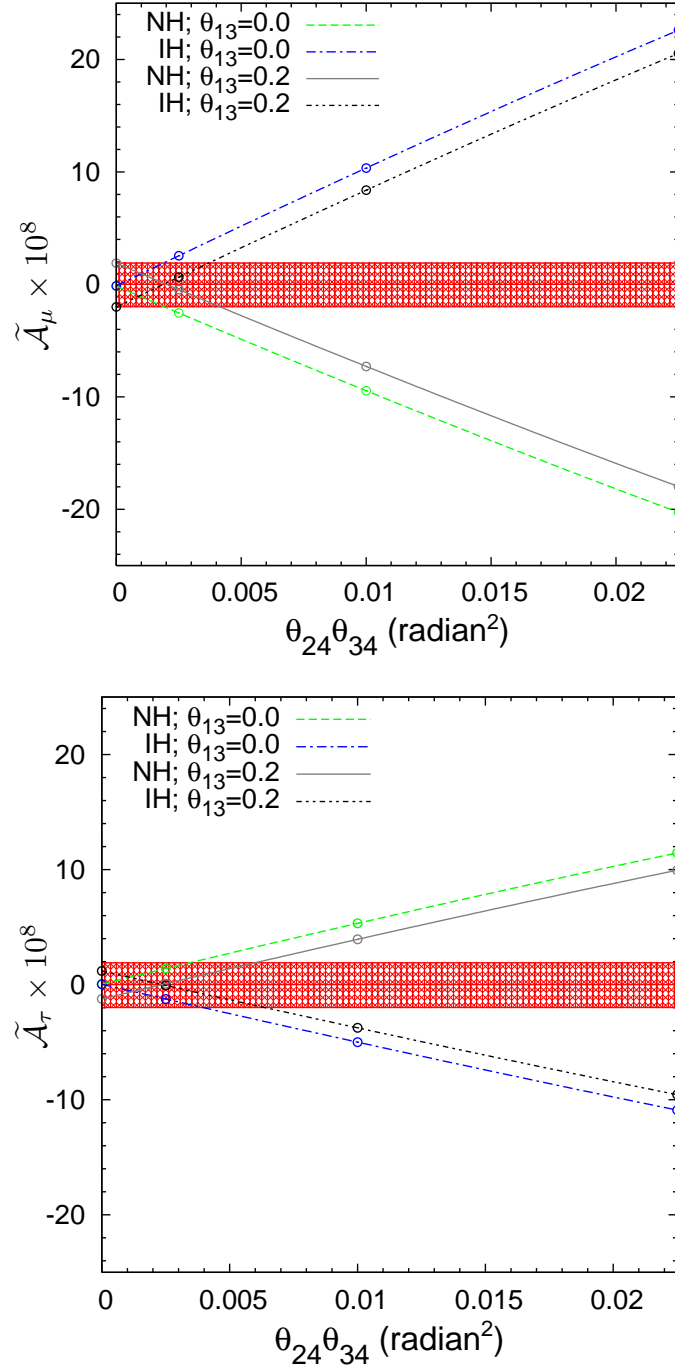


Figure 2.3: The integrated asymmetries $\tilde{\mathcal{A}}_\mu$ and $\tilde{\mathcal{A}}_\tau$ as functions of sterile mixing parameters at a neutrino factory. We use $\theta_{24} = \theta_{34}$ and $\delta_{24} = 0$. The rest of the parameters are the same as in Fig. 2.2. The statistical errors are smaller than the circles shown in the plots.

asymmetries depend on the sign of Δm_{32}^2 , sterile mixing also makes it possible to distinguish between normal and inverted hierarchies.

If we have a 50 kt detector that can detect e^-/e^+ and identify their charge², we can use the observable

$$\mathcal{R}_e(E) \equiv \frac{N_e^{\text{far}}(E)}{N_e^{\text{near}}(E)} \quad (2.25)$$

and the integrated quantity

$$\tilde{\mathcal{R}}_e \equiv \frac{N_e^{\text{far}}(E > 25\text{GeV})}{N_e^{\text{near}}(E > 25\text{GeV})} \quad (2.26)$$

for detecting the sterile neutrino contribution. Note that there is no difference between the two hierarchies, or between ν_e and $\bar{\nu}_e$, as far as the expected probabilities are concerned. From Fig. 2.4, it may be seen that for $\theta_{14} \gtrsim 0.06$, the sterile mixing signals can be clearly discerned at 3σ C.L. in worst case scenario. If the bound on θ_{13} becomes stronger, even smaller values of θ_{14} may be identified. On the other hand, an higher actual value of θ_{13} helps in the identification of sterile mixing even at lower θ_{14} values.

The ‘‘platinum’’ channel $P_{\mu e}$ at the neutrino factories is not affected by the sterile mixing, not just to $\mathcal{O}(\lambda^2)$, but even at $\mathcal{O}(\lambda^3)$. Indeed, going to one higher order in the λ -perturbation, we get

$$\begin{aligned} P_{\mu e} = & \frac{\Delta_{32}^2 \sin^2(\Delta_e - \Delta_{32})}{(\Delta_e - \Delta_{32})^2} \left[2\theta_{13}^2 + 4\theta_{13}^2(\tilde{\theta}_{23} - \theta_{13}) \right] \\ & + 2\theta_{13}\Delta_{21}\Delta_{32} \sin(2\theta_{12}) \sin\Delta_{32} \frac{\cos(\Delta_e - \Delta_{32} - \delta_{13})}{(\Delta_e - \Delta_{32})} \cdot \frac{\sin\Delta_e}{\Delta_e} + \mathcal{O}(\lambda^4). \end{aligned} \quad (2.27)$$

For getting $P_{\bar{\mu} \bar{e}}$, one just needs to replace $\Delta_e \rightarrow -\Delta_e$ and $\delta_{13} \rightarrow -\delta_{13}$. Thus this channel, being free of any sterile contaminations to $\mathcal{O}(\lambda^3)$, is suitable for determining the parameters in the standard three flavor analysis. Nevertheless, the neutrino factory will be able to probe the $P_{\mu e}$ channel upto an accuracy of 10^{-4} and hence may be useful in putting bounds on the $\mathcal{O}(\lambda^4)$ sterile

²Charge identification is needed in order to get rid of the error due to misidentification of the wrong sign leptons produced due to $\nu_\mu \rightarrow \nu_e$ or $\bar{\nu}_\mu \rightarrow \bar{\nu}_e$ oscillations. A magnetized iron calorimeter with thin iron strips, or a liquid Ar detector [111, 112], may serve the purpose. If charge identification is not possible, as in a water Cherenkov detector for example, the background due to the wrong sign lepton will have to be taken into account.

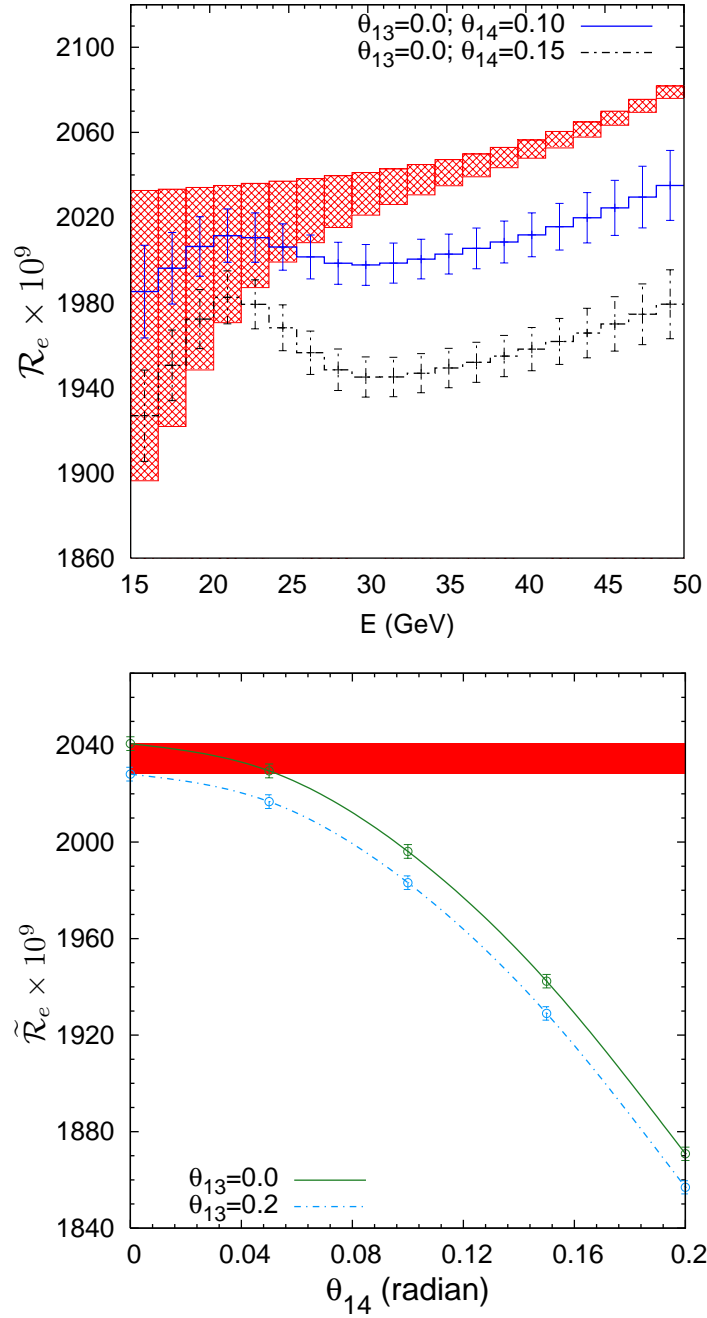


Figure 2.4: The observables $\mathcal{R}_e(E)$ and $\tilde{\mathcal{R}}_e$ at a neutrino factory, where e^-/e^+ and their charge may be identified. The active neutrino mixing parameters are the same as that in Fig. 2.2. The sterile mixing parameters are taken to be $\theta_{24} = \theta_{34} = 0$ and $\Delta m_{42}^2 = 0.1 \text{ eV}^2$. Any increase in Δm_{42}^2 , or nonzero value of θ_{24}/θ_{34} are not expected to have any significant effect on this observable. The result is insensitive to $\text{sgn}(\Delta m_{32}^2)$.

contributions.

2.4 Generalization to any number of sterile neutrinos

If the LSND results [6] are taken to be valid, a single sterile neutrino is not enough to describe all the data from short baseline experiments. However, two or more sterile neutrinos with $\Delta m_{j1}^2 \sim 1$ eV ($j > 3$) and $|\mathcal{U}_{ej}\mathcal{U}_{\mu j}| \sim \mathcal{O}(0.01-0.1)$ are consistent with all data [18]. Some avenues for probing the mixing parameters and distinguishing between different mass orderings in such a case have already been suggested [84, 113, 114]. It is therefore desirable to extend our formalism to more sterile neutrinos.

The analytical treatment in Sec. 2.2 for the case of one sterile neutrino may be generalized easily to any arbitrary number n of sterile neutrinos. The $(3+n) \times (3+n)$ mixing matrix \mathcal{U}_{3+n} may be written in the block form as

$$\begin{aligned} \mathcal{U}_{3+n} &\equiv \begin{pmatrix} [U^{AA}]_{3 \times 3} & [U^{AS}]_{3 \times n} \\ [U^{SA}]_{n \times 3} & [U^{SS}]_{n \times n} \end{pmatrix} \\ &\equiv \mathcal{W} \cdot \mathcal{V} \equiv \begin{pmatrix} [W^{AA}]_{3 \times 3} & [W^{AS}]_{3 \times n} \\ [W^{SA}]_{n \times 3} & [W^{SS}]_{n \times n} \end{pmatrix} \begin{pmatrix} [V^{AA}]_{3 \times 3} & [0]_{3 \times n} \\ [0]_{n \times 3} & [V^{SS}]_{n \times n} \end{pmatrix}, \end{aligned} \tag{2.28}$$

where $V^{AA} \equiv U_{23}(\theta_{23}, 0) U_{13}(\theta_{13}, \delta_{13}) U_{12}(\theta_{12}, 0)$ is the standard mixing matrix for three active neutrino flavors, and V^{SS} is the matrix that mixes the n sterile neutrinos among themselves. Since the assignment of “flavor” eigenstates to the sterile species is arbitrary, we choose the basis such that the flavor and mass eigenstates of the sterile neutrinos coincide in the absence of any active-sterile mixing, i.e. $V^{SS} = I_{n \times n}$. The matrix \mathcal{W} parameterizes the mixing between active and sterile states, and in general may be represented by a product of matrices $U_{ij}(\theta_{ij}, \delta_{ij})$ as defined in Eq. (2.3), with $i \leq 3$ and $j > 3$.

In addition, we assume that all the active-sterile mixing is small, which is borne out by the recent 3+2 neutrino fit to LSND, MiniBooNE as well as the

short baseline disappearance data [18]. This allows us to write

$$W^{AS} \equiv \begin{pmatrix} [W^{eS}]_{1 \times n} \\ [W^{\mu S}]_{1 \times n} \\ [W^{\tau S}]_{1 \times n} \end{pmatrix} \equiv \lambda \begin{pmatrix} [X^{eS}]_{1 \times n} \\ [X^{\mu S}]_{1 \times n} \\ [X^{\tau S}]_{1 \times n} \end{pmatrix} \equiv \lambda X^{AS}. \quad (2.29)$$

If terms of $\mathcal{O}(\lambda^3)$ and smaller are neglected, the unitary matrix \mathcal{W} may be written in its most general form as

$$\mathcal{W} = \begin{pmatrix} \left[I - \lambda^2 \frac{X^{AS}(X^{AS})^\dagger}{2} \right]_{3 \times 3} & [\lambda X^{AS}]_{3 \times n} \\ [-\lambda (X^{AS})^\dagger]_{n \times 3} & \left[I - \lambda^2 \frac{(X^{AS})^\dagger X^{AS}}{2} \right]_{n \times n} \end{pmatrix} + \mathcal{O}(\lambda^3). \quad (2.30)$$

The net leptonic mixing matrix \mathcal{U}_{3+n} in Eq. (2.28) can then be written as

$$\mathcal{U}_{3+n} = \begin{pmatrix} \left[\left(I - \frac{W^{AS}(W^{AS})^\dagger}{2} \right) V^{AA} \right]_{3 \times 3} & [W^{AS}]_{3 \times n} \\ [-(W^{AS})^\dagger V^{AA}]_{n \times 3} & \left[I - \frac{(W^{AS})^\dagger W^{AS}}{2} \right]_{n \times n} \end{pmatrix} + \mathcal{O}(\lambda^3). \quad (2.31)$$

For the active mixing angles in V^{AA} , we use the same λ -expansion as in Eq. (2.7), i.e. $\theta_{13} \equiv \chi_{13}\lambda$ and $\theta_{23} \equiv \pi/4 + \tilde{\theta}_{23} \equiv \pi/4 + \chi_{23}\lambda$. We also treat $\Delta m_{21}^2/\Delta m_{32}^2$ to be a small quantity, and denote it formally by $\Delta m_{21}^2/\Delta m_{32}^2 \equiv \eta\lambda^2$, as in Eq. (2.8). The quantities η, χ_{ij} as well as all the elements of X^{AS} are taken to be $\mathcal{O}(1)$ parameters.

Following the same systematic expansion procedure delineated in Sec. 2.2 in the case of one sterile neutrino, we obtain the neutrino flavor conversion (or survival) probabilities for an initial ν_μ beam to be

$$P_{\mu e} \approx 2\theta_{13}^2 \Delta_{32}^2 \frac{\sin^2(\Delta_e - \Delta_{32})}{(\Delta_e - \Delta_{32})^2} + \mathcal{O}(\lambda^3), \quad (2.32)$$

$$\begin{aligned} P_{\mu\mu} \approx & \cos^2 \Delta_{32} + 4\tilde{\theta}_{23}^2 \sin^2 \Delta_{32} - \Delta_{21} \sin^2 \theta_{12} \sin 2\Delta_{32} + \frac{\theta_{13}^2 \Delta_{32}}{(\Delta_e - \Delta_{32})^2} \times \\ & \left\{ -2\Delta_{32} \cos \Delta_{32} \sin \Delta_e \sin(\Delta_e - \Delta_{32}) + \Delta_e(\Delta_e - \Delta_{32}) \sin 2\Delta_{32} \right\} \\ & - 2[W^{\mu S}(W^{\mu S})^\dagger] \cos^2 \Delta_{32} + 2\text{Re}[W^{\tau S}(W^{\mu S})^\dagger] \Delta_n \sin 2\Delta_{32} + \mathcal{O}(\lambda^3), \end{aligned} \quad (2.33)$$

$$\begin{aligned}
P_{\mu\tau} \approx & \sin^2 \Delta_{32} - 4\tilde{\theta}_{23}^2 \sin^2 \Delta_{32} + \Delta_{21} \sin^2 \theta_{12} \sin 2\Delta_{32} + \frac{\theta_{13}^2 \Delta_{32}}{(\Delta_e - \Delta_{32})^2} \times \\
& \left\{ 2\Delta_{32} \sin \Delta_{32} \cos \Delta_e \sin (\Delta_e - \Delta_{32}) - \Delta_e (\Delta_e - \Delta_{32}) \sin 2\Delta_{32} \right\} \\
& - ([W^{\mu S}(W^{\mu S})^\dagger] + [W^{\tau S}(W^{\tau S})^\dagger]) \sin^2 \Delta_{32} \\
& - 2\text{Re}[W^{\tau S}(W^{\mu S})^\dagger] \Delta_n \sin 2\Delta_{32} - \text{Im}[W^{\tau S}(W^{\mu S})^\dagger] \sin 2\Delta_{32} + \mathcal{O}(\lambda^3) .
\end{aligned} \tag{2.34}$$

Here we have assumed $|\Delta m_{32}^2|, |A_{e,n}| \ll |\Delta m_{42}^2|$, and have averaged out the oscillating terms of the form $\cos(\Delta m_{42}^2 L/E)$, as before. The sterile contribution to the CP violation in these channels is then

$$P_{\mu\mu} - P_{\bar{\mu}\bar{\mu}} \approx (P_{\mu\mu} - P_{\bar{\mu}\bar{\mu}})_{3\nu} + 4\text{Re}[W^{\tau S}(W^{\mu S})^\dagger] \Delta_n \sin 2\Delta_{32} , \tag{2.35}$$

$$\begin{aligned}
P_{\mu\tau} - P_{\bar{\mu}\bar{\tau}} \approx & (P_{\mu\tau} - P_{\bar{\mu}\bar{\tau}})_{3\nu} - 4\text{Re}[W^{\tau S}(W^{\mu S})^\dagger] \Delta_n \sin 2\Delta_{32} \\
& - 2\text{Im}[W^{\tau S}(W^{\mu S})^\dagger] \sin 2\Delta_{32} .
\end{aligned} \tag{2.36}$$

For an initial ν_e beam, the corresponding flavor conversion probabilities are

$$P_{ee} \approx 1 - 4\theta_{13}^2 \Delta_{32}^2 \frac{\sin^2(\Delta_e - \Delta_{32})}{(\Delta_e - \Delta_{32})^2} - 2[W^{eS}(W^{eS})^\dagger] + \mathcal{O}(\lambda^3) , \tag{2.37}$$

$$P_{e\mu} \approx 2\theta_{13}^2 \Delta_{32}^2 \frac{\sin^2(\Delta_e - \Delta_{32})}{(\Delta_e - \Delta_{32})^2} + \mathcal{O}(\lambda^3) , \tag{2.38}$$

$$P_{e\tau} \approx 2\theta_{13}^2 \Delta_{32}^2 \frac{\sin^2(\Delta_e - \Delta_{32})}{(\Delta_e - \Delta_{32})^2} + \mathcal{O}(\lambda^3) . \tag{2.39}$$

The mixing matrix \mathcal{U}_{3+n} in Eq. (2.31) reduces to the 4×4 mixing matrix \mathcal{U}_4 given in Eq. (2.2) in the case of one sterile neutrino simply by taking $n = 1$ and using the substitution

$$W^{eS} \rightarrow \theta_{14} e^{-i\delta_{14}} , \quad W^{\mu S} \rightarrow \theta_{24} e^{-i\delta_{24}} , \quad W^{\tau S} \rightarrow \theta_{34} . \tag{2.40}$$

As a result, the bounds obtained on $\theta_{14}, \theta_{24}, \theta_{34}$ and δ_{24} in the 4-neutrino analysis can be directly translated to bounds on the combinations $[W^{eS}(W^{eS})^\dagger]$, $[W^{\mu S}(W^{\mu S})^\dagger]$, $[W^{\tau S}(W^{\tau S})^\dagger]$ and the real and imaginary parts of $[W^{\tau S}(W^{\mu S})^\dagger]$. Note that the expressions in Eqs. (2.15)–(2.22) obtained in the special case of only one sterile neutrino can be obtained from the general expressions in Eqs. (2.32)–(2.39) simply with the substitutions (2.40). Specifically, the bounds obtained on $\theta_{24}\theta_{34}$ in Sec. 2.3 using the observables $\tilde{\mathcal{A}}_\mu, \tilde{\mathcal{A}}_\tau$ are simply

bounds on $\text{Re}[W^{\tau S}(W^{\mu S})^\dagger]$. Similarly, the bound obtained on θ_{14} through $\tilde{\mathcal{R}}_e$ is simply the bound on $[W^{eS}(W^{eS})^\dagger]^{1/2}$.

The above argument also implies that, at least in the region of validity of our analytic approximations, the only combinations of active-sterile mixing parameters that may be bounded by data are the four quantities $[W^{eS}(W^{eS})^\dagger]$, $[W^{\mu S}(W^{\mu S})^\dagger]$, $[W^{\tau S}(W^{\tau S})^\dagger]$ and $[W^{\tau S}(W^{\mu S})^\dagger]$, irrespective of the number of sterile species. For example, in the 3+2 scenario, the mixing matrix $\mathcal{U} \equiv \mathcal{U}_5$ may be written as

$$\begin{aligned} \mathcal{U}_5 = & U_{45}(\theta_{45}, \delta_{45}) \cdot U_{35}(\theta_{35}, \delta_{35}) \cdot U_{25}(\theta_{25}, \delta_{25}) \cdot U_{15}(\theta_{15}, \delta_{15}) \cdot U_{34}(\theta_{34}, \delta_{34}) \cdot \\ & U_{24}(\theta_{24}, \delta_{24}) \cdot U_{14}(\theta_{14}, \delta_{14}) \cdot U_{23}(\theta_{23}, \delta_{23}) \cdot U_{13}(\theta_{13}, \delta_{13}) \cdot U_{12}(\theta_{12}, \delta_{12}), \end{aligned} \quad (2.41)$$

where $\theta_{45} = 0$, and $\theta_{ij} \sim \mathcal{O}(\lambda)$ for $j > 3$. One may, in addition, choose some of the phases δ_{ij} to be vanishing by proper redefinitions of leptonic phases. With the mixing matrix \mathcal{U}_5 in Eq. (2.41), the substitution

$$\begin{pmatrix} W^{eS} \\ W^{\mu S} \\ W^{\tau S} \end{pmatrix} = \begin{pmatrix} \theta_{14}e^{-i\delta_{14}} & \theta_{15}e^{-i\delta_{15}} \\ \theta_{24}e^{-i\delta_{24}} & \theta_{25}e^{-i\delta_{25}} \\ \theta_{34}e^{-i\delta_{34}} & \theta_{35}e^{-i\delta_{35}} \end{pmatrix} \quad (2.42)$$

would give the relevant combinations of the sterile mixing parameters:

$$\begin{aligned} [W^{eS}(W^{eS})^\dagger] &= \theta_{14}^2 + \theta_{15}^2, \\ [W^{\mu S}(W^{\mu S})^\dagger] &= \theta_{24}^2 + \theta_{25}^2, \\ [W^{\tau S}(W^{\tau S})^\dagger] &= \theta_{34}^2 + \theta_{35}^2, \\ [W^{\tau S}(W^{\mu S})^\dagger] &= \theta_{24}\theta_{34}e^{i(\delta_{24}-\delta_{34})} + \theta_{25}\theta_{35}e^{i(\delta_{25}-\delta_{35})}. \end{aligned} \quad (2.43)$$

The expected bounds obtained in Sec. 2.3 then would correspond to

$$\theta_{24}\theta_{34} \cos(\delta_{24} - \delta_{34}) + \theta_{25}\theta_{35} \cos(\delta_{25} - \delta_{35}) < 0.005, \quad \sqrt{\theta_{14}^2 + \theta_{15}^2} < 0.06. \quad (2.44)$$

at 3σ C.L. if the neutrino factory set up, like what we have stated above, cannot see any sterile neutrino signature in the observables $\tilde{\mathcal{A}}_\mu$, $\tilde{\mathcal{A}}_\tau$ or $\tilde{\mathcal{R}}_e$. These bounds will act as a stringent test of the scenario with multiple sterile neutrinos [18].

2.5 Summary

Heavy sterile neutrinos may play an important role in astrophysics and cosmology, for example in r-process nucleosynthesis or as dark matter. Neutrino oscillation experiments, mainly the short baseline ones, have already put severe constraints on the extent of mixing of these sterile neutrinos with the active ones. If the LSND results are taken to be valid, at least two sterile neutrinos are in fact needed to describe all data.

Our aim in this chapter has been to check whether the sterile neutrinos so constrained can still give rise to observable signals at future experiments, and whether these signals can be cleanly identified in spite of our current lack of knowledge of all parameters in the mixing of three active neutrinos. This would lead to an estimation of bounds on the sterile mixing parameters that can be obtained with neutrino oscillation experiments.

The number of neutrino mixing parameters increase quadratically with the number of neutrinos, and only certain combinations are expected to be relevant for the observed neutrino flavor conversions. In order to identify these combinations in an analytically tractable manner, we have exploited the smallness of certain parameters to carry out a systematic expansion in an arbitrarily defined small parameter, $\lambda \equiv 0.2$. The small quantities $\theta_{14}, \theta_{24}, \theta_{34}, \theta_{13}, \theta_{23} - \pi/4$, and $\Delta m_{\odot}^2 / \Delta m_{\text{atm}}^2$ have been formally written as powers of λ times $\mathcal{O}(1)$ numbers, and neutrino conversion probabilities correct to $\mathcal{O}(\lambda^2)$ have been obtained using techniques of Rayleigh-Schrödinger perturbation theory. We have also neglected terms proportional to $\Delta m_{\text{atm}}^2 / \Delta m_{42}^2$, and averaged away the fast oscillating terms like $\cos(\Delta m_{42}^2 L/E)$ since $|\Delta m_{42}^2 L/E| \gg 1$ in typical long baseline experiments.

It has been observed that the conversion probabilities $P_{\mu e}, P_{e\mu}$ or $P_{e\tau}$ get no sterile contribution to $\mathcal{O}(\lambda^2)$. For $P_{\mu\mu}$ and $P_{\mu\tau}$, sterile mixing gives contributions proportional to θ_{24}^2 and $(\theta_{24}^2 + \theta_{34}^2)$ respectively. In addition, there is a CP violating contribution proportional to $\theta_{24}\theta_{34}$ to both these quantities. The survival probability P_{ee} gets modified simply by a term proportional to θ_{14}^2 . There is no dependence on the mass of the sterile neutrino, since oscillations containing Δm_{42}^2 have been averaged out. It has been observed that as long as the neutrinos do not pass through the core of the earth, the probabilities obtained through our analytic approximations match the exact numerical ones

rather well. Note that the sterile contribution to the conversion probabilities at long baseline experiments appears at $\mathcal{O}(\lambda^2)$, which is at a lower order than the appearance of CP violation in the active sector or the sterile contribution to short baseline appearance experiments.

Whereas the contribution due to the currently unknown θ_{13} decreases at high energies due to the earth matter effects, the sterile contribution stays almost constant, and therefore the energy range $E = 10\text{--}50$ GeV is suitable for distinguishing the sterile “signal” above the θ_{13} “background”. The CP violating part of the sterile contribution builds up with increasing L , and hence longer baselines are preferable. This naturally leads to the consideration of neutrino factories with $E_\mu = 50$ GeV and baseline of a few thousand km as the desirable setup, with lepton charge identification capability and a near detector for calibration purposes.

For illustration we have taken the far detector to be near the magic baseline of ≈ 7000 km, and choose three observables, $\tilde{\mathcal{A}}_\mu$ and $\tilde{\mathcal{A}}_\tau$ that correspond to the CP asymmetries in the μ and τ channels respectively, and $\tilde{\mathcal{R}}_e$, which corresponds to the disappearance in the electron channel. The background in these channels is obtained by varying over the unknown values of θ_{13}, θ_{23} and the CP phase δ_{13} . It has been observed that the signal rises above this background for $\tilde{\mathcal{A}}_\mu$ and $\tilde{\mathcal{A}}_\tau$ when $\theta_{24}\theta_{34} \gtrsim 0.005$ (3σ), and for $\tilde{\mathcal{R}}_e$ when $\theta_{14} \gtrsim 0.06$ rad (3σ). The range of θ_{i4} probed is limited mainly by the unknown value of θ_{13} . The limit on θ_{13} may be brought down by a factor of two or more at the reactor experiments like Double CHOOZ [115] or Daya Bay [116], and indeed at the neutrino factories themselves [117]. The values of θ_{i4} that can be probed then decrease by approximately the same factor.

Note that we have only chosen to analyze a few specific observables whose dependence on the sterile mixing is analytically transparent. A complete analysis that fits for all the parameters simultaneously may give rise to more stringent constraints. The long baseline experiments thus have the capability of tightening the limits on the sterile mixing angles by almost an order of magnitude over the current ones, or identify sterile neutrinos if their mixing is indeed above such a value. Note that if the sterile mixing is identified through $\tilde{\mathcal{A}}_\mu$ or $\tilde{\mathcal{A}}_\tau$, the neutrino mass hierarchy – normal vs. inverted – is also identified.

In the light of the recent results that show that LSND, MiniBooNE and the earlier null-result short baseline experiments can be consistent if the number

of sterile neutrinos is two or more, we have also extended our formalism to include any number of sterile neutrinos. The number of distinct combinations of sterile mixing parameters remains the same, irrespective of the number of sterile neutrinos. We have given explicit expressions for such combinations, and the neutrino conversion probabilities in terms of them. The limits obtained on θ_{i4} through the 4ν analysis can easily be translated to the corresponding combinations of these parameters in the general case. Indeed, the bounds on the sterile mixing parameters obtained from the measurements described in this chapter would act as stringent tests of the scenarios with multiple sterile neutrinos.

Chapter 3

Type-III seesaw: RG evolution of neutrino masses and mixing

In this chapter, we consider the renormalization group evolution of the neutrino masses and the mixing parameters in the framework of the standard model (SM) of particle physics, extended by the addition of fermionic triplets to give rise to the small active neutrino masses through the Type-III seesaw mechanism.

3.1 Introduction

The very fact that the three active neutrinos have tiny masses requires extension of the standard model (SM) of particle physics. The most favored mechanisms to generate such small neutrino masses are the so called seesaw mechanisms which need the introduction of one or more heavy fields, while maintaining the $SU(3)_C \times SU(2)_L \times U(1)_Y$ gauge group structure of the SM. As discussed in Chapter 1, there can be three types of seesaws if one demands that the low energy small neutrino masses are generated by addition of only one kind of heavy field at the high scale. These are known as Type-I, Type-II and Type-III seesaw. Amongst them, Type-I and Type-III require additional fermionic fields. Type-I is already discussed in Chapter 1 in detail. Type-II requires addition of extra Higgs fields. Type-III seesaw mechanism is mediated by heavy fermion triplets transforming in the adjoint representation of $SU(2)_L$ and has been considered earlier in [82, 93]. Very recently there has been a

renewed interest in these type of models. The smallness of neutrino masses usually implies the mass of the heavy particle to be high $\sim 10^{11-15}$ GeV, as shown in Chapter 1. However, it is also possible that one or more of the triplets have masses near the TeV scale, making it possible to search for their signatures at the LHC [118, 119, 120, 121, 122]. In such models, the Yukawa couplings need to be small to suppress the neutrino mass, if no fine tuning of the parameters is assumed. Lepton flavor violating decays in the context of Type-III seesaw models have also been considered in [123]. Recently it has also been suggested that the neutral member of the triplet can serve as the dark matter and can be instrumental in generating small neutrino mass radiatively [124].

Fermions in the adjoint representation fit naturally into the 24-dimensional representation of SU(5), and can rectify the two main problems encountered in SU(5) Grand Unified Theory (GUT) models, viz. generation of neutrino masses and gauge coupling unification [118, 119, 125, 126, 127]. The latter requirement constrains the fermionic triplets to be of mass below TeV for $M_{\text{GUT}} \sim 10^{16}$ GeV, making the model testable at the LHC. Leptogenesis mediated by triplet fermions has been explored in [128, 129, 130]. MSSM extended by triplet fermions has recently been considered in [131].

In this chapter we consider the RG evolution of neutrino masses and mixing parameters in the Type-III seesaw scenario with nondegenerate heavy fermion triplets, when the low energy effective theory is the SM. We evaluate the contributions of these fermion triplets to the wavefunction, mass and coupling constant renormalization of the SM fields and of the triplet fields themselves. We obtain the β -functions for RG evolution of the Yukawa couplings, the Higgs self-coupling, the Majorana mass matrix of the fermion triplets, the gauge couplings, and the low energy effective vertex obtained by integrating out the heavy triplets, including the extra contribution due to the additional triplets still coupled to the theory. We obtain analytic expressions for the running of the masses, mixing angles and phases in a basis where all the quantities are well-defined at every point in the parameter space including $\theta_{13} = 0$. We also solve the RG equations numerically and present some illustrative examples of running of masses and mixing angles.

3.2 The Type-III seesaw model

3.2.1 The Lagrangian

In the Type-III seesaw, there are right handed fermionic triplet Σ_R added to the SM at the high scale which is singlet under $U(1)_Y$ to meet the requirement that the theory must be anomaly free, while transform as a triplet in the adjoint representation of $SU(2)_L$. In the basis of the Pauli matrices $\{\sigma^1, \sigma^2, \sigma^3\}$, this triplet can be represented as

$$\Sigma_R = \begin{pmatrix} \Sigma_R^0/\sqrt{2} & \Sigma_R^+ \\ \Sigma_R^- & -\Sigma_R^0/\sqrt{2} \end{pmatrix} \equiv \frac{\Sigma_R^i \sigma^i}{\sqrt{2}}, \quad (3.1)$$

where $\Sigma_R^\pm = (\Sigma_R^1 \mp i\Sigma_R^2)\sqrt{2}$. For the sake of simplicity of further calculations, we combine Σ_R with its CP conjugate Σ_R^C to construct

$$\Sigma \equiv \Sigma_R + \Sigma_R^C. \quad (3.2)$$

Clearly, Σ also transforms in the adjoint representation of $SU(2)_L$. Note that though formally $\Sigma = \Sigma^C$, the individual elements of Σ are not all Majorana particles. While the diagonal elements of Σ are indeed Majorana spinors which represent the neutral component of Σ , the off-diagonal elements are charged Dirac spinors.

Introduction of this triplet field will introduce new terms in the Lagrangian. The net Lagrangian is

$$\mathcal{L} = \mathcal{L}_{SM} + \mathcal{L}_\Sigma, \quad (3.3)$$

where

$$\mathcal{L}_\Sigma = \mathcal{L}_{\Sigma,kin} + \mathcal{L}_{\Sigma,mass} + \mathcal{L}_{\Sigma,Yukawa}. \quad (3.4)$$

Here,

$$\mathcal{L}_{\Sigma,kin} = \text{Tr}[\bar{\Sigma}i\not{D}\Sigma], \quad (3.5)$$

$$\mathcal{L}_{\Sigma,mass} = -\frac{1}{2}\text{Tr}[\bar{\Sigma}M_\Sigma\Sigma], \quad (3.6)$$

$$\mathcal{L}_{\Sigma,Yukawa} = -\bar{l}_L\sqrt{2}Y_\Sigma^\dagger\Sigma\tilde{\phi} - \phi^T\varepsilon^T\bar{\Sigma}\sqrt{2}Y_\Sigma l_L, \quad (3.7)$$

where

$$\varepsilon = \begin{pmatrix} 0 & 1 \\ -1 & 0 \end{pmatrix} \quad (3.8)$$

is the completely anti-symmetric tensor in the $SU(2)_L$ space. Here we have not written the generation indices explicitly. M_Σ is the Majorana mass matrix of the heavy fermion triplets and Y_Σ is the Yukawa coupling. The SM fields l_L , ϕ and $\tilde{\phi}$ are $SU(2)_L$ doublets and can be written as

$$l_L = \begin{pmatrix} \nu_L \\ e_L^- \end{pmatrix}_{Y=-1}, \quad \phi = \begin{pmatrix} \phi^+ \\ \phi^0 \end{pmatrix}_{Y=1}, \quad \tilde{\phi} = \varepsilon\phi^* = \begin{pmatrix} \phi^{0*} \\ -\phi^- \end{pmatrix}_{Y=-1}. \quad (3.9)$$

Each member of the $SU(2)_L$ doublet l_L is a 4-component Dirac spinor. Since the fermion triplet Σ is in the adjoint representation of $SU(2)_L$, the covariant derivative of Σ is defined as

$$D_\mu \Sigma = \partial_\mu \Sigma + ig_2 [W_\mu, \Sigma], \quad (3.10)$$

where g_2 is the $SU(2)_L$ gauge coupling.

All the Feynman diagrams for the new vertices involving the triplet fermionic field Σ as well as those involving the SM particles are given in the Appendix B.

3.2.2 The seesaw

The new term \mathcal{L}_Σ in the Lagrangian, as shown in Eq. (3.4), can be expanded as [123]

$$\begin{aligned} \mathcal{L}_\Sigma = & \left(\bar{\Psi} i \not{\partial} \Psi + \bar{\Sigma}_R^0 i \not{\partial} \Sigma_R^0 + \text{h.c.} \right) \\ & + g_2 \left(W_\mu^+ \bar{\Sigma}_R^0 \gamma^\mu P_R \Psi + W_\mu^+ \bar{\Sigma}_R^{0C} \gamma^\mu P_L \Psi + \text{h.c.} \right) - g_2 W_\mu^3 \bar{\Psi} \gamma^\mu \Psi \\ & - \bar{\Psi} M_\Sigma \Psi - \left(\frac{1}{2} \bar{\Sigma}_R^0 M_\Sigma \Sigma_R^{0C} + \text{h.c.} \right) \\ & - \left(\phi^0 \bar{\Sigma}_R^0 Y_\Sigma \nu_L + \sqrt{2} \phi^0 \bar{\Psi} Y_\Sigma l_L + \phi^+ \bar{\Sigma}_R^0 Y_\Sigma l_L - \sqrt{2} \phi^+ \nu_L^C Y_\Sigma^T \Psi + \text{h.c.} \right), \end{aligned} \quad (3.11)$$

where we have defined the four component Dirac spinor

$$\Psi \equiv \Sigma_R^{+C} + \Sigma_R^-, \quad (3.12)$$

for our convenience, while the neutral component of Σ_R is still in the two component notation. In Eq. (3.11), the first two lines come from $\mathcal{L}_{\Sigma,kin}$, the third line corresponds to the Majorana mass term in $\mathcal{L}_{\Sigma,mass}$ and the terms in the last line corresponds to the Yukawa coupling terms in $\mathcal{L}_{\Sigma,Yukawa}$, as given in Eqs. (3.5)–(3.7). After the electroweak symmetry breaking, the mass matrix for the neutral fields become

$$\mathcal{L} \ni -\frac{1}{2} \begin{pmatrix} \overline{\nu_L^C} & \overline{\Sigma_R^0} \end{pmatrix} \begin{pmatrix} 0 & \mathfrak{m}_D \\ \mathfrak{m}_D^T & \mathbb{M}_\Sigma \end{pmatrix} \begin{pmatrix} \nu_L \\ \Sigma_R^{0C} \end{pmatrix} + \text{h.c.}, \quad (3.13)$$

where $\mathfrak{m}_D = (v/\sqrt{2})Y_\Sigma^T$ is the Dirac mass matrix of the neutral fields. Thus the mass matrix in Eq. (3.13) looks the same as that obtained in Eq. (1.8) and hence for large \mathbb{M}_Σ , diagonalization of the mass matrix will produce light active neutrino states via seesaw mechanism,

$$\mathfrak{m}_\nu = -\mathfrak{m}_D \mathbb{M}_\Sigma^{-1} \mathfrak{m}_D^T, \quad (3.14)$$

as obtained in the Section 1.2.1. The seesaw achieved here with the help of the neutral component of the fermionic triplet is known as the Type-III seesaw mechanism. Eq. (3.13) also implies that there will be a mixing between the light and the heavy neutral states, however the mixing angle will be $\mathcal{O}(\mathfrak{m}_D/\mathbb{M}_\Sigma)$ and hence very small for large \mathbb{M}_Σ .

3.2.3 Corrections to the charged lepton mass

Since the heavy fermion triplets added to the SM at the high scale have charged components also, they will modify the masses of the charged leptons belonging to the SM, in addition to the generation of the small active neutrino masses. With the addition of the triplet fields, the mass term of the charged lepton

sector becomes

$$\begin{aligned}
 \mathcal{L} \ni & - \begin{pmatrix} \bar{l}_R & \bar{\Psi}_R \end{pmatrix} \begin{pmatrix} m_L & 0 \\ \sqrt{2}m_D^T & M_\Sigma \end{pmatrix} \begin{pmatrix} l_L \\ \Psi_L \end{pmatrix} \\
 & - \begin{pmatrix} \bar{l}_L & \bar{\Psi}_L \end{pmatrix} \begin{pmatrix} m_L & \sqrt{2}m_D^* \\ 0 & M_\Sigma \end{pmatrix} \begin{pmatrix} l_R \\ \Psi_R \end{pmatrix} \\
 = & - \begin{pmatrix} \bar{l}_R & \bar{\Psi}_R \end{pmatrix} \mathcal{M}_c \begin{pmatrix} l_L \\ \Psi_L \end{pmatrix} - \begin{pmatrix} \bar{l}_L & \bar{\Psi}_L \end{pmatrix} \mathcal{M}_c^\dagger \begin{pmatrix} l_R \\ \Psi_R \end{pmatrix}, \quad (3.15)
 \end{aligned}$$

where m_L is the Dirac mass matrix of the SM charged leptons and

$$\mathcal{M}_c \equiv \begin{pmatrix} m_L & 0 \\ \sqrt{2}m_D^T & M_\Sigma \end{pmatrix} \quad (3.16)$$

denotes the complete mass matrix for the charged leptons after electroweak symmetry breaking. Eq. (3.16) shows that the inclusion of the charged fermions as components of the heavy triplets does not change the masses of the charged leptons of the SM. However, there will be mixing between the states l_L - Ψ_L and l_R - Ψ_R , but the mixing angle is small in the $m_D, m_L \ll M_\Sigma$ limit.

3.2.4 The effective vertex

In the low energy limit of the extended standard model, we have an effective theory which will be described by the SM Lagrangian with the additional operators obtained by integrating out the heavy fermion triplets added to it. The lowest dimensional one of such operators is the dimension-5 operator [31]

$$\mathcal{L}_\kappa = \kappa_{fg} \left(\bar{l}_L^C{}^f \sigma^i \varepsilon \phi \right) \left(\phi^T \sigma^i \varepsilon l_L^g \right) + \text{h.c.}, \quad (3.17)$$

$$= -\kappa_{fg} \left(\bar{l}_{Lc}^C{}^f \phi_a l_{Lb}^g \phi_d \right) \frac{1}{2} (\varepsilon_{ac} \varepsilon_{bd} + \varepsilon_{ab} \varepsilon_{cd}) + \text{h.c.}, \quad (3.18)$$

where κ is a symmetric complex matrix with mass dimension (-1) . Generation indices $f, g \in \{1, 2, 3\}$ are shown explicitly and $a, b, c, d \in \{1, 2\}$ are the $SU(2)_L$ indices. In writing Eq. (3.18) we have used

$$\begin{aligned}
 (\sigma^i)_{ab} (\sigma^i)_{cd} &= 2\delta_{ad} \delta_{bc} - \delta_{ab} \delta_{cd} \\
 \Rightarrow (\sigma^i \varepsilon)_{ba} (\sigma^i \varepsilon)_{dc} &= 2\varepsilon_{da} \varepsilon_{bc} - \varepsilon_{ba} \varepsilon_{dc}
 \end{aligned} \quad (3.19)$$

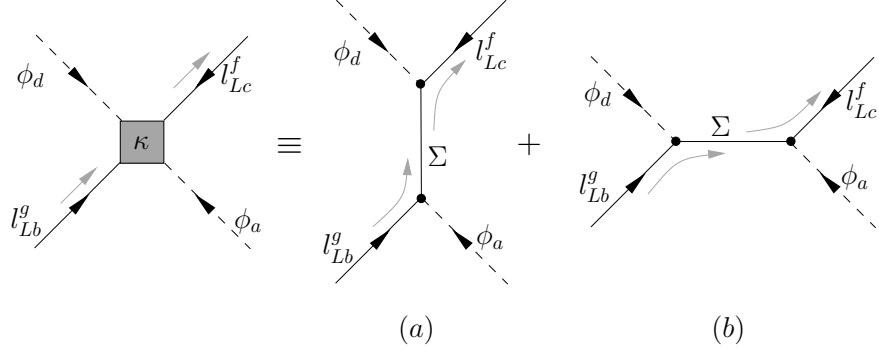


Figure 3.1: The effective vertex κ at an energy $\mu \ll M_1$, after all the heavy fermions have been decoupled from the theory. $f, g \in \{1, 2, 3\}$ are the generation indices. The $SU(2)_L$ and generation indices for Σ are not shown explicitly since they are summed over.

and utilizing the $\phi_d \leftrightarrow \phi_a$ symmetry, we can write

$$2\varepsilon_{da}\varepsilon_{bc} - \varepsilon_{ba}\varepsilon_{dc} = \frac{1}{2}(\varepsilon_{ab}\varepsilon_{dc} + \varepsilon_{db}\varepsilon_{ac}) . \quad (3.20)$$

The relevant diagrams in the complete theory giving rise to the effective operators in the low energy limit are shown in Fig 3.1. The ‘‘shaded box’’ on the left hand side represents the effective low energy vertex κ , while $\mathcal{A}_{(a)}$ and $\mathcal{A}_{(b)}$ are the amplitudes of the diagrams labeled as (a) and (b) on the right hand side. The amplitudes are given by

$$\mathcal{A}_{(a)} = i\mu^\epsilon (Y_\Sigma^T \mathbb{M}_\Sigma^{-1} Y_\Sigma)_{fg} [(\varepsilon^T \sigma^i)_{ab} (\varepsilon^T \sigma^i)_{cd}] P_L , \quad (3.21)$$

$$\mathcal{A}_{(b)} = i\mu^\epsilon (Y_\Sigma^T \mathbb{M}_\Sigma^{-1} Y_\Sigma)_{fg} [(\varepsilon^T \sigma^i)_{db} (\varepsilon^T \sigma^i)_{ca}] P_L , \quad (3.22)$$

with $\epsilon = 4 - D$ where D is the dimensionality that we introduce in order to use dimensional regularization. Note that $\mathcal{A}_{(b)}$ is obtained from $\mathcal{A}_{(a)}$ just by $d \leftrightarrow a$ interchange. Using Eq. (3.19) one finally gets

$$\mathcal{A}_{(a)} + \mathcal{A}_{(b)} = -i\mu^\epsilon (Y_\Sigma^T \mathbb{M}_\Sigma^{-1} Y_\Sigma)_{fg} (\varepsilon_{ab}\varepsilon_{cd} + \varepsilon_{ac}\varepsilon_{bd}) P_L . \quad (3.23)$$

This is equal to the left hand side of Fig. 3.1 with the identification

$$\kappa = 2Y_\Sigma^T \mathbb{M}_\Sigma^{-1} Y_\Sigma . \quad (3.24)$$

Equation (3.24) gives the Feynman rule for the low energy effective vertex

κ , as shown in the Appendix B. From Eqs. (3.24) and (3.18), one gets the neutrino mass after spontaneous symmetry breaking to be

$$\mathbf{m}_\nu = -\frac{v^2}{2} Y_\Sigma^T \mathbb{M}_\Sigma^{-1} Y_\Sigma \quad (3.25)$$

which is the Type-III seesaw relation. Here, v denotes the vacuum expectation value of the Higgs field.

3.3 Radiative corrections in Type-III seesaw

3.3.1 Sequential decoupling of heavy fermions

As mentioned in Sections 3.2.2 and 3.2.4, after electroweak symmetry breaking the light neutrino mass matrix is given by

$$\mathbf{m}_\nu = -\frac{v^2}{2} Y_\Sigma^T \mathbb{M}_\Sigma^{-1} Y_\Sigma . \quad (3.26)$$

In this section we would like to study the radiative corrections to the quantity

$$\mathbb{R} \equiv Y_\Sigma^T \mathbb{M}_\Sigma^{-1} Y_\Sigma , \quad (3.27)$$

which is the quantity of interest at different energy scales and finally gives the light neutrino mass matrix as $\mathbf{m}_\nu = -\frac{v^2}{2} \mathbb{R}$, after spontaneous symmetry breaking.

Let us consider the most general case when there are r triplets having masses $M_1 < M_2 < \dots < M_{r-1} < M_r$. Above the heaviest mass M_r , all the r -triplets are coupled to the theory and contribute to \mathbb{R} as

$$\mathbb{R} = Q^{(r+1)} , \quad (3.28)$$

where $Q^{(r+1)}$ denotes the contribution from the r coupled triplet fields and is given by

$$Q^{(r+1)} = Y_\Sigma^{(r+1)T} \mathbb{M}_\Sigma^{(r+1)-1} Y_\Sigma^{(r+1)} \quad (\mu > M_r) . \quad (3.29)$$

Here $Y_\Sigma^{(r+1)}$ is a $[r \times n_F]$ dimensional matrix (n_F is the number of flavors, which

is 3 in our case), given as

$${}^{(r+1)}Y_\Sigma = \begin{pmatrix} (y_\Sigma)_{1,1} & \cdots & (y_\Sigma)_{1,n_F} \\ \vdots & & \vdots \\ (y_\Sigma)_{r,1} & \cdots & (y_\Sigma)_{r,n_F} \end{pmatrix}. \quad (3.30)$$

${}^{(r+1)}\mathbb{M}_\Sigma$ is a $[r \times r]$ matrix and Q as well as \mathbb{R} is a $[n_F \times n_F]$ dimensional matrix. We use the super-indices just to keep track of the number of coupled fields. Below the scale M_r , the heaviest triplet decouples from the theory. Integrating out this degree of freedom gives rise to an effective operator ${}^{(r)}\kappa$. The matching condition at $\mu = M_r$ is

$${}^{(r)}\kappa_{ij} \Big|_{M_r} = 2(Y_\Sigma^T)_{ir} (M_r)^{-1} (Y_\Sigma)_{rj} \Big|_{M_r}, \quad (3.31)$$

where no summation over ‘ r ’ is implied and $i, j \in \{1, 2, \dots, n_F\}$. This condition ensures the continuity of \mathbb{R} at $\mu = M_r$. In order to get the value of the threshold M_r , we need to write the above matching condition in the basis where $\mathbb{M}_\Sigma = \text{Diag}(M_1, M_2, \dots, M_r)$. Here it is worth mentioning that the matching scale has to be found carefully since \mathbb{M}_Σ itself runs with the energy scale, i.e. $M_i = M_i(\mu)$. The threshold scale M_i is therefore to be understood as $M_i(\mu = M_i)$.

In the energy range $M_{r-1} < \mu < M_r$, \mathbb{R} will be given as

$$\mathbb{R} = \frac{1}{2}{}^{(r)}\kappa + Q. \quad (3.32)$$

The first term in Eq. (3.32) is the contribution of the integrated out triplet of mass M_r through the effective operator ${}^{(r)}\kappa$. The second term represents the contribution of the remaining $(r - 1)$ heavy fermion triplets, which are still coupled to the theory. ${}^{(r)}\mathbb{M}_\Sigma$ is now a $[(r - 1) \times (r - 1)]$ matrix while ${}^{(r)}Y_\Sigma$ is a $[(r - 1) \times n_F]$ dimensional matrix given as

$$Y_\Sigma \rightarrow \left. \begin{pmatrix} (y_\Sigma)_{1,1} & \cdots & (y_\Sigma)_{1,n_F} \\ \vdots & & \vdots \\ (y_\Sigma)_{r-1,1} & \cdots & (y_\Sigma)_{r-1,n_F} \\ 0 & \cdots & 0 \end{pmatrix} \right\} = {}^{(r)}Y_\Sigma, \quad (3.33)$$

$\left. \vphantom{\begin{pmatrix} (y_\Sigma)_{1,1} & \cdots & (y_\Sigma)_{1,n_F} \\ \vdots & & \vdots \\ (y_\Sigma)_{r-1,1} & \cdots & (y_\Sigma)_{r-1,n_F} \\ 0 & \cdots & 0 \end{pmatrix}} \right\} M_r \text{ integrated out.}$

Finally $\overset{(r)}{\mathbb{M}}_\Sigma$ and $\overset{(r)}{Y}_\Sigma$ constitute $\overset{(r)}{Q}$, which is $[n_F \times n_F]$ dimensional.

The matching condition at $\mu = M_{r-1}$ is

$$\overset{(r-1)}{\kappa}_{ij} \Big|_{M_{r-1}} = \overset{(r)}{\kappa}_{ij} \Big|_{M_{r-1}} + 2(\overset{(r)}{Y}_\Sigma^T)_{i(r-1)} (M_{r-1})^{-1} (\overset{(r)}{Y}_\Sigma)_{(r-1)j} \Big|_{M_{r-1}}, \quad (3.34)$$

where no summation over ‘ $(r-1)$ ’ is to be taken.

Generalizing the above sequence, we can say that if we consider the intermediate energy region between the $(n-1)^{\text{th}}$ and the n^{th} threshold, i.e. $M_n > \mu > M_{n-1}$, then all the heavy triplets from masses M_r down to M_n have been decoupled. In this region the Yukawa matrix $\overset{(n)}{Y}_\Sigma$ will be $[(n-1) \times n_F]$ dimensional that couples the $(n-1)$ coupled triplets with n_F flavors and will be given as

$$Y_\Sigma \rightarrow \left(\begin{array}{ccc} (y_\Sigma)_{1,1} & \cdots & (y_\Sigma)_{1,n_F} \\ \vdots & & \vdots \\ (y_\Sigma)_{n-1,1} & \cdots & (y_\Sigma)_{n-1,n_F} \\ \hline 0 & \cdots & 0 \\ \vdots & & \vdots \\ 0 & \cdots & 0 \end{array} \right) \left. \vphantom{\begin{array}{ccc} (y_\Sigma)_{1,1} & \cdots & (y_\Sigma)_{1,n_F} \\ \vdots & & \vdots \\ (y_\Sigma)_{n-1,1} & \cdots & (y_\Sigma)_{n-1,n_F} \\ \hline 0 & \cdots & 0 \\ \vdots & & \vdots \\ 0 & \cdots & 0 \end{array}} \right\} = \overset{(n)}{Y}_\Sigma, \quad (3.35)$$

heavy triplets with
masses $M_n - M_r$
integrated out .

$\overset{(n)}{\mathbb{M}}_\Sigma$ will be $[(n-1) \times (n-1)]$ dimensional matrix involving the mass terms of all the coupled triplets. In this energy range \mathbb{R} will be

$$\mathbb{R} = \frac{1}{2} \overset{(n)}{\kappa} + \overset{(n)}{Q}, \quad (3.36)$$

with

$$\overset{(n)}{Q} \equiv \overset{(n)}{Y}_\Sigma^T \overset{(n)}{\mathbb{M}}_\Sigma^{-1} \overset{(n)}{Y}_\Sigma. \quad (3.37)$$

Note that \mathbb{R} , κ and Q are $[n_F \times n_F]$ matrices. The matching condition at $\mu = M_n$ is given by Eq. (3.34) with r replaced by $(n+1)$.

At low energies $\mu < M_1$, when all the heavy triplets are decoupled, $Q(\mu) = \overset{(1)}{Q}(\mu) = 0$ and $\mathbb{R}(\mu) = (1/2)\overset{(1)}{\kappa}(\mu)$. Fig. 3.2 shows the expressions for \mathbb{R} at different energy scales for the case of three fermion triplets *i.e.* for $r = 3$. When $\mu < M_1$, all the heavy triplets will get decoupled and thus only $\overset{(1)}{\kappa}$ will contribute. Finally the light neutrino mass matrix m_ν is obtained as

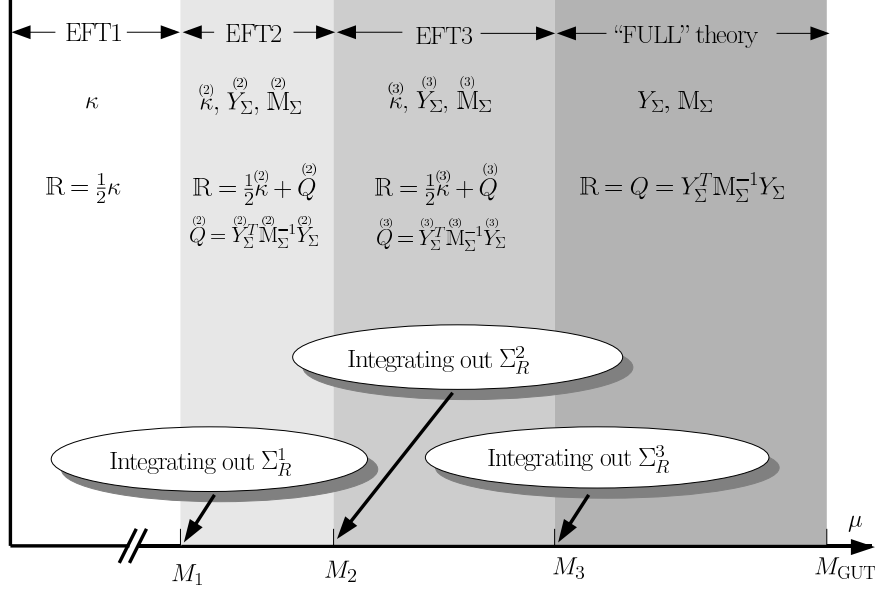


Figure 3.2: Sequential decoupling of the heavy fermion triplets and construction of \mathbb{R} at different energy scales, for $r = 3$. Finally the light neutrino mass matrix is given as $\mathfrak{m}_\nu \equiv -\frac{v^2}{2}\mathbb{R}$ after spontaneous symmetry breaking, where v is the vacuum expectation value of the SM Higgs.

$\mathfrak{m}_\nu \equiv -\frac{v^2}{2}\mathbb{R}$, after the electroweak symmetry breaking.

For the sake of convenience and to be consistent with the existing literature, we will refer to $\mathfrak{m}_\nu = -\frac{v^2}{2}\mathbb{R}$ as the effective light neutrino mass matrix at any energy scale, in the rest of the thesis. However, it must be understood that the quantity ‘ v ’ is present only after electroweak symmetry breaking and hence, strictly speaking, this relation is valid only in that energy regime, while \mathbb{R} is a well-defined quantity at all energy scales.

3.3.2 Dimensional regularization and renormalization

Now we consider the radiative corrections to the fields, masses and couplings in our model, on the lines of that performed in [34, 75] in the context of Type-I seesaw. The wavefunction renormalizations are defined as

$$\psi_B^f = \left(Z_\psi^{\frac{1}{2}} \right)_{fg} \psi^g, \quad (3.38)$$

where $\psi \in \{l_L, q_L, e_R, u_R, d_R\}$. We denote the renormalized quantities as X and the corresponding bare fields as X_B . For the fermion triplets

$$\Sigma_B^{fi} = \left(Z_{\Sigma}^{\frac{1}{2}} \right)_{fg} \Sigma^{gi} . \quad (3.39)$$

For the doublet Higgs

$$\phi_B = Z_{\phi}^{\frac{1}{2}} \phi , \quad (3.40)$$

whereas

$$A_B = Z_A^{\frac{1}{2}} A \quad (3.41)$$

for the gauge bosons where $A \in \{B, W^i, G^A\}$. For the Faddeev-Popov ghosts one has

$$c_B = Z_c^{\frac{1}{2}} c , \quad (3.42)$$

however the ghosts will not appear in the RG evolution of the relevant quantities at one loop level. We introduce the abbreviation

$$\delta Z_X = Z_X - 1 , \quad (3.43)$$

where Z_X denotes the renormalization constant of any of the relevant quantities X .

We will use the dimensional regularization and the minimal subtraction scheme for renormalization. In this renormalization formalism, the counter terms are defined such that they only cancel out the divergent parts. Thus the renormalization constants are of the form

$$Z_X = 1 + \sum_{k \geq 1} \delta Z_{X,k} \frac{1}{\epsilon^k} , \quad (3.44)$$

where the $\delta Z_{X,k}$ are independent of ϵ . In our scenario, at the one loop level, the renormalization constants are proportional to $1/\epsilon$. The final results of course will be independent of the particular regularization as well as the renormalization scheme used for the calculations.

The diagrams contributing to the renormalization constants of different quantities are all shown explicitly in Appendix C. The renormalization constants

of different quantities are given by

$$\delta Z_\phi = -\frac{1}{16\pi^2} \left(2T - \frac{3}{10}(3 - \xi_1)g_1^2 - \frac{3}{2}(3 - \xi_2)g_2^2 \right) \frac{1}{\epsilon}, \quad (3.45)$$

$$\delta Z_{l_L} = -\frac{1}{16\pi^2} \left(Y_e^\dagger Y_e + 3Y_\Sigma^{(n)\dagger} Y_\Sigma^{(n)} + \frac{3}{10}\xi_1 g_1^2 + \frac{3}{2}\xi_2 g_2^2 \right) \frac{1}{\epsilon}, \quad (3.46)$$

$$\delta Z_{e_R} = -\frac{1}{16\pi^2} \left(2Y_e Y_e^\dagger + \frac{6}{5}\xi_1 g_1^2 \right) \frac{1}{\epsilon}, \quad (3.47)$$

$$\delta Z_\Sigma = -\frac{1}{16\pi^2} \left[\left(2Y_\Sigma^{(n)\dagger} Y_\Sigma^{(n)} + 4\xi_2 g_2^2 \right) P_R + \left(2(Y_\Sigma^{(n)} Y_\Sigma^{(n)\dagger})^* + 4\xi_2 g_2^2 \right) P_L \right] \frac{1}{\epsilon} \quad (3.48)$$

where we have used the R_ξ gauge, and the GUT normalization of the gauge couplings [32].

The Yukawa couplings are renormalized as¹

$$\delta Z_{Y_e} = -\frac{1}{16\pi^2} \left(-6Y_\Sigma^{(n)\dagger} Y_\Sigma^{(n)} + \frac{9}{10}(2 + \xi_1)g_1^2 + \frac{3}{2}\xi_2 g_2^2 \right) \frac{1}{\epsilon}, \quad (3.49)$$

$$\delta Z_{Y_\Sigma} = -\frac{1}{16\pi^2} \left(2Y_e^\dagger Y_e - \frac{3}{10}\xi_1 g_1^2 - \frac{1}{2}(12 + 7\xi_2)g_2^2 \right) \frac{1}{\epsilon}, \quad (3.50)$$

while the Majorana neutrino mass matrix gets renormalized as

$$\delta Z_{M_\Sigma} = -\frac{1}{16\pi^2} (12 + 4\xi_2) g_2^2 \frac{1}{\epsilon}. \quad (3.51)$$

The addition of the right handed fermion triplets to the SM will contribute one extra diagram to the renormalization of the Higgs self-coupling λ , as shown in the diagram (G1) of the Appendix C. This contribution will be²

$$\delta Z_\lambda|_{\text{new}} = -\frac{5i}{4\pi^2} \text{Tr} \left[Y_\Sigma^{(n)\dagger} Y_\Sigma^{(n)} Y_\Sigma^{(n)\dagger} Y_\Sigma^{(n)} \right] (\delta_{ab}\delta_{cd} + \delta_{ac}\delta_{bd}) \frac{1}{\epsilon}. \quad (3.52)$$

¹ In [65] the contributions of fermion triplets to some of the above renormalization constants are calculated in the context of SM extended with these fields. Their conventions of field normalizations are different and hence the results may differ upto numerical constants in certain cases. However, their Eq. (19) for δY_ν , which is the same quantity as our δZ_{Y_Σ} in Eq. (3.50), is missing the $Y_e^\dagger Y_e$ term. The source of this term is the diagram labeled as (F2) in Appendix C. The extra contribution to δZ_{Y_e} from the fermion triplets has also not been calculated in [65].

² Note that Ref. [65] gives this quantity ($\delta\lambda$ in their Eq. (20)) to be of the form $\text{Tr}(Y_\Sigma^\dagger Y_\Sigma)$. However, the additional contribution to the Higgs quartic coupling δZ_λ should be of the form $\text{Tr}(Y_\Sigma^\dagger Y_\Sigma Y_\Sigma^\dagger Y_\Sigma)$, since it comes from the diagram (G1) in Appendix C.

Finally for the effective vertex $\kappa^{(n)}$, the renormalization constant is

$$\delta\kappa = -\frac{1}{16\pi^2} \left[2 \kappa^{(n)} (Y_e^\dagger Y_e) + 2 (Y_e^\dagger Y_e)^T \kappa^{(n)} - \lambda \kappa^{(n)} - \left(\frac{3}{2} - \xi_1 \right) g_1^2 \kappa^{(n)} - \left(\frac{3}{2} - 3\xi_2 \right) g_2^2 \kappa^{(n)} \right] \frac{1}{\epsilon}. \quad (3.53)$$

We observe that there is no contribution from the fermion triplet Σ in the loop, which means that $\delta\kappa^{(n)}$ will not directly depend on the fermion triplets still coupled to the theory. However, during RG evolution an indirect dependence will creep in via the other couplings.

3.3.3 Calculation of the β functions

To calculate the β functions for the RG evolution of the Yukawa couplings, Majorana mass matrix, the effective vertex κ and other relevant quantities, we consider the relations between the bare (X_B) and the corresponding renormalized (X) quantities given by

$$Z_\Sigma^{T\frac{1}{2}} M_{\Sigma B} Z_\Sigma^{\frac{1}{2}} = Z_{M_\Sigma} M_\Sigma, \quad (3.54)$$

$$Z_{\Sigma R}^{\frac{1}{2}} Y_{\Sigma B} Z_\phi^{\frac{1}{2}} Z_{l_L}^{\frac{1}{2}} = \mu^{\frac{\epsilon}{2}} Y_\Sigma Z_{Y_\Sigma}, \quad (3.55)$$

$$Z_{eR}^{\frac{1}{2}} Y_{eB} Z_\phi^{\frac{1}{2}} Z_{l_L}^{\frac{1}{2}} = \mu^{\frac{\epsilon}{2}} Y_e Z_{Y_e}, \quad (3.56)$$

$$Z_{l_L}^{T\frac{1}{2}} Z_\phi^{\frac{1}{2}} \kappa_B Z_\phi^{\frac{1}{2}} Z_{l_L}^{\frac{1}{2}} = \mu^\epsilon (\kappa + \delta\kappa), \quad (3.57)$$

where $Z_{\Sigma R} = P_R Z_\Sigma$. We further use the functional differentiation method as in [75] to find the β functions for the Yukawa couplings as

$$16\pi^2 \beta_{Y_e} = Y_e \left(\frac{3}{2} Y_e^\dagger Y_e + \frac{15}{2} Y_\Sigma^\dagger Y_\Sigma + T - \frac{9}{4} g_1^2 - \frac{9}{4} g_2^2 \right), \quad (3.58)$$

$$16\pi^2 \beta_{Y_\Sigma} = Y_\Sigma \left(\frac{5}{2} Y_e^\dagger Y_e + \frac{5}{2} Y_\Sigma^\dagger Y_\Sigma + T - \frac{9}{20} g_1^2 - \frac{33}{4} g_2^2 \right), \quad (3.59)$$

$$16\pi^2 \beta_{Y_u} = Y_u \left(\frac{3}{2} Y_u^\dagger Y_u - \frac{3}{2} Y_d^\dagger Y_d + T - \frac{17}{20} g_1^2 - \frac{9}{4} g_2^2 - 8g_3^2 \right), \quad (3.60)$$

$$16\pi^2 \beta_{Y_d} = Y_d \left(\frac{3}{2} Y_d^\dagger Y_d - \frac{3}{2} Y_u^\dagger Y_u + T - \frac{1}{4} g_1^2 - \frac{9}{4} g_2^2 - 8g_3^2 \right). \quad (3.61)$$

Here

$$T = \text{Tr} \left[Y_e^\dagger Y_e + 3Y_\Sigma^\dagger Y_\Sigma + 3Y_u^\dagger Y_u + 3Y_d^\dagger Y_d \right], \quad (3.62)$$

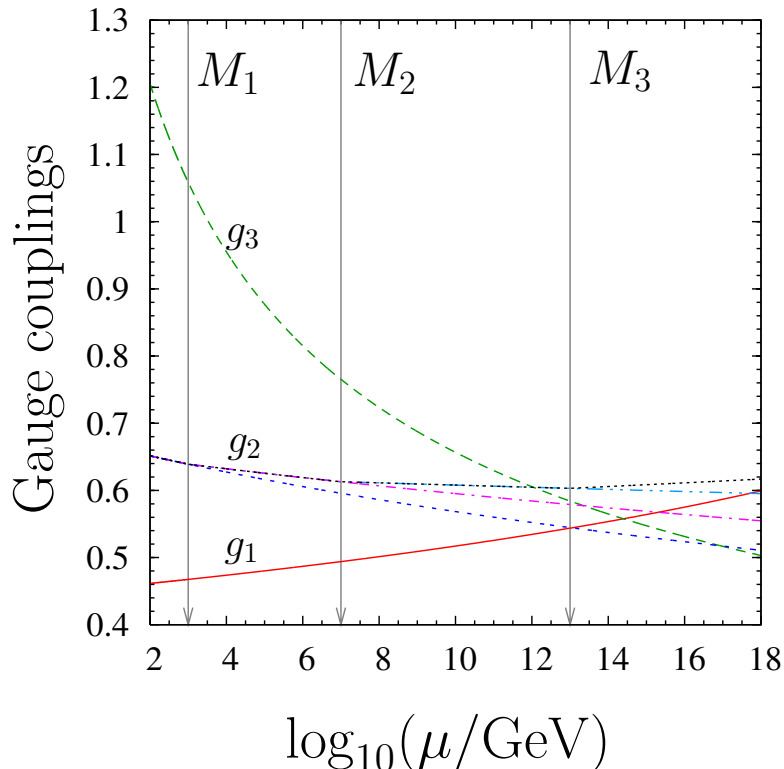


Figure 3.3: The solid (red) line and the dashed (green) lines show the energy scale variations of g_1 and g_3 respectively in the SM, which is unaffected in Type-III seesaw. The dotted (blue) line gives the SM running of g_2 , while dot-dashed (magenta), dot-dot-dashed (sky) and densely dotted (black) lines show the running if there were one, two or three fermion triplets respectively.

and $\beta_X \equiv \mu(dX/d\mu)$. Note that $Y_\Sigma^{(n)}$ is given in Eq. (3.35), with $(n-1)$ the number of heavy fermion triplets still coupled to the theory.

Since the fermion triplets have non-zero $SU(2)_L$ charge, they couple to the W bosons and hence will affect the RG evolution of the gauge coupling g_2 via

$$16\pi^2\beta_{g_2} = b_2g_2^3, \quad (3.63)$$

where

$$b_2 = -\frac{19}{6} + \frac{4(n-1)}{3}. \quad (3.64)$$

Note that if the number of heavy fermion triplets is ≤ 2 , the value of b_2 is always negative. On the other hand, if the number is ≥ 3 , then b_2 becomes positive above the mass scale M_3 . Adding fermion triplets shifts the g_1 - g_2

intersection to higher energy scales, and the g_2 - g_3 intersection to lower energy scales, as can be seen from Fig. 3.3. The exact situation would depend on the values of M_i .

The RG evolution of λ is given by

$$16\pi^2\beta_\lambda = 6\lambda^2 - 3\lambda \left(\frac{3}{5}g_1^2 + 3g_2^2 \right) + 3g_2^4 + \frac{3}{2} \left(\frac{3}{5}g_1^2 + g_2^2 \right)^2 + 4\lambda T - 8 \operatorname{Tr}[Y_e^\dagger Y_e Y_e^\dagger Y_e + 3Y_u^\dagger Y_u Y_u^\dagger Y_u + 3Y_d^\dagger Y_d Y_d^\dagger Y_d] - 20 \operatorname{Tr}[Y_\Sigma^\dagger Y_\Sigma Y_\Sigma^\dagger Y_\Sigma]. \quad (3.65)$$

As it is evident from Eq. (3.65), the last term is the new contribution to the β -function from the heavy triplets still coupled to the theory.

The RG evolution of the Majorana mass matrix of the heavy triplet fermions is given by

$$16\pi^2\beta_{\mathbb{M}_\Sigma} = \left[\left(Y_\Sigma^{(n)} Y_\Sigma^{(n)\dagger} \right) P_L + \left(Y_\Sigma^{(n)} Y_\Sigma^{(n)\dagger} \right)^* P_R \right] \mathbb{M}_\Sigma + \mathbb{M}_\Sigma \left[\left(Y_\Sigma^{(n)} Y_\Sigma^{(n)\dagger} \right)^* P_L + \left(Y_\Sigma^{(n)} Y_\Sigma^{(n)\dagger} \right) P_R \right] - 12g_2^2 \mathbb{M}_\Sigma, \quad (3.66)$$

where it is always possible to separate the components of different chirality to get the left-chiral part as

$$16\pi^2\beta_{\mathbb{M}_\Sigma} = \left(Y_\Sigma^{(n)} Y_\Sigma^{(n)\dagger} \right) \mathbb{M}_\Sigma + \mathbb{M}_\Sigma \left(Y_\Sigma^{(n)} Y_\Sigma^{(n)\dagger} \right)^T - 12g_2^2 \mathbb{M}_\Sigma, \quad (3.67)$$

since $P_L + P_R = \mathbb{I}$. Thus all the β -functions are gauge-independent, as they should be. The anomalous dimension of \mathbb{M}_Σ is

$$-16\pi^2\gamma_{\mathbb{M}_\Sigma}^{(0)} = \mathbb{M}_\Sigma^{-1} \left[\left(Y_\Sigma^{(n)} Y_\Sigma^{(n)\dagger} \right) P_L + \left(Y_\Sigma^{(n)} Y_\Sigma^{(n)\dagger} \right)^* P_R \right] \mathbb{M}_\Sigma + \left[\left(Y_\Sigma^{(n)} Y_\Sigma^{(n)\dagger} \right)^* P_L + \left(Y_\Sigma^{(n)} Y_\Sigma^{(n)\dagger} \right) P_R \right] - 12g_2^2. \quad (3.68)$$

Similar to the left-chiral component of $\beta_{\mathbb{M}_\Sigma}$ in Eq. (3.67), the left-chiral component of $\gamma_{\mathbb{M}_\Sigma}^{(0)}$ is

$$-16\pi^2\gamma_{\mathbb{M}_\Sigma}^{(0)} = \mathbb{M}_\Sigma^{-1} \left(Y_\Sigma^{(n)} Y_\Sigma^{(n)\dagger} \right) \mathbb{M}_\Sigma + \left(Y_\Sigma^{(n)} Y_\Sigma^{(n)\dagger} \right)^* - 12g_2^2. \quad (3.69)$$

As seen from Eq. (3.36) and the definition of the effective neutrino mass matrix $\mathbb{m}_\nu \equiv -\frac{v^2}{2}\mathbb{R}$, the RG evolution of the light neutrino mass matrix \mathbb{m}_ν is controlled by the evolutions of both $\kappa^{(n)}$ and $Q^{(n)}$, which are given by

$$16\pi^2\beta_\kappa = \alpha_\kappa\kappa + P_\kappa^T\kappa + \kappa P_\kappa, \quad (3.70)$$

$$16\pi^2\beta_Q = \alpha_Q Q + P_Q^T Q + Q P_Q, \quad (3.71)$$

with

$$P_\kappa = \frac{3}{2}Y_\Sigma^\dagger Y_\Sigma - \frac{3}{2}Y_e^\dagger Y_e; \quad \alpha_\kappa = 2T + \lambda - 3g_2^2, \quad (3.72)$$

$$P_Q = \frac{3}{2}Y_\Sigma^\dagger Y_\Sigma + \frac{5}{2}Y_e^\dagger Y_e; \quad \alpha_Q = 2T - \frac{9}{10}g_1^2 - \frac{9}{2}g_2^2. \quad (3.73)$$

3.4 RG running of neutrino masses and mixing angles

To derive the RG evolution for the neutrino masses and mixings we follow the standard procedure [34, 61]. At any energy scale μ , the neutrino mass matrix \mathbb{m}_ν can be diagonalized by a unitary transformation via

$$U_\nu(\mu)^T \mathbb{m}_\nu(\mu) U_\nu(\mu) = \text{Diag}(m_1(\mu), m_2(\mu), m_3(\mu)). \quad (3.74)$$

In a basis where Y_e is diagonal, the neutrino mixing matrix is given as

$$U_{\text{PMNS}} = U_\nu, \quad (3.75)$$

where U_{PMNS} is the Pontecorvo-Maki-Nakagawa-Sakata neutrino mixing matrix [9, 10, 11, 12]. From Eqs. (3.58) it is seen that above and between the thresholds, off-diagonal terms will be generated in Y_e even if we start with a diagonal Y_e at the high scale, due to the $Y_\Sigma^\dagger Y_\Sigma$ terms. These terms will give additional contributions to the evolution of different parameters. In the presence of Y_e with off-diagonal entries, the neutrino mixing matrix will be given as

$$U_{\text{PMNS}} = U_e^\dagger U_\nu, \quad (3.76)$$

	C_e	C_Σ	D_e	D_Σ	α_e	α_ν
$\mu > M_3$	$\frac{5}{2}$	$\frac{3}{2}$	$\frac{3}{2}$	$\frac{15}{2}$	$T - \frac{9}{4}g_1^2 - \frac{9}{4}g_2^2$	$2T - \frac{9}{10}g_1^2 - \frac{9}{2}g_2^2$
$\mu < M_1$	$-\frac{3}{2}$	0	$\frac{3}{2}$	0	$T - \frac{9}{4}g_1^2 - \frac{9}{4}g_2^2$	$2T + \lambda - 3g_2^2$

Table 3.1: Coefficients of the β -functions governing the running of neutrino masses and mixings in the energy regimes $\mu > M_3$ and $\mu < M_1$. The quantity T is defined in Eq. (3.62).

where U_e is the unitary matrix that diagonalizes $Y_e^\dagger Y_e$ by a unitary transformation. The parametrization of U_{PMNS} is shown in Eq. (1.1) in Chapter 1.

In this work, we consider $r = 3$ heavy fermion triplets, one for each generation. Then Y_Σ is a 3×3 matrix at high scale when all the three triplets are coupled, and is identically zero for $\mu < M_1$. The RG evolution of the neutrino parameters is then controlled by

$$16\pi^2\beta_{Y_e} = Y_e F + \alpha_e Y_e, \quad (3.77)$$

$$16\pi^2\beta_{\mathbf{m}_\nu} = P^T \mathbf{m}_\nu + \mathbf{m}_\nu P + \alpha_\nu \mathbf{m}_\nu, \quad (3.78)$$

where

$$P = C_e Y_e^\dagger Y_e + C_\Sigma Y_\Sigma^\dagger Y_\Sigma, \quad (3.79)$$

$$F = D_e Y_e^\dagger Y_e + D_\Sigma Y_\Sigma^\dagger Y_\Sigma. \quad (3.80)$$

Eqs. (3.77) and (3.78) are essentially the same as the β -functions given in Eqs. (3.58), (3.70) and (3.71), which we rewrite in the above form for later discussions. For $\mu > M_3$ and $\mu < M_1$, the evolutions of Y_e and \mathbf{m}_ν can be written in simple analytic forms, using Table 3.1. Note that for $\mu > M_3$ the running of the neutrino masses will be governed by β_Q and so P in Eq. (3.79) is the same as P_Q as defined in Eq. (3.73). On the other hand, for $\mu < M_1$, we have $P = P_\kappa$ as given in Eq. (3.72). P and F are 3×3 matrices, with the rows and columns representing generations. We denote the elements of P and F by P_{fg} and F_{fg} . The coefficient of P_{fg} and F_{fg} in the running of Y_e and \mathbf{m}_ν can be read off directly from [61], since the structure of Eqs. (3.77) and (3.78) remain the same both in Type-I and Type-III seesaw. The values of P_{fg}

and F_{fg} themselves will however be different because of different underlying theories. The values of the relevant coefficients in Type-III seesaw are shown in Table 3.1.

If we consider the running equations in the basis $\mathcal{P}_\delta = \{m_i; \theta_{12}, \theta_{13}, \theta_{23}; \phi_i; \delta\}$, then both δ and $\dot{\delta}$ become ill-defined at $\theta_{13} = 0$ [34, 35] and as a consequence, $\dot{\theta}_{13}$ also becomes ill-defined because of its δ dependence. This is only an apparent singularity. One can get rid of it by imposing a particular value of $\cot \delta$ at $\theta_{13} = 0$ [34, 35] or by using the basis $\mathcal{P}_J = \{m_i; \theta_{12}, \theta_{23}, \theta_{13}^2; \phi_i; J_{\text{CP}}, J'_{\text{CP}}\}$, where the singularity does not appear at all [57]. We will elaborate on this issue later on in Chapter 4. Here J_{CP} and J'_{CP} are defined as

$$J_{\text{CP}} \equiv \frac{1}{2} s_{12} c_{12} s_{23} c_{23} s_{13} c_{13}^2 \sin \delta, \quad (3.81)$$

$$J'_{\text{CP}} \equiv \frac{1}{2} s_{12} c_{12} s_{23} c_{23} s_{13} c_{13}^2 \cos \delta. \quad (3.82)$$

In the limit $\theta_{13} \rightarrow 0$, $J_{\text{CP}}, J'_{\text{CP}} \rightarrow 0$. From the point of view of the experiments also, the Jarlskog invariant J_{CP} is the quantity which appears in the probability expressions for CP violation in neutrino oscillation experiments, and is therefore directly measurable. J'_{CP} is needed in order to have complete information on δ , since J_{CP} has no information on the sign of $\cos \delta$. We also choose to write the RG evolution for θ_{13}^2 instead of θ_{13} as is traditionally done. This quantity turns out to have a smooth behavior at $\theta_{13} = 0$. Moreover, since $\theta_{13} \geq 0$ by convention, the complete information about θ_{13} lies within θ_{13}^2 . The information about the Dirac phase will be present in $J_{\text{CP}}, J'_{\text{CP}}$.

The running of masses and the Majorana phases does not depend on the Dirac phase to the lowest order in θ_{13} . Hence the RG evolution equations do not change with the change in basis $\mathcal{P}_\delta \rightarrow \mathcal{P}_J$. Running of the two large mixing angles θ_{12} and θ_{23} , as given in Table 3.2, is also the same as that in the \mathcal{P}_δ basis since the quantities \mathcal{S}_{ij} and \mathcal{Q}_{ij}^\pm , defined as

$$\mathcal{Q}_{13}^\pm = \frac{|m_3 \pm m_1 e^{2i\phi_1}|^2}{\Delta m_{\text{atm}}^2 (1+\zeta)}, \quad \mathcal{Q}_{23}^\pm = \frac{|m_3 \pm m_2 e^{2i\phi_2}|^2}{\Delta m_{\text{atm}}^2}, \quad \mathcal{Q}_{12}^\pm = \frac{|m_2 e^{2i\phi_2} \pm m_1 e^{2i\phi_1}|^2}{\Delta m_{\text{sol}}^2}, \quad (3.83)$$

$$\mathcal{S}_{13} = \frac{m_1 m_3 \sin 2\phi_1}{\Delta m_{\text{atm}}^2 (1+\zeta)}, \quad \mathcal{S}_{23} = \frac{m_2 m_3 \sin 2\phi_2}{\Delta m_{\text{atm}}^2}, \quad \mathcal{S}_{12} = \frac{m_1 m_2 \sin (2\phi_1 - 2\phi_2)}{\Delta m_{\text{sol}}^2}, \quad (3.84)$$

depend on the mass eigenvalues and Majorana phases only. However the running of θ_{13}^2 , as seen from the Table 3.2, depends on the quantities $\tilde{\mathcal{A}}_{ij}^\pm$,

	$32\pi^2 \theta_{12}$	$32\pi^2 \theta_{23}$
P_{11}	$Q_{12}^+ \sin 2\theta_{12}$	0
P_{22}	$-Q_{12}^+ \sin 2\theta_{12} c_{23}^2$	$(Q_{23}^+ c_{12}^2 + Q_{13}^+ s_{12}^2) \sin 2\theta_{23}$
P_{33}	$-Q_{12}^+ \sin 2\theta_{12} s_{23}^2$	$-(Q_{23}^+ c_{12}^2 + Q_{13}^+ s_{12}^2) \sin 2\theta_{23}$
$\text{Re}P_{21}$	$2Q_{12}^+ \cos 2\theta_{12} c_{23}$	$(Q_{23}^+ - Q_{13}^+) \sin 2\theta_{12} s_{23}$
$\text{Re}P_{31}$	$-2Q_{12}^+ \cos 2\theta_{12} s_{23}$	$(Q_{23}^+ - Q_{13}^+) \sin 2\theta_{12} c_{23}$
$\text{Re}P_{32}$	$Q_{12}^+ \sin 2\theta_{12} \sin 2\theta_{23}$	$2(Q_{23}^+ c_{12}^2 + Q_{13}^+ s_{12}^2) \cos 2\theta_{23}$
$\text{Im}P_{21}$	$4\mathcal{S}_{12} c_{23}$	$2(\mathcal{S}_{23} - \mathcal{S}_{13}) \sin 2\theta_{12} s_{23}$
$\text{Im}P_{31}$	$-4\mathcal{S}_{12} s_{23}$	$2(\mathcal{S}_{23} - \mathcal{S}_{13}) \sin 2\theta_{12} c_{23}$
$\text{Im}P_{32}$	0	$4(\mathcal{S}_{23} c_{12}^2 + \mathcal{S}_{13} s_{12}^2)$

	$64\pi^2 \overline{\theta_{13}^2}$
P_{11}	0
P_{22}	$(\tilde{\mathcal{A}}_{23}^+ - \tilde{\mathcal{A}}_{13}^+) \sin 2\theta_{12} \sin 2\theta_{23}$
P_{33}	$-(\tilde{\mathcal{A}}_{23}^+ - \tilde{\mathcal{A}}_{13}^+) \sin 2\theta_{12} \sin 2\theta_{23}$
$\text{Re}P_{21}$	$4(\tilde{\mathcal{A}}_{13}^+ c_{12}^2 + \tilde{\mathcal{A}}_{23}^+ s_{12}^2) s_{23}$
$\text{Re}P_{31}$	$4(\tilde{\mathcal{A}}_{13}^+ c_{12}^2 + \tilde{\mathcal{A}}_{23}^+ s_{12}^2) c_{23}$
$\text{Re}P_{32}$	$2(\tilde{\mathcal{A}}_{23}^+ - \tilde{\mathcal{A}}_{13}^+) \sin 2\theta_{12} \cos 2\theta_{23}$
$\text{Im}P_{21}$	$4(\tilde{\mathcal{B}}_{13}^- c_{12}^2 + \tilde{\mathcal{B}}_{23}^- s_{12}^2) s_{23}$
$\text{Im}P_{31}$	$4(\tilde{\mathcal{B}}_{13}^- c_{12}^2 + \tilde{\mathcal{B}}_{23}^- s_{12}^2) c_{23}$
$\text{Im}P_{32}$	$2(\tilde{\mathcal{B}}_{23}^- - \tilde{\mathcal{B}}_{13}^-) \sin 2\theta_{12}$

Table 3.2: Coefficients of P_{fg} in the RG evolution equations of the mixing angles θ_{12} , θ_{13}^2 and θ_{23} , in the limit $\theta_{13} \rightarrow 0$.

$\tilde{\mathcal{B}}_{ij}^\pm$ defined as

$$\tilde{\mathcal{A}}_{13}^\pm = \frac{4(m_1^2 + m_3^2) J'_{\text{CP}} \pm 8m_1 m_3 (J'_{\text{CP}} \cos 2\phi_1 + J_{\text{CP}} \sin 2\phi_1)}{a\Delta m_{\text{atm}}^2 (1 + \zeta)}, \quad (3.85)$$

$$\tilde{\mathcal{A}}_{23}^\pm = \frac{4(m_2^2 + m_3^2) J'_{\text{CP}} \pm 8m_2 m_3 (J'_{\text{CP}} \cos 2\phi_2 + J_{\text{CP}} \sin 2\phi_2)}{a\Delta m_{\text{atm}}^2}, \quad (3.86)$$

$$\tilde{\mathcal{B}}_{13}^\pm = \frac{4(m_1^2 + m_3^2) J_{\text{CP}} \pm 8m_1 m_3 (J_{\text{CP}} \cos 2\phi_1 - J'_{\text{CP}} \sin 2\phi_1)}{a\Delta m_{\text{atm}}^2 (1 + \zeta)}, \quad (3.87)$$

$$\tilde{\mathcal{B}}_{23}^\pm = \frac{4(m_2^2 + m_3^2) J_{\text{CP}} \pm 8m_2 m_3 (J_{\text{CP}} \cos 2\phi_2 - J'_{\text{CP}} \sin 2\phi_2)}{a\Delta m_{\text{atm}}^2}, \quad (3.88)$$

where $a \equiv s_{12} c_{12} s_{23} c_{23}$. Clearly these quantities depend on J_{CP} , J'_{CP} in addition

	$64\pi^2 \dot{J}_{CP}/a$	$64\pi^2 \dot{J}'_{CP}/a$
P_{11}	0	0
P_{22}	$-4a\mathcal{G}_s^+$	$2a(\mathcal{G}_0^- - 2\mathcal{G}_c^-)$
P_{33}	$4a\mathcal{G}_s^-$	$-2a(\mathcal{G}_0^- - 2\mathcal{G}_c^-)$
$\text{Re}P_{21}$	$4s_{23}\mathcal{G}_s^+$	$2s_{23}(\mathcal{G}_0^+ + 2\mathcal{G}_c^+)$
$\text{Re}P_{31}$	$4c_{23}\mathcal{G}_s^+$	$2c_{23}(\mathcal{G}_0^+ + 2\mathcal{G}_c^+)$
$\text{Re}P_{32}$	$-2 \sin 2\theta_{12} \cos 2\theta_{23} \mathcal{G}_s^-$	$\sin 2\theta_{12} \cos 2\theta_{23} (\mathcal{G}_0^- - 2\mathcal{G}_c^-)$
$\text{Im}P_{21}$	$2s_{23}(\mathcal{G}_0^+ - 2\mathcal{G}_c^+)$	$4s_{23}\mathcal{G}_s^+$
$\text{Im}P_{31}$	$2c_{23}(\mathcal{G}_0^+ - 2\mathcal{G}_c^+)$	$4c_{23}\mathcal{G}_s^+$
$\text{Im}P_{32}$	$\sin 2\theta_{12}(\mathcal{G}_0^- + 2\mathcal{G}_c^-)$	$-2 \sin 2\theta_{12}\mathcal{G}_s^-$

Table 3.3: Coefficients of P_{fg} in the RG evolution equations of the Jarlskog invariant J_{CP} , the quantity $J'_{CP} \equiv J_{CP} \cot \delta$, in the limit $\theta_{13} \rightarrow 0$. The convention used here is $a \equiv s_{12}c_{12}s_{23}c_{23}$, and $J_{CP} \equiv (a/2)s_{13}c_{13}^2 \sin \delta$.

to the masses and Majorana phases. The coefficients for the RG evolution of J_{CP} and J'_{CP} are presented in Table 3.3, where the quantities $\mathcal{G}_{0,c,s}^\pm$ are given by

$$\mathcal{G}_0^\pm = \frac{m_2^2 + m_3^2}{\Delta m_{\text{atm}}^2} \pm \frac{m_1^2 + m_3^2}{\Delta m_{\text{atm}}^2 (1 + \zeta)}, \quad (3.89)$$

$$\mathcal{G}_s^\pm = \frac{m_1 m_3 \sin 2\phi_1}{\Delta m_{\text{atm}}^2 (1 + \zeta)} \pm \frac{m_2 m_3 \sin 2\phi_2}{\Delta m_{\text{atm}}^2}, \quad (3.90)$$

$$\mathcal{G}_c^\pm = \frac{m_1 m_3 \cos 2\phi_1}{\Delta m_{\text{atm}}^2 (1 + \zeta)} \pm \frac{m_2 m_3 \cos 2\phi_2}{\Delta m_{\text{atm}}^2}. \quad (3.91)$$

Thus all the the quantities appearing in the evolution equations (3.85) – (3.91) have finite well-defined limits for $\theta_{13} \rightarrow 0$ in the \mathcal{P}_J basis.

The expressions for the running of masses and Majorana phases are the same as the ones obtained in [61] for the Type-I seesaw mechanism. Tables 3.4 and 3.5 show the running of the masses m_i and the difference between the Majorana phases $|\phi_1 - \phi_2|$ respectively.

Even if one starts with diagonal Y_e (i.e. $Y_e = \text{Diag}(y_e, y_\mu, y_\tau)$) at the high scale, non-zero off-diagonal elements of Y_e will be generated through Eqs. (3.77) – (3.80) since $Y_\Sigma^\dagger Y_\Sigma^{(n)}$ is not diagonal. These off-diagonal elements will give additional contributions to the running of masses and mixing above and between the thresholds through F and α_e . Since α_e is flavor diagonal, it will contribute to the running of y_e, y_μ and y_τ , while off-diagonal components of F will contribute additional terms in the β -functions of angles and phases, as

	$16\pi^2 \dot{m}_1/m_1$	$16\pi^2 \dot{m}_2/m_2$	$16\pi^2 \dot{m}_3/m_3$
α_ν	1	1	1
P_{11}	$2c_{12}^2$	$2s_{12}^2$	0
P_{22}	$2s_{12}^2 c_{23}^2$	$2c_{12}^2 c_{23}^2$	$2s_{23}^2$
P_{33}	$2s_{12}^2 s_{23}^2$	$2c_{12}^2 s_{23}^2$	$2c_{23}^2$
$\text{Re}P_{21}$	$-2 \sin 2\theta_{12} c_{23}$	$2 \sin 2\theta_{12} c_{23}$	0
$\text{Re}P_{31}$	$2 \sin 2\theta_{12} s_{23}$	$-2 \sin 2\theta_{12} s_{23}$	0
$\text{Re}P_{32}$	$-2 \sin 2\theta_{23} s_{12}^2$	$-2 \sin 2\theta_{23} c_{12}^2$	$2 \sin 2\theta_{23}$
$\text{Im}P_{21}$	0	0	0
$\text{Im}P_{31}$	0	0	0
$\text{Im}P_{32}$	0	0	0

Table 3.4: Coefficients of P_{fg} in the RG evolution equations of the neutrino masses m_i $\{i = 1, 2, 3\}$, in the limit $\theta_{13} \rightarrow 0$.

	$32\pi^2(\dot{\phi}_1 - \dot{\phi}_2)$
P_{11}	$-4\mathcal{S}_{12} \cos 2\theta_{12}$
P_{22}	$4\mathcal{S}_{12} c_{23}^2 \cos 2\theta_{12}$
P_{33}	$4\mathcal{S}_{12} s_{23}^2 \cos 2\theta_{12}$
$\text{Re}P_{21}$	$-8\mathcal{S}_{12} c_{23} \cos 2\theta_{12} \cot 2\theta_{12}$
$\text{Re}P_{31}$	$8\mathcal{S}_{12} s_{23} \cos 2\theta_{12} \cot 2\theta_{12}$
$\text{Re}P_{32}$	$-4\mathcal{S}_{12} \cos 2\theta_{12} \sin 2\theta_{23}$
$\text{Im}P_{21}$	$-4\mathcal{Q}_{12}^- c_{23} \cot 2\theta_{12}$
$\text{Im}P_{31}$	$4\mathcal{Q}_{12}^- s_{23} \cot 2\theta_{12}$
$\text{Im}P_{32}$	0

Table 3.5: Coefficients of P_{fg} in the RG evolution equations of the Majorana phase difference $(\phi_1 - \phi_2)$, in the limit $\theta_{13} \rightarrow 0$.

tabulated in Table 3.6 and Table 3.7, respectively. These contributions will just get added to the P_{fg} contribution for the evolution of the quantities in Tables 3.2, 3.3, 3.5. Note that the F_{fg} coefficients are $\lesssim \mathcal{O}(1)$, whereas the P_{fg} coefficients are $\gtrsim \mathcal{O}(m_i^2/\Delta m_{\text{atm}}^2)$. Since the running is significant only when $m_i^2 \gg \Delta m_{\text{atm}}^2$, in almost all the region of interest P_{fg} contributions dominate over the F_{fg} contribution.

Note that the analytical expressions obtained in Eq. (3.83) onwards, and those given in the tables, are valid only in the two extreme regions $\mu > M_3$ and $\mu < M_1$. For the intermediate energy scales, m_ν will receive contributions from both $\kappa^{(n)}$ and $Q^{(n)}$. In the SM these two quantities have non-identical evolutions, as seen from Eqs. (3.70) and (3.71), and therefore the net evolution of Y_e and m_ν is rather complicated. We perform it numerically in the next section.

	$16\pi^2 \dot{\theta}_{12}^{U_e}$	$16\pi^2 \dot{\theta}_{13}^{U_e}$	$16\pi^2 \dot{\theta}_{23}^{U_e}$
F_{11}	0	0	0
F_{22}	0	0	0
F_{33}	0	0	0
$\text{Re}F_{21}$	$-c_{23}$	$-4s_{23}J'_{\text{CP}}/a$	0
$\text{Re}F_{31}$	s_{23}	$-4c_{23}J'_{\text{CP}}/a$	0
$\text{Re}F_{32}$	0	0	1
$\text{Im}F_{21}$	0	$-4s_{23}J_{\text{CP}}/a$	0
$\text{Im}F_{31}$	0	$-4c_{23}J_{\text{CP}}/a$	0
$\text{Im}F_{32}$	0	0	0

Table 3.6: Coefficients of F_{fg} in the RG evolution equations of all the angles (θ_{12} , θ_{13}^2 , θ_{23}), in the limit $\theta_{13} \rightarrow 0$. The convention used here is $a \equiv s_{12}c_{12}s_{23}c_{23}$, and $J_{\text{CP}} \equiv (a/2)s_{13}c_{13}^2 \sin \delta$. We neglect y_e and y_μ compared to y_τ , and take vanishing flavor phases.

	$16\pi^2 \dot{J}_{\text{CP}}^{U_e}$	$16\pi^2 \dot{J}'_{\text{CP}}^{U_e}$	$16\pi^2 \dot{\phi}_1^{U_e}$	$16\pi^2 \dot{\phi}_2^{U_e}$
F_{11}	0	0	0	0
F_{22}	0	0	0	0
F_{33}	0	0	0	0
$\text{Re}F_{21}$	0	$-s_{23}a/2$	0	0
$\text{Re}F_{31}$	0	$-c_{23}a/2$	0	0
$\text{Re}F_{32}$	0	0	0	0
$\text{Im}F_{21}$	$-s_{23}a/2$	0	$c_{23}c_{12}/s_{12}$	$-c_{23}s_{12}/c_{12}$
$\text{Im}F_{31}$	$-c_{23}a/2$	0	$-s_{23}c_{12}/s_{12}$	$s_{23}s_{12}/c_{12}$
$\text{Im}F_{32}$	0	0	$-1/(c_{23}s_{23})$	$-1/(c_{23}s_{23})$

Table 3.7: Coefficients of F_{fg} in the RG evolution equations of J_{CP} , J'_{CP} and the Majorana phases ϕ_i in the limit $\theta_{13} \rightarrow 0$. The convention used here is $a \equiv s_{12}c_{12}s_{23}c_{23}$, and $J_{\text{CP}} \equiv (a/2)s_{13}c_{13}^2 \sin \delta$. We neglect y_e and y_μ compared to y_τ , and take vanishing flavor phases.

3.5 Illustrative examples of RG running of the masses and mixing

In this section we numerically calculate the RG evolution of the masses and mixing parameters within the Type-III seesaw model including the impact of running between the thresholds. This analysis is done by imposing suitable matching conditions (3.34) at the thresholds. For illustration, we start at $\mu_0 = 10^{16}$ GeV and choose the basis in which Y_e is diagonal, so that $U_{\text{PMNS}} = U_\nu$. We further choose U_ν at this high scale to be the bimaximal mixing matrix

$U_{\nu, \text{bimax}}$ [45, 132, 133, 134, 135], i.e. $\theta_{12} = \theta_{23} = \pi/4$ and $\theta_{13} = 0$. This scenario is clearly inconsistent with the current data in the absence of RG evolution. We shall check if the radiative corrections to the masses and mixing angles can make it consistent with the data at the low scale.

If the low energy theory in the complete energy range $\mu < \mu_0$ is the SM, then θ_{12} decreases as the energy scale decreases, however the running is not sufficient to achieve compatibility with the low energy data. If the low energy theory is the MSSM, then θ_{12} increases with decreasing energy scale [136], so that compatibility with the data is not possible. However, it has been shown in [59, 137, 138] in the context of Type-I seesaw mechanism, that the inclusion of threshold effects can make the mixing angle θ_{12} decrease substantially as we go to lower energy scale and can give the correct values consistent with the Large Mixing Angle (LMA) solution. In this section we study the evolution from bi-maximal mixing at high scale in the context of Type-III seesaw scenario, including the seesaw threshold effects.

We write the neutrino mass matrix as

$$\mathbb{m}_\nu = U_{\nu, \text{bimax}}^* \text{Diag}(m_1, m_2, m_3) U_{\nu, \text{bimax}}^\dagger, \quad (3.92)$$

with $\delta_e = \delta_\mu = \delta_\tau = 0$ at the high scale. Given the masses of the three fermion triplets and the light neutrino masses at the high scale, one can determine a Y_Σ at the high scale³ that satisfies the seesaw relation $\mathbb{m}_\nu = -(v^2/2)Y_\Sigma^T \mathbb{M}_\Sigma^{-1} Y_\Sigma$. We then evolve the parameters using the analysis of Section 3.4.

Among the neutrino mixing angles, θ_{12} is expected to be the most sensitive to RG effects. Table 3.2 shows that $\dot{\theta}_{12}$ is proportional to \mathcal{Q}_{12}^+ and \mathcal{S}_{12} , which are in turn proportional to $(m_i^2/\Delta m_{\text{sol}}^2)$ as can be seen from Eqs. (3.83) and (3.84). For the other angles θ_{ij} , the corresponding quantities \mathcal{Q}_{ij}^+ and \mathcal{S}_{ij} are proportional to $(m_i^2/\Delta m_{\text{atm}}^2)$, so the evolution of these angles is smaller. The direction of θ_{12} evolution depends on the details of the Yukawa coupling matrix and masses of the heavy fermions.

Since the values of Majorana phases at the low scale are completely unknown, we first consider the case where $\phi_1 = \phi_2 = 0$. In this case the CP violation

³ The solution for Y_Σ need not be unique, however any one of the solutions would suffice for the illustration. For practicality, we first choose an ‘‘trial’’ Y_Σ , calculate the corresponding \mathbb{M}_Σ from the seesaw relation, and then apply the basis transformation that makes \mathbb{M}_Σ diagonal and takes the ‘‘trial’’ Y_Σ to its final form.

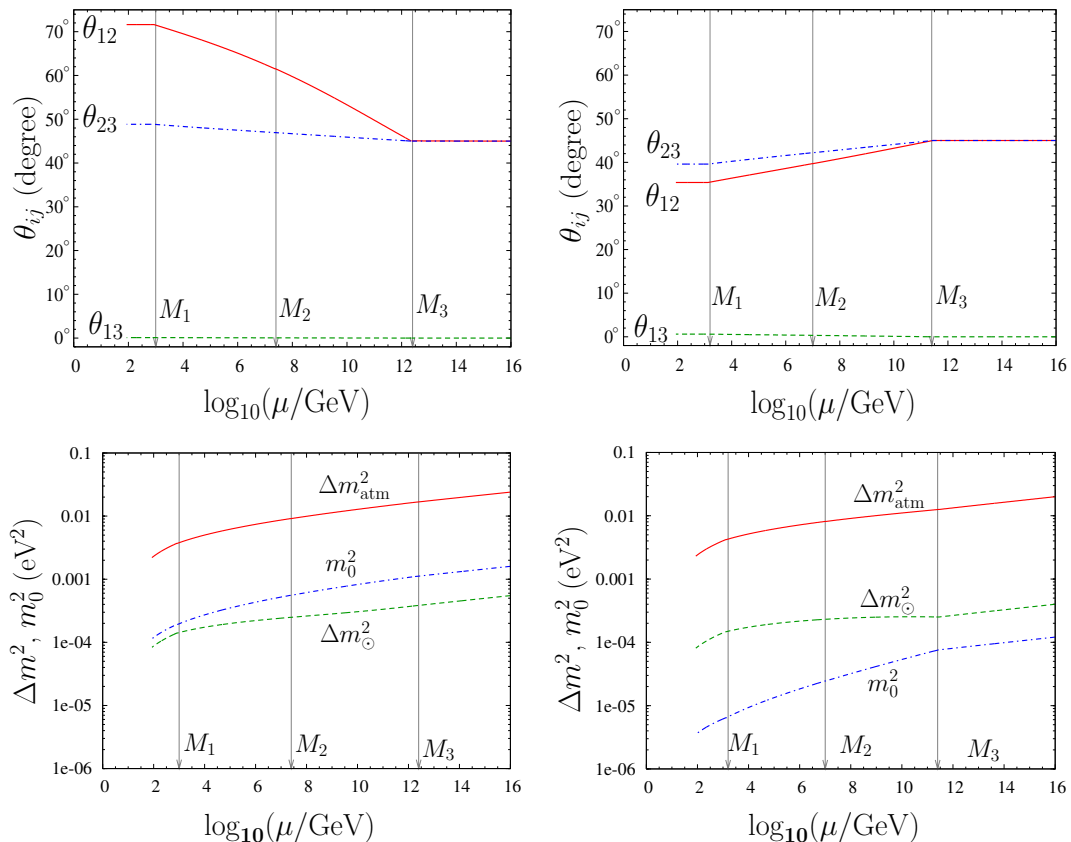


Figure 3.4: RG evolution of mixing angles and mass squared differences, starting from bimaximal mixing at $\mu_0 = 10^{16}$ GeV, for normal mass ordering and hierarchical neutrino masses. The left panels represent the scenario where the Majorana phases vanish at μ_0 . The right panel shows a representative case of nonzero Majorana phases ($\phi_1 = 89.0^\circ$, $\phi_2 = 0.4^\circ$) at μ_0 . The values of parameters at the high scale have been chosen such that the Δm^2 's and g_2 at the low scale are reproduced.

will remain zero at all energy scales. The left panels of Fig. 3.4 show the running of mixing angles and mass squared differences for the normal mass ordering in this scenario. It is observed that θ_{12} in the intermediate energy region changes more rapidly than in the extreme regions, however this change is in the opposite direction to what is required. As a result, bimaximal mixing at the high scale is not compatible with the low energy data in our model when the Majorana phases vanish. With nonzero Majorana phases, however, it is possible to achieve compatibility with the low scale data, as can be seen from the right panels of the figure.

The lower panels of Fig. 3.4 show the evolution of m_0 , the lowest mass scale,

and the two mass squared differences. As can be observed, the running of masses is quite substantial in Type-III seesaw, as compared to the SM, the MSSM [35], or the Type-I seesaw [59]. Most of this running occurs in the intermediate energy range $M_1 < \mu < M_3$, where threshold effects play a crucial role in enhancing the running. Note that the values of m_0 required to cause substantial running of mixing angles is quite small: in the case of vanishing (non vanishing) Majorana phases, we have taken $m_0 = 0.04(0.01)$ eV at $\mu = \mu_0$. Thus, even at extremely small m_0 , substantial running of neutrino parameters can be present in the Type-III seesaw.

The example of the bimaximal mixing discussed above was just for illustration. However, it brings out certain salient features of the RG running in Type-III seesaw scenario. The running of neutrino masses can be quite substantial here in the intermediate energy range. Moreover, threshold effects can enhance the extent of running of mixing angles, as well as the direction of the evolution, similar to the Type-I seesaw scenario [59]. Majorana phases are also seen to play an important role in determining the extent and the direction of RG running of neutrino mixing parameters.

In Fig. 3.5, we illustrate the RG evolution of parameters when the neutrino masses are quasi-degenerate. We have taken the parameter values at the high scale to achieve compatibility with the low scale data, without imposing any special symmetry. However in order to bring out certain salient features of the RG evolution that are independent of the threshold effects, we have chosen a small θ_{13} value, $|\phi_1 - \phi_2| \approx \pi/2$, and $Y_\Sigma^\dagger Y_\Sigma$ to be almost diagonal in the charged lepton basis, with hierarchical eigenvalues. These conditions ensure that P_{21} and P_{31} are small, and \mathcal{S}_{12} vanishes, so that from Table 3.5, the evolution of $(\phi_1 - \phi_2)$ is extremely small. Thus $|\phi_1 - \phi_2|$ is expected to stay close to $\pi/2$ even after evolution, which is verified by the figure. Moreover, combined with $m_1 \approx m_2$, the choice $|\phi_1 - \phi_2| \approx \pi/2$ makes \mathcal{Q}_{12}^+ extremely small, thus restricting the θ_{12} evolution.

It is observed that the running of θ_{23} is now large, owing to $m_0^2/\Delta m_{\text{atm}}^2 \sim 1$. This makes it possible to mimic maximal mixing accidentally, even if the mixing generated at the high scale is arbitrary. The value of θ_{13} also quadruples from its high scale value. The Dirac phase, which was chosen to vanish at μ_0 , is generated by the RG evolution. The running of Dirac as well as Majorana phases is substantial between the thresholds.

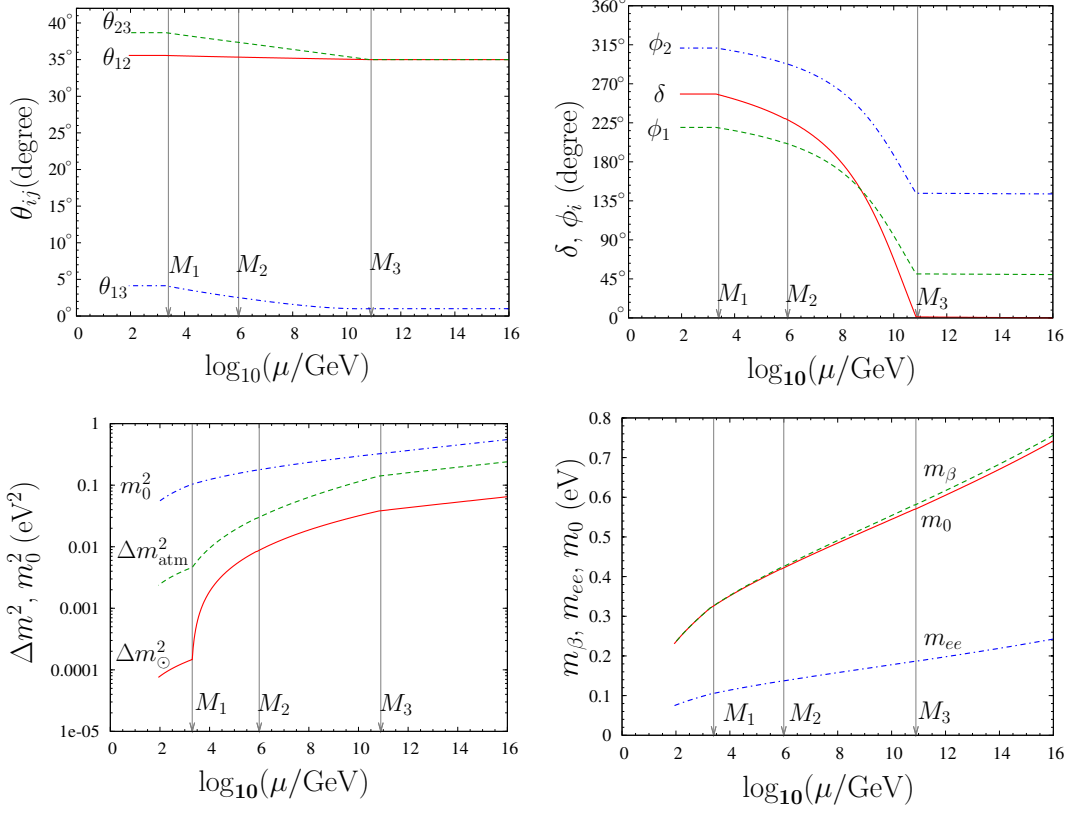


Figure 3.5: RG evolution of mixing angles, mass squared differences, and CP violating phases, for quasi-degenerate neutrino masses and normal mass ordering. The values of parameters at the high scale have been chosen such that the Δm^2 's and g_2 at the low scale are reproduced. Note that for the Majorana phases ϕ_i , the regions $(0^\circ - 180^\circ)$ and $(180^\circ - 360^\circ)$ should be identified with each other.

The right hand bottom panel of Fig. 3.5 shows the energy evolution of $m_\beta \equiv \sqrt{\sum_i |U_{ei}|^2 m_i^2}$, the effective neutrino mass measured in the Tritium beta decay experiments [17], as well as $m_{ee} \equiv |\sum_i U_{ei}^2 m_i|$, the effective neutrino Majorana mass in the neutrinoless double beta decay. Note that since θ_{13} is small, $m_1 \approx m_2 \approx m_0$, and since $|\phi_1 - \phi_2| \approx \pi/2$ in addition, we have $m_{ee} \approx m_0 \cos 2\theta_{12}$. Also in the quasi-degenerate case, the sum of neutrino masses that is restricted by cosmology is $\sum m_i \approx 3m_0$. The large running of these masses suggests that, even if the beta decay experiments were to bound m_β to ≤ 0.3 eV, or the neutrinoless double beta decay experiments were to bound m_{ee} to ≤ 0.1 eV, or the cosmological observations were to restrict m_0 at the low scale to ≤ 0.3 eV, the value of m_0 generated at the high scale can still be substantially larger.

It is thus observed that in Type-III seesaw, the RG evolution of masses, angles as well as CP violating phases can be significant between the thresholds even at low m_0 values. The reason behind this, as well as the exact dependence of the evolution on the mass thresholds and Majorana phases, needs to be studied in further detail for a better understanding of the allowed neutrino parameter space at high energies.

3.6 Summary

In this chapter we have studied the RG evolution of neutrino masses and mixing parameters in the context of Type-III seesaw mechanism mediated by heavy fermions Σ transforming as triplets under $SU(2)_L$. Tree level exchange of such particles gives rise to an effective operator $\kappa_5 l_L l_L \phi \phi$ below their lowest mass threshold. If one or more such triplets are present in the model, they affect the RG evolution of wavefunctions, masses and couplings. We compute these extra contributions using dimensional regularization and minimal subtraction scheme. We calculate the beta functions for the Yukawa couplings Y_e , Y_u , Y_d and Y_Σ , the $SU(2)_L$ gauge coupling g_2 , the Higgs self-coupling λ , the heavy fermion triplet mass matrix M_Σ , and finally the light neutrino mass matrix m_ν . We do our calculation in the R_ξ gauge and show the gauge invariance explicitly by demonstrating that the terms containing ξ are not present in the β -functions.

It is found that the presence of the triplets does not give rise to any additional diagram for the effective vertex κ . However, the presence of these fields is felt indirectly in the running of κ through their contribution to the evolution of the other quantities. Since the fermion triplets couple to W bosons, the evolution of the $SU(2)_L$ gauge coupling g_2 is significantly affected, with more than two Σ triplets changing the sign of the β function for g_2 . This may also have implications for the unification of gauge couplings. In turn, the masses of the Σ 's are also affected substantially due to the coupling with g_2 .

We give the analytic expressions for the RG evolutions of the neutrino masses and mixing above the highest mass threshold and below the lowest one. However, we use a basis $\mathcal{P}_J = \{m_i, \theta_{12}, \theta_{23}, \theta_{13}^2, \phi_i, J_{\text{CP}}, J'_{\text{CP}}\}$ instead of the commonly used basis $\mathcal{P}_\delta = \{m_i, \theta_{12}, \theta_{23}, \theta_{13}, \phi_i, \delta\}$. The advantage of \mathcal{P}_J is that in this basis all the evolution equations are explicitly non-singular at all points in

the parameter space including at $\theta_{13} = 0$. This specific issue will be discussed in detail in Chapter 4.

We consider the scenario with three triplets having non-degenerate masses and include the effect of successive decoupling of the heavy triplets at their respective mass thresholds by imposing suitable matching conditions at each mass scale. We present illustrative examples of running of masses and mixings by numerical diagonalization of the effective neutrino mass matrix. Although the running of masses and mixing angles is not very large in the SM, in our model the running can be large due to threshold effects of the heavy triplets. In particular we find that starting from bi-maximal mixing at high scale it is possible to generate low scale values of masses and mixing angles for the normal hierarchical neutrino spectrum. However, this requires non-zero values of the Majorana phases. Indeed it is observed that the presence of threshold effects and Majorana phases can influence the evolution of the mixing angles significantly.

In conclusion, the work in this chapter studies threshold effects in the context of the Type-III seesaw mechanism. It is crucial for testing the viability of a high scale theory with low scale data. Indeed it is seen that theories that are excluded by the data in the absence of RG running can become viable once these effects are included. In order to determine the allowed neutrino parameter space at the high scale, a detailed exploration of the dependence of RG effects on various parameters is necessary. This is all the more important in view of the onset of the precision era in neutrino physics.

Chapter 4

RG evolution near $\theta_{13} = 0$

4.1 Introduction

The current experimental ranges for the different neutrino mixing parameters are given in the Table 1.1 of Chapter 1, which shows that while two of the mixing angles θ_{12} and θ_{23} are large, the third angle θ_{13} is small and may even be zero. There is a whole class of models with $\theta_{13} \approx 0$ that are consistent with data [139]. $\theta_{23} = \pi/4$ and $\theta_{13} = 0$ are allowed by the current data and their origin has been traced to an exact $\mu - \tau$ exchange symmetry in the neutrino mass matrix [140, 141, 142, 143, 144]. Such symmetries can be realized by models based on the discrete non-abelian symmetry groups like A_4 [145, 146, 147], D_4 [148, 149], S_3 [150, 151, 152, 153, 154], S_4 [155, 156, 157, 158]. Special cases of an exact $\mu - \tau$ symmetric matrix corresponding to a L_e symmetry for normal ordering [159], $L_e - L_\mu - L_\tau$ symmetry for inverted ordering [160, 161, 162, 163, 164, 165] and $L_\mu - L_\tau$ symmetry for quasidegenerate neutrinos can give $\theta_{13} = 0$ [166]. Any deviation from this value would indicate breaking of these symmetries. Models with discrete abelian symmetries can also make θ_{13} vanish [167]. Models involving certain texture zeroes in the neutrino Yukawa matrix or certain scaling relations between Majorana matrix elements can also predict zero or almost vanishing θ_{13} [168, 169, 170, 171, 172]. SO(10) models with certain structures for Dirac mass matrices [173, 174, 175], or those with a SO(3) symmetry can predict $\theta_{13} \lesssim 10^{-4}$ with a normal mass ordering [176].

Most of the symmetries in these models are obeyed at the high scale, and are broken at the low scale by, for example, radiative corrections. If the radiative

corrections are large enough, any trace of the original symmetry may be wiped out. However in the context of a specific model, the compatibility between the high scale symmetry and low scale measurements can still be verified. This needs a careful study of the renormalization group (RG) evolution of the neutrino mass matrix and the mixing parameters. The basic formalism for calculating this evolution has been established in [32, 33, 34, 35, 36], as already discussed in Chapter 3. Specific features of the evolution, like the stability of mixing angles and masses [177, 178, 179, 180], possible occurrence of fixed points [181, 182, 183], evolution of nearly degenerate Majorana neutrinos [45, 46, 48, 49, 50, 51, 52, 53, 184], or the generation of large mixing angles from small angles at the high scale [38, 39, 40, 41, 42, 43, 44], have been explored. Radiative generation of \mathcal{U}_{e3} starting from zero value at high scale has been studied in [54, 55, 56, 185], while its effect on lepton flavor violating decays are examined in the framework of SUSY-GUTs in [186]. Threshold effects on masses and mixings, due to the decoupling of heavy particles involved in the neutrino mass generation, have also been estimated [60, 61, 187, 188]. These effects can revive [59, 137, 138] the bimaximal mixing scenario [132, 189], which predicts $\theta_{13} = 0$.

Analytical expressions for the RG evolution of the neutrino masses and mixing parameters in the low energy effective theory have been obtained through an expansion in the small parameter θ_{13} [34]. For a quantity $X \in \{m_i, \theta_{ij}, \phi_i\}$, the evolution may be written as

$$\dot{X} = A_X + \mathcal{O}(\theta_{13}), \quad (4.1)$$

where dot represents the derivative with respect to $t \equiv \ln(\mu/\text{GeV})/(16\pi^2)$, with μ the relevant energy scale. Here A_X is independent of θ_{13} , but is a function of $m_i, \theta_{12}, \theta_{23}, \phi_i, \delta$ in general. In the context of quark-lepton complementarity, approximate but transparent analytical expressions were obtained in [136] where a further expansion in the small parameter $\Delta_\tau \propto y_\tau^2(1 + \tan^2 \beta)$ was employed. Here y_τ is the Yukawa coupling of the tau lepton and $\tan \beta$ the ratio of vacuum expectation values of the two Higgses in minimal supersymmetric standard model (MSSM). Such an expansion was used to constrain the allowed values of mixing angles in the context of tri-bimaximal mixing [190, 191] and to distinguish between various symmetry-based relations at the high scale by comparing the low scale θ_{13} values [192].

A subtle but important issue arises in the evolution of the Dirac phase δ at $\theta_{13} = 0$. With the parameterization in [34], the evolution formally takes the form

$$\dot{\delta} = \frac{D_\delta}{\theta_{13}} + A_\delta + \mathcal{O}(\theta_{13}), \quad (4.2)$$

such that the derivative of δ formally diverges at vanishing θ_{13} , indicating an apparent singularity. This is an unphysical singularity: all the elements of the mixing matrix U_{PMNS} evolve continuously, and the peculiar evolution of δ is related to the fact that δ is undefined at $\theta_{13} = 0$. This argument is in fact used in [34] to assert that D_δ identically vanishes when $\theta_{13} = 0$, which leads to a specific value of $\cot \delta$ which is a function of $\{m_i, \phi_i\}$ at $\theta_{13} = 0$. Ref. [183] has examined this prescription in various limits in the parameter space.

Hence it is important to study this issue of apparent singularity at $\theta_{13} = 0$ carefully. While the above prescription for choosing the value of δ at $\theta_{13} \rightarrow 0$ works practically when one needs to start with vanishing θ_{13} , a few conceptual problems remain. Firstly, when $\theta_{13} = 0$, the value of δ chosen should not make a difference to the RG evolution since δ is an unphysical quantity at this point. Secondly, it is not *a priori* clear whether the prescription would work when $\theta_{13} = 0$ is reached during the process of RG evolution. Indeed, getting the required value of δ precisely when $\theta_{13} = 0$ may seem like fine tuning. The prescription in [34], though practical, does not tell us the origin of this apparent coincidence. Here we analyze this problem in more detail, and find an explanation in terms of the evolution of the complex quantity $\mathcal{U}_{e3} = \sin \theta_{13} e^{-i\delta}$ in the parameter plane $\text{Re}(\mathcal{U}_{e3})\text{--}\text{Im}(\mathcal{U}_{e3})$.

We also evolve an alternative formalism where the singularity does not arise at all. This is based on the observation that the set of quantities $\mathcal{P}_J \equiv \{m_i, \theta_{12}, \theta_{23}, \theta_{13}^2, \phi_i, J_{\text{CP}}, J'_{\text{CP}}\}$, where $J_{\text{CP}} = \frac{1}{2} s_{12} c_{12} s_{23} c_{23} s_{13} c_{13}^2 \sin \delta$ is the Jarlskog invariant and $J'_{\text{CP}} = \frac{1}{2} s_{12} c_{12} s_{23} c_{23} s_{13} c_{13}^2 \cos \delta$, have the same information as the set $\mathcal{P}_\delta \equiv \{m_i, \theta_{12}, \theta_{23}, \theta_{13}, \phi_i, \delta\}$. We therefore write the evolution equations in terms of the former set and explicitly show that the complete evolution may be studied without any reference to diverging quantities. We confirm numerically that the evolutions with both the parameterizations indeed match with each other and with the exact numerical one.

With the conceptual issue clarified, we numerically study the extent to which θ_{13} may be generated through RG running in the class of models with $\theta_{13} = 0$

at the high scale, where the low energy effective theory is the standard model (SM) or the minimal supersymmetric standard model (MSSM). This evolution turns out to be extremely sensitive to the mass of the lightest neutrino m_0 , the neutrino mass ordering and the Majorana phases. Another experimentally observable quantity that depends on these parameters is the effective Majorana mass m_{ee} which is explored by the neutrinoless double beta decay experiments. Correlated constraints can therefore be obtained on θ_{13} , m_0 and m_{ee} , the quantities for which only upper bounds are available currently but which may be measured in the next generation experiments. For the case of MSSM, it will also depend on the value of $\tan\beta$.

4.2 Apparent singularity in δ -evolution at $\theta_{13} = 0$ and RG evolution in the complex \mathcal{U}_{e3} plane

Analytic studies of the evolution of neutrino parameters till date have been mostly performed with the parameter set $\mathcal{P}_\delta \equiv \{m_i, \theta_{12}, \theta_{23}, \theta_{13}, \phi_i, \delta\}$. The RG evolution equations for the mixing parameters in this \mathcal{P}_δ basis are given in Appendix D. As can be seen, all the evolution equations obtained are continuous and non-singular, except the equation for the Dirac CP phase δ , which is given by

$$\dot{\delta} = \frac{D_\delta}{\theta_{13}} + A_\delta + \mathcal{O}(\theta_{13}), \quad (4.3)$$

where

$$D_\delta = \frac{C y_\tau^2}{2} \sin 2\theta_{12} \sin 2\theta_{23} \frac{m_3}{\Delta m_{31}^2} \times \left[m_1 \sin(2\phi_1 - \delta) - (1 + \zeta) m_2 \sin(2\phi_2 - \delta) + \zeta m_3 \sin \delta \right], \quad (4.4)$$

$$\begin{aligned}
 A_\delta = & 2C y_\tau^2 \left[\frac{m_1 m_2}{\Delta m_\odot^2} s_{23}^2 \sin(2\phi_1 - 2\phi_2) \right. \\
 & + \frac{m_1 m_3}{\Delta m_{31}^2} (c_{12}^2 c_{23}^2 \sin(2\delta - 2\phi_1) + s_{12}^2 \cos 2\theta_{23} \sin 2\phi_1) \\
 & \left. + \frac{m_2 m_3}{\Delta m_{\text{atm}}^2} (s_{12}^2 c_{23}^2 \sin(2\delta - 2\phi_2) + c_{12}^2 \cos 2\theta_{23} \sin 2\phi_2) \right]. \quad (4.5)
 \end{aligned}$$

Here $\zeta = \Delta m_\odot^2 / \Delta m_{\text{atm}}^2$ and C is a constant which depends on the underlying effective theory in the energy regime considered. Eq. (4.3) clearly suggests that $\dot{\delta}$ diverges for $\theta_{13} \rightarrow 0$. This problem is overcome by requiring that $D_\delta = 0$ at $\theta_{13} = 0$, which gives the following condition on δ at $\theta_{13} = 0$ [34]:

$$\cot \delta = \frac{m_1 \cos 2\phi_1 - (1 + \zeta)m_2 \cos 2\phi_2 - \zeta m_3}{m_1 \sin 2\phi_1 - (1 + \zeta)m_2 \sin 2\phi_2}. \quad (4.6)$$

The above prescription works for the calculation of evolution when one starts with vanishing θ_{13} . However on the face of it, it seems to imply that the CP phase δ , which does not have any physical meaning at the point $\theta_{13} = 0$, should attain a particular value depending on the masses and Majorana phases, as given in Eq. (4.6). Also, the situation when $\theta_{13} = 0$ is reached during the course of the RG evolution has not been studied so far, so it is not clear if the prescription needs to be introduced by hand in such a case, or whether the RG evolution equations stay valid while passing through $\theta_{13} = 0$. Getting the required value of δ precisely when $\theta_{13} = 0$ would seem to need fine tuning, unless we are able to figure out the origin of this apparent coincidence, and show that this value of δ is a natural limit of the RG evolution.

The problem also propagates to the evolution of θ_{13} , since it depends in turn on δ :

$$\begin{aligned}
 \dot{\theta}_{13} &= A_{13} + \mathcal{O}(\theta_{13}), \quad (4.7) \\
 A_{13} &= \frac{C y_\tau^2}{2} \sin 2\theta_{12} \sin 2\theta_{23} \frac{m_3}{\Delta m_{31}^2} \times \\
 & \quad [m_1 \cos(2\phi_1 - \delta) - (1 + \zeta)m_2 \cos(2\phi_2 - \delta) - \zeta m_3 \cos \delta]. \quad (4.8)
 \end{aligned}$$

The evolution of all the other quantities, viz. $\theta_{12}, \theta_{23}, m_i, \phi_i$ is independent of δ upto $\mathcal{O}(\theta_{13}^0)$ [34], so these quantities do not concern us here.

In order to understand the nature of the apparent singularity in δ , we explore the RG evolution of the complex quantity $\mathcal{U}_{e3} = \sin \theta_{13} e^{-i\delta}$. We start with

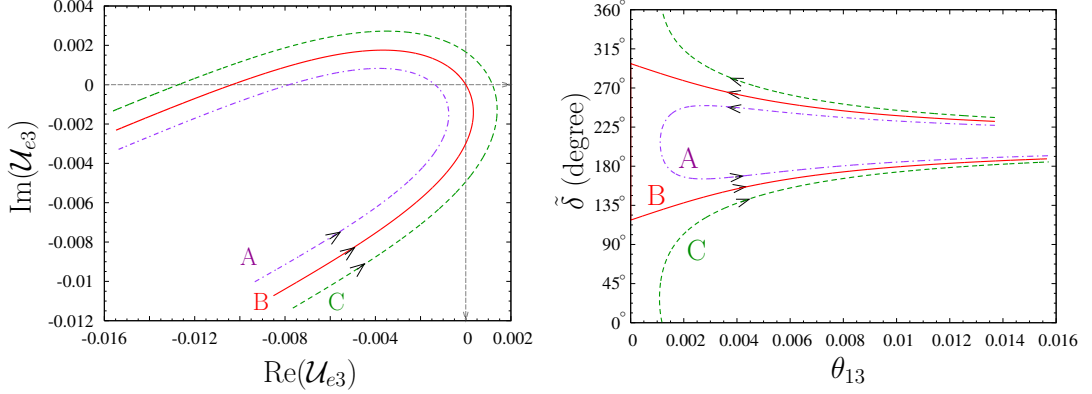


Figure 4.1: The left panel shows the evolution in the $\text{Re}(\mathcal{U}_{e3})$ – $\text{Im}(\mathcal{U}_{e3})$ parameter plane, whereas The right panel shows the corresponding evolution in the θ_{13} – $\tilde{\delta}$ plane. The values of the parameters chosen at $\mu_0 = 10^{12}$ GeV are: $\tan \beta = 50$, $m_0 = 0.0585 \text{ eV}^2$, $\Delta m_{\odot}^2 = 4.22 \times 10^{-5} \text{ eV}^2$, $\Delta m_{\text{atm}}^2 = 3.91 \times 10^{-3} \text{ eV}^2$, $\theta_{12} = 32.84^\circ$, $\theta_{23} = 43.71^\circ$ and $\theta_{13} = 0.014$ rad. The Majorana phases are taken to be $\phi_1 = 58.9^\circ$ and $\phi_2 = 159.15^\circ$. The Dirac CP phase is 124.0° for case A (violet, dash-dotted line), 128.447° for case B (red, solid line) and 133.0° for case C (green, dashed line).

three representative values of δ at the energy scale $\mu_0 = 10^{12}$ GeV, with the other parameters chosen such that $\theta_{13} \lesssim 10^{-3}$ at $\mu \approx 10^9$ GeV. The left panel of Fig. 4.1 shows the evolution in the complex \mathcal{U}_{e3} plane. The right panel shows the corresponding evolution in the θ_{13} – $\tilde{\delta}$ plane, with $\tilde{\delta} \equiv 2\pi - \delta$. The following observations may be made from the figures:

(a) Though all the parameter values at the high scale are very close, and though in all cases θ_{13} decreases to a very small value before it starts to increase, θ_{13} does not vanish during the evolution in all the cases. Indeed, the value of δ chosen at the high scale, in order to make θ_{13} vanish during its evolution, needs to be extremely fine-tuned. This is because

$$\sin^2 \theta_{13} = [\text{Re}(\mathcal{U}_{e3})]^2 + [\text{Im}(\mathcal{U}_{e3})]^2, \quad (4.9)$$

so that one needs both the real and imaginary components of \mathcal{U}_{e3} to vanish simultaneously, which needs a coincidence. Note that when both the CP violating phases δ and ϕ_i vanish at the high scale, $\text{Im}(\mathcal{U}_{e3}) = 0$ automatically throughout the evolution. Then starting from a non-zero value at high scale, θ_{13} can be made to vanish simply by requiring $\text{Re}(\mathcal{U}_{e3}) = 0$ so that no fine tuning is needed.

(b) With the definition $\tilde{\delta} \equiv 2\pi - \delta$ we have $\mathcal{U}_{e3} \equiv s_{13}e^{i\tilde{\delta}}$ and thus $\tilde{\delta}$ is the

phase of \mathcal{U}_{e3} which can be read off easily from the $\text{Re}(\mathcal{U}_{e3})$ – $\text{Im}(\mathcal{U}_{e3})$ plot. The values of δ chosen at $\mu_0 = 10^{12}$ GeV are such that $\tilde{\delta}$ is in the third quadrant, so $\text{Re}(\mathcal{U}_{e3}) < 0$ and $\text{Im}(\mathcal{U}_{e3}) < 0$ at this scale. At the end of the evolution, at $\mu = 10^4$ GeV, $\tilde{\delta}$ returns to the third quadrant. During its evolution, $\tilde{\delta}$ may change its quadrant zero, one or multiple times. The value of θ_{13} need not vanish completely during the RG evolution, as is represented by the scenarios A and C. Scenario B is the one where $\text{Re}(\mathcal{U}_{e3})$ and $\text{Im}(\mathcal{U}_{e3})$ vanish at the same point, and therefore θ_{13} passes through zero during its evolution.

(c) In scenario A, since $\text{Re}(\mathcal{U}_{e3})$ stays negative, $\tilde{\delta}$ simply moves from the third quadrant to the second, and then returns to the third in a continuous manner. In scenario C on the other hand, $\tilde{\delta}$ has to pass through the fourth, first and second quadrant in sequence to finally return to the third quadrant. However its evolution is continuous, the apparent jump at the lowest θ_{13} values in the right panel of Fig. 4.1 is just the identification of 0° and 360° .

(d) In scenario B, $\tilde{\delta}$ starts in the third quadrant and moves continuously to the fourth quadrant. However it propagates to the second quadrant directly through the origin, thus bypassing the first quadrant entirely. Its value at the origin can be well-defined through the limit

$$\cot \tilde{\delta}_0 \equiv \lim_{\text{Re}(\mathcal{U}_{e3}), \text{Im}(\mathcal{U}_{e3}) \rightarrow 0} \frac{\text{Re}(\mathcal{U}_{e3})}{\text{Im}(\mathcal{U}_{e3})} = \lim_{\text{Re}(\mathcal{U}_{e3}), \text{Im}(\mathcal{U}_{e3}) \rightarrow 0} \frac{\frac{d}{dt} \text{Re}(\mathcal{U}_{e3})}{\frac{d}{dt} \text{Im}(\mathcal{U}_{e3})} \quad (4.10)$$

where we have used L'Hospital's rule to compute the limit since both the numerator and denominator in this ratio tend to zero at the limiting point.

Since

$$\text{Re}(\mathcal{U}_{e3}) = \sin \theta_{13} \cos \delta, \quad \text{Im}(\mathcal{U}_{e3}) = -\sin \theta_{13} \sin \delta, \quad (4.11)$$

we have

$$\cot \tilde{\delta}_0 = -\frac{A_{13} \cos \delta - D_\delta \sin \delta}{A_{13} \sin \delta + D_\delta \cos \delta}, \quad (4.12)$$

and using Eqs. (4.4) and (4.8), one obtains

$$\cot \tilde{\delta}_0 = -\frac{m_1 \cos 2\phi_1 - (1 + \zeta)m_2 \cos 2\phi_2 - \zeta m_3}{m_1 \sin 2\phi_1 - (1 + \zeta)m_2 \sin 2\phi_2}. \quad (4.13)$$

Since $\delta = 2\pi - \tilde{\delta}$, this is equivalent to

$$\cot \delta_0 = \frac{m_1 \cos 2\phi_1 - (1 + \zeta)m_2 \cos 2\phi_2 - \zeta m_3}{m_1 \sin 2\phi_1 - (1 + \zeta)m_2 \sin 2\phi_2}, \quad (4.14)$$

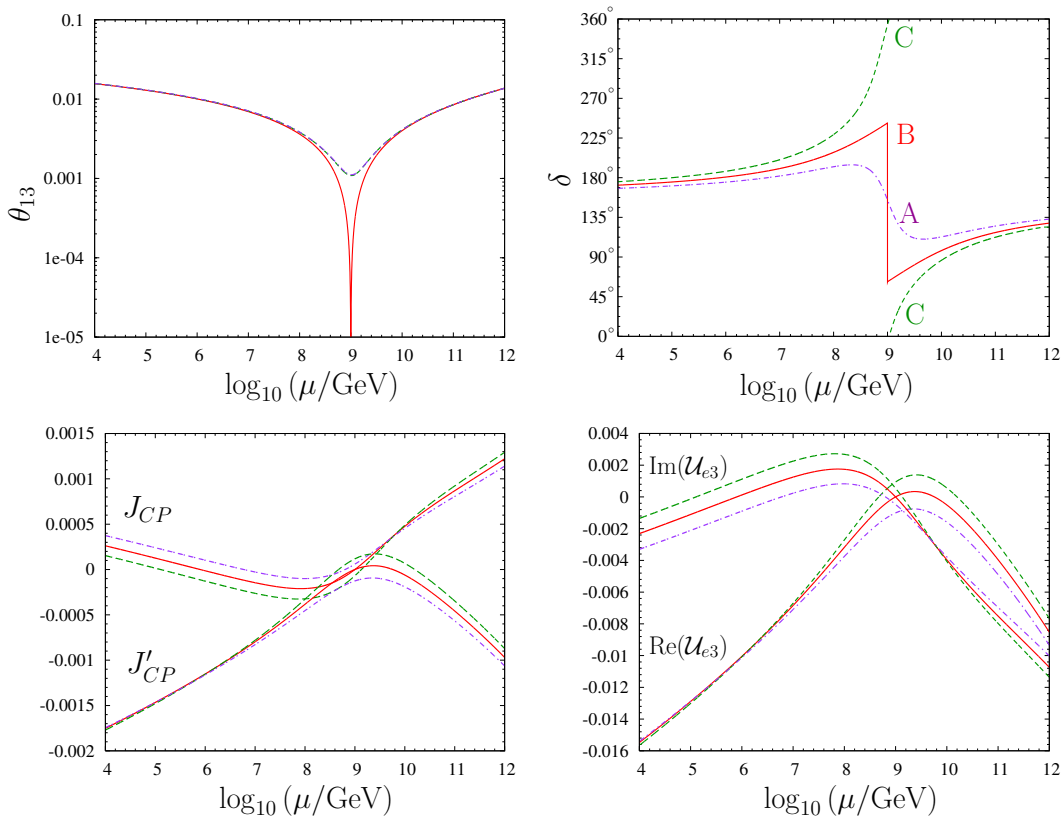


Figure 4.2: The evolution of θ_{13} , δ , $\text{Re}(\mathcal{U}_{e3})$, $\text{Im}(\mathcal{U}_{e3})$, J_{CP} and J'_{CP} as functions of the energy scale μ , in the scenarios A (violet, dash-dotted line), B (red, solid line) and C (green, dashed line).

which corresponds exactly to the value of $\cot \delta$ in Eq. (4.6), which had been prescribed in [34]. We have thus shown that the prescription follows directly from the procedure of taking the limit of δ as $\text{Re}(\mathcal{U}_{e3})$ and $\text{Im}(\mathcal{U}_{e3})$ go to zero simultaneously.

The net evolution of θ_{13} and δ as functions of the energy scale has been shown in the top panels of Fig. 4.2. The evolution of δ clearly has a discontinuity at $\theta_{13} = 0$ in scenario B, where its value changes by π . Though the origin of this discontinuity has now been well understood, it is important to have a clear evolution of parameters that reflect the continuous nature of the evolution of elements of the neutrino mixing matrix U_{PMNS} . This can clearly be achieved by using the parameters $\text{Re}(\mathcal{U}_{e3})$ and $\text{Im}(\mathcal{U}_{e3})$. However, we prefer to use the Jarlskog invariant J_{CP} , as defined in Eq. (3.81) in Chapter 3, which appears in the probability expressions relevant for the neutrino oscillation experiments, and is therefore more directly measurable than the real and imaginary parts

of \mathcal{U}_{e3} . Since J_{CP} has information only about $\sin \delta$, we need its partner J'_{CP} , as defined already in Eq. (3.82) in Chapter 3, to keep track of the quadrant in which δ lies. The evolutions of $(J_{\text{CP}}, J'_{\text{CP}})$ are very similar to those of $(\text{Re}(\mathcal{U}_{e3}), \text{Im}(\mathcal{U}_{e3}))$, as can be seen from the bottom panels of Fig. 4.2.

4.3 RG evolution equations in terms of the parameter set \mathcal{P}_J

We now calculate the RG evolution of the Jarlskog invariant J_{CP} and its partner J'_{CP} as defined in (3.82), and get to a set of evolution equations that are nonsingular everywhere, even at $\theta_{13} = 0$. The RG evolution equation for J_{CP} and J'_{CP} are obtained as

$$\dot{J}_{\text{CP}} = A_J + \mathcal{O}(\theta_{13}), \quad (4.15)$$

$$\dot{J}'_{\text{CP}} = A'_J + \mathcal{O}(\theta_{13}), \quad (4.16)$$

with

$$A_J = Cy_\tau^2 s_{12}^2 c_{12}^2 s_{23}^2 c_{23}^2 \frac{m_3}{\Delta m_{31}^2} \left[m_1 \sin 2\phi_1 - (1 + \zeta) m_2 \sin 2\phi_2 \right], \quad (4.17)$$

$$A'_J = Cy_\tau^2 s_{12}^2 c_{12}^2 s_{23}^2 c_{23}^2 \frac{m_3}{\Delta m_{31}^2} \left[m_1 \cos 2\phi_1 - (1 + \zeta) m_2 \cos 2\phi_2 - \zeta m_3 \right]. \quad (4.18)$$

We also choose to write the RG evolution for θ_{13}^2 instead of θ_{13} , as is traditionally done. This quantity turns out to have a nonsingular behavior at $\theta_{13} = 0$. Moreover, since $\theta_{13} \geq 0$ by convention, the complete information about θ_{13} lies within θ_{13}^2 . Also, the possible ‘‘sign problem’’¹ of θ_{13} is avoided. In terms of

¹Usually the convention used in defining the elements of U_{PMNS} is to take the angles θ_{ij} to lie in the first quadrant. \mathcal{U}_{e3} can then take both positive or negative values depending on the choice of the CP phase δ . In the formulation of Eq. (4.8) the sign of A_{13} can be such that θ_{13} can assume negative values during the course of evolution and in such situations one will have to talk about the evolution of $|\theta_{13}|$. Our formulation in terms of θ_{13}^2 , as shown in Eq. (4.19), naturally avoids this problem.

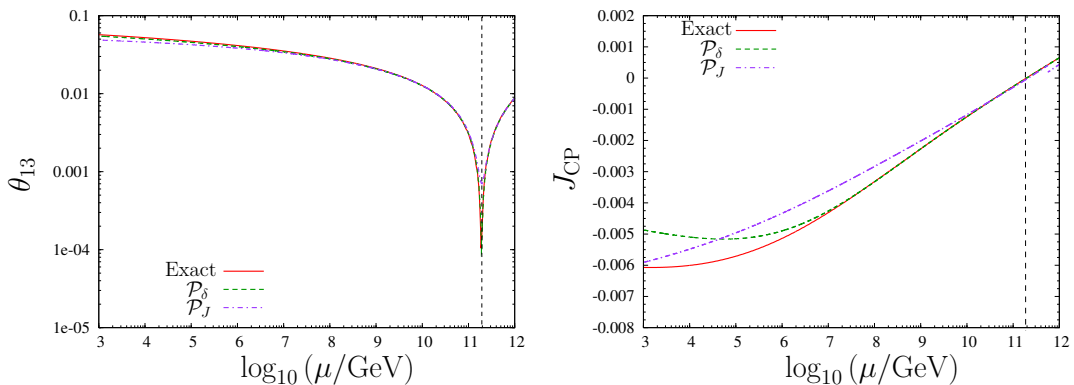


Figure 4.3: Comparison of the RG evolution of θ_{13} and J_{CP} from the analytic expressions in \mathcal{P}_δ basis (green, dashed line) and \mathcal{P}_J basis (blue, dotted line) with the exact numeric one (red, solid line). The parameters chosen at the high scale $\mu_0 = 10^{12}$ GeV are: $\tan\beta = 50$, $m_0 = 0.05$ eV², $\Delta m_\odot^2 = 0.00008$ eV², $\Delta m_{\text{atm}}^2 = 0.0026$ eV², $\theta_{12} = 34.5^\circ$, $\theta_{23} = 42.5^\circ$ and $\theta_{13} = 0.5^\circ$. The phases are taken to be $\delta = 40^\circ$, $\phi_1 = 25^\circ$ and $\phi_2 = 105^\circ$.

the new parameters J_{CP} and J'_{CP} , the RG evolution equations for θ_{13}^2 becomes

$$\dot{\theta}_{13}^2 = A_{13}^{sq} + \mathcal{O}(\theta_{13}^2), \quad (4.19)$$

$$A_{13}^{sq} = 8C y_\tau^2 \frac{m_3}{\Delta m_{31}^2} \left\{ J_{\text{CP}} [m_1 \sin 2\phi_1 - (1 + \zeta)m_2 \sin 2\phi_2] + J'_{\text{CP}} [m_1 \cos 2\phi_1 - (1 + \zeta)m_2 \cos 2\phi_2 - \zeta m_3] \right\}. \quad (4.20)$$

Thus the evolution equations in basis \mathcal{P}_J are all non-singular and continuous at every point. In particular, even when δ shows a discontinuity, J_{CP} as well as J'_{CP} change in a continuous manner.

In Fig. 4.3, we show the RG evolution of θ_{13} (left panel) and J_{CP} (right panel), as obtained from the analytic expressions in \mathcal{P}_δ basis as well as in the \mathcal{P}_J basis, along with the exact numerical solution, for some chosen values of parameters. It shows that the approximate running equations agree with each other to an accuracy of $\mathcal{O}(\theta_{13})$.

4.4 Bounds on θ_{13} at low scale

We now consider all the theories that predict $\theta_{13} = 0$ at the high scale and try to see the nature of running of the masses and mixing parameters with the energy scale. For high scale we consider $\mu_0 = 10^{12}$ GeV and implement

the symmetry $\theta_{13} = 0$ at this scale, which we also take to be the mass of the lightest heavy particle responsible for the seesaw mechanism. We choose this value of μ_0 since it is consistent with the current neutrino mass squared differences and seesaw mechanism with Dirac mass of the heaviest neutrino around 1–100 GeV [193]. This scale is also desirable for successful leptogenesis [194]. However, our results are only logarithmically sensitive to this choice and hence our conclusions will be robust against variations of μ_0 . Also, this would allow us to compare our bounds with those obtained in [191, 192] for specific models like tri-bimaximal mixing at the high scale. The values of the other parameters at high energy are chosen such that their low scale values are compatible with experiments. For the absolute mass scale of neutrinos, we take the cosmological bound of $m_0 \lesssim 0.5$ eV [16] at the laboratory energy.

We consider the scenarios where the effective theory below μ_0 is the SM or the MSSM. We then estimate the maximum value that θ_{13} can gain through radiative corrections. This can be obtained from

$$\begin{aligned} \theta_{13} &\equiv \left| \int_{t_0}^t A_{13} dt + \mathcal{O}(\theta_{13}) \right| & (4.21) \\ &\approx \frac{|C|\Delta_\tau}{2} \sin 2\theta_{12} \sin 2\theta_{23} \frac{m_3}{|\Delta m_{31}^2|} \times \\ &\quad |m_1 \cos(2\phi_1 - \delta) - (1 + \zeta)m_2 \cos(2\phi_2 - \delta) - \zeta m_3 \cos \delta| \\ &\quad + \mathcal{O}(\Delta_\tau \theta_{13}, \Delta_\tau^2), & (4.22) \end{aligned}$$

where $t_0 \equiv \ln(\mu_0/\text{GeV})/(16\pi^2)$, $C = -3/2$ for SM and $C = 1$ for MSSM. Note that we can use the parameter set \mathcal{P}_δ here since apart from the starting point, where δ is unphysical and hence is irrelevant completely, the evolution in terms of this set is also continuous everywhere. Moreover it is convenient to talk about Dirac and Majorana phases while putting bounds on quantities. In Eq. (4.22), Δ_τ is defined as

$$\Delta_\tau^{\text{SM}} \equiv -\frac{1}{32\pi^2} \left(\frac{g_2 m_\tau}{M_W} \right)^2 \ln \left(\frac{\mu_0}{\mu} \right) \quad (4.23)$$

in the SM, where g_2 is the $\text{SU}(2)_L$ gauge coupling, whereas m_τ and M_W are the τ lepton and W boson masses respectively. In the MSSM,

$$\Delta_\tau^{\text{MSSM}} \equiv -\frac{1}{32\pi^2} \left(\frac{g_2 m_\tau}{M_W} \right)^2 (1 + \tan^2 \beta) \ln \left(\frac{\mu_0}{\mu} \right). \quad (4.24)$$

Numerically, one has $\Delta_\tau^{\text{SM}} \approx -1.4 \times 10^{-5}$ and $\Delta_\tau^{\text{MSSM}} \approx -1.4 \times 10^{-5}(1 + \tan^2 \beta)$, where $\tan \beta$ can take values upto ~ 50 , and so one can treat these quantities as small parameters. We explicitly indicate the neglected powers of these parameters in Eq. (4.22).

In order to get the maximum θ_{13} value possible, for any value of the lowest neutrino mass m_0 , all the coefficients of the masses m_i in Eq. (4.22) should have the same sign (which we choose to be positive) and the maximum possible magnitude. This can be achieved with the choice

$$2\phi_1 - \delta_0 = 0, \quad |2\phi_2 - \delta_0| = \pi, \quad (4.25)$$

which gives us

$$\theta_{13}^{\text{max}} \approx \frac{|C|\Delta_\tau}{2} \sin 2\theta_{12} \sin 2\theta_{23} \frac{m_3}{|\Delta m_{31}^2|} [m_1 + (1 + \zeta)m_2 + |\zeta m_3 \cos \delta_0|] \quad (4.26)$$

$$\leq \frac{|C|\Delta_\tau}{2} \sin 2\theta_{12} \sin 2\theta_{23} \frac{m_3}{|\Delta m_{31}^2|} [m_1 + (1 + \zeta)m_2 + |\zeta| m_3]. \quad (4.27)$$

The right hand side of Eq. (4.27) corresponds to choosing the phases shown in Table 4.1 for Eq. (4.22). As seen, these phases depend only on whether the neutrino mass ordering is normal or inverted, and not on the low energy effective theory (SM or MSSM). However, the value itself will indeed depend on the effective theory considered. Note that in this procedure of bounding θ_{13} , the actual value of δ_0 did not need to be used, a considerable simplification achieved at the expense of a small overestimation.

	δ	ϕ_1	ϕ_2
Normal ordering	π	$\pi/2$	0
Inverted ordering	0	0	$\pi/2$

Table 4.1: Phase choices in SM and MSSM that give the maximum radiative correction for θ_{13} .

To estimate θ_{13}^{max} that can be generated at the low scale, we take the optimal values of the other quantities in their current 3σ allowed ranges [195]. We are allowed to do this since the corrections to θ_{13} due to the evolutions of the other quantities will formally be $\mathcal{O}(\Delta_\tau^2)$ [136]. The quantity that may run quite a bit is θ_{12} , however the running is extremely small in the SM and θ_{12} always increases in the MSSM, so we use the maximum allowed value of $\sin 2\theta_{12}$ in

Eq. (4.27) for our estimation. The values of m_1 , m_2 and m_3 depend on Δm_{\odot}^2 , Δm_{atm}^2 , m_0 as well as the chosen mass ordering. The running of masses and the mass squared differences are governed by the Yukawa couplings of up-type quarks and the $U(1)_Y$ and $SU(2)_L$ gauge couplings. For SM, these evolutions depend also on the Higgs boson self coupling, and Yukawa couplings of down-type quarks and charged leptons. But θ_{13} , as given in Eq. (4.27), will be independent of these quantities to the leading order in Δ_τ and thus considering Δm_{\odot}^2 , Δm_{atm}^2 in the current 3σ range is expected to give the correct estimate to this order. This assumption can be seen to be valid *a posteriori* from the comparison between analytic and numerical results that follow.

4.4.1 θ_{13} at the low scale in the SM

We first consider the case when the effective low energy theory below μ_0 is the SM. Running of the masses and mixing parameters is considered from $\mu_0 = 10^{12}$ GeV to the current experimental scale ($\sim M_Z$). The scatter points in Fig. 4.4 are obtained by keeping $\theta_{13} = 0$ and varying the other two mixing angles randomly in the range 0 to $\pi/2$, whereas the phases are varied between 0 to 2π . The masses at the high scale are varied within 0–1.0 eV, so that the lightest neutrino mass m_0 at the low scale varies between 0 and 0.5 eV. Thus each point represents a different high energy theory with $\theta_{13} = 0$ at the high scale. The upper bound can be analytically estimated through Eq. (4.27), which depends on the neutrino mass ordering through the phase choices made in Table 4.1 and the value of Δ_τ^{SM} is given in Eq. (4.23).

From Fig. 4.4 it is seen that the maximum value gained radiatively by θ_{13} is rather small, being $\lesssim 3 \times 10^{-3}$ in the range $0 \leq m_0 \leq 0.5$ eV for both the mass orderings. Hence if future experiments measure θ_{13} greater than this limit, all the theories with $\theta_{13} = 0$ at the high scale and SM as the low energy effective theory will be ruled out completely². If the upper limit for m_0 is brought down by KATRIN [17] to $m_0 \lesssim 0.2$ eV, even lower θ_{13} values will be excluded for this class of theories. Note that for m_0 of this order, the effective electron neutrino mass measured by KATRIN will essentially be the same as m_0 .

²Note however that if we consider multi-Higgs doublet SM with additional discrete symmetries to ensure $\theta_{13} = 0$ at high scale, then for $m_0 > 0.2$ eV, the value of $\sin^2 \theta_{13}$ can be as large as 10^{-2} [185].

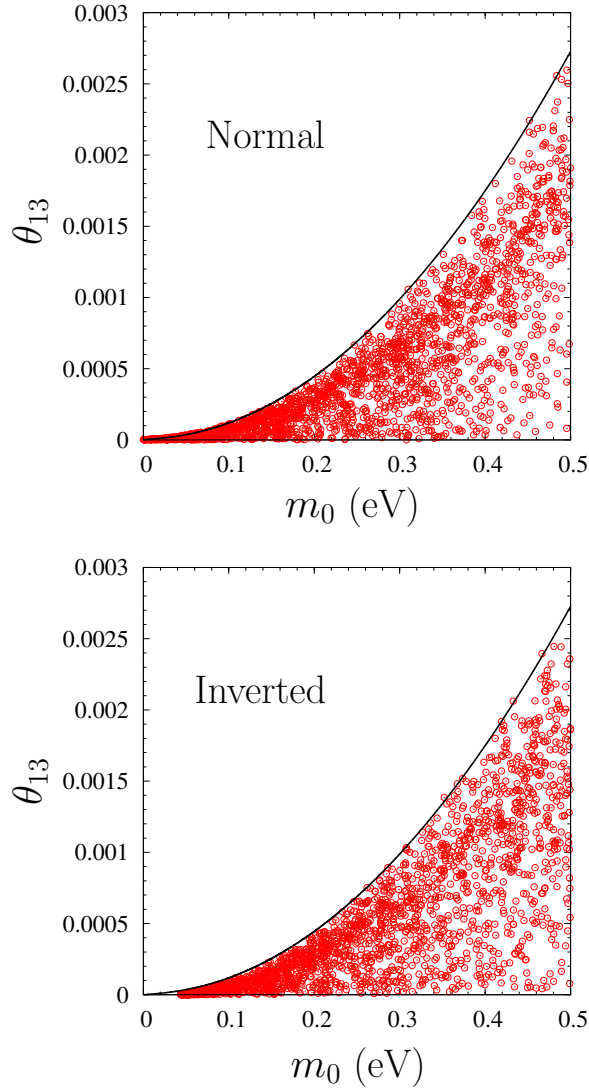


Figure 4.4: Scatter points show the low energy θ_{13} as a function of the lightest neutrino mass m_0 at the low scale, for both normal (left panel) and inverted (right panel) mass ordering. Each point represents a different high energy theory with $\theta_{13} = 0$ obtained by varying the other parameters at the high scale randomly. The solid (black) line gives the maximum attainable θ_{13} for a given m_0 , calculated using the analytic bound in Eq. (4.27), the current 3σ limits of the masses and mixings at the low scale, and the phase values as given in Table 4.1.

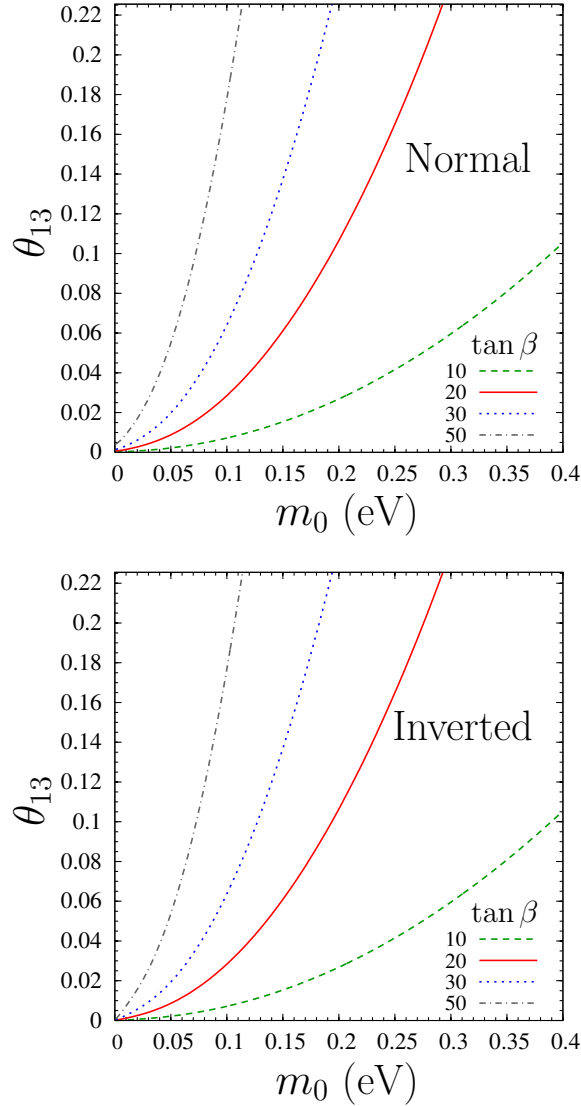


Figure 4.5: Maximum θ_{13} obtained at the low scale as a function of the lightest neutrino mass m_0 at the low scale for $\tan \beta = 10, 20, 30$ and 50 in the normal (left panel) and inverted (right panel) mass ordering. The plots show that simultaneous measurement of θ_{13} and m_0 will help in ruling out of a class of high energy theories with $\theta_{13} = 0$. However there is a strong dependence on the upper limit of $\tan \beta$.

4.4.2 θ_{13} at the low scale from MSSM

When MSSM is the low energy effective theory, the evolution of the neutrino parameters is proportional to $(1 + \tan^2 \beta)$, as is seen from Eq. (4.24), where $\tan \beta$ may take values up to ~ 50 . Thus, considerably larger running of θ_{13} may

be expected at large $\tan\beta$. The variation of θ_{13} as a function of m_0 is shown in Fig. 4.5. From the figure it can be concluded that with the current limit of m_0 , the radiative correction to $\theta_{13} = 0$ at the high scale can be large enough to reach the present upper bound of θ_{13} at laboratory energy. However, for a given $m_0 \lesssim 0.1$ eV, the maximum θ_{13} these theories can generate is significantly lower for the whole $\tan\beta$ range. For example, if m_0 happens to be 0.08 eV, the maximum θ_{13} for $\tan\beta = 50$ is $\theta_{13} \sim 0.12$, i.e. $\sin^2 2\theta_{13} \sim 0.056$. Such a θ_{13} regime will be probed by the next generation neutrino oscillation experiments like Double CHOOZ [115], Daya Bay [116], T2K [196]. Since the tritium beta decay experiment KATRIN [17] plans to probe $m_0 \sim 0.2$ eV only, it may not be enough to rule out theories with larger $\tan\beta$.

However, the neutrinoless double beta decay ($0\nu\beta\beta$) experiments will measure the effective Majorana mass of the electron neutrino

$$m_{ee} = \left| c_{12}^2 c_{13}^2 m_1 e^{2i(\phi_1 - \delta)} + s_{12}^2 c_{13}^2 m_2 e^{2i(\phi_2 - \delta)} + s_{13}^2 m_3 \right|, \quad (4.28)$$

The value of m_{ee} will allow us to estimate the m_0 range, albeit with a large uncertainty owing to the complete lack of knowledge of the phases δ , ϕ_1 and ϕ_2 currently. The present upper bound on the average neutrino mass is $m_{ee} < 1.1$ eV [80], whereas the proposed next generation experiments like COBRA[197], CUORE [198], EXO[199], GERDA [200], Super-NEMO[201], MOON [202] plan to probe m_{ee} in the range as low as $0.01 \text{ eV} \leq m_{ee} \leq 0.1 \text{ eV}$. Therefore, combined measurement of θ_{13} and m_{ee} may enable us to put some bound on the theories with large $\tan\beta$.

The expression for m_{ee} in (4.28) can be expanded in terms of the parameter $\delta_\odot \equiv \Delta m_\odot^2 / m_0^2$, which is small in the range $m_{ee} > 0.01$ eV, and the small parameter θ_{13} , to get

$$m_{ee} = m_0 \cos 2\theta_{12} \left(1 - \frac{\delta_\odot}{2} \frac{s_{12}^2}{\cos 2\theta_{12}} - \theta_{13}^2 \right) - \theta_{13}^2 \sqrt{m_0^2 + \Delta m_{\text{atm}}^2} + \mathcal{O}(\delta_\odot^2, \delta_\odot \theta_{13}^2, \theta_{13}^3) \quad (4.29)$$

for normal mass ordering, where the phases are chosen as given in Table 4.1. For inverted mass ordering,

$$m_{ee} = \cos 2\theta_{12} (1 - \epsilon) \sqrt{m_0^2 + |\Delta m_{\text{atm}}^2|} + \mathcal{O}(\delta_\odot^2, \delta_\odot \theta_{13}^2, \theta_{13}^3), \quad (4.30)$$

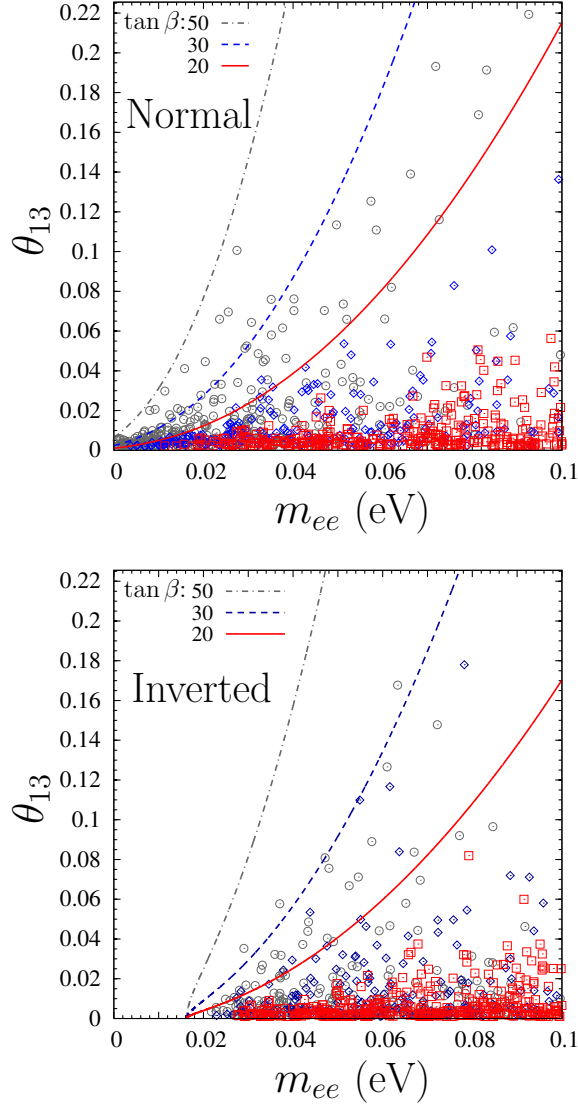


Figure 4.6: Scatter points show the value of θ_{13} generated at the low scale as a function of m_{ee} , for normal (left panel) and inverted (right panel) ordering. Each point represents a different high energy theory with $\theta_{13} = 0$. Different symbols (colors) correspond to different ranges of $\tan \beta$, *viz.* squares (red) for $1.0 \leq \tan \beta \leq 20.0$, diamonds (blue) for $20.0 \leq \tan \beta \leq 30.0$ and circles (gray) for $30.0 \leq \tan \beta \leq 50.0$. The lines show analytic estimates of θ_{13}^{\max} : solid (red) line for $\tan \beta = 20.0$, dashed (blue) line for $\tan \beta = 30.0$ and dot-dashed (gray) line for $\tan \beta = 50.0$.

where

$$\epsilon = \frac{\delta_{\odot}}{2} \frac{c_{12}^2}{\cos 2\theta_{12}(1 + \Delta)} + \theta_{13}^2 \left(1 - \frac{1}{\cos 2\theta_{12} \sqrt{1 + \Delta}} \right). \quad (4.31)$$

The quantity $\Delta \equiv |\Delta m_{\text{atm}}^2|/m_0^2$ is bounded from below, while for inverted mass ordering δ_{\odot} is a small parameter ($\sim \mathcal{O}(10^{-1})$) in the range $m_{ee} > 0.02$ eV, so that ϵ is small in this range. The analytic expressions in Eqs. (4.29) and (4.30) are valid for $m_{ee} > 0.01$ eV and $m_{ee} > 0.02$ eV respectively. In this domain of validity, we invert the relations (4.29) and (4.30) to obtain m_0 in terms of m_{ee} , and then use Eq. (4.27) for an analytic estimation of θ_{13}^{max} . For the m_{ee} values outside the range of validity, one has to estimate numerically the minimum allowed m_{ee} for a given m_0 and then use Eq. (4.27) to determine θ_{13}^{max} . These estimations are shown in Fig. 4.6 for various $\tan\beta$ values. The scattered points are the low scale predictions calculated numerically, which show the correlated constraints in the parameter space of θ_{13} and m_{ee} . It may be noted that the analytic bounds on θ_{13} obtained here as a function of m_{ee} are generous overestimations, mainly due to the error in the estimation of m_0 for a given m_{ee} .

Note that bounds on θ_{13} at the low scale generated by RG evolution have been studied earlier in the context of specific neutrino mixing scenarios at the high scale, like the quark-lepton complementarity or tri-bimaximal mixing [192], or correlated generation of Δm_{21}^2 and θ_{13} [54, 55]. The bounds obtained in this section, which are applicable not only for all the models with $\theta_{13} = 0$ at the high scale, but to all the models with $\theta_{13} = 0$ anytime during their RG evolution, subsumes the earlier analyses with specific models.

4.5 Summary

If the neutrino mixing angle θ_{13} is extremely small, it could point towards some flavor symmetry in the lepton sector. There is indeed a large class of theories of neutrino mass that predict extremely small or even vanishing θ_{13} . However, such predictions are normally valid at the high scale where the masses of the heavy particle responsible for neutrino mass generation lie. Below this scale, radiative corrections give rise to RG evolution of the neutrino mixing parameters, which in principle can wipe out signatures of such symmetries. In this chapter, we have explored the RG evolution of all such theories collectively.

The RG evolution with the traditional parameter set $\mathcal{P}_{\delta} = \{m_i, \theta_{ij}, \phi_i, \delta\}$ involves an apparent singularity in the evolution of the Dirac phase δ when $\theta_{13} = 0$. This singularity is unphysical, since all the elements of the neutrino

mixing matrix U_{PMNS} are continuous at $\theta_{13} = 0$, and in fact the value of δ there should be immaterial. A practical solution to this situation has already been proposed, which involves prescribing a specific value of $\cot \delta$ when one starts the RG evolution of a model with $\theta_{13} = 0$. However, if θ_{13} vanishes during the evolution, getting the required value of δ exactly at that point looks like fine tuning. This issue is relevant to the class of models under consideration, since θ_{13} is already very close to zero at the high scale.

We have explored the apparent singularity in δ by analyzing the evolution of the complex quantity \mathcal{U}_{e3} , which stays continuous throughout the RG evolution. We have found that a fine tuning is indeed required, but that is to ensure that θ_{13} exactly vanishes. In general, if the CP violating Dirac and Majorana phases take nontrivial values, one does not pass through $\theta_{13} = 0$ even when one starts with θ_{13} very close to zero. One needs rather finely tuned values for the starting values of the neutrino mixing parameters, unless one introduces a symmetry like CP conservation, which makes the Dirac and Majorana phases vanish everywhere. Since the latter assumption is used commonly in literature, one tends to miss the fact that getting $\theta_{13} = 0$ during RG evolution is possible only in a small region of the parameter space.

However, if the parameters happen to be tuned such that θ_{13} vanishes exactly, we have shown that the limiting value of δ as $\theta_{13} \rightarrow 0$ is indeed the one given by the prescription mentioned above. Moreover, we have shown that if one is starting from $\theta_{13} = 0$, one need not give any specific value to δ , which is an undefined quantity at that point. An infinitesimally nonzero θ_{13} automatically ensures the correct values of δ . We have also proposed an alternate parameterization using the parameter set $\mathcal{P}_J = \{m_i, \theta_{12}, \theta_{23}, \theta_{13}^2, \phi_i, J_{\text{CP}}, J'_{\text{CP}}\}$, where all the parameters are well-defined everywhere and any seemingly nonsingular behavior is avoided.

For models with exactly vanishing θ_{13} at the high scale, we have studied the generation of nonzero θ_{13} through radiative corrections. We have considered two scenarios, one when the low energy effective theory is the SM, and the other where it is the MSSM. The radiatively generated θ_{13} values are correlated with the absolute neutrino mass scale m_0 . This scale will be probed by the future experiments on tritium beta decay, and indirectly by the neutrinoless double beta decay experiments. If the value of m_0 is indeed restricted to the value ~ 0.2 eV which KATRIN will probe, the maximum value of θ_{13}

generated can only be $\lesssim 3 \times 10^{-3}$ in the SM scenario. With the MSSM, the running can be much higher for large $\tan\beta$, such that the current bound of $\theta_{13} < 0.22$ may be reached. In this scenario, we have correlated the bound on θ_{13} with the effective neutrino Majorana mass m_{ee} to be measured in the next generation neutrinoless double beta decay experiments. The whole class of models considered in this chapter can then be ruled out from future measurements of θ_{13} , m_{ee} and $\tan\beta$.

Chapter 5

Conclusions

Heavy sterile neutrinos may play an important role in astrophysics and cosmology, for example in r-process nucleosynthesis or as dark matter. Neutrino oscillation experiments, mainly the short baseline (SBL) ones, have already put severe constraints on the extent of mixing of these sterile neutrinos with the active ones. Recently it has been pointed out that to satisfy LSND, MiniBooNE and the SBL appearance data simultaneously, at least two sterile neutrinos with $\Delta m^2 \sim \mathcal{O}(1) \text{ eV}^2$ are in fact needed. At the same time, the current experimental values of the mass squared differences of the three active neutrinos, combined with the bound on the sum of the neutrino masses coming from cosmology and astrophysics, indicate that neutrino masses are orders of magnitude smaller than the masses of the quarks and the charged leptons.

In the framework of the standard model (SM) of particle physics, neutrinos are massless at the tree level as well as at loop level. Hence one has to extend the SM in order to explain the tiny active neutrino masses observed experimentally. The most favored mechanisms to generate such small neutrino masses are the seesaw mechanisms, in which small active neutrino masses are generated at some high energy scale. But since the experimental data are available at the laboratory energy scales, one needs to include the effects of renormalization group (RG) evolution. Unlike the quark sector where RG evolutions are quite small, the effect of RG evolution on the neutrino masses and the mixing parameters are important.

In this thesis we have explored the neutrino oscillation phenomenology on two fronts. In the first part we have checked whether the sterile neutrinos obeying

the constraints from astrophysics, cosmology and neutrino oscillation data can still give rise to observable signals at future long baseline experiments, and whether these signals can be cleanly identified in spite of our current lack of knowledge of the parameters in the mixing of three active neutrinos. We have also estimated the bounds on the sterile neutrino parameters that can be obtained at these experiments. In the light of the recent results that show that LSND, MiniBooNE and the earlier null-result SBL appearance experiments can be consistent if the number of sterile neutrinos is two or more, we have also extended our formalism to include any number of sterile neutrinos. We have given explicit expressions for the sterile mixing combinations to which long baseline experiments are sensitive, and the neutrino conversion probabilities in terms of them. The limits obtained on active-sterile mixing parameters through the 4ν analysis can easily be translated to the corresponding combinations of these parameters in the general case. It can be seen that the bounds on the sterile mixing parameters obtained from the measurements described here would act as stringent tests of the scenarios with multiple sterile neutrinos.

The sterile neutrinos required to fit all the oscillation data, help r -process nucleosynthesis or act as the warm dark matter are too light to serve as the seesaw particles giving small active neutrino masses at the high scale. On the other hand, if we have a heavy right-handed Majorana fermion in the high energy renormalizable theory to generate the neutrino mass via seesaw (Type-I or Type-III), the mixing angle with the active species will be $\lesssim 3 \cdot 10^{-5}$ for a mass $\gtrsim 10$ keV, and hence will not affect the signal at the future long baseline experiments.

In the second part of the thesis we have considered the Type-III seesaw scenario when heavy right-handed Majorana fermion triplets have been added to the SM at the high energy scale, so that they produce the small active neutrino masses through the Type-III seesaw mechanism. At energies lower than the mass of the respective heavy fermion, the particle gets decoupled from the theory, and contributes to the active neutrino masses through the non-renormalizable effective operator. We have used the dimensional regularization and the minimal subtraction (MS) scheme to compute the beta functions in the renormalizable R_ξ gauge and studied the RG evolution of the neutrino masses and mixing parameters in the high energy renormalizable theory as well as the low energy effective theory. We have pointed out some salient features of the RG evolution of the neutrino masses and the mixing parameters in this model,

and also the important role of the threshold effects and Majorana phases in the evolution of mixing angles through illustrative examples.

Some subtle issues are present when $\theta_{13} = 0$ is reached, either at the high scale or during evolution. This is essentially because of the fact that the Dirac CP phase δ becomes unphysical when $\theta_{13} = 0$. We have analyzed this problem for a better understanding and also presented an alternative formalism which enables one to determine analytically the change in the neutrino masses and mixing parameters due to RG evolution unambiguously, even when the evolution involves the $\theta_{13} = 0$ point. Finally we have considered the models which predict $\theta_{13} = 0$ at the high scale and estimated the maximum value of θ_{13} that can be generated through RG evolution. We have obtained a correlated constraint on θ_{13} and the lightest neutrino mass m_0 , for both the mass orderings and with the SM as the low energy effective theory. It has been seen that for both the mass orderings, $\theta_{13} \lesssim 3 \times 10^{-3}$ for $0 \leq m_0 \leq 0.5$ eV, so that future measurements of θ_{13} and m_0 may be able to rule out this whole class of models considered here. It has also been observed that if the low energy effective theory is the minimal supersymmetric standard model (MSSM), the running can be much higher for large $\tan\beta$, and the current bound of $\theta_{13} < 0.22$ may be reached. In this scenario, we have correlated the bound on θ_{13} with the effective neutrino Majorana mass m_{ee} to be measured in the next generation neutrinoless double beta decay experiments. The whole class of models considered can then be ruled out from future measurements of θ_{13}, m_{ee} and $\tan\beta$.

In summary, we have studied some aspects of light sterile neutrinos (masses $\gtrsim 0.1$ eV) and fermionic triplets (masses \sim TeV), in the light of current experimental bounds on the neutrino masses and mixing parameters. A more exhaustive numerical study is in progress. Such studies combined with the precision data from future neutrino experiments and possible collider signatures of new physics will guide the direction of future research and will help in a better understanding of the fundamental interactions.

Appendix A

Calculation of neutrino flavor survival/conversion probabilities

AS.1 Effective Hamiltonian to second order in a small parameter λ

In order to calculate the neutrino conversion (survival) probabilities in the presence of a sterile neutrino, we define an auxiliary small parameter $\lambda \equiv 0.2$, write all the small quantities as $a\lambda^n$ where a and n are some constants, and then perform a formal expansion of the effective Hamiltonian in powers of λ . This enables us to use the second order perturbation theory to get results accurate to $\mathcal{O}(\lambda^2)$.

We have defined the small quantities in the problem as

$$\theta_{14} = \chi_{14}\lambda, \quad \theta_{24} = \chi_{24}\lambda, \quad \theta_{34} = \chi_{34}\lambda, \quad (\text{A.1})$$

$$\theta_{13} = \chi_{13}\lambda, \quad \theta_{23} - \pi/4 = \chi_{23}\lambda, \quad \Delta m_{\odot}^2/\Delta m_{\text{atm}}^2 = \eta\lambda^2. \quad (\text{A.2})$$

As argued in Sec. 2.2, we need to diagonalize the effective Hamiltonian H_v , given in Eq. (2.11). This Hamiltonian matrix may be expanded in powers of λ as

$$H_v = \frac{\Delta m_{32}^2}{2E} [h_0 + \lambda h_1 + \lambda^2 h_2 + \mathcal{O}(\lambda^3)]. \quad (\text{A.3})$$

Here, the leading term is

$$h_0 = \begin{pmatrix} a_n + a_e \cos^2 \theta_{12} & a_e \cos \theta_{12} \sin \theta_{12} & 0 & 0 \\ a_e \cos \theta_{12} \sin \theta_{12} & a_n + a_e \sin^2 \theta_{12} & 0 & 0 \\ 0 & 0 & a_n + 1 & 0 \\ 0 & 0 & 0 & \sigma \end{pmatrix}, \quad (\text{A.4})$$

where

$$a_{e,n} \equiv A_{e,n}/\Delta m_{32}^2; \quad \sigma \equiv \Delta m_{42}^2/\Delta m_{32}^2 \approx \pm \Delta m_{\text{st}}^2/\Delta m_{\text{atm}}^2.$$

We take the neutrinos to be traversing through a constant matter density, so that $a_{e,n}$ are constants.

The subleading term in (A.3) is

$$h_1 = \begin{pmatrix} 0 & 0 & a_e \chi_{13} \cos \theta_{12} e^{-i\delta_{13}} & (a_e + a_n) \chi_{14} e^{-i\delta_{14}} \cos \theta_{12} - \frac{a_n}{\sqrt{2}} \sin \theta_{12} (\chi_{24} e^{-i\delta_{24}} - \chi_{34}) \\ 0 & 0 & a_e \chi_{13} \sin \theta_{12} e^{-i\delta_{13}} & (a_e + a_n) \chi_{14} e^{-i\delta_{14}} \sin \theta_{12} + \frac{a_n}{\sqrt{2}} \cos \theta_{12} (\chi_{24} e^{-i\delta_{24}} - \chi_{34}) \\ \cdot & \cdot & 0 & \frac{a_n}{\sqrt{2}} (\chi_{24} e^{-i\delta_{24}} + \chi_{34}) \\ \cdot & \cdot & \cdot & 0 \end{pmatrix}. \quad (\text{A.5})$$

The matrix h_1 is hermitian, so we do not write its lower triangular elements for the sake of brevity. Note that all the elements of h_1 are $\mathcal{O}(1)$.

The expression for the matrix h_2 in (A.3) is rather complicated, we just give its ten independent elements separately here for the sake of completeness. The diagonal elements are

$$\begin{aligned} h_2^{11} &= -\Delta_{32}\eta - [a_e \chi_{13}^2 + (a_e + a_n) \chi_{14}^2] \cos^2 \theta_{12} \\ &\quad - \frac{a_n}{2} (\chi_{24}^2 + \chi_{34}^2 - 2\chi_{24}\chi_{34} \cos \delta_{24}) \sin^2 \theta_{12} \\ &\quad - \sqrt{2} (a_e + a_n) \chi_{14} [\chi_{34} \cos \delta_{14} - \chi_{24} \cos(-\delta_{14} + \delta_{24})] \sin \theta_{12} \cos \theta_{12}, \\ h_2^{22} &= -[a_e \chi_{13}^2 + (a_e + a_n) \chi_{14}^2] \sin^2 \theta_{12} \\ &\quad - \frac{a_n}{2} (\chi_{24}^2 + \chi_{34}^2 - 2\chi_{24}\chi_{34} \cos \delta_{24}) \cos^2 \theta_{12} \\ &\quad + \sqrt{2} (a_e + a_n) \chi_{14} [\chi_{34} \cos \delta_{14} - \chi_{24} \cos(-\delta_{14} + \delta_{24})] \sin \theta_{12} \cos \theta_{12}, \\ h_2^{33} &= -\frac{a_n}{2} (\chi_{24}^2 + \chi_{34}^2 + 2\chi_{24}\chi_{34} \cos \delta_{24}) + a_e \chi_{13}^2, \\ h_2^{44} &= a_n (\chi_{24}^2 + \chi_{34}^2) + (a_e + a_n) \chi_{14}^2, \end{aligned} \quad (\text{A.6})$$

while the off-diagonal elements are

$$\begin{aligned}
 h_2^{12} &= -[a_e \chi_{13}^2 + (a_e + a_n) \chi_{14}^2] \sin \theta_{12} \cos \theta_{12} \\
 &\quad + \frac{a_n}{2} (\chi_{24}^2 + \chi_{34}^2 - 2\chi_{24}\chi_{34} \cos \delta_{24}) \sin \theta_{12} \cos \theta_{12} \\
 &\quad + \frac{(a_e + a_n)}{\sqrt{2}} \chi_{14} [\chi_{34} \cos \delta_{14} - \chi_{24} \cos(-\delta_{14} + \delta_{24})] \cos 2\theta_{12} \\
 &\quad + i \frac{(a_e + a_n)}{2} \chi_{14} [-\chi_{34} \sin \delta_{14} - \chi_{24} \sin(-\delta_{14} + \delta_{24})] , \\
 h_2^{13} &= -\frac{(\chi_{24} e^{i\delta_{24}} + \chi_{34})}{2} \left[\sqrt{2} (a_e + a_n) \chi_{14} e^{-i\delta_{14}} \cos \theta_{12} \right. \\
 &\quad \left. - a_n (\chi_{24} e^{-i\delta_{24}} - \chi_{34}) \sin \theta_{12} \right] , \\
 h_2^{23} &= -\frac{(\chi_{24} e^{i\delta_{24}} + \chi_{34})}{2} \left[\sqrt{2} (a_e + a_n) \chi_{14} e^{-i\delta_{14}} \sin \theta_{12} \right. \\
 &\quad \left. + a_n (\chi_{24} e^{-i\delta_{24}} - \chi_{34}) \cos \theta_{12} \right] , \\
 h_2^{14} &= \frac{a_n}{\sqrt{2}} (\chi_{24} e^{-i\delta_{24}} + \chi_{34}) (-\chi_{13} e^{-i\delta_{13}} \cos \theta_{12} + \chi_{23} \sin \theta_{12}) , \\
 h_2^{24} &= -\frac{a_n}{\sqrt{2}} (\chi_{24} e^{-i\delta_{24}} + \chi_{34}) (\chi_{13} e^{-i\delta_{13}} \sin \theta_{12} + \chi_{23} \cos \theta_{12}) , \\
 h_2^{34} &= \frac{a_n}{\sqrt{2}} \chi_{23} (\chi_{24} e^{-i\delta_{24}} - \chi_{34}) + (a_e + a_n) \chi_{13} \chi_{14} e^{i(\delta_{13} - \delta_{14})} . \quad (\text{A.7})
 \end{aligned}$$

Note that all the elements of h_2 are $\mathcal{O}(1)$ or smaller. The dependence on Δm_{\odot}^2 appears only at this order, and only in the element h_2^{11} .

AS.2 Calculation of the flavor survival/conversion probabilities

Using the above formal expansion of the effective Hamiltonian, one can compute the eigenvalues and eigenvectors of H_v correct up to $\mathcal{O}(\lambda^2)$ by using the techniques of time independent perturbation theory. The complete set of four normalized eigenvectors gives the unitary matrix \tilde{U} that diagonalizes H_v through Eq. (2.13). Using Eq. (2.12), we can then compute the unitary matrix \mathcal{U}_m that diagonalizes H_f through Eq. (2.9). The matrix \mathcal{U}_m and the eigenvalues of H_v (or H_f) allow us to calculate the neutrino flavor conversion

probabilities from

$$P_{\alpha\beta} \equiv P(\nu_\alpha \rightarrow \nu_\beta) = \left| \sum_i [\mathcal{U}_m]_{\alpha i} [\mathcal{U}_m]_{\beta i}^* \exp \left[i \frac{(-\tilde{m}_i^2)L}{2E} \right] \right|^2, \quad (\text{A.8})$$

as given in Eq. (2.10). The complete expressions, accurate to $\mathcal{O}(\lambda^2)$, are given below.

$$P_{\mu e} = 2\lambda^2 \chi_{13}^2 \Delta_{32}^2 \frac{\sin^2(\Delta_e - \Delta_{32})}{(\Delta_e - \Delta_{32})^2} + \mathcal{O}(\lambda^3), \quad (\text{A.9})$$

$$\begin{aligned} P_{\mu\mu} = & \cos^2 \Delta_{32} + 4\lambda^2 \chi_{23}^2 \sin^2 \Delta_{32} - \lambda^2 \eta \sin^2 \theta_{12} \Delta_{32} \sin 2\Delta_{32} \\ & + \frac{\lambda^2 \chi_{13}^2 \Delta_{32}}{(-\Delta_e + \Delta_{32})^2} \times \\ & \{-2\Delta_{32} \cos \Delta_{32} \sin \Delta_e \sin(\Delta_e - \Delta_{32}) + \Delta_e(\Delta_e - \Delta_{32}) \sin 2\Delta_{32}\} \\ & + \lambda^2 \chi_{24}^2 Q_1 + \lambda^2 \chi_{34}^2 Q_2 + \lambda^2 \chi_{24} \chi_{34} \cos \delta_{24} Q_3 + \mathcal{O}(\lambda^3), \end{aligned} \quad (\text{A.10})$$

$$\begin{aligned} P_{\mu\tau} = & \sin^2 \Delta_{32} - 4\lambda^2 \chi_{23}^2 \sin^2 \Delta_{32} + \lambda^2 \eta \sin^2 \theta_{12} \Delta_{32} \sin 2\Delta_{32} \\ & + \frac{\lambda^2 \chi_{13}^2 \Delta_{32}}{(-\Delta_e + \Delta_{32})^2} \times \\ & \{-2\Delta_{32} \cos \Delta_e \sin \Delta_{32} \sin(\Delta_{32} - \Delta_e) + \Delta_e(-\Delta_e + \Delta_{32}) \sin 2\Delta_{32}\} \\ & + \lambda^2 (\chi_{24}^2 + \chi_{34}^2) Q_4 + \lambda^2 \chi_{24} \chi_{34} (\cos \delta_{24} Q_5 + \sin \delta_{24} Q_6) + \mathcal{O}(\lambda^3), \end{aligned} \quad (\text{A.11})$$

where we have invoked the shorthand

$$\Delta_e \equiv \frac{A_e L}{4E_\nu}, \quad \Delta_n \equiv \frac{A_n L}{4E_\nu}, \quad \Delta_{32} \equiv \frac{\Delta m_{32}^2 L}{4E_\nu}, \quad \Delta_{42} \equiv \frac{\Delta m_{42}^2 L}{4E_\nu}. \quad (\text{A.12})$$

and defined the quantities Q_i $\{i = 1, 6\}$ as

$$\begin{aligned} Q_1 \equiv & \frac{1}{4(\Delta_n + \Delta_{32} - \Delta_{42})^2 (-\Delta_n + \Delta_{42})^2} \times \\ & \left\{ -(\Delta_n(\Delta_{32} - 2\Delta_{42}) + 2\Delta_{42}(-\Delta_{32} + \Delta_{42}))^2 \cos 2\Delta_{32} \right. \\ & + (\Delta_n \Delta_{32} - 2(\Delta_n + \Delta_{32})\Delta_{42} + 2\Delta_{42}^2)^2 \cos(2\Delta_n - 2\Delta_{42}) \\ & + 2\Delta_n^2 \Delta_{32} (\Delta_n - \Delta_{42})(\Delta_n + \Delta_{32} - \Delta_{42}) \sin 2\Delta_{32} \\ & \left. - 2(\Delta_n \Delta_{32} - 2(\Delta_n + \Delta_{32})\Delta_{42} + 2\Delta_{42}^2)^2 \sin^2(\Delta_n + \Delta_{32} - \Delta_{42}) \right\}, \end{aligned} \quad (\text{A.13})$$

$$Q_2 \equiv \frac{\Delta_n^2 \Delta_{32}}{2(\Delta_n + \Delta_{32} - \Delta_{42})^2 (-\Delta_n + \Delta_{42})^2} \times \left\{ (\Delta_n - \Delta_{42})(\Delta_n + \Delta_{32} - \Delta_{42}) \sin 2\Delta_{32} - 2\Delta_{32} \cos \Delta_{32} \sin(\Delta_n - \Delta_{42}) \sin(\Delta_n + \Delta_{32} - \Delta_{42}) \right\}, \quad (\text{A.14})$$

$$Q_3 \equiv \frac{\Delta_n (\Delta_n (\Delta_{32} - 2\Delta_{42}) + 2\Delta_{42} (-\Delta_{32} + \Delta_{42})) \cos \Delta_{32}}{(\Delta_n + \Delta_{32} - \Delta_{42})^2 (-\Delta_n + \Delta_{42})^2} \times \left\{ 2(\Delta_n - \Delta_{42})(\Delta_n + \Delta_{32} - \Delta_{42}) \sin \Delta_{32} + \Delta_{32} [-\cos \Delta_{32} + \cos(2\Delta_n + \Delta_{32} - 2\Delta_{42})] \right\}, \quad (\text{A.15})$$

$$Q_4 \equiv \frac{1}{8(\Delta_n + \Delta_{32} - \Delta_{42})^2 (-\Delta_n + \Delta_{42})^2} \left\{ 4\Delta_n (\Delta_{32} - 2\Delta_{42})(\Delta_{32} - \Delta_{42})\Delta_{42} - 4(\Delta_{32} - \Delta_{42})^2 \Delta_{42}^2 - 2\Delta_n^2 (\Delta_{32}^2 - 2\Delta_{32}\Delta_{42} + 2\Delta_{42}^2) + 2 \left[-2\Delta_n (\Delta_{32} - 2\Delta_{42})(\Delta_{32} - \Delta_{42})\Delta_{42} + 2(\Delta_{32} - \Delta_{42})^2 \Delta_{42}^2 + \Delta_n^2 (\Delta_{32}^2 - 2\Delta_{32}\Delta_{42} + 2\Delta_{42}^2) \right] \cos 2\Delta_{32} + \Delta_n \Delta_{32} \sin \Delta_{32} \left[-8\Delta_n (\Delta_n - \Delta_{42})(\Delta_n + \Delta_{32} - \Delta_{42}) \cos \Delta_{32} - 4[\Delta_n (\Delta_{32} - 2\Delta_{42}) + 2\Delta_{42} (-\Delta_{32} + \Delta_{42})] \sin(\Delta_{32} - 2\Delta_{42} + 2\Delta_n) \right] \right\}, \quad (\text{A.16})$$

$$Q_5 \equiv \frac{\sin \Delta_{32}}{2(\Delta_n + \Delta_{32} - \Delta_{42})^2 (-\Delta_n + \Delta_{42})^2} \times \left\{ \Delta_n [\Delta_n (\Delta_{32} - 2\Delta_{42}) + \Delta_{42} (-\Delta_{32} + \Delta_{42})] \times [4(\Delta_n - \Delta_{42})(\Delta_n + \Delta_{32} - \Delta_{42}) \cos \Delta_{32} + 2\Delta_{32} \sin \Delta_{32}] + 2 \left[-2\Delta_n (\Delta_{32} - 2\Delta_{42})(\Delta_{32} - \Delta_{42})\Delta_{42} + 2(\Delta_{32} - \Delta_{42})^2 \Delta_{42}^2 + \Delta_n^2 (\Delta_{32}^2 - 2\Delta_{32}\Delta_{42} + 2\Delta_{42}^2) \right] \sin(2\Delta_n + \Delta_{32} - 2\Delta_{42}) \right\}, \quad (\text{A.17})$$

$$Q_6 \equiv \frac{-4(\Delta_{32} - \Delta_{42})\Delta_{42} \sin(\Delta_n - \Delta_{42}) \sin \Delta_{32} \sin(\Delta_n + \Delta_{32} - \Delta_{42})}{(\Delta_n + \Delta_{32} - \Delta_{42})(-\Delta_n + \Delta_{42})}. \quad (\text{A.18})$$

Here we are interested in heavy sterile neutrinos, we may take $|\Delta m_{32}^2| \ll |\Delta m_{42}^2|$. Also, since $|\Delta m_{32}^2 L/E| \sim \mathcal{O}(1)$, we have $|\Delta m_{42}^2 L/E| \gg 1$ and the oscillating terms of the form $\cos(\Delta m_{42}^2 L/E)$ may be averaged out. In the long baseline experiments, we are interested in the energy range 1–50 GeV. Even at the higher end of the energy spectrum, taking the density of the earth mantle to be ≈ 5 g/cc, we get $A_e \approx 2 \times 10^{-2}$ eV² and $A_n \approx -1 \times 10^{-2}$ eV² for neutrinos,

so we also approximate $|A_{e,n}| \ll |\Delta m_{42}^2|$ wherever appropriate. With these approximations, the neutrino flavor conversion (or survival) probabilities for an initial ν_μ may be written as

$$P_{\mu e} \approx 2\theta_{13}^2 \Delta_{32}^2 \frac{\sin^2(\Delta_e - \Delta_{32})}{(\Delta_e - \Delta_{32})^2} + \mathcal{O}(\lambda^3), \quad (\text{A.19})$$

$$\begin{aligned} P_{\mu\mu} \approx & \cos^2 \Delta_{32} + 4\tilde{\theta}_{23}^2 \sin^2 \Delta_{32} - \Delta_{21} \sin^2 \theta_{12} \sin 2\Delta_{32} \\ & + \frac{\theta_{13}^2 \Delta_{32}}{(\Delta_e - \Delta_{32})^2} \times \\ & \left\{ -2\Delta_{32} \cos \Delta_{32} \sin \Delta_e \sin(\Delta_e - \Delta_{32}) + \Delta_e(\Delta_e - \Delta_{32}) \sin 2\Delta_{32} \right\} \\ & - 2\theta_{24}^2 \cos^2 \Delta_{32} + 2\theta_{24}\theta_{34}\Delta_n \cos \delta_{24} \sin 2\Delta_{32} + \mathcal{O}(\lambda^3), \end{aligned} \quad (\text{A.20})$$

$$\begin{aligned} P_{\mu\tau} \approx & \sin^2 \Delta_{32} - 4\tilde{\theta}_{23}^2 \sin^2 \Delta_{32} + \Delta_{21} \sin^2 \theta_{12} \sin 2\Delta_{32} \\ & + \frac{\theta_{13}^2 \Delta_{32}}{(\Delta_e - \Delta_{32})^2} \times \\ & \left\{ 2\Delta_{32} \sin \Delta_{32} \cos \Delta_e \sin(\Delta_e - \Delta_{32}) - \Delta_e(\Delta_e - \Delta_{32}) \sin 2\Delta_{32} \right\} \\ & - (\theta_{24}^2 + \theta_{34}^2) \sin^2 \Delta_{32} - \theta_{24}\theta_{34}(2\Delta_n \cos \delta_{24} + \sin \delta_{24}) \sin 2\Delta_{32} + \mathcal{O}(\lambda^3), \end{aligned} \quad (\text{A.21})$$

which are the same as those obtained in Eqs. (2.15)–(2.17) in Chapter 2.

For an incident ν_e , the probabilities $P_{e\alpha}$ are

$$P_{ee} = 1 - 4\theta_{13}^2 \Delta_{32}^2 \frac{\sin^2(\Delta_e - \Delta_{32})}{(\Delta_e - \Delta_{32})^2} - 4\theta_{14}^2 \Delta_{42}^2 \frac{\sin^2(\Delta_e + \Delta_n - \Delta_{42})}{(\Delta_e + \Delta_n - \Delta_{42})^2} + \mathcal{O}(\lambda^3), \quad (\text{A.22})$$

$$P_{e\mu} = 2\theta_{13}^2 \Delta_{32}^2 \frac{\sin^2(\Delta_e - \Delta_{32})}{(\Delta_e - \Delta_{32})^2} + \mathcal{O}(\lambda^3), \quad (\text{A.23})$$

$$P_{e\tau} = 2\theta_{13}^2 \Delta_{32}^2 \frac{\sin^2(\Delta_e - \Delta_{32})}{(\Delta_e - \Delta_{32})^2} + \mathcal{O}(\lambda^3), \quad (\text{A.24})$$

which with these approximations can be simplified to

$$P_{ee} \approx 1 - 4\theta_{13}^2 \Delta_{32}^2 \frac{\sin^2(\Delta_e - \Delta_{32})}{(\Delta_e - \Delta_{32})^2} - 2\theta_{14}^2 + \mathcal{O}(\lambda^3), \quad (\text{A.25})$$

$$P_{e\mu} = P_{e\tau} = 2\theta_{13}^2 \Delta_{32}^2 \frac{\sin^2(\Delta_e - \Delta_{32})}{(\Delta_e - \Delta_{32})^2} + \mathcal{O}(\lambda^3), \quad (\text{A.26})$$

as given in Eqs. (2.20)–(2.22) in Chapter 2.

Appendix B

Feynman diagrams in Type-III seesaw

BS.1 Feynman rules involving the fermion triplet

In this appendix, we list the Feynman rules involving the fermion triplets Σ . Following [203], we introduce the fermion flow arrow for the leptons, which is the gray arrow in the diagrams. The black arrows indicate the lepton number flow. However interactions involving Σ may violate lepton numbers and thus the Σ line does not carry any lepton flow arrow. For the lepton number conserving interactions, the two arrows are parallel for particles, and antiparallel for the charge-conjugate fields. The Feynman rules are also given for the effective operator in the low energy limit of the theory obtained by integrating out these heavy fermion triplets.

BS.1.1 Propagator

$$\begin{array}{c} \xrightarrow{\hspace{1.5cm}} \\ \hline \Sigma^{gj} \qquad \qquad \qquad \Sigma^{fi} \end{array} = \frac{i(\not{p} + M_f)}{p^2 - M_f^2 + i\epsilon} \delta_{fg} \delta_{ij}$$

BS.1.2 Yukawa interactions

$$\phi_a = -i\mu^{\epsilon/2} (Y_{\Sigma}^{\dagger})_{fg} (\sigma^i \varepsilon)_{ba} P_R$$

$$\phi_a = -i\mu^{\epsilon/2} (Y_{\Sigma}^T)_{fg} (\varepsilon^T \sigma^i)_{ba} P_L$$

$$\phi_a = -i\mu^{\epsilon/2} (Y_{\Sigma})_{gf} (\varepsilon^T \sigma^i)_{ab} P_L$$

$$\phi_a = -i\mu^{\epsilon/2} (Y_{\Sigma}^*)_{gf} (\sigma^i \varepsilon)_{ab} P_R$$

BS.1.3 Gauge boson interactions

$$= -i\mu^{\frac{\epsilon}{2}} g_2 \gamma^{\mu} (i\varepsilon^{jik}) \delta_{gf}$$

BS.1.4 Counterterms

$$= i \left[\not{p} (\delta Z_{\Sigma})_{fg} - (\delta Z_{\mathbb{M}_{\Sigma}} \mathbb{M}_{\Sigma})_{fg} \right] \delta_{ij}$$

$$\phi_a = -i\mu^{\epsilon/2} (\delta Z_{Y_{\Sigma}}^{\dagger} Y_{\Sigma}^{\dagger})_{fg} (\sigma^i \varepsilon)_{ba} P_R$$

$$\phi_a = -i\mu^{\epsilon/2} (\delta Z_{Y_\Sigma} Y_\Sigma)_{gf} (\varepsilon^T \sigma^i)_{ab} P_L$$

$$\phi_a = -i\mu^{\epsilon/2} (\delta Z_{Y_\Sigma}^T Y_\Sigma^T)_{fg} (\varepsilon^T \sigma^i)_{ba} P_L$$

$$\phi_a = -i\mu^{\epsilon/2} (\delta Z_{Y_\Sigma}^* Y_\Sigma^*)_{gf} (\sigma^i \varepsilon)_{ab} P_R$$

BS.1.5 Effective vertex κ

$$= i\mu^{\epsilon/2} \kappa_{fg} \frac{1}{2} (\varepsilon_{ab} \varepsilon_{cd} + \varepsilon_{ad} \varepsilon_{bc}) P_L$$

$$= i\mu^{\epsilon/2} (\kappa^\dagger)_{fg} \frac{1}{2} (\varepsilon_{ab} \varepsilon_{cd} + \varepsilon_{ad} \varepsilon_{bc}) P_R$$

BS.1.6 Counterterms for κ

$$= i\mu^{\epsilon/2} (\delta\kappa)_{fg} \frac{1}{2} (\varepsilon_{ab}\varepsilon_{cd} + \varepsilon_{ad}\varepsilon_{bc}) P_L$$

$$= i\mu^{\epsilon/2} (\delta\kappa^\dagger)_{fg} \frac{1}{2} (\varepsilon_{ab}\varepsilon_{cd} + \varepsilon_{ad}\varepsilon_{bc}) P_R$$

BS.2 Feynman rules for the SM fields

Here we list the Feynman rules involving the SM fields only, also given in [75], which are needed for our calculations. The directions of the arrows should be interpreted in the same way as stated at the beginning of Appendix BS.1.

BS.2.1 Propagators

$$\frac{\longrightarrow}{q_{La}^g} \longrightarrow \frac{\longrightarrow}{q_{Lb}^f} = \frac{i\cancel{p}}{p^2+i\epsilon} \delta_{fg} \delta_{ab} \quad ; \quad \frac{\longrightarrow}{X_R^g} \longrightarrow \frac{\longrightarrow}{X_R^f} = \frac{i\cancel{p}}{p^2+i\epsilon} \delta_{fg} \quad , \quad X \in \{u, d\}$$

$$\frac{\longrightarrow}{l_{La}^g} \longrightarrow \frac{\longrightarrow}{l_{Lb}^f} = \frac{i\cancel{p}}{p^2+i\epsilon} \delta_{fg} \delta_{ab} \quad ; \quad \frac{\longrightarrow}{e_R^g} \longrightarrow \frac{\longrightarrow}{e_R^f} = \frac{i\cancel{p}}{p^2+i\epsilon} \delta_{fg}$$

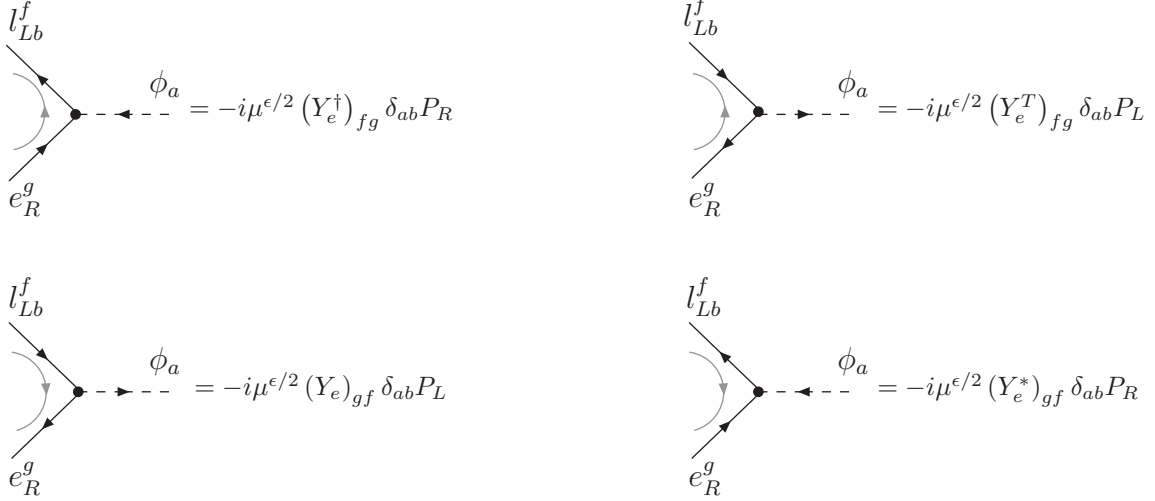
$$\frac{\longleftarrow}{l_{La}^g} \longleftarrow \frac{\longleftarrow}{l_{Lb}^f} = \frac{-i\cancel{p}}{p^2+i\epsilon} \delta_{gf} \delta_{ab} \quad ; \quad \frac{\longleftarrow}{e_R^g} \longleftarrow \frac{\longleftarrow}{e_R^f} = \frac{-i\cancel{p}}{p^2+i\epsilon} \delta_{gf}$$

$$\frac{\text{---}}{\phi_a} \text{---} \frac{\text{---}}{\phi_b} = \frac{i}{p^2 - m_\phi^2 + i\epsilon} \delta_{ab}$$

$$\frac{\text{~~~~~}}{X^\mu} \text{~~~~~} \frac{\text{~~~~~}}{X^\nu} = \frac{i(-\eta^{\mu\nu} + (1-\xi)p^\mu p^\nu / p^2)}{p^2 + i\epsilon} \quad ; \quad X \in \{B, W^i\}$$

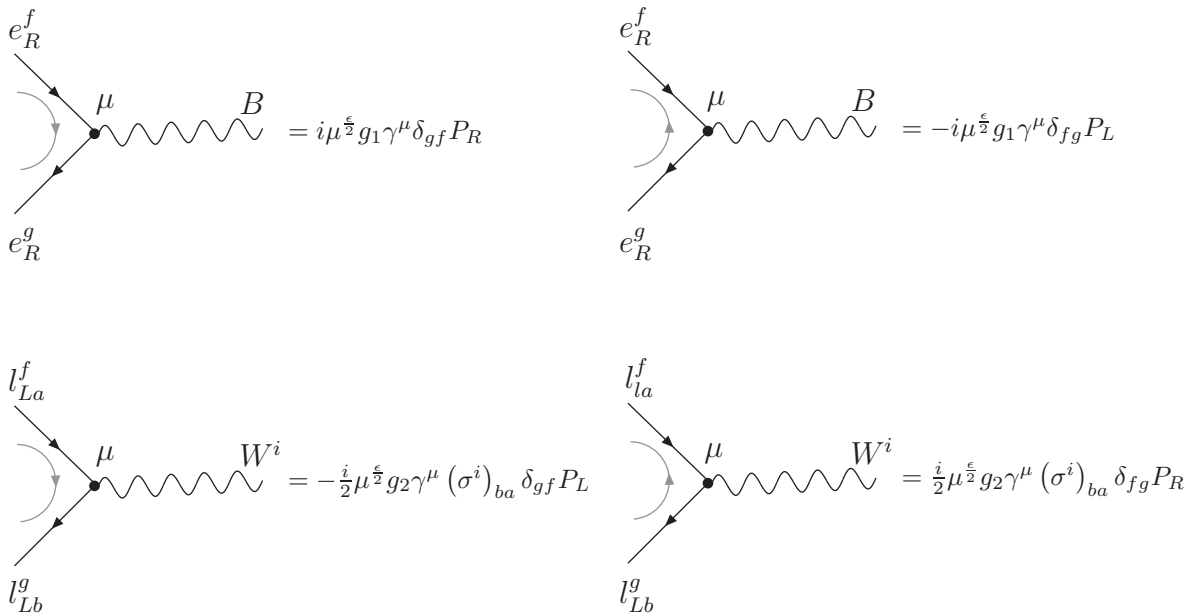
where $\xi = \xi_1$ for B boson and $\xi = \xi_2$ for W boson.

BS.2.2 Yukawa interactions



Similar Feynman rules, as those in the left panel, are there for Yukawa interactions of q_L - u_R and q_L - d_R with the Higgs ϕ having coefficients Y_u and Y_d respectively.

BS.2.3 Gauge boson – lepton interactions



$$l_{La}^f \text{ --- } \mu \text{ --- } B \text{ --- } l_{Lb}^g = \frac{i}{2} \mu^{\frac{\epsilon}{2}} g_1 \gamma^\mu \delta_{gf} \delta_{ab} P_L$$

$$l_{La}^f \text{ --- } \mu \text{ --- } B \text{ --- } l_{Lb}^g = -\frac{i}{2} \mu^{\frac{\epsilon}{2}} g_1 \gamma^\mu \delta_{fg} \delta_{ab} P_R$$

BS.2.4 Gauge boson – Higgs interactions

$$\phi_a \text{ --- } \mu \text{ --- } B \text{ --- } \phi_b = -\frac{i}{2} \mu^{\frac{\epsilon}{2}} g_1 (p_\mu + q_\mu) \delta_{ab}$$

$$\phi_a \text{ --- } \mu \text{ --- } W^i \text{ --- } \phi_b = -\frac{i}{2} \mu^{\frac{\epsilon}{2}} g_2 (p_\mu + q_\mu) (\sigma^i)_{ba}$$

The vertices involving two Higgses and two gauge bosons are not shown since they do not appear explicitly in our analysis.

BS.2.5 Higgs self-interaction

$$= -i \mu^\epsilon \lambda \frac{1}{2} (\delta_{ac} \delta_{bd} + \delta_{bc} \delta_{ad})$$

BS.2.6 Counterterms

$$l_{La}^f \text{ --- } \otimes \text{ --- } l_{Lb}^g = i \not{p} (\delta Z_{l_L})_{gf} P_L \delta_{ba}$$

$$l_{La}^f \text{ --- } \otimes \text{ --- } l_{Lb}^g = -i \not{p} (\delta Z_{l_L})_{fg} P_L \delta_{ba}$$

$$e_R^f \text{ --- } \otimes \text{ --- } e_R^g = i \not{p} (\delta Z_{e_R})_{gf} P_R$$

$$e_R^f \text{ --- } \otimes \text{ --- } e_R^g = -i \not{p} (\delta Z_{e_R})_{fg} P_R$$

$$\phi_a \text{ --- } \otimes \text{ --- } \phi_b = i (p^2 \delta Z_\phi - \delta m_\phi^2) \delta_{ba}$$

Appendix C

Calculation of renormalization constants

In this appendix we show the Feynman diagrams contributing to the renormalization constants of different quantities and evaluate them to determine the renormalization constants. Note that for particles in the loop, we suppress the flavor as well as the $SU(2)_L$ indices.

We will use the dimensional regularization and the minimal subtraction (MS) scheme for renormalization. In the MS scheme the counterterms are defined such that they only cancel the divergent parts. Hence the renormalization constants are defined as

$$Z_i = 1 + \sum_{k \geq 1} \delta Z_{i,k} \frac{1}{\epsilon}, \quad (\text{C.1})$$

where $\delta Z_{i,k}$ are independent of $\epsilon \equiv 4 - d$, d being the space-time dimension. At the one-loop level the sum reduces to the term proportional to $1/\epsilon$.

The calculations are done in the general renormalizable R_ξ gauge, and then the very fact that the final beta-functions must be independent of the choice of gauge is verified. The calculations are done considering the gauge bosons W^i and B to be massless, and strictly speaking the bosonic propagators considered are correct before electroweak symmetry breaking only. However the results are assumed to be true at energies below the symmetry breaking also.

CS.1 Doublet Higgs wavefunction and mass (Z_ϕ and δm_ϕ^2)

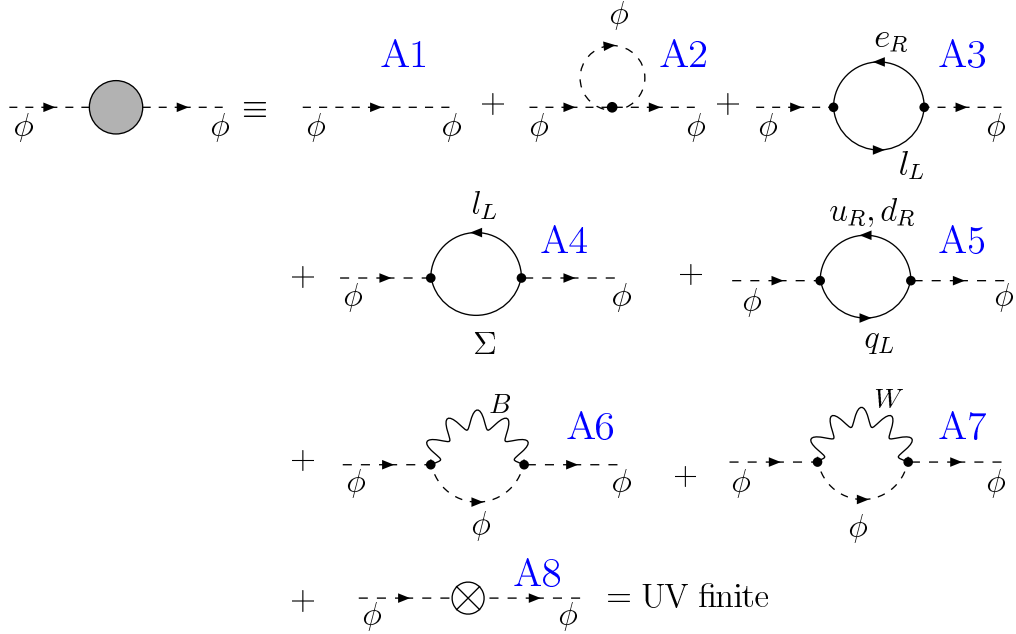


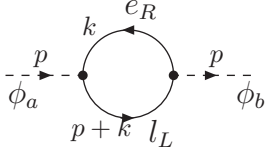
Figure C.1: Feynman diagrams contributing to the one loop correction of the doublet Higgs self-energy.

Let us evaluate the Feynman diagrams shown in the Fig. C.1 that contributes to the renormalization of the doublet Higgs wavefunction and its mass.

$$\begin{aligned}
 \text{A2 : } & \text{Diagram showing a loop of } \phi \text{ with external lines } \phi_a \text{ and } \phi_b \text{ and internal lines } p \text{ and } k. \\
 & = (-i^2) \frac{3}{2} \mu^\epsilon \lambda \delta_{ab} \int \frac{d^d k}{(2\pi)^d} \frac{1}{k^2 - m_\phi^2} \\
 & = -\frac{3i}{2} \mu^\epsilon \lambda \delta_{ab} I_{0,1}(m_\phi^2, \epsilon) \\
 & = \frac{3i}{16\pi^2} \lambda m_\phi^2 \delta_{ab} \frac{1}{\epsilon} + \text{UV finite} . \tag{C.2}
 \end{aligned}$$

The d -dimensional integral defined here is given explicitly in the Section CS.9.

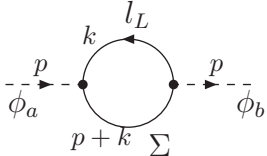
A3 :



$$\begin{aligned}
 &= (-1)i^2\mu^\epsilon\text{Tr}(Y_e^\dagger Y_e)\delta_{ab}\int\frac{d^dk}{(2\pi)^d}\text{Tr}\left[P_L\frac{i(\not{p}+\not{k})}{(p+k)^2}P_R\frac{i\not{k}}{k^2}\right] \\
 &= -\mu^\epsilon\text{Tr}(Y_e^\dagger Y_e)\delta_{ab}\int\frac{d^dk}{(2\pi)^d}\frac{2(p+k)\cdot k}{k^2(p+k)^2} \\
 &= 2i\mu^\epsilon\text{Tr}(Y_e^\dagger Y_e)\delta_{ab}\left[I_{0,1}(0,\epsilon)+p^2\int_0^1dx(1-x)I_{0,2}(\Delta(x),\epsilon)\right], \\
 &= \frac{i}{8\pi^2}\text{Tr}(Y_e^\dagger Y_e)\delta_{ab}p^2\frac{1}{\epsilon}+\text{UV finite}. \tag{C.3}
 \end{aligned}$$

Here $\Delta(x) = (1-x)^2p^2 - (1-x)p^2$. The trace is evaluated as given in Eq. (C.56). Here we have used the Clifford algebra in d -dimension as described in Section CS.10 and the Feynman parameterization as shown in the Section CS.11. The overall negative sign comes because of the fermion loop.

A4 :

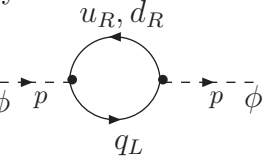


$$\begin{aligned}
 &= (-1)i^2\mu^\epsilon\text{Tr}(Y_\Sigma^\dagger Y_\Sigma)(\varepsilon^T\sigma^i\sigma^i\varepsilon)_{ab}\int\frac{d^dk}{(2\pi)^d}\text{Tr}\left[P_R\frac{i(\not{p}+\not{k}+\mathbb{M}_\Sigma)}{[(p+k)^2-\mathbb{M}_\Sigma^2]}P_L\frac{i\not{k}}{k^2}\right] \\
 &= -\mu^\epsilon\text{Tr}(3Y_\Sigma^\dagger Y_\Sigma)\delta_{ab}\int\frac{d^dk}{(2\pi)^d}\frac{2(p+k)\cdot k}{k^2[(p+k)^2-\mathbb{M}_\Sigma^2]} \\
 &= 2i\mu^\epsilon\text{Tr}(3Y_\Sigma^\dagger Y_\Sigma)\delta_{ab}\left[I_{0,1}(\mathbb{M}_\Sigma^2,\epsilon)+p^2\int_0^1dx(1-x)I_{0,2}(\Delta(x,\mathbb{M}_\Sigma^2),\epsilon)\right], \\
 &= \frac{i}{8\pi^2}\text{Tr}(3Y_\Sigma^\dagger Y_\Sigma)\delta_{ab}(p^2-2\mathbb{M}_\Sigma^2)\frac{1}{\epsilon}+\text{UV finite}, \tag{C.4}
 \end{aligned}$$

where $\Delta(x, \mathbb{M}_\Sigma^2) = (1-x)^2p^2 - (1-x)p^2 + \mathbb{M}_\Sigma^2$. Here σ^i are the Pauli matrices and $\sum\sigma^i\sigma^i = 3$. ε is the antisymmetric matrix in $\text{SU}(2)_L$ and $\varepsilon^T\varepsilon = \varepsilon\varepsilon^T = \mathbb{1}$.

Similarly we can evaluate the diagram A5 to get

A5 :



$$= \frac{i}{8\pi^2}\text{Tr}(3Y_u^\dagger Y_u + 3Y_d^\dagger Y_d)\delta_{ab}p^2\frac{1}{\epsilon}+\text{UV finite}. \tag{C.5}$$

A6 :

$$\begin{aligned}
 &= \frac{i^2}{4} \mu^\epsilon g_1^2 \delta_{ab} \int \frac{d^d k}{(2\pi)^d} (2p_\mu + k_\mu) i \frac{-\eta^{\mu\nu} + (1 - \xi_1) \frac{k^\mu k^\nu}{k^2}}{k^2} (2p_\nu + k_\nu) \frac{i}{(p+k)^2 - m_\phi^2} \\
 &= \frac{1}{4} \mu^\epsilon g_1^2 \delta_{ab} \int \frac{d^d k}{(2\pi)^d} \frac{-(2p+k)^2 + (1 - \xi_1) \frac{1}{k^2} [k \cdot (2p+k)]^2}{k^2 [(p+k)^2 - m_\phi^2]} \\
 &= \frac{i}{32\pi^2} g_1^2 \delta_{ab} (-3p^2 + \xi_1 p^2 - \xi_1 m_\phi^2) \frac{1}{\epsilon} + \text{UV finite} . \tag{C.6}
 \end{aligned}$$

Similarly

A7 :

$$= \frac{3i}{32\pi^2} g_1^2 \delta_{ab} (-3p^2 + \xi_2 p^2 - \xi_2 m_\phi^2) \frac{1}{\epsilon} + \text{UV finite} , \tag{C.7}$$

where the difference of factor 3 is because of the fact that the W bosons form a triplet in $SU(2)_L$.

Then using the definition of counter term A8 in the minimal subtraction scheme and demanding that the counter terms will only cancel the divergences, the renormalization constants are evaluated to be

$$\delta Z_\phi = -\frac{1}{16\pi^2} \left(2T - \frac{3}{10} (3 - \xi_1) g_1^2 - \frac{3}{2} (3 - \xi_2) g_2^2 \right) \frac{1}{\epsilon} , \tag{C.8}$$

$$\delta m_\phi^2 = \frac{1}{16\pi^2} \left(3\lambda m_\phi^2 - \frac{3}{10} \xi_1 g_1^2 m_\phi^2 - \frac{3}{2} \xi_2 g_2^2 m_\phi^2 - 4 \text{Tr}[3Y_\Sigma^\dagger Y_\Sigma] \mathbb{M}_\Sigma^2 \right) \frac{1}{\epsilon} . \tag{C.9}$$

CS.2 Left-handed lepton wavefunction (Z_{l_L})

Now let us evaluate the Feynman diagrams that contribute to the renormalization constant Z_{l_L} at the one loop level, as shown in Fig C.2.

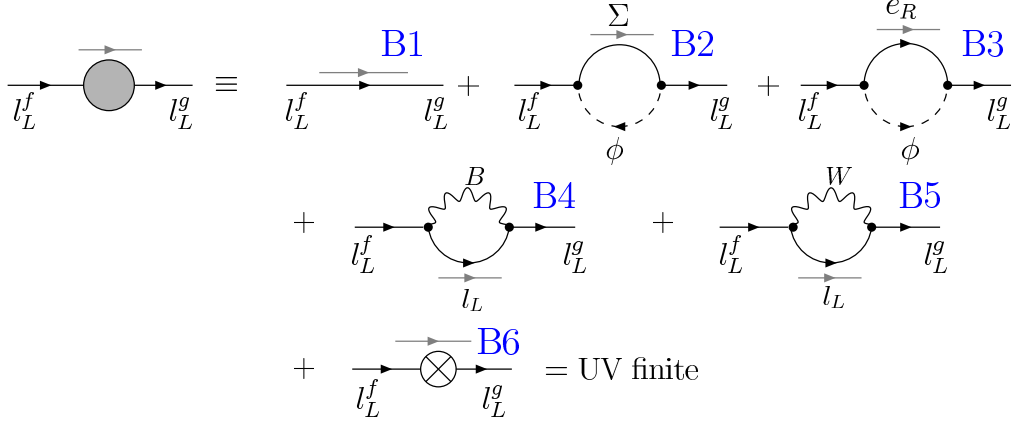


Figure C.2: Feynman diagrams contributing to the one loop correction to the self-energy of the lepton doublet l_L .

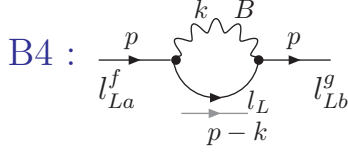
$$\begin{aligned}
 \text{B2 : } & \text{Diagram with } \Sigma \text{ and } \phi \text{ loop} \\
 &= i^2 \mu^\epsilon \left(Y_{\Sigma}^\dagger Y_{\Sigma} \right)_{gf} (\sigma^i \varepsilon^T \varepsilon \sigma^i)_{ba} \int \frac{d^d k}{(2\pi)^d} P_R \frac{i(\not{k} + M_{\Sigma})}{k^2 - M_{\Sigma}^2} P_L \frac{i}{(k-p)^2 - m_{\phi}^2} \\
 &= 3\mu^\epsilon \left(Y_{\Sigma}^\dagger Y_{\Sigma} \right)_{gf} \delta_{ab} P_R \int \frac{d^d k}{(2\pi)^d} \frac{\not{k}}{(k^2 - M_{\Sigma}^2)[(k-p)^2 - m_{\phi}^2]} \\
 &= 3i\mu^\epsilon \left(Y_{\Sigma}^\dagger Y_{\Sigma} \right)_{gf} \delta_{ab} \not{p} P_L \int_0^1 dx I_{0,2}(\Delta(x, M_{\Sigma}), \epsilon) \\
 &= \frac{3i}{16\pi^2} \left(Y_{\Sigma}^\dagger Y_{\Sigma} \right)_{gf} \delta_{ab} \not{p} P_L \frac{1}{\epsilon} + \text{UV finite} . \tag{C.10}
 \end{aligned}$$

Here $\Delta(x, M_{\Sigma}) = x^2 p^2 - x p^2 + x m_{\phi}^2 + (1-x) M_{\Sigma}^2$.

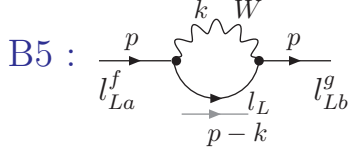
$$\begin{aligned}
 \text{B3 : } & \text{Diagram with } e_R \text{ and } \phi \text{ loop} \\
 &= i^2 \mu^\epsilon (Y_e^\dagger Y_e)_{gf} \delta_{ba} \int \frac{d^d k}{(2\pi)^d} P_R \frac{i\not{k}}{k^2} P_L \frac{i}{(p-k)^2 - m_{\phi}^2}
 \end{aligned}$$

$$\begin{aligned}
 &= i\mu^\epsilon (Y_e^\dagger Y_e)_{gf} \delta_{ba} \not{p} P_L \int_0^1 dx I_{0,2}(\Delta(x), \epsilon) \\
 &= \frac{i}{16\pi^2} (Y_e^\dagger Y_e)_{gf} \delta_{ba} \not{p} P_L \frac{1}{\epsilon} + \text{UV finite} ,
 \end{aligned} \tag{C.11}$$

where $\Delta(x) = x^2 p^2 - xp^2 + xm_\phi^2$.



$$\begin{aligned}
 &= \frac{i^2}{4} \mu^\epsilon g_1^2 \delta_{gf} \delta_{ab} \int \frac{d^d k}{(2\pi)^d} \gamma_\mu P_L \frac{i(\not{p} - \not{k})}{(p-k)^2} \gamma_\nu P_L i \frac{-\eta^{\mu\nu} + (1-\xi_1) \frac{k^\mu k^\nu}{k^2}}{k^2} \\
 &= \frac{1}{4} \mu^\epsilon g_1^2 \delta_{gf} \delta_{ab} P_R \int \frac{d^d k}{(2\pi)^d} \frac{2(\not{p} - \not{k}) + (1-\xi_1)(\not{k} \not{p} \not{k} - \not{k} k^2)/k^2}{k^2 (p-k)^2} \\
 &= \frac{i}{32\pi^2} \xi_1 g_1^2 \delta_{gf} \delta_{ab} \not{p} P_L \frac{1}{\epsilon} + \text{UV finite} .
 \end{aligned} \tag{C.12}$$



$$= \frac{3i}{32\pi^2} \xi_2 g_1^2 \delta_{gf} \delta_{ab} \not{p} P_L \frac{1}{\epsilon} + \text{UV finite} . \tag{C.13}$$

Finally, using the counter term B6, the wavefunction renormalization can be calculated in the minimal subtraction scheme to get

$$\delta Z_{l_L} = -\frac{1}{16\pi^2} \left(Y_e^\dagger Y_e + 3Y_\Sigma^\dagger Y_\Sigma + \frac{3}{10} \xi_1 g_1^2 + \frac{3}{2} \xi_2 g_2^2 \right) \frac{1}{\epsilon} . \tag{C.14}$$

CS.3 Wavefunction and mass of fermion triplet (Z_Σ and Z_{M_Σ})

Now we evaluate the Feynman diagrams shown in the Fig C.3, which contribute to the self-energy correction of the fermionic triplet Σ at one loop.

$$\begin{aligned}
 & \Sigma^{fi} \text{ (with grey circle) } \Sigma^{gj} \equiv \Sigma^{fi} \xrightarrow{\text{C1}} \Sigma^{gj} + \Sigma^{fi} \text{ (with } \phi \text{ loop and } l_L \text{)} \xrightarrow{\text{C2}} \Sigma^{gj} \\
 & + \Sigma^{fi} \text{ (with } W \text{ loop and } \Sigma \text{)} \xrightarrow{\text{C3}} \Sigma^{gj} + \Sigma^{fi} \text{ (with } \otimes \text{)} \xrightarrow{\text{C4}} \Sigma^{gj} \\
 & = \text{UV finite}
 \end{aligned}$$

Figure C.3: Feynman diagrams contributing to the one loop correction to the self-energy of the fermion triplet $\Sigma \equiv \Sigma_R + \Sigma_R^C$.

C2 :

$$\begin{aligned}
 & = i^2 \mu^\epsilon \left(Y_\Sigma Y_\Sigma^\dagger \right)_{gf} \text{Tr}(\varepsilon^T \sigma^j \sigma^i \varepsilon) \int \frac{d^d k}{(2\pi)^d} P_L \frac{i \not{k}}{k^2} P_R \frac{i}{(p-k)^2 - m_\phi^2} \\
 & = 2\mu^\epsilon \left(Y_\Sigma Y_\Sigma^\dagger \right)_{gf} \delta_{ij} P_L \int \frac{d^d k}{(2\pi)^d} P_L \frac{\not{k}}{k^2 [(p-k)^2 - m_\phi^2]} \\
 & = 2i\mu^\epsilon \left(Y_\Sigma Y_\Sigma^\dagger \right)_{gf} \delta_{ij} \not{p} P_R \int_0^1 dx I_{0,2}(\Delta(x), \epsilon) \\
 & = \frac{i}{8\pi^2} \left(Y_\Sigma Y_\Sigma^\dagger \right)_{gf} \delta_{ij} \not{p} P_R \frac{1}{\epsilon} + \text{UV finite}, \tag{C.15}
 \end{aligned}$$

where $\Delta(x) = x^2 p^2 - xp^2 + xm_\phi^2$ and we have used $\text{Tr}(\sigma^i \sigma^j) = 2\delta_{ij}$.

C3 :

$$\begin{aligned}
 & = -2i^4 \mu^\epsilon g_2^2 \delta_{ij} \delta_{gf} \int \frac{d^d k}{(2\pi)^d} \gamma^\mu \frac{i(\not{p} - \not{k} + M_\Sigma)}{(p-k)^2 - M_\Sigma^2} \gamma_\nu i \frac{-\eta^{\mu\nu} + (1-\xi_2) \frac{k^\mu k^\nu}{k^2}}{k^2} \\
 & = 2\mu^\epsilon g_2^2 \delta_{ij} \delta_{gf} \int \frac{d^d k}{(2\pi)^d} \frac{2(\not{p} - \not{k}) - (3 + \xi_2) M_\Sigma + (1 - \xi_2) \not{k} (\not{p} - \not{k}) \not{k} / k^2}{k^2 [(p-k)^2 - M_\Sigma^2]}
 \end{aligned}$$

$$\begin{aligned}
 &= 2i\mu^\epsilon g_2^2 \delta_{ij} \delta_{gf} \left[\left(\frac{1}{2} \not{p} - \mathbb{M}_\Sigma \right) (3 + \xi_2) \int_0^1 dx I_{0,2}(\Delta(x, \mathbb{M}_\Sigma^2), \epsilon) \right. \\
 &\quad \left. + (-3 + \xi_2) \not{p} \int_0^1 x dx I_{0,2}(\Delta(x, \mathbb{M}_\Sigma^2), \epsilon) \right] \\
 &= \frac{i}{4\pi^2} g_2^2 \delta_{ij} \delta_{gf} [\xi_2 \not{p} - (3 + \xi_2) \mathbb{M}_\Sigma] \frac{1}{\epsilon} + \text{UV finite} , \tag{C.16}
 \end{aligned}$$

where we have used $\varepsilon^{ijk} \varepsilon^{ljk} = -2\delta_{il}$ and $\Delta(x, \mathbb{M}_\Sigma^2) = x^2 p^2 - x p^2 + x \mathbb{M}_\Sigma^2$.

Using the above results, and the definition of the counter term in C4, we get the renormalization constants in the minimal subtraction scheme to be

$$\delta Z_\Sigma = -\frac{1}{16\pi^2} \left[\left(2Y_\Sigma Y_\Sigma^\dagger + 4\xi_2 g_2^2 \right) P_R + \left(2(Y_\Sigma Y_\Sigma^\dagger)^* + 4\xi_2 g_2^2 \right) P_L \right] \frac{1}{\epsilon} , \tag{C.17}$$

$$\delta Z_{\mathbb{M}_\Sigma} = -\frac{1}{16\pi^2} (12 + 4\xi_2) g_2^2 \frac{1}{\epsilon} . \tag{C.18}$$

The term proportional to P_L in δZ_Σ comes from the Feynman diagram similar to C2, where the particles in the closed loop flow in the opposite direction.

CS.4 Right-handed charged lepton wavefunction (Z_{e_R})

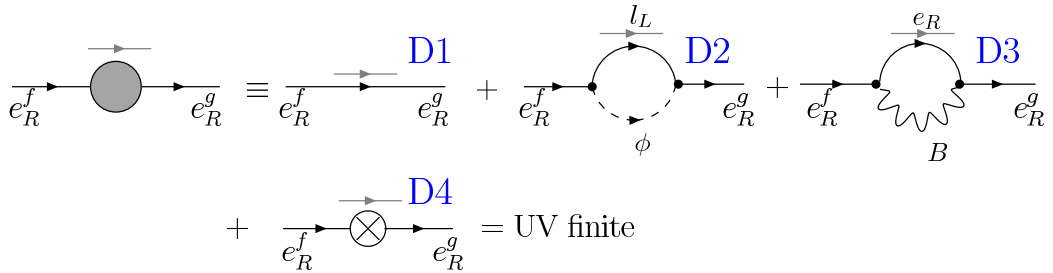
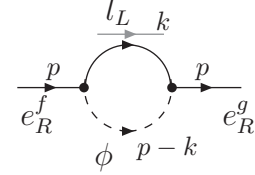


Figure C.4: Feynman diagrams contributing to the one loop correction to the self-energy of the fermion singlet e_R .

Let us now evaluate the Feynman diagrams that contribute to δZ_{e_R} , as shown in Fig C.4.

As can be seen, the diagram D2 can be evaluated in a quite similar way to B3 in Section CS.2 to get

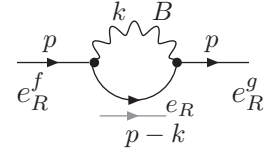
D2 :



$$= \frac{i}{8\pi^2} (Y_e Y_e^\dagger)_{gf} \not{P}_R \frac{1}{\epsilon} + \text{UV finite} , \quad (\text{C.19})$$

while the evaluation of D3 will be similar to that of B5 and produce

D3 :



$$= \frac{i}{8\pi^2} \xi_1 g_1^2 \delta_{gf} \not{P}_R \frac{1}{\epsilon} + \text{UV finite} . \quad (\text{C.20})$$

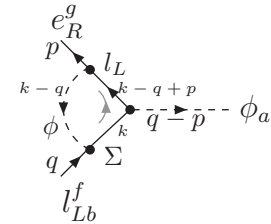
Thus finally using the definition of the counter term in D4 the wavefunction renormalization constant can be obtained as

$$\delta Z_{e_R} = -\frac{1}{16\pi^2} \left(2Y_e Y_e^\dagger + \frac{6}{5} \xi_1 g_1^2 \right) \frac{1}{\epsilon} . \quad (\text{C.21})$$

CS.5 $l_L e_R \phi$ Yukawa vertex (Z_{Y_e})

Fig C.5 shows the Feynman diagrams that contribute to the one loop correction of the $l_L - e_R - \phi$ vertex in the SM. Let us now evaluate the diagrams explicitly.

E2 :



$$= -i^6 \mu^{3\epsilon/2} (Y_e Y_\Sigma^\dagger Y_\Sigma)_{gf} (\sigma^i \varepsilon)_{xa} (\varepsilon^T \sigma^i)_{xb} P_L \times$$

$$\int \frac{d^d k}{(2\pi)^d} \frac{\not{k} (\not{k} - \not{q} + \not{p})}{(k^2 - M_\Sigma^2) [(k-q)^2 - m_\phi^2] (k-q+p)^2} \quad (\text{C.22})$$

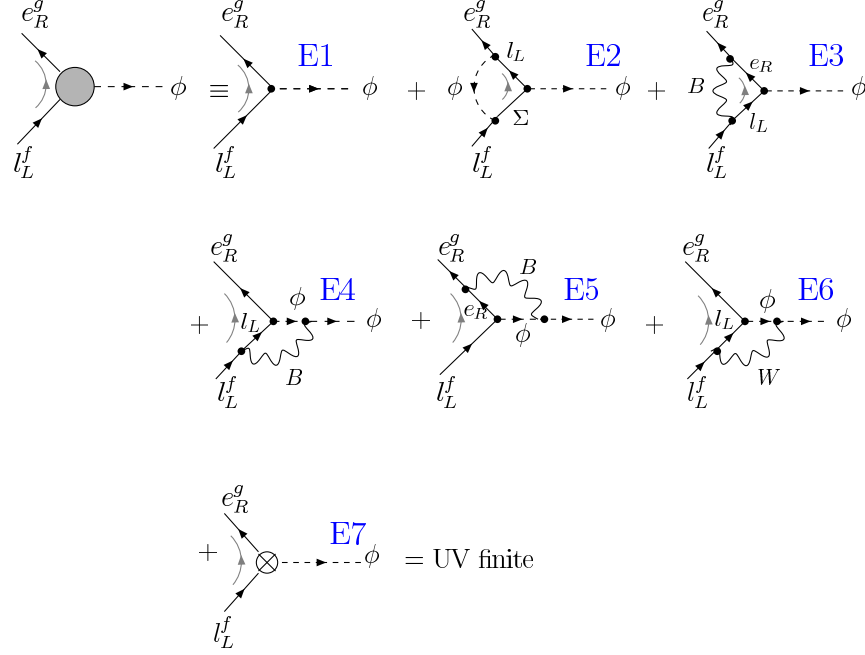
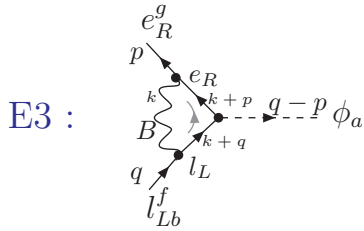


Figure C.5: Feynman diagrams contributing to the one loop correction of the $l_L e_R \phi$ Yukawa vertex.

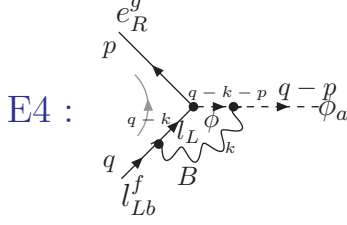
$$\begin{aligned}
 &= i\mu^{3\epsilon/2} \left(3Y_e Y_\Sigma^\dagger Y_\Sigma \right)_{gf} \delta_{ba} P_L \int_0^1 dx dy I_{2,3}(\Delta(x, y, M_\Sigma^2, m_\phi^2), \epsilon) + \text{UV finite} \\
 &= \frac{3i}{8\pi^2} \left(Y_e Y_\Sigma^\dagger Y_\Sigma \right)_{gf} \delta_{ba} P_L \frac{1}{\epsilon} + \text{UV finite} , \tag{C.23}
 \end{aligned}$$

where $\Delta(x, y, M_\Sigma^2, m_\phi^2) \equiv (xq)^2 + y^2(p-q)^2 - xq^2 - y(p-q)^2 + (1-x-y)M_\Sigma^2 + xm_\phi^2$ and $(\sigma^i \varepsilon)_{xa} (\varepsilon^T \sigma^i)_{xb} = 3\delta_{ab}$.



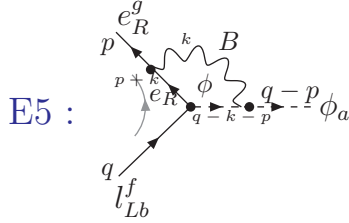
$$\begin{aligned}
 &= -\frac{i^6}{2} \mu^{3\epsilon/2} g_1^2 (Y_e)_{gf} \delta_{ba} P_L \int \frac{d^d k}{(2\pi)^d} \frac{(\not{q} + \not{k}) \gamma_\nu [-\eta^{\mu\nu} + (1 - \xi_1) \frac{k^\mu k^\nu}{k^2}] \gamma_\mu (\not{p} + \not{k})}{k^2 (k+p)^2 (k+q)^2} \\
 &= -\frac{i}{2} \mu^{3\epsilon/2} (3 + \xi_1) g_1^2 (Y_e)_{gf} \delta_{ba} P_L \int_0^1 dx I_{0,2}(\Delta(x), \epsilon) + \text{UV finite} \\
 &= -\frac{i}{16\pi^2} (3 + \xi_1) g_1^2 (Y_e)_{gf} \delta_{ba} P_L \frac{1}{\epsilon} + \text{UV finite} , \tag{C.24}
 \end{aligned}$$

where $\Delta(x) \equiv [xp + (1-x)q]^2 - xp^2 - (1-x)q^2$.



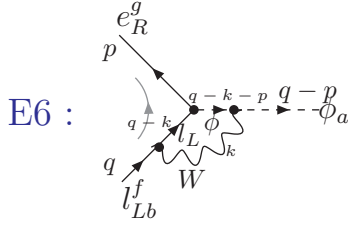
$$\begin{aligned}
 &= -\frac{g_1^2}{4} \mu^{3\epsilon/2} (Y_e)_{gf} \delta_{ba} P_L \times \\
 &\quad \int \frac{d^d k}{(2\pi)^d} \frac{(q-k)\gamma_\nu [-\eta^{\mu\nu} + (1-\xi_1) \frac{k^\mu k^\nu}{k^2}] [2(q_\mu - p_\mu) - k_\mu]}{(q-k)^2 k^2 [(q-k-p)^2 - m_\phi^2]} \\
 &= -\frac{g_1^2}{4} \mu^{3\epsilon/2} (Y_e)_{gf} \delta_{ba} P_L \int_0^1 dx dy (-i\xi_1) I_{2,3}(\Delta(x, y, m_\phi^2), \epsilon) + \text{UV finite} \\
 &= \frac{i}{32\pi^2} \xi_1 g_1^2 (Y_e)_{gf} \delta_{ba} P_L \frac{1}{\epsilon} + \text{UV finite} . \tag{C.25}
 \end{aligned}$$

Here $\Delta(x, y, m_\phi^2) \equiv [xp + (x+y)q]^2 + xm_\phi^2 - x(p+q)^2 - yq^2$.



$$\begin{aligned}
 &= \frac{i^6}{2} g_1^2 \mu^{3\epsilon/2} (Y_e)_{gf} \delta_{ba} P_L \times \\
 &\quad \int \frac{d^d k}{(2\pi)^d} \frac{(2q_\mu - 2p_\mu - k_\mu) [-\eta^{\mu\nu} + (1-\xi_1) \frac{k^\mu k^\nu}{k^2}] \gamma_\nu (\not{p} + \not{k})}{k^2 [(q-p-k)^2 - m_\phi^2] (p+k)^2} \\
 &= -\frac{i}{2} \xi_1 g_1^2 (Y_e)_{gf} \delta_{ba} P_L \int_0^1 dx I_{0,2}(\Delta(x, m_\phi^2), \epsilon) + \text{UV finite} \\
 &= -\frac{i}{16\pi^2} \xi_1 g_1^2 (Y_e)_{gf} \delta_{ba} P_L \frac{1}{\epsilon} + \text{UV finite} . \tag{C.26}
 \end{aligned}$$

Here $\Delta(x, m_\phi^2) \equiv (1-x)^2 p^2 - (1-x)p^2 + x^2(p-q)^2 - x(p-q)^2 + xm_\phi^2$. The diagram shown in E6 can be evaluated in a similar way as E4 to get



$$= -\frac{3i}{32\pi^2}\xi_2 g_2^2 (Y_e)_{gf} \delta_{ba} P_L \frac{1}{\epsilon} + \text{UV finite} . \quad (\text{C.27})$$

The factor ‘3’ comes because of the fact that W forms a triplet under $SU(2)_L$, while B is a singlet. The difference in sign is there because of the sign difference between the coupling of the lepton doublet l_L with these two gauge bosons.

Then finally, using the definition of the counter term in E7, the renormalization constant for the Yukawa interaction vertex $l_L e_R \phi$ will be given by

$$\delta Z_{Y_e} = -\frac{1}{16\pi^2} \left(-6Y_\Sigma^\dagger Y_\Sigma + \frac{9}{5} \left(1 + \frac{1}{2}\xi_1 \right) g_1^2 + \frac{3}{2}\xi_2 g_2^2 \right) \frac{1}{\epsilon} . \quad (\text{C.28})$$

CS.6 $l_L \Sigma \phi$ Yukawa vertex (Z_{Y_Σ})

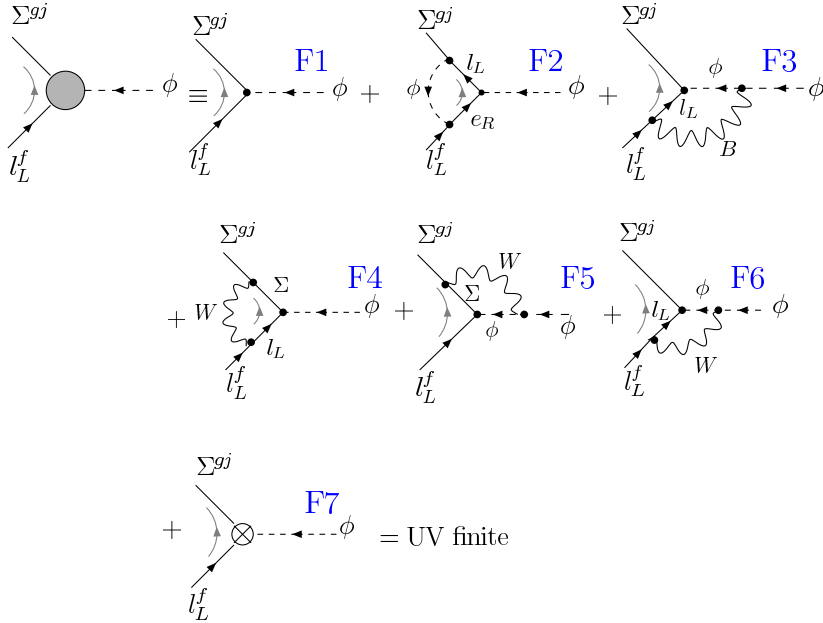
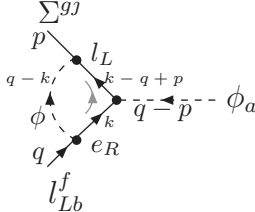


Figure C.6: Feynman diagrams contributing to the one loop correction of the $l_L \Sigma \phi$ Yukawa vertex.

Fig C.6 shows the Feynman diagrams that contribute to the one loop correction

of the $l_L - \Sigma - \phi$ vertex in the Type-III seesaw scenario. Let us now evaluate the diagrams explicitly.

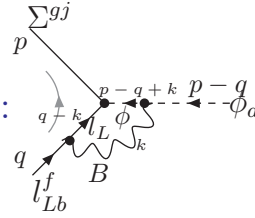
F2 :



$$\begin{aligned}
 &= -i^6 \mu^{3\epsilon/2} (Y_\Sigma Y_e^\dagger Y_e)_{gf} (\varepsilon^T \sigma^j)_{ba} P_L \int \frac{d^d k}{(2\pi)^d} \frac{\not{k}(\not{k} - \not{q} + \not{p})}{k^2(k-q+p)^2[(q-k)^2 - m_\phi^2]} \\
 &= \mu^{3\epsilon/2} (Y_\Sigma Y_e^\dagger Y_e)_{gf} (\varepsilon^T \sigma^j)_{ba} P_L i \int_0^1 dx I_{0,2}(\Delta(x, m_\phi^2), \epsilon) + \text{UV finite} \\
 &= \frac{i}{8\pi^2} (Y_\Sigma Y_e^\dagger Y_e)_{gf} (\varepsilon^T \sigma^j)_{ba} P_L \frac{1}{\epsilon} + \text{UV finite} , \tag{C.29}
 \end{aligned}$$

with $\Delta(x, m_\phi^2) \equiv x^2(p-q)^2 - x(p-q)^2 + (1-x)^2q^2 - (1-x)q^2 + (1-x)m_\phi^2$.

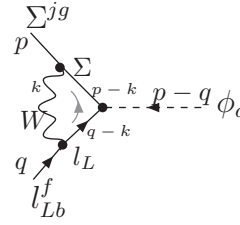
F3 :



$$\begin{aligned}
 &= \frac{i^6}{4} \mu^{3\epsilon/2} g_1^2 (Y_\Sigma)_{gf} (\varepsilon^T \sigma^j)_{ba} P_L \times \\
 &\quad \int \frac{d^d k}{(2\pi)^d} \frac{(\not{q} - \not{k}) \gamma_\mu [-\eta^{\mu\nu} + (1-\xi_1) \frac{k^\mu k^\nu}{k^2}] (2p_\nu - 2q_\nu + k_\nu)}{k^2(q-k)^2[(p-q+k)^2 - m_\phi^2]} \\
 &= -\frac{i}{4} \mu^{3\epsilon/2} \xi_1 g_1^2 (Y_\Sigma)_{gf} (\varepsilon^T \sigma^j)_{ba} P_L \int_0^1 dx I_{0,2}(\Delta(x, m_\phi^2), \epsilon) + \text{UV finite} \\
 &= -\frac{i}{32\pi^2} \xi_1 g_1^2 (Y_\Sigma)_{gf} (\varepsilon^T \sigma^j)_{ba} P_L \frac{1}{\epsilon} + \text{UV finite} , \tag{C.30}
 \end{aligned}$$

where $\Delta(x, m_\phi^2) \equiv x^2(p-q)^2 - x(p-q)^2 + (1-x)^2q^2 - (1-x)q^2 + xm_\phi^2$.

F4 :

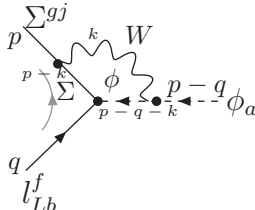


$$= -\frac{i^6}{2} \mu^{3\epsilon/2} g_2^2 (Y_\Sigma)_{gf} [(\sigma^{iT} \varepsilon^T \sigma^m)_{ba} i\varepsilon^{jim}] P_L \times$$

$$\begin{aligned}
 & \int \frac{d^d k}{(2\pi)^d} \frac{(\not{q} - \not{k})\gamma_\nu[-\eta^{\mu\nu} + (1 - \xi_2)\frac{k^\mu k^\nu}{k^2}]\gamma_\mu(\not{p} - \not{k} + \mathbb{M}_\Sigma)}{k^2(q - k)^2[(p - k)^2 - \mathbb{M}_\Sigma^2]} \\
 &= -i\mu^{3\epsilon/2}(3 + \xi_2)g_2^2(Y_\Sigma)_{gf}(\varepsilon^T \sigma^j)_{ba} P_L \int_0^1 dx I_{0,2}(\Delta(x, \mathbb{M}_\Sigma^2), \epsilon) + \text{UV finite} \\
 &= -\frac{i}{8\pi^2}(3 + \xi_2)g_2^2(Y_\Sigma)_{gf}(\varepsilon^T \sigma^j)_{ba} P_L \frac{1}{\epsilon} + \text{UV finite}, \tag{C.31}
 \end{aligned}$$

where $i\varepsilon^{mij}(\sigma^{iT} \varepsilon^T \sigma^m)_{ab} \equiv 2(\varepsilon^T \sigma^j)_{ba}$.

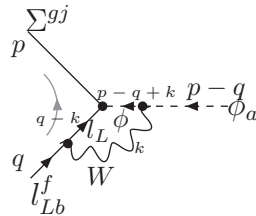
F5 :



$$\begin{aligned}
 &= -\frac{i^6}{2}g_2^2\mu^{3\epsilon/2}(Y_\Sigma)_{gf}(\sigma^{iT} \varepsilon^T \sigma^m)_{ab} P_L \times \\
 & \int \frac{d^d k}{(2\pi)^d} \frac{(2p_\mu - 2q_\mu - k_\mu)[-\eta^{\mu\nu} + (1 - \xi_2)\frac{k^\mu k^\nu}{k^2}]\gamma_\nu(\not{p} - \not{k} + \mathbb{M}_\Sigma)}{k^2[(p - q - k)^2 - m_\phi^2][(p - k)^2 - \mathbb{M}_\Sigma^2]} \\
 &= -i\xi_2 g_2^2 \mu^{3\epsilon/2} (Y_\Sigma)_{gf} (\varepsilon^T \sigma^j)_{ba} P_L \int_0^1 dx I_{0,2}(\Delta(x, m_\phi^2, \mathbb{M}_\Sigma^2), \epsilon) + \text{UV finite} \\
 &= -\frac{i}{8\pi^2} \xi_2 g_2^2 (Y_\Sigma)_{gf} (\varepsilon^T \sigma^j)_{ba} P_L \frac{1}{\epsilon} + \text{UV finite}. \tag{C.32}
 \end{aligned}$$

Here $\Delta(x, m_\phi^2, \mathbb{M}_\Sigma^2) \equiv (1 - x)^2 p^2 - (1 - x)p^2 + (1 - x)\mathbb{M}_\Sigma^2 + x^2(p - q)^2 - x(p - q)^2 + xm_\phi^2$. The diagram F6 can be evaluated in a similar way as F3 to get

F6 :



$$= \frac{i}{32\pi^2} \xi_1 g_1^2 (Y_\Sigma)_{gf} (\varepsilon^T \sigma^j)_{ba} P_L \frac{1}{\epsilon} + \text{UV finite}, \tag{C.33}$$

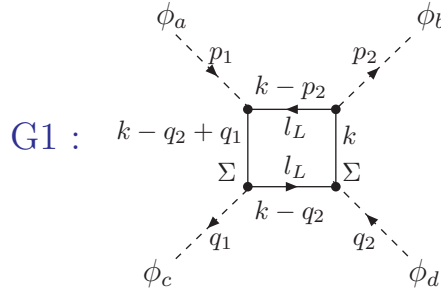
where we have used $(\varepsilon^T \sigma^j)^T = \varepsilon^T \sigma^j \forall j$. The extra ‘-’ sign comes because of the difference in sign between the W and B boson couplings with l_L .

Then finally using the relation shown in Fig C.6 and using the minimal subtraction scheme to define the counter term F7, we find the renormalization

constant to be

$$\delta Z_{Y_\Sigma} = -\frac{1}{16\pi^2} \left(2Y_e^\dagger Y_e - \frac{3}{10} \xi_1 g_1^2 - \frac{1}{2} (12 + 7\xi_2) g_2^2 \right) \frac{1}{\epsilon}. \quad (\text{C.34})$$

CS.7 The extra diagram contributing to the renormalization of Higgs self-coupling λ



$$\begin{aligned} &= -(-i\mu^{\epsilon/2})^4 \text{Tr} \left[Y_\Sigma^\dagger Y_\Sigma Y_\Sigma^\dagger Y_\Sigma \right] (\varepsilon^T \sigma^i \sigma^j \varepsilon)_{ab} (\varepsilon^T \sigma^j \sigma^i \varepsilon)_{dc} \times \\ &\quad \int \frac{d^d k}{(2\pi)^d} \text{Tr} \left[\frac{P_R \not{k} (\not{k} - \not{q}_2) (\not{k} - \not{q}_2 + \not{q}_1) (\not{k} - \not{q}_2)}{(k^2 - M_\Sigma^2) (k - q_2)^2 (k - p_2)^2 [(k - q_2 + q_1)^2 - M_\Sigma^2]} \right] \\ &= -\frac{i}{4\pi^2} \text{Tr} \left[Y_\Sigma^\dagger Y_\Sigma Y_\Sigma^\dagger Y_\Sigma \right] (\delta_{ab} \delta_{cd} + 4\delta_{ac} \delta_{bd}) \frac{1}{\epsilon} + \text{UV finite}. \quad (\text{C.35}) \end{aligned}$$

It is clear from the Feynman diagram that $a \leftrightarrow d$ or $b \leftrightarrow c$ interchange will produce diagrams which will contribute similarly to the amplitude and finally one gets the amplitude to be

$$= -\frac{5i}{4\pi^2} \text{Tr} \left[Y_\Sigma^\dagger Y_\Sigma Y_\Sigma^\dagger Y_\Sigma \right] (\delta_{ab} \delta_{cd} + \delta_{ac} \delta_{bd}) \frac{1}{\epsilon} + \text{UV finite}.$$

CS.8 Renormalization constant of the effective vertex κ

Fig C.7 shows the Feynman diagrams that contribute to the renormalization of the effective low energy vertex κ at the one loop level. As we have already mentioned in Chapter 3, in the intermediate energy scales the fermion triplets

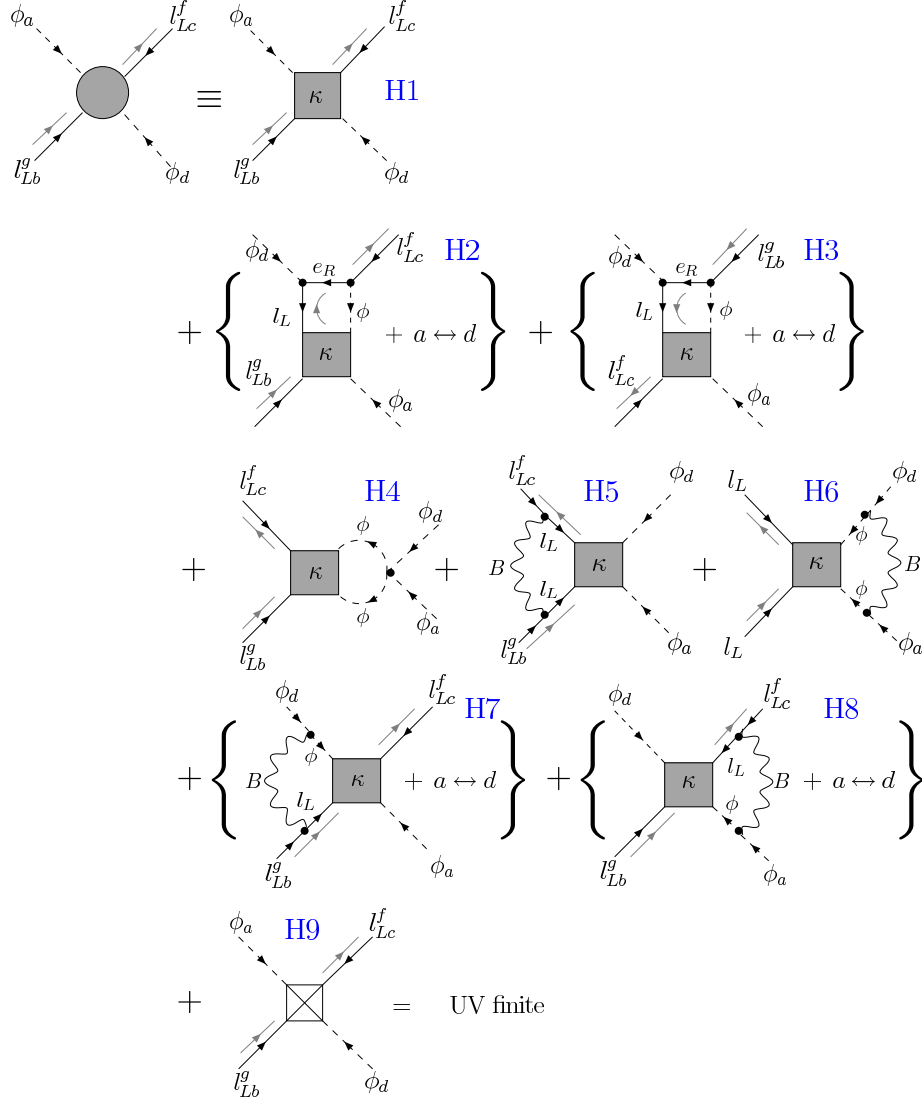


Figure C.7: Feynman diagrams contributing to the one loop correction of the effective vertex κ .

still coupled to the theory do not contribute. Thus the renormalization constant Z_κ remains the same at all energies and also in different seesaw models and is given by

$$\begin{aligned} \delta\kappa = & -\frac{1}{16\pi^2} \left[2\kappa (Y_e^\dagger Y_e) + 2 (Y_e^\dagger Y_e)^T \kappa - \lambda\kappa \right. \\ & \left. - \left(\frac{3}{2} - \xi_1 \right) g_1^2 \kappa - \left(\frac{3}{2} - 3\xi_2 \right) g_2^2 \kappa \right] \frac{1}{\epsilon}. \end{aligned} \quad (\text{C.36})$$

CS.9 Evaluation of d -dimensional momentum integrals

In this section, we write down the d -dimensional integrals explicitly, which have been used in evaluating the diagrams in Sections CS.1 – CS.8.

$$\begin{aligned}
 I_{m,n}(\Delta, \epsilon) &= \int \frac{d^d l_E}{(2\pi)^d} \frac{l_E^m}{(l_E^2 + \Delta)^n} \\
 &= \frac{1}{(4\pi)^{d/2}} \frac{\Gamma(n - \frac{d+m}{2}) \Gamma(\frac{d+m}{2})}{\Gamma(\frac{d}{2}) \Gamma(n)} \left(\frac{1}{\Delta}\right)^{n - \frac{d+m}{2}}, \quad (\text{C.37})
 \end{aligned}$$

where l_E is the momentum of the particle in the loop in Euclidean space and is given as $l_E^0 \equiv -il^0$ and $\vec{l}_E \equiv \vec{l}$ and Δ is some function independent of the momentum l_E . The quantity ϵ is defined as $\epsilon \equiv 4 - d$. The explicit form of $I_{m,n}(\Delta, \epsilon)$ for some specific m, n values are given below, which have been used in the calculation of the diagrams in Section CS.1 - CS.5.

$$I_{0,1}(\Delta, \epsilon) = \frac{\Delta}{16\pi^2} \left(-\frac{2}{\epsilon} + \gamma - 1 + \mathcal{O}(\epsilon) \right), \quad (\text{C.38})$$

$$I_{0,2}(\Delta, \epsilon) = \frac{1}{16\pi^2} \left(\frac{2}{\epsilon} - \gamma + \mathcal{O}(\epsilon) \right), \quad (\text{C.39})$$

$$I_{2,3}(\Delta, \epsilon) = \frac{1}{16\pi^2} \left(\frac{2}{\epsilon} - \gamma + \mathcal{O}(\epsilon) \right), \quad (\text{C.40})$$

where $\gamma \equiv 0.577216$ is the Euler-Mascheroni constant.

CS.10 Clifford algebra in d dimensions

In this section, we write down the Clifford algebra in general d -dimension, which have been used in evaluating the diagrams in Sections CS.1 – CS.8.

Let $\eta^{\mu\nu}$ be the Minkowski metric tensor in d -dimension. Then

$$\eta^{\mu\nu} = \eta^{\nu\mu}, \quad (\text{C.41})$$

$$\eta^{\mu\rho} \eta_\rho^\mu = \eta^{\mu\nu}, \quad (\text{C.42})$$

$$\eta_{\mu\nu} \eta^{\mu\nu} = d, \quad (\text{C.43})$$

and the definition of the Clifford algebra is

$$\{\gamma^\mu, \gamma^\nu\} = 2\eta^{\mu\nu} . \quad (\text{C.44})$$

Using the above relations, one can get

$$\gamma_\mu \gamma^\mu = d , \quad (\text{C.45})$$

$$\gamma_\nu \not{d} \gamma^\nu = (2 - d) \not{d} , \quad (\text{C.46})$$

$$\gamma_\nu \not{d} \not{b} \gamma^\nu = 4a \cdot b - (4 - d) \not{d} \not{b} , \quad (\text{C.47})$$

$$\gamma_\nu \not{d} \not{b} \not{c} \gamma^\nu = -2 \not{c} \not{b} \not{d} + (4 - d) \not{d} \not{b} \not{c} . \quad (\text{C.48})$$

The traces involving gamma matrices are given below.

$$\text{Tr}(\mathbb{1}) = 4 , \quad (\text{C.49})$$

$$\text{Tr}(\not{d} \not{b}) = 4a \cdot b , \quad (\text{C.50})$$

$$\text{Tr}(\text{odd number of } \gamma\text{'s}) = 0 , \quad (\text{C.51})$$

$$\text{Tr}(\not{d} \not{b} \not{c} \not{d}) = 4 [(a \cdot b)(c \cdot d) - (a \cdot c)(b \cdot d) + (a \cdot d)(b \cdot c)] \quad (\text{C.52})$$

Thus the traces of γ matrices not involving γ_5 remains the same as those in 4-dimension.

The issue of γ_5 in dimensional regularization is somewhat delicate, since the 4-dimensional definition leads to inconsistencies. However, it is consistent to use “naive dimensional regularization” [204], where γ_5 anticommutes with all other Dirac matrices to give

$$\{\gamma_5, \gamma^\mu\} = 0 , \quad (\text{C.53})$$

and also satisfies

$$\text{Tr}(\gamma_5) = 0 , \quad (\text{C.54})$$

$$\text{Tr}(\gamma_5 \not{d} \not{b}) = 0 . \quad (\text{C.55})$$

Defining γ_5 in this way, one faces the problem that the quantity $\text{Tr}(\gamma_5 \not{d} \not{b} \not{c} \not{d})$ is not defined in a consistent way. However as long as this quantity does not appear in the calculations explicitly, the above “naive” definition of γ_5 works

fine. Hence we will stick to this definition. With this definition one gets

$$\mathrm{Tr}(P_R d\not{b}) = \mathrm{Tr}(P_L d\not{b}) = 2a.b . \quad (\text{C.56})$$

There is another approach where γ_5 is defined as $\gamma_5 \equiv i\gamma^0\gamma^1\gamma^2\gamma^3$, and thus is an intrinsically 4-dimensional object. In that case Eq. (C.53) is replaced by mixed commutation and anticommutation relations since now γ_5 now commutes with γ^μ for $\mu = 0, 1, 2, 3$ and anticommutes with the other γ^μ . This is the dimensional regularization method suggested by 't Hooft and Veltman [205] and this method is free from any inconsistencies stated above.

CS.11 Feynman parameterization

Feynman parameterization has been used in Sections CS.1 – CS.8 in order to evaluate the d -dimensional integrals. We describe this parameterization below.

$$\frac{1}{AB} = \int_0^1 dx \frac{1}{[xA + (1-x)B]^2} , \quad (\text{C.57})$$

$$\frac{1}{AB^n} = \int_0^1 dx dy \delta(x+y-1) \frac{ny^{n-1}}{[xA+yB]^{n+1}} , \quad (\text{C.58})$$

$$\frac{1}{A_1 A_2 \cdots A_n} = \int_0^1 dx_1 dx_2 \cdots dx_n \delta\left(\sum x_i - 1\right) \frac{(n-1)!}{[\sum x_i A_i]^n} , \quad (\text{C.59})$$

$$\frac{1}{A_1^{m_1} A_2^{m_2} \cdots A_n^{m_n}} = \int_0^1 dx_1 dx_2 \cdots dx_n \delta\left(\sum x_i - 1\right) \frac{\prod x_i^{m_i-1}}{[\sum x_i A_i]^{\sum m_i}} \frac{\Gamma(\sum m_i)}{\prod \Gamma(m_i)} . \quad (\text{C.60})$$

After one uses the suitable Feynman parameterization to the d -dimensional momentum integral, the standard form as given in Section CS.9 by change of variables. The integrals over the auxiliary Feynman parameters may not be solved analytically always.

Appendix D

RG evolution equations of masses and mixing parameters

The renormalization group (RG) evolution for some variable $X \in \{m_i, \theta_{ij}, \phi_i\}$ can be written in the most general form as

$$\dot{X} = A_X^{\mathcal{P}} + \frac{D_X^{\mathcal{P}}}{\theta_{13}} + \theta_{13} B_X^{\mathcal{P}} + \mathcal{O}(\theta_{13}^2), \quad (\text{D.1})$$

where \mathcal{P} denotes the basis in which the quantities are written. We have $D_X^{\mathcal{P}} \equiv 0 \forall X$ and for $\mathcal{P} = \mathcal{P}_J, \mathcal{P}_\delta$ except for $X = \delta$ when $\mathcal{P} = \mathcal{P}_\delta$. The coefficients in $\mathcal{P} = \mathcal{P}_\delta$ are given below.

$$A_{12}^{\mathcal{P}_\delta} = -\frac{C y_\tau^2}{2} \sin 2\theta_{12} s_{23}^2 \left[\frac{m_1^2 + m_2^2 + 2m_1 m_2 \cos(2\phi_1 - 2\phi_2)}{\Delta m_\odot^2} \right], \quad (\text{D.2})$$

$$A_{23}^{\mathcal{P}_\delta} = -\frac{C y_\tau^2}{2} \left[\frac{c_{12}^2 |m_2 + m_3 e^{2i\phi_2}|^2}{\Delta m_{\text{atm}}^2} + \frac{s_{12}^2 |m_1 + m_3 e^{2i\phi_1}|^2}{\Delta m_{31}^2} \right], \quad (\text{D.3})$$

$$A_{13}^{\mathcal{P}_\delta} = \frac{C y_\tau^2}{2} \sin 2\theta_{12} \sin 2\theta_{23} \frac{m_3}{\Delta m_{31}^2} \times [m_1 \cos(\delta - 2\phi_1) - m_2(1 + \zeta) \cos(\delta - 2\phi_2) - \zeta m_3 \cos \delta], \quad (\text{D.4})$$

where $\zeta \equiv \Delta m_{\odot}^2 / \Delta m_{\text{atm}}^2$.

$$A_{\phi_1}^{\mathcal{P}_\delta} = 2C y_\tau^2 \left\{ \cos 2\theta_{23} \frac{m_3}{\Delta m_{31}^2} [m_1 s_{12}^2 \sin 2\phi_1 + m_2(1 + \zeta) c_{12}^2 \sin 2\phi_2] + c_{12}^2 s_{23}^2 \frac{m_1 m_2}{\Delta m_{\odot}^2} \sin(2\phi_1 - 2\phi_2) \right\}, \quad (\text{D.5})$$

$$A_{\phi_2}^{\mathcal{P}_\delta} = 2C y_\tau^2 \left\{ \cos 2\theta_{23} \frac{m_3}{\Delta m_{31}^2} [m_1 s_{12}^2 \sin 2\phi_1 + m_2(1 + \zeta) c_{12}^2 \sin 2\phi_2] + s_{12}^2 s_{23}^2 \frac{m_1 m_2}{\Delta m_{\odot}^2} \sin(2\phi_1 - 2\phi_2) \right\}. \quad (\text{D.6})$$

From the expressions given above, it can be seen that $A_X^{\mathcal{P}_\delta}, \forall X \in \{\theta_{ij}, \phi_i\}$, are independent of δ and hence we have $A_X^{\mathcal{P}_J} \equiv A_X^{\mathcal{P}_\delta}$.

The coefficients involved in $\dot{\delta}$, $A_\delta^{\mathcal{P}_\delta}$ and $D_\delta^{\mathcal{P}_\delta}$ are given by

$$A_\delta^{\mathcal{P}_\delta} = 2C y_\tau^2 \left\{ \frac{m_1 m_2}{\Delta m_{\odot}^2} s_{23}^2 \sin(2\phi_1 - 2\phi_2) + \frac{m_3}{\Delta m_{31}^2} [c_{23}^2 (m_1 c_{12}^2 \sin(2\delta - 2\phi_1) + m_2(1 + \zeta) s_{12}^2 \sin(2\delta - 2\phi_2)) + \cos 2\theta_{23} (m_1 s_{12}^2 \sin 2\phi_1 + m_2(1 + \zeta) c_{12}^2 \sin 2\phi_2)] \right\}, \quad (\text{D.7})$$

$$D_\delta^{\mathcal{P}_\delta} = C y_\tau^2 s_{12} c_{12} s_{23} c_{23} \left\{ \left(\frac{\zeta m_3^2}{\Delta m_{31}^2} + \frac{m_2^2}{\Delta m_{\text{atm}}^2} - \frac{m_1^2}{\Delta m_{31}^2} \right) \sin \delta - \frac{2m_1 m_3}{\Delta m_{31}^2} \sin(\delta - 2\phi_1) + \frac{2m_2 m_3}{\Delta m_{\text{atm}}^2} \sin(\delta - 2\phi_2) \right\} \quad (\text{D.8})$$

The other $A_X^{\mathcal{P}}$ appearing in the basis \mathcal{P}_J are $A_J^{\mathcal{P}_J}, A_J^{\prime \mathcal{P}_J}$ and are given as

$$A_J^{\mathcal{P}_J} = C y_\tau^2 s_{12}^2 c_{12}^2 s_{23}^2 c_{23}^2 \frac{m_3}{\Delta m_{31}^2} [m_1 \sin 2\phi_1 - m_2(1 + \zeta) \sin 2\phi_2], \quad (\text{D.9})$$

$$A_J^{\prime \mathcal{P}_J} = C y_\tau^2 s_{12}^2 c_{12}^2 s_{23}^2 c_{23}^2 \frac{m_3}{\Delta m_{31}^2} [m_1 \cos 2\phi_1 - m_2(1 + \zeta) \cos 2\phi_2 - \zeta m_3]. \quad (\text{D.10})$$

Thus the evolution equations in the \mathcal{P}_J basis are all continuous and well-behaved at all points in the parameter space, including $\theta_{13} = 0$.

The running of the neutrino masses are given as

$$\dot{m}_1 = [\alpha + Cy_\tau^2 (2 \sin^2 \theta_{12} \sin^2 \theta_{23} + G_1^{\mathcal{P}})] m_1 , \quad (\text{D.11})$$

$$\dot{m}_2 = [\alpha + Cy_\tau^2 (2 \cos^2 \theta_{12} \sin^2 \theta_{23} + G_2^{\mathcal{P}})] m_2 , \quad (\text{D.12})$$

$$\dot{m}_3 = [\alpha + 2Cy_\tau^2 \cos^2 \theta_{13} \cos^2 \theta_{23}] m_1 . \quad (\text{D.13})$$

As can be seen from Eqs. (D.11)-(D.13), the quantities $G_i^{\mathcal{P}}$ depends on the choice of basis. In the \mathcal{P}_δ basis they can be given as

$$G_1^{\mathcal{P}_\delta} = -\sin \theta_{13} \sin 2\theta_{12} \sin 2\theta_{23} \cos \delta + 2 \sin^2 \theta_{13} \cos^2 \theta_{12} \cos^2 \theta_{23} , \quad (\text{D.14})$$

$$G_2^{\mathcal{P}_\delta} = \sin \theta_{13} \sin 2\theta_{12} \sin 2\theta_{23} \cos \delta + 2 \sin^2 \theta_{13} \sin^2 \theta_{12} \cos^2 \theta_{23} , \quad (\text{D.15})$$

while in the \mathcal{P}_J basis they become

$$G_1^{\mathcal{P}_J} = -\frac{8J'_{\text{CP}}}{\cos^2 \theta_{13}} + 2 \sin^2 \theta_{13} \cos^2 \theta_{12} \cos^2 \theta_{23} , \quad (\text{D.16})$$

$$G_2^{\mathcal{P}_J} = \frac{8J'_{\text{CP}}}{\cos^2 \theta_{13}} + 2 \sin^2 \theta_{13} \sin^2 \theta_{12} \cos^2 \theta_{23} . \quad (\text{D.17})$$

Here we define $a \equiv \sin \theta_{12} \cos \theta_{12} \sin \theta_{23} \cos \theta_{23}$.

Bibliography

- [1] Fukuda, Y. et al. *Phys. Rev. Lett.* **81**, 1562–1567 (1998). [ix](#), [1](#)
- [2] Ahmad, Q. R. et al. *Phys. Rev. Lett.* **87**, 071301 (2001). [ix](#), [2](#)
- [3] Araki, T. et al. *Phys. Rev. Lett.* **94**, 081801 (2005). [ix](#), [2](#)
- [4] Ahn, M. H. et al. *Phys. Rev. Lett.* **90**, 041801 (2003). [ix](#)
- [5] Ahn, M. H. et al. *Phys. Rev.* **D74**, 072003 (2006). [ix](#), [1](#)
- [6] Aguilar, A. et al. *Phys. Rev.* **D64**, 112007 (2001). [ix](#), [5](#), [15](#), [33](#)
- [7] Armbruster, B. et al. *Phys. Rev.* **D65**, 112001 (2002). [ix](#), [xiv](#), [5](#), [16](#), [19](#)
- [8] Aguilar-Arevalo, A. A. et al. *Phys. Rev. Lett.* **98**, 231801 (2007). [ix](#), [xiv](#), [5](#), [16](#), [19](#)
- [9] Pontecorvo, B. *Sov. Phys. JETP* **7**, 172–173 (1958). [ix](#), [3](#), [57](#)
- [10] Pontecorvo, B. *Sov. Phys. JETP* **26**, 984–988 (1968). [ix](#), [3](#), [57](#)
- [11] Gribov, V. N. and Pontecorvo, B. *Phys. Lett.* **B28**, 493 (1969). [ix](#), [3](#), [57](#)
- [12] Maki, Z., Nakagawa, M., and Sakata, S. *Prog. Theor. Phys.* **28**, 870–880 (1962). [ix](#), [3](#), [57](#)
- [13] Schwetz, T., Tortola, M., and Valle, J. W. F. *New J. Phys.* **10**, 113011 (2008). [x](#), [xiv](#), [2](#), [3](#), [4](#)
- [14] Fogli, G. L., Lisi, E., Marrone, A., Palazzo, A., and Rotunno, A. M. *Phys. Rev. Lett.* **101**, 141801 (2008). [x](#), [xiv](#), [4](#)
- [15] Bandyopadhyay, A., Choubey, S., Goswami, S., Petcov, S. T., and Roy, D. P. (2008). [x](#), [xiv](#), [4](#)

- [16] Hannestad, S. *Phys. Rev. Lett.* **95**, 221301 (2005). [x](#), [5](#), [81](#)
- [17] Robertson, R. G. H. *J. Phys. Conf. Ser.* **120**, 052028 (2008). [x](#), [xxiii](#), [xxviii](#), [5](#), [67](#), [83](#), [86](#)
- [18] Maltoni, M. and Schwetz, T. *Phys. Rev.* **D76**, 093005 (2007). [x](#), [xvii](#), [xviii](#), [6](#), [7](#), [16](#), [17](#), [33](#), [34](#), [36](#)
- [19] Kusenko, A. *AIP Conf. Proc.* **917**, 58–68 (2007). [x](#), [6](#), [10](#), [11](#), [16](#)
- [20] McLaughlin, G. C., Fetter, J. M., Balantekin, A. B., and Fuller, G. M. *Phys. Rev.* **C59**, 2873–2887 (1999). [x](#), [6](#)
- [21] Hidaka, J. and Fuller, G. M. *Phys. Rev.* **D76**, 083516 (2007). [x](#), [6](#)
- [22] Kusenko, A. *Int. J. Mod. Phys.* **D13**, 2065–2084 (2004). [x](#), [6](#)
- [23] Riemer-Sorensen, S., Hansen, S. H., and Pedersen, K. *Astrophys. J.* **644**, L33–L36 (2006). [xi](#), [6](#)
- [24] Munyaneza, F. and Biermann, P. L. (2006). [xi](#), [6](#)
- [25] de Gouvea, A. *Phys. Rev.* **D72**, 033005 (2005). [xi](#), [7](#)
- [26] Asaka, T. and Shaposhnikov, M. *Phys. Lett.* **B620**, 17–26 (2005). [xi](#), [7](#)
- [27] Asaka, T., Blanchet, S., and Shaposhnikov, M. *Phys. Lett.* **B631**, 151–156 (2005). [xi](#), [7](#)
- [28] Sahu, N. and Yajnik, U. A. *Phys. Lett.* **B635**, 11–16 (2006). [xi](#), [7](#)
- [29] Chakraborty, J., Dighe, A., Goswami, S., and Ray, S. (2008). [xi](#), [xiii](#), [13](#)
- [30] Dighe, A. and Ray, S. *Phys. Rev.* **D76**, 113001 (2007). [xi](#), [7](#)
- [31] Weinberg, S. *Phys. Rev. Lett.* **43**, 1566–1570 (1979). [xii](#), [10](#), [46](#)
- [32] Chankowski, P. H. and Pokorski, S. *Int. J. Mod. Phys.* **A17**, 575–614 (2002). [xii](#), [xxi](#), [13](#), [53](#), [72](#)
- [33] Babu, K. S., Leung, C. N., and Pantaleone, J. T. *Phys. Lett.* **B319**, 191–198 (1993). [xii](#), [13](#), [72](#)

- [34] Antusch, S., Drees, M., Kersten, J., Lindner, M., and Ratz, M. *Phys. Lett.* **B519**, 238–242 (2001). [xii](#), [xiii](#), [xxiii](#), [xxv](#), [xxvi](#), [13](#), [51](#), [57](#), [59](#), [72](#), [73](#), [75](#), [78](#)
- [35] Antusch, S., Kersten, J., Lindner, M., and Ratz, M. *Nucl. Phys.* **B674**, 401–433 (2003). [xii](#), [xiii](#), [xxv](#), [xxvi](#), [13](#), [59](#), [66](#), [72](#)
- [36] Antusch, S., Drees, M., Kersten, J., Lindner, M., and Ratz, M. *Phys. Lett.* **B525**, 130–134 (2002). [xii](#), [13](#), [72](#)
- [37] Fukuyama, T. and Okada, N. *JHEP* **11**, 011 (2002). [xii](#), [13](#)
- [38] Tanimoto, M. *Phys. Lett.* **B360**, 41–46 (1995). [xii](#), [13](#), [72](#)
- [39] Haba, N., Okamura, N., and Sugiura, M. *Prog. Theor. Phys.* **103**, 367–377 (2000). [xii](#), [13](#), [72](#)
- [40] Balaji, K. R. S., Dighe, A. S., Mohapatra, R. N., and Parida, M. K. *Phys. Rev. Lett.* **84**, 5034–5037 (2000). [xii](#), [13](#), [72](#)
- [41] Balaji, K. R. S., Dighe, A. S., Mohapatra, R. N., and Parida, M. K. *Phys. Lett.* **B481**, 33–38 (2000). [xii](#), [13](#), [72](#)
- [42] Balaji, K. R. S., Mohapatra, R. N., Parida, M. K., and Paschos, E. A. *Phys. Rev.* **D63**, 113002 (2001). [xii](#), [13](#), [72](#)
- [43] Mohapatra, R. N., Parida, M. K., and Rajasekaran, G. *Phys. Rev.* **D69**, 053007 (2004). [xii](#), [13](#), [72](#)
- [44] Agarwalla, S. K., Parida, M. K., Mohapatra, R. N., and Rajasekaran, G. *Phys. Rev.* **D75**, 033007 (2007). [xii](#), [13](#), [72](#)
- [45] Vissani, F. (1997). [xii](#), [13](#), [64](#), [72](#)
- [46] Branco, G. C., Rebelo, M. N., and Silva-Marcos, J. I. *Phys. Rev. Lett.* **82**, 683–686 (1999). [xii](#), [13](#), [72](#)
- [47] Casas, J. A., Espinosa, J. R., Ibarra, A., and Navarro, I. *Nucl. Phys.* **B556**, 3–22 (1999). [xii](#), [13](#)
- [48] Casas, J. A., Espinosa, J. R., Ibarra, A., and Navarro, I. *Nucl. Phys.* **B569**, 82–106 (2000). [xii](#), [13](#), [72](#)

- [49] Haba, N., Matsui, Y., Okamura, N., and Sugiura, M. *Prog. Theor. Phys.* **103**, 145–150 (2000). [xii](#), [13](#), [72](#)
- [50] Adhikari, R., Ma, E., and Rajasekaran, G. *Phys. Lett.* **B486**, 134–139 (2000). [xii](#), [13](#), [72](#)
- [51] Joshipura, A. S., Rindani, S. D., and Singh, N. N. *Nucl. Phys.* **B660**, 362–372 (2003). [xii](#), [13](#), [72](#)
- [52] Joshipura, A. S. and Mohanty, S. *Phys. Rev.* **D67**, 091302 (2003). [xii](#), [13](#), [72](#)
- [53] Xing, Z.-z. and Zhang, H. *Commun. Theor. Phys.* **48**, 525 (2007). [xii](#), [13](#), [72](#)
- [54] Joshipura, A. S. *Phys. Lett.* **B543**, 276–282 (2002). [xii](#), [13](#), [72](#), [88](#)
- [55] Joshipura, A. S. and Rindani, S. D. *Phys. Rev.* **D67**, 073009 (2003). [xii](#), [13](#), [72](#), [88](#)
- [56] Mei, J.-w. and Xing, Z.-z. *Phys. Rev.* **D70**, 053002 (2004). [xii](#), [13](#), [72](#)
- [57] Dighe, A., Goswami, S., and Ray, S. (2008). [xii](#), [xiii](#), [xxviii](#), [13](#), [59](#)
- [58] King, S. F. and Singh, N. N. *Nucl. Phys.* **B591**, 3–25 (2000). [xiii](#), [13](#)
- [59] Antusch, S., Kersten, J., Lindner, M., and Ratz, M. *Phys. Lett.* **B544**, 1–10 (2002). [xiii](#), [13](#), [64](#), [66](#), [72](#)
- [60] Mohapatra, R. N., Parida, M. K., and Rajasekaran, G. *Phys. Rev.* **D71**, 057301 (2005). [xiii](#), [13](#), [72](#)
- [61] Antusch, S., Kersten, J., Lindner, M., Ratz, M., and Schmidt, M. A. *JHEP* **03**, 024 (2005). [xiii](#), [xxiii](#), [13](#), [57](#), [58](#), [61](#), [72](#)
- [62] Mei, J.-w. *Phys. Rev.* **D71**, 073012 (2005). [xiii](#), [13](#)
- [63] Schmidt, M. A. *Phys. Rev.* **D76**, 073010 (2007). [xiii](#), [13](#)
- [64] Chao, W. and Zhang, H. *Phys. Rev.* **D75**, 033003 (2007). [xiii](#), [13](#)
- [65] Gogoladze, I., Okada, N., and Shafi, Q. *Phys. Lett.* **B668**, 121–125 (2008). [xiii](#), [13](#), [53](#)

- [66] Declais, Y. et al. *Nucl. Phys.* **B434**, 503–534 (1995). [xiv](#), [16](#), [19](#)
- [67] Astier, P. et al. *Phys. Lett.* **B570**, 19–31 (2003). [xiv](#), [1](#), [16](#), [19](#)
- [68] Dydak, F. et al. *Phys. Lett.* **B134**, 281 (1984). [xiv](#), [1](#), [16](#), [19](#)
- [69] Hosaka, J. et al. *Phys. Rev.* **D74**, 032002 (2006). [xiv](#), [19](#)
- [70] Apollonio, M. et al. *Eur. Phys. J.* **C27**, 331–374 (2003). [xiv](#), [19](#)
- [71] Huber, P., Lindner, M., and Winter, W. *Nucl. Phys.* **B645**, 3–48 (2002). [xvi](#), [27](#)
- [72] Dziewonski, A. M. and Anderson, D. L. *Phys. Earth Planet. Interiors* **25**, 297–356 (1981). [xvi](#), [24](#), [27](#)
- [73] Huber, P., Lindner, M., and Winter, W. *Comput. Phys. Commun.* **167**, 195 (2005). [xvii](#), [27](#)
- [74] Huber, P., Kopp, J., Lindner, M., Rolinec, M., and Winter, W. *Comput. Phys. Commun.* **177**, 432–438 (2007). [xvii](#), [27](#)
- [75] Kersten, J. *Diploma Thesis*, web-address (2001). [xxi](#), [51](#), [54](#), [106](#)
- [76] Michael, D. G. et al. *Phys. Rev. Lett.* **97**, 191801 (2006). [1](#)
- [77] Fukuda, S. et al. *Phys. Rev. Lett.* **86**, 5656–5660 (2001). [2](#)
- [78] Bahcall, J. N., Gonzalez-Garcia, M. C., and Pena-Garay, C. *JHEP* **07**, 054 (2002). [2](#)
- [79] Kraus, C. et al. *Eur. Phys. J.* **C40**, 447–468 (2005). [5](#)
- [80] Klapdor-Kleingrothaus, H. V. et al. *Eur. Phys. J.* **A12**, 147–154 (2001). [5](#), [86](#)
- [81] Komatsu, E. et al. *Astrophys. J. Suppl.* **180**, 330–376 (2009). [5](#)
- [82] Foot, R., Lew, H., He, X. G., and Joshi, G. C. *Z. Phys.* **C44**, 441 (1989). [6](#), [11](#), [41](#)
- [83] Choubey, S., Harries, N. P., and Ross, G. G. *Phys. Rev.* **D74**, 053010 (2006). [7](#)

- [84] Choubey, S., Harries, N. P., and Ross, G. G. *Phys. Rev.* **D76**, 073013 (2007). [7](#), [33](#)
- [85] Awasthi, R. L. and Choubey, S. *Phys. Rev.* **D76**, 113002 (2007). [7](#)
- [86] Minkowski, P. *Phys. Lett.* **B67**, 421 (1977). [9](#)
- [87] Yanagida, T. *Proceedings of the Workshop on the Unified Theory and the Baryon Number in the Universe*. KEK, Tsukuba, Japan, (1979). [9](#)
- [88] Gell-Mann, M, R. P. and Slansky, R. *Complex spinors and unified theories*. Supergravity. North Holland, Amsterdam, (1979). [9](#)
- [89] Glashow, S. L. *The future of elementary particle physics*. Proceedings of the 1979 Cargèse Summer Institute on Quarks and Leptons. Plenum Press, New York, (1980). [9](#)
- [90] Mohapatra, R. N. and Senjanovic, G. *Phys. Rev. Lett.* **44**, 912 (1980). [9](#)
- [91] Magg, M. and Wetterich, C. *Phys. Lett.* **B94**, 61 (1980). [11](#)
- [92] Lazarides, G., Shafi, Q., and Wetterich, C. *Nucl. Phys.* **B181**, 287 (1981). [11](#)
- [93] Ma, E. and Roy, D. P. *Nucl. Phys.* **B644**, 290–302 (2002). [11](#), [41](#)
- [94] Chankowski, P. H. and Pluciennik, Z. *Phys. Lett.* **B316**, 312–317 (1993). [13](#)
- [95] Yao, W. M. et al. *J. Phys.* **G33**, 1–1232 (2006). [15](#)
- [96] Ahmad, Q. R. et al. *Phys. Rev. Lett.* **89**, 011301 (2002). [15](#)
- [97] Chauhan, B. C. and Pulido, J. *JHEP* **12**, 040 (2004). [15](#)
- [98] Fukuda, S. et al. *Phys. Rev. Lett.* **85**, 3999–4003 (2000). [16](#)
- [99] Fogli, G. L., Lisi, E., and Marrone, A. *Phys. Rev.* **D64**, 093005 (2001). [16](#), [19](#)
- [100] Nakaya, T. (2002). [16](#), [19](#)
- [101] Choudhury, D. and Datta, A. (2006). [16](#), [19](#)

- [102] Donini, A., Maltoni, M., Meloni, D., Migliozzi, P., and Terranova, F. *JHEP* **12**, 013 (2007). [16](#)
- [103] Donini, A. and Meloni, D. *Eur. Phys. J.* **C22**, 179–186 (2001). [16](#)
- [104] Donini, A., Lusignoli, M., and Meloni, D. *Nucl. Phys.* **B624**, 405–422 (2002). [16](#)
- [105] Goswami, S., Bandyopadhyay, A., and Choubey, S. *Nucl. Phys. Proc. Suppl.* **143**, 121–128 (2005). [19](#)
- [106] Akhmedov, E. K., Johansson, R., Lindner, M., Ohlsson, T., and Schwetz, T. *JHEP* **04**, 078 (2004). [23](#)
- [107] Albright, C. H. et al. (2004). [27](#)
- [108] Athar, M. S. et al. . A Report of the INO Feasibility Study. Updated from the earlier Interim Report of May 1, 2005. [27](#)
- [109] Messier, M. D. . UMI-99-23965. [27](#)
- [110] Paschos, E. A. and Yu, J. Y. *Phys. Rev.* **D65**, 033002 (2002). [27](#)
- [111] Ereditato, A. and Rubbia, A. *Nucl. Phys. Proc. Suppl.* **155**, 233–236 (2006). [31](#)
- [112] Ereditato, A. and Rubbia, A. *Nucl. Phys. Proc. Suppl.* **154**, 163–178 (2006). [31](#)
- [113] Goswami, S. and Rodejohann, W. *JHEP* **10**, 073 (2007). [33](#)
- [114] Bandyopadhyay, A. and Choubey, S. (2007). [33](#)
- [115] Ardellier, F. et al. (2006). [38](#), [86](#)
- [116] Guo, X. et al. (2007). [38](#), [86](#)
- [117] Huber, P., Lindner, M., Rolinec, M., and Winter, W. *Phys. Rev.* **D74**, 073003 (2006). [38](#)
- [118] Bajc, B. and Senjanovic, G. *JHEP* **08**, 014 (2007). [42](#)
- [119] Bajc, B., Nemevsek, M., and Senjanovic, G. *Phys. Rev.* **D76**, 055011 (2007). [42](#)

- [120] Abada, A., Biggio, C., Bonnet, F., Gavela, M. B., and Hambye, T. *JHEP* **12**, 061 (2007). [42](#)
- [121] Franceschini, R., Hambye, T., and Strumia, A. *Phys. Rev.* **D78**, 033002 (2008). [42](#)
- [122] del Aguila, F. and Aguilar-Saavedra, J. A. *Nucl. Phys.* **B813**, 22–90 (2009). [42](#)
- [123] Abada, A., Biggio, C., Bonnet, F., Gavela, M. B., and Hambye, T. *Phys. Rev.* **D78**, 033007 (2008). [42](#), [44](#)
- [124] Ma, E. and Suematsu, D. *Mod. Phys. Lett.* **A24**, 583–589 (2009). [42](#)
- [125] Fileviez Perez, P. *Phys. Rev.* **D76**, 071701 (2007). [42](#)
- [126] Dorsner, I. and Fileviez Perez, P. *JHEP* **06**, 029 (2007). [42](#)
- [127] Mohapatra, R. N., Okada, N., and Yu, H.-B. *Phys. Rev.* **D78**, 075011 (2008). [42](#)
- [128] Blanchet, S. and Fileviez Perez, P. *JCAP* **0808**, 037 (2008). [42](#)
- [129] Fischler, W. and Flauger, R. *JHEP* **09**, 020 (2008). [42](#)
- [130] Blanchet, S. and Fileviez Perez, P. (2008). [42](#)
- [131] Di Chiara, S. and Hsieh, K. *Phys. Rev.* **D78**, 055016 (2008). [42](#)
- [132] Barger, V. D., Pakvasa, S., Weiler, T. J., and Whisnant, K. *Phys. Lett.* **B437**, 107–116 (1998). [64](#), [72](#)
- [133] Baltz, A. J., Goldhaber, A. S., and Goldhaber, M. *Phys. Rev. Lett.* **81**, 5730–5733 (1998). [64](#)
- [134] Jezabek, M. and Sumino, Y. *Phys. Lett.* **B440**, 327–331 (1998). [64](#)
- [135] Altarelli, G. and Feruglio, F. *Phys. Lett.* **B439**, 112–118 (1998). [64](#)
- [136] Dighe, A., Goswami, S., and Roy, P. *Phys. Rev.* **D73**, 071301 (2006). [64](#), [72](#), [82](#)
- [137] Miura, T., Shindou, T., and Takasugi, E. *Phys. Rev.* **D68**, 093009 (2003). [64](#), [72](#)

- [138] Shindou, T. and Takasugi, E. *Phys. Rev.* **D70**, 013005 (2004). [64](#), [72](#)
- [139] Albright, C. H. and Chen, M.-C. *Phys. Rev.* **D74**, 113006 (2006). [71](#)
- [140] Fukuyama, T. and Nishiura, H. (1997). [71](#)
- [141] Mohapatra, R. N. and Nussinov, S. *Phys. Rev.* **D60**, 013002 (1999). [71](#)
- [142] Lam, C. S. *Phys. Lett.* **B507**, 214–218 (2001). [71](#)
- [143] Grimus, W. and Lavoura, L. *JHEP* **07**, 045 (2001). [71](#)
- [144] Grimus, W. and Lavoura, L. *Acta Phys. Polon.* **B32**, 3719–3734 (2001). [71](#)
- [145] Ma, E. and Rajasekaran, G. *Phys. Rev.* **D64**, 113012 (2001). [71](#)
- [146] Babu, K. S., Ma, E., and Valle, J. W. F. *Phys. Lett.* **B552**, 207–213 (2003). [71](#)
- [147] Altarelli, G. and Feruglio, F. *Nucl. Phys.* **B741**, 215–235 (2006). [71](#)
- [148] Grimus, W., Joshipura, A. S., Kaneko, S., Lavoura, L., and Tanimoto, M. *JHEP* **07**, 078 (2004). [71](#)
- [149] Ishimori, H. et al. *Phys. Lett.* **B662**, 178–184 (2008). [71](#)
- [150] Harrison, P. F., Perkins, D. H., and Scott, W. G. *Phys. Lett.* **B458**, 79–92 (1999). [71](#)
- [151] Harrison, P. F., Perkins, D. H., and Scott, W. G. *Phys. Lett.* **B530**, 167 (2002). [71](#)
- [152] Harrison, P. F. and Scott, W. G. *Phys. Lett.* **B557**, 76 (2003). [71](#)
- [153] Grimus, W. and Lavoura, L. *JHEP* **08**, 013 (2005). [71](#)
- [154] Koide, Y. *Phys. Rev.* **D73**, 057901 (2006). [71](#)
- [155] Brown, T., Pakvasa, S., Sugawara, H., and Yamanaka, Y. *Phys. Rev.* **D30**, 255 (1984). [71](#)
- [156] Ma, E. *Phys. Lett.* **B632**, 352–356 (2006). [71](#)
- [157] Koide, Y. *JHEP* **08**, 086 (2007). [71](#)

- [158] Lam, C. S. *Phys. Rev. Lett.* **101**, 121602 (2008). [71](#)
- [159] Vissani, F. *JHEP* **11**, 025 (1998). [71](#)
- [160] Petcov, S. T. *Phys. Lett.* **B110**, 245–249 (1982). [71](#)
- [161] Joshipura, A. S. *Phys. Rev.* **D60**, 053002 (1999). [71](#)
- [162] Joshipura, A. S. and Rindani, S. D. *Phys. Lett.* **B464**, 239–243 (1999). [71](#)
- [163] Lavoura, L. *Phys. Rev.* **D62**, 093011 (2000). [71](#)
- [164] Lavoura, L. and Grimus, W. *JHEP* **09**, 007 (2000). [71](#)
- [165] Altarelli, G. and Franceschini, R. *JHEP* **03**, 047 (2006). [71](#)
- [166] Choubey, S. and Rodejohann, W. *Eur. Phys. J.* **C40**, 259–268 (2005). [71](#)
- [167] Low, C. I. *Phys. Rev.* **D70**, 073013 (2004). [71](#)
- [168] Watanabe, A. and Yoshioka, K. *JHEP* **05**, 044 (2006). [71](#)
- [169] Mohapatra, R. N. and Rodejohann, W. *Phys. Lett.* **B644**, 59–66 (2007). [71](#)
- [170] Blum, A., Mohapatra, R. N., and Rodejohann, W. *Phys. Rev.* **D76**, 053003 (2007). [71](#)
- [171] Branco, G. C., Emmanuel-Costa, D., Rebelo, M. N., and Roy, P. *Phys. Rev.* **D77**, 053011 (2008). [71](#)
- [172] Goswami, S. and Watanabe, A. *Phys. Rev.* **D79**, 033004 (2009). [71](#)
- [173] Albright, C. H. and Barr, S. M. *Phys. Rev.* **D64**, 073010 (2001). [71](#)
- [174] Shafi, Q. and Tavartkiladze, Z. *Phys. Lett.* **B633**, 595–601 (2006). [71](#)
- [175] Oshimo, N. *Nucl. Phys.* **B668**, 258–272 (2003). [71](#)
- [176] Masina, I. *Phys. Lett.* **B633**, 134–140 (2006). [71](#)
- [177] Ellis, J. R. and Lola, S. *Phys. Lett.* **B458**, 310–321 (1999). [72](#)
- [178] Haba, N. and Okamura, N. *Eur. Phys. J.* **C14**, 347–365 (2000). [72](#)

- [179] Ma, E. *J. Phys.* **G25**, L97–L100 (1999). [72](#)
- [180] Haba, N., Matsui, Y., Okamura, N., and Suzuki, T. *Phys. Lett.* **B489**, 184–193 (2000). [72](#)
- [181] Chankowski, P. H., Krolkowski, W., and Pokorski, S. *Phys. Lett.* **B473**, 109–117 (2000). [72](#)
- [182] Pantaleone, J. T., Kuo, T.-K., and Wu, G.-H. *Phys. Lett.* **B520**, 279–288 (2001). [72](#)
- [183] Luo, S. and Xing, Z.-z. *Phys. Lett.* **B637**, 279–286 (2006). [72](#), [73](#)
- [184] Petcov, S. T., Shindou, T., and Takanishi, Y. *Nucl. Phys.* **B738**, 219–242 (2006). [72](#)
- [185] Grimus, W. and Lavoura, L. *Eur. Phys. J.* **C39**, 219–227 (2005). [72](#), [83](#)
- [186] Calibbi, L., Faccia, A., Masiero, A., and Vempati, S. K. *JHEP* **07**, 012 (2007). [72](#)
- [187] Chankowski, P. H. and Wasowicz, P. *Eur. Phys. J.* **C23**, 249–258 (2002). [72](#)
- [188] Antusch, S., Kersten, J., Lindner, M., and Ratz, M. *Phys. Lett.* **B538**, 87–95 (2002). [72](#)
- [189] Jezabek, M. and Sumino, Y. *Phys. Lett.* **B457**, 139–146 (1999). [72](#)
- [190] Dighe, A., Goswami, S., and Rodejohann, W. *Phys. Rev.* **D75**, 073023 (2007). [72](#)
- [191] Goswami, S., Petcov, S., Ray, S., and Rodejohann, W. (2009). [72](#), [81](#)
- [192] Dighe, A., Goswami, S., and Roy, P. *Phys. Rev.* **D76**, 096005 (2007). [72](#), [81](#), [88](#)
- [193] Mohapatra, R. N., Setzer, N., and Spinner, S. *Phys. Rev.* **D73**, 075001 (2006). [81](#)
- [194] Buchmuller, W., Di Bari, P., and Plumacher, M. *Nucl. Phys.* **B665**, 445–468 (2003). [81](#)
- [195] Amsler, C. et al. *Phys. Lett.* **B667**, 1 (2008). [82](#)

- [196] Zito, M. *J. Phys. Conf. Ser.* **110**, 082023 (2008). [86](#)
- [197] Stewart, D. Y. *Nucl. Instrum. Meth.* **A580**, 342–345 (2007). [86](#)
- [198] Cremonesi, O. et al. *Phys. Atom. Nucl.* **69**, 2083–2089 (2006). [86](#)
- [199] Hall, C. *AIP Conf. Proc.* **870**, 532–535 (2006). [86](#)
- [200] Kroninger, K. *J. Phys. Conf. Ser.* **110**, 082010 (2008). [86](#)
- [201] Barabash, A. S. *J. Phys. Conf. Ser.* **39**, 347–349 (2006). [86](#)
- [202] Nakamura, H. et al. *J. Phys. Conf. Ser.* **39**, 350–352 (2006). [86](#)
- [203] Denner, A., Eck, H., Hahn, O., and Kublbeck, J. *Nucl. Phys.* **B387**, 467–484 (1992). [103](#)
- [204] Buras, A. J. and Weisz, P. H. *Nucl. Phys.* **B333**, 66 (1990). [126](#)
- [205] 't Hooft, G. and Veltman, M. J. G. *Nucl. Phys.* **B44**, 189–213 (1972). [127](#)